Pluronic F127 as Transient Barrier for Vascularized Cortical Organoids on-a-Chip

MSc. Biomedical Engineering

Maarten Lemmens

Delft University of Technology

Pluronic F127 as Transient Barrier for Vascularized Cortical Organoids on-a-Chip

by

Maarten Lemmens

to obtain the degree of

Master of Science
in Biomedical Engineering

at the Delft University of Technology,

to be defended publicly on Thursday June 27, 2024 at 9:00 AM.

Student number:	5609828	
Project duration:	December 1, 2023 – June 27, 2024	
Thesis committee:	Dr. Clementine Boutry,	TU Delft, supervisor
	Dr. Massimo Mastrangeli,	TU Delft
	Dr. G.A. (Georgy) Filonenko,	TU Delft
	Elena Aprea,	TU Delft, Daily supervisor

This thesis is confidential and cannot be made public until December 31, 2024.

Acknowledgement

The completion of this Master's thesis has been a wonderful journey, and it would not have been possible without the support, guidance, and encouragement of many individuals. I am deeply grateful to all who have contributed to this work and my development as a researcher.

First and foremost, I would like to express my gratitude towards Dr. Clementine Boutry, for her continuous support and insightful guidance throughout this project. She provided me with the opportunity to undertake this extremely educative project, with extensive practical experience. I am thankful for the received degree of autonomy and always positive and clear directions. I also express sincere appreciation to my thesis committee members Dr. Massimo Mastrangeli and Dr. Georgy Filonenko their invested time and insights.

Special thanks goes to Elena Aprea, my daily supervisor, for her unconditional support and constant feedback. Her guidance was crucial in navigating the challenges faced during this project. Her valuable insights significantly contributed to the progress and successfully completion of my thesis.

This project wouldn't be a success without the interdisciplinary nature, facilitated by collaborations with Dr.Femke de Vrij, Dr. Valeria Orlova, Mark van der Kroeg, and Dr. Marc Vila Cuenca. Their valuable input and feedback provided a successful collaboration between three institutions. I would also like to thank NOCI and hDMT. Their investment in scientific research and development has been crucial for this project.

Special thanks go to Mascha Slingerland, Hande Aydogmus, Dr. Stephen Eustace and Sebastian Couweleers for their guidance throughout this project. Their technical expertise and willingness to assist have been invaluable.

I would also like to express my gratitude to the ECTM community with the Biodegradable- and Organ-on-a-Chip groups in particular. Thanks for the joyful times and positivity during our weekly meetings. The constructive feedback and encouraging atmosphere provided were invaluable to create a collaborative and productive research environment.

Maarten Lemmens
Delft, June 2024

Summary

Organ-on-a-chip (OoC) technology has revolutionized the biomedical research field by offering dynamic platforms which accurately mimic physiological environments of human tissue. This technology has become a promising option to study human biology *in vitro*, including disease modeling, drug screening and personalized medicine. Organoids, 3D cell cultures derived from human stem cells, represent a promising tool to investigate 3D tissue growth *in vitro*. However, integration of vasculature in these organoids remains a significant challenge. Establishment of vasculature is essential to enable significant organoid growth, allowing nutrient and oxygen supply and waste removal.

This report aims to develop a Pluronic F127 based hydrogel as a transient barrier in an OoC-platform that combines cell cultures of Vasculature-on-a-Chip and cortical brain organoids. This transient barrier separates the two cell cultures until sufficient maturation of the cortical organoid. Due to thermoreversible gelation, the Pluronic F127 hydrogel barrier can be removed from the barrier channel by a decrease in temperature. Pluronic F127 and di-acrylated Pluronic F127 hydrogels were synthesizes and characterized using rheometry, differential scanning calorimetry and degradation testing to determine the optimal Pluronic F127 hydrogel. Simultaneously, optimization of the OoC-platform was done by fabrication of the platform using Polydimethylsiloxane (PDMS).

It was shown that the OoC platform for Vascularized Organoids-on-a-Chip could effectively by fabricated using PDMS molding. This was achieved through both PDMS-PDMS and PDMS-glass bonding. Pluronic F127 hydrogels were shown to be a viable option to function as a transient barrier for Vascularized Organoids-on-a-Chip. Pluronic F127 hydrogels effectively blocked fluid flow through the barrier channel for seven days. To increase this time, di-acrylated Pluronic F127 was synthesizes. A degree of acrylation of 57% was achieved. This was shown to be insufficient to significantly increase the longevity of Pluronic F127 hydrogels.

Further research needs to be done to find the optimal synthesis and photo-polymerization conditions of di-acrylated Pluronic F127 hydrogels. Ideally, di-acrylated Pluronic F127 hydrogels exhibit a low degradation rate while maintaining the thermoreversible properties of Pluronic F127 hydrogels.

Contents

List of Figures

List of Tables

Nomenclature

Abbreviations

Abbreviation	Definition
2PP	Two-photon polymerization
AM	Additive manufacturing
APTES	(3-Aminopropyl)triethoxysilane
CDCL3	Deuterated chloroform
DLP	Digital light processing
DoD	Drop-on-demand
DSC	Differential scanning calorimetry
EB	Embryoid bodies
EC	Endothelial cell
EGM-2	Endothelial Cell Growth Medium-2
F127DA	Di-acrylated Pluronic F127
FEP	Fluorinated ethylene propylene
FDM	Fused deposition modeling
hiPSC	Human induced pluripotent stem cell
H-NMR	Hydrogen-nuclear magnetic resonance
HUVEC	Human umbilical vein endothelial cell
i3DP	Inkjet printing
IPA	Isopropylalcohol
OoC	Organ-on-a-Chip
PBS	Phosphate buffered saline
PDMS	Polydimethylsiloxane
PEEK	Polyether Ether Ketone
PEO	Polyoxyethylene
PET	Poly(ethylene terephthalate)
PMMA	Poly(methyl methacrylate)
POMaC	Poly(octamethylene maleate (anhydride) citrate)
PPO	Polyoxypropylene
Pt	Platinum
RPM	Revolutions-per-minute
SLA	Stereolithography
UV	Ultaviolet
VEGF	vascular endothelial growth factor
VoC	Vasculature-on-a-Chip
VSMC	Vascular smooth muscle cell

1

Introduction

Traditional *in vitro* two-dimensional cell cultures lack to accurately simulate the complex living environment of cells *in vivo*. Simultaneously, *in vivo* monitoring in humans is the least accessible method for direct physiological investigation, while animal models lack to reliably resemble human physiology [1]. Therefore, development of models that accurately simulate the human physiology is important. Organ-on-a-chip models are a promising solution. These models offer the ability to finely manipulate the cell environment to resemble human physiology [2].During development of Organ-on-a-chip models, it is important to consider the anatomical structures and environment of the target organ. Through this way, Organ-on-a-chip model can accurately resemble the target organ, by adjusted to mechanical an biochemical environment accordingly [3].

Recent years have seen an advancement in development of organoids and organoids-on-a-chip [3]. Organoids are three dimensional self-organizing cell cultures of a specific organ or tissue derived from human cells. Organoids can accurately resemble the morphology and function of their respective organ [4]. In particular, cortical organoids have shown to provide an opportunity to model human brain development and function. Something which is often inaccessible for direct experimentation [5]. However, the main limitation of achieving completely functional organoid it the lack or rational tissue size [3]. The lack of oxygen and nutrient supply it considered the major cause of cell death in organoids. Therefore, perfusion of vascularization in organoid is required for further development.

A major complication to achieve vascularization within organoids is the inherently different culturing approach of both cell cultures. Blood vessels in the human body are exposed to pulsating blood flow, causing substantial shear stresses on endothelial cells [6]. This shear stress is required for the growth of blood vessels. Simultaneously, cortical organoids are fragile cell cultures requiring a static environment. To allow both cell cultures to be grown simultaneously, the Organ-on-a-chip platform should comply with the requirements of both cell cultures. Therefore, an Organ-on-a-chip platform designed with a barrier in between both cell cultures can be utilized [7].

Pluronic F127 is a promising option to be used as a transient barrier between both cell cultures. Pluronic F127 molecules dissolved in water can form stable and transparent hydrogels, if both temperature and concentration are high enough [8]. These hydrogels exhibit thermoreversible properties allowing them to become liquid when the temperature is lowered. This work focused on the development of biocompatible Organ-on-a-chip platforms and the characterization and integration of conventional- and di-acrylated Pluronic F127 hydrogels in Organoid-on-a-chip platforms.

In this report, first the current state of the art of the fabrication and materials of organ-on-a-chip platforms will be discussed. This is concluded with a comparison of the advantages and disadvantages of each fabrication method. Protocol of cortical organoid- and vasculature growth will be discussed afterwards. The state of the art chapter is finalized with a discussion on Pluronic F127 hydrogels. The methods and materials chapter precisely shows the conducted experiments, including the characterization of the hydrogels and fabrication of the organ-on-a-chip platform. This chapter is followed by the results of those experiments and an outlook section for future studies. Finally, the results are discussed and recommendations for further research are proposed before the report is concluded.

2

State of the Art

2.1. Organ-on-a-Chip

Organ-on-a-Chip (OoC) is a scientific and technological development which couples biology to microtechnology to mimic aspects of human physiology [1]. OoC platforms utilize microfluidic channels to manipulate the microenvironment. These microfluidic platforms are designed in a precise manner so that cells behave similarly as they would in human organs. Although these platforms are much simpler than human organs, it is believed that OoC devices can accurately mimic the human physiological environment due to accurate control of the microenvironment. *In vivo* models still exceed engineered tissue approaches [9]. However, *in vivo* physiological processes are the least accessible method for direct investigation despite recent advances in *in vivo* imaging [1]. On the other hand, 2D and 3D cell cultures, sacrifice in many aspects to *in vivo* relevance. OoC can be seen as a bridge between these two technologies. It offers the ability to work with complex cell cultures, while being able to manipulate the environment by precisely tuning parameters, such as concentration gradients, shear force and tissue-boundaries, to determine cell-cell interaction and chemical- and electrical signaling [10, 11, 12].

Why is OoC needed? OoC technology is driven by a need to better understand human physiology underlying health and disease [1]. This opens a pathway to find new approaches to improves human conditions, which is especially needed in the pharmaceutical industry. OoC can drastically accelerate the development process of drugs. Simultaneously, cosmetics, food and chemical industries can benefit form OoC technologies as an alternative for *in vivo* testing. Moreover, since 2D cell cultures fail to accurately simulate physiological conditions, animal models are often required for proper verification. However, due to differences in species between humans and animals, animal models are often poor predictors of human physiology [13]. Besides, both *in vivo* models and 2D cell cultures fail to accurately represent the pathophysiology of neurodegenerative diseases such as Alzheimer's disease [14]. Simultaneously, high costs and ethical issues form barriers for *in vivo* animal models. OoC might function as a suitable alternative for *in vivo* testing models.

What are the applications of OoC? OoC technologies can by applicable for multiple different applications, for which they are often specifically developed. Some of the most promising applications of OoC devices are listed below.

- **Testing of pharmaceutical and chemical compounds:** OoC technologies have mainly focused on drug development. The majority of drugs fail at a late stage of development. The ability to test drugs for efficacy and toxicity in pre-clinical trials is therefore a huge advantage for pharmaceutical companies [1]. OoC technologies can be used to in pre-clinical and clinical trials. However, OoC models would become more complex in later stages of development. Where initial stages require simpler and highly focused systems, later stages would require multi-organ models to completely predict physiological effects. Multi-organ models have the potential to provide this information in pre-clinical studies [15].

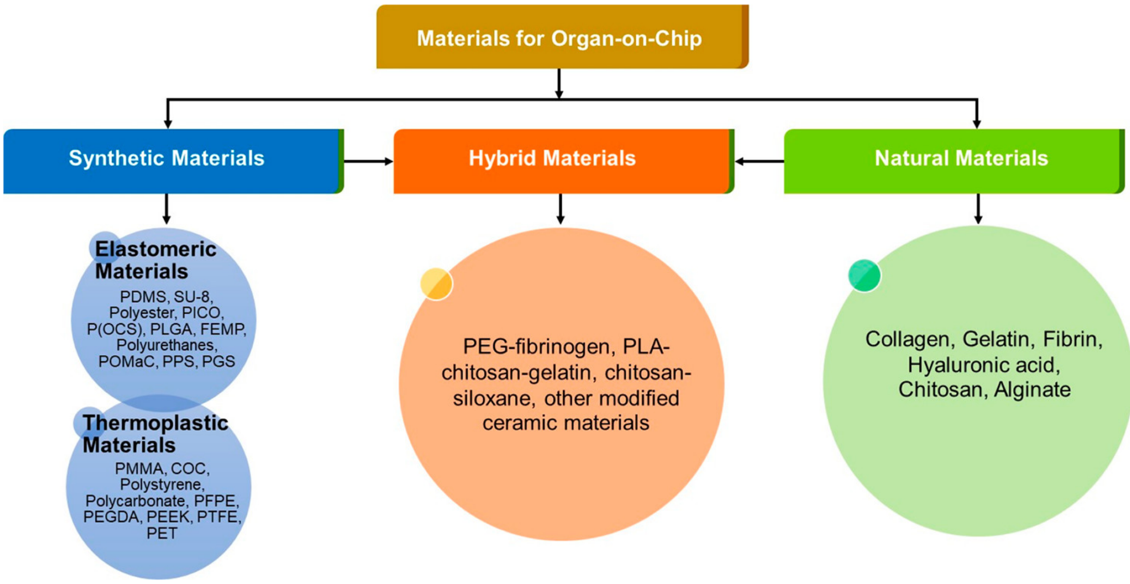

Figure 2.1: Classification of used materials for Organ-on-a-Chip platforms [19].

- **Testing of biomaterials:** Many surgical- and medical devices and medical implants rely on the usage of biomaterials [1]. Biomaterials are matter, substances, constructs or surfaces which are designed to interact with biological systems [16]. OoC models can be used to determine the biocompatibility of these biomaterials in and environment which represents the organs or tissue for which the biomaterial is used [1]. To test biomaterials in OoC platforms, biomaterials require miniaturization. Moreover, the miniaturized sample should also be representative for the situation of the full scale model in the human body. By actively controlling the microenvironment, systematic studies can be done to test for specific properties of the biomaterial. These properties might influence cell- or tissue behavior, such as adhesion, proliferation and differentiation [1].
- **Disease modeling:** OoC technologies allow for modeling of diseases in a human environment. Currently, most disease modeling is done using animal models. However, animal physiology can differ substantial from human physiology. This can severely inhibit the utility of these models. In OoC technologies, human specific environments can be created to study human diseases [1]. Moreover, by incorporating patient specific derived stem cells in the OoC platform, genetic factors can be integrated in the specific disease modeling. Moreover, disease modeling on OoC platforms can become extremely valuable for the pharmaceutical compound testing for rare disease. Especially since these diseases often lack proper clinical trials due to the absence of patients [1].
- **Mimicking cell environment:** OoC technologies are widely used to mimic and manipulate environmental factors to determine the effect on cell phenotype and function. Moreover, biochemical and mechanical factors can be closely controlled in OoC technologies. This allow for systematic testing of the effects of each factor on human physiology, which in turn increase the understanding thereof [1].
- **Personalized medicine:** OoC technologies could also be used in personalized medicine. By implementing patient specific cells in the OoC platform, it will reflect on the individual physiology of the patient. This creates new possibilities to test for patient-specific pharmaceutical efficacy and toxicity and customized treatment methods [17].

2.2. Typical Materials used in Organ-on-a-Chip Platforms

Choosing a suitable material is of vital importance for the fabrication of an efficient OoC platform [18]. The chosen material influences different aspects of the OoC platform, including the performance, visualization and experimental results. Important parameters to consider when choosing a material include the transparency, gas permeability, biocompatibility and costs. Different materials used in the fabrication of OoC platforms are shown in Fig. 2.1.

2.2.1. Elastomeric Materials

Elastomers are widely used in the fabrication of microfluidic development, due to their ease of fabrication and low cost. Elastomers consist of cross-linked polymeric chains which can be stretched or compressed under applied forces. Polydimethylsiloxane (PDMS) is the most widely used type of elastomer for OoC fabrication, due to its low cost, availability, transparency, elasticity, biocompatibility and gas permeability [19]. In the context of this work, it is important to notice that PDMS based OoC platforms have been shown to be biocompatible with vascularization and brain organoids [20, 21]. However, OoC platforms made from PDMS also have several drawbacks. First, PDMS can have an influence on the concentration of soluble factors in growth media due to absorption of small molecules [22]. Second, cured PDMS can still have remaining uncured oligomers which can leach into surrounding solutions and penetrate the membranes of cells [23]. Last, due to unstable surface properties, PDMS channels can swell under exposure of some organic solvents, which causes changes in dimension and surface properties [19].

Alternative elastomeric materials which can be used for the fabrication of OoC platforms include SU-8 polymers, poly(octamethylene maleate (anhydride) citrate) (POMaC), polyesters, polyurethane and propylene [19]. Depending on the application of the OoC platform, one material is more suitable than the other. SU-8 polymers and polyesters cane be optically transparent, while POMaC is biodegradable [19, 24].

2.2.2. Thermoplastic Materials

Thermoplastic materials can be molded after elevation of temperature. This trait allows thermoplastic materials to be suitable for mass-productions. Moreover, many thermoplastic materials are optically transparent, inexpensive and biocompatible, making them and interesting choice for the fabrication of OoC platforms [19]. A widely used thermoplastic materials is poly(methyl methacrylate) (PMMA). PMMA is a biocompatible, transparent polymer with good gas permeability and solvent resistance. Other frequently used thermoplastic materials include polystyrene, polycarbonate, polyether Ether Ketone (PEEK) and poly(ethylene terephthalate) (PET) [19]. In the context of this work, it is important to discuss thermoplastic materials used in additive manufacturing such as liquid resins.

2.2.2.1. Polyacrylate Resins

Thermoplastic can be provided in the form of liquid resins. After polymerization, these materials take the form of hard plastics and behave as thermoplastics. Frequently used resin materials include acrylate- and methacrylate based resins [25]. Polymerization converts single monomers into stable polymers through a reaction activated by heat, light or chemical activators [26]. Due to the nature of polymerization, OoC platforms made of polyacrylate resins can be fabricated using additive manufacturing techniques. This allows for a wide variation of biomedical applications and rapid prototyping. The obtained hardened polymers can exhibit high optical transparency, cytocompatibility and resolution [27].

However, manufacturing OoC platforms from polyacrylate resins can have several drawbacks. In the context of OoC platform fabrication, the cytocompatibility is of particular interest. This has proven to be challenging as the used resins commonly comprise toxic monomers, such as acrylates, methacrylates or urethanes [27]. The conversion from monomers to polymers in these resins is never complete, which results in residual monomers or other toxic products such as methyl methacrylate or methacrylic acid [28]. 3D-printed devices cured by light were found to contain levels of residual monomers. Especially if these resins are not properly cured they can be highly toxic. If these resins are overcured, the mechanical performance can be affected. In some common 3D printing resins, toxicity has been recorded even after post-processing in their fully cured states [29].

2.2.3. Natural Material

Natural materials are better suited to provide a representative environment for cells to develop, migrate and proliferate compared to previously mentioned materials. Hydrogels made of commonly found materials in nature can be used as tissue scaffolds. These materials include collagen, gelatin, chitosan and fibrin [19]. Collagen is the most abundant protein found in the human body. It can be used to provide support to tissue and closely resemble the extracellular matrix [18]. In combination with other chemical cross-linking agents, the stability and mechanical properties of hydrogels containing collagen can be improved to make them suitable for OoC applications. Simultaneously, gelatin is a biocompatible and biodegradable polymer. It can be used as matrix and stabilizer for implanted materials [19]. Despite many attractive properties, hydrogels with natural materials are not widely used for the manufacturing of microfluidic devices because of their low stiffness and difficulties with microfabrication [18, 30].

2.2.4. Inorganic Materials

Inorganic materials used in OoC fabrication mainly include glass and silicon. They are favored because of their surface stability, variability, heat conductivity and solvent comparability [19]. Silicon was the first material used in microfluidics. Silicon is especially suited for many microfabrication techniques including etching, laser processing and bonding. Moreover, silicon has well suited mechanical properties and is relatively inexpensive [18]. Glass is also often used because of its optical transparency and high resistance towards chemicals and mechanical stress [19]. However, glass suffers from low gas-permeability, which is required for growth of cell cultures. Glass is suitable for the fabrication of microfluidic devices as it can be used in photolithography, wet etching and laser cutting [18, 31].

2.3. Fabrication Methods for Organ-on-a-Chip Platforms

Multiple different fabrication methods have been established for the manufacturing of OoC platforms. Additive manufacturing processes capable of fabrication structures ranging from several microns to multiple centimeters are starting to challenge soft lithography as a prototyping approach for microfluidic fabrication [32]. Different manufacturing approach have their respective advantages and disadvantages. Choosing the optimal fabrication method depends on the required resolutions and desired materials. Below, several approaches for the manufacturing of microfluidic devices are discussed, including additive manufacturing, soft lithography and injection molding.

2.3.1. Additive Manufacturing

Additive manufacturing (AM) technologies allow for the creation of fast, high-resolution and low cost fabrication of microscale devices [33]. Additive manufacturing refers to the fabrication of parts using a layer-by-layer fabrication technique [18]. Several techniques are discussed below, including Inkjet printing, Fused deposition modeling, stereolithography and two-photon polymerization. AM allows for rapid prototyping of microfluidic devices, making it a suitable method for the fabrication of microfluidic devices for Organ-on-a-Chip applications.

2.3.1.1. Inkjet Printing (i3DP)

Inkjet printing (i3DP) is based on a technology which operates in continuous or drop-on-demand (DoD) mode. Continues mode is used for lower viscosity ink. However, for the fabrication of microfluidics, DoD mode is used as this generates smaller droplets with higher placement accuracy [32, 34]. A pulse is generated either thermally or piezoelectrically. Thermal pulse generation is performed through localized heating to form vaporized bubbles which eject as ink droplets. Piezoelectric materials generate pulses through deformation of piezoelectric elements, which push droplets out of the nozzle.

i3DP can be divided between powder-based and photopolymer-based printing. Powder-based printing is based on a bed of solid powder particles, which are bonded with adhesive solution supplied through the inkjet printer nozzle (Fig. 2.2A) [32]. A layer of powder is deposited in the build chamber and spread using a roller. The printer nozzle provides droplets of adhesive materials on the target areas, after which these areas are cured. If a layer is complete, an additional powder layer is placed and the process repeats. All the uncured powder serves as support for the printed part and can be reused later. The powder size (50 - 100 µm), shape and density determines the resolution of the printer [32].
Photopolymer-based inkjet printing deposit tiny drops of build material to form the desired object. After the droplets are deposited on the desired place, they are cured using UV light. Using multiple nozzles, up to 14 different materials can be printed simultaneously. This allows for a wide range of materials, properties and colors in a single build.

Theoretically, i3DP can be used to print microfluidics with high resolution. However, in reality this high resolutions are not reached. Therefore, i3DP printing can be used to print microfluidics with microchan-

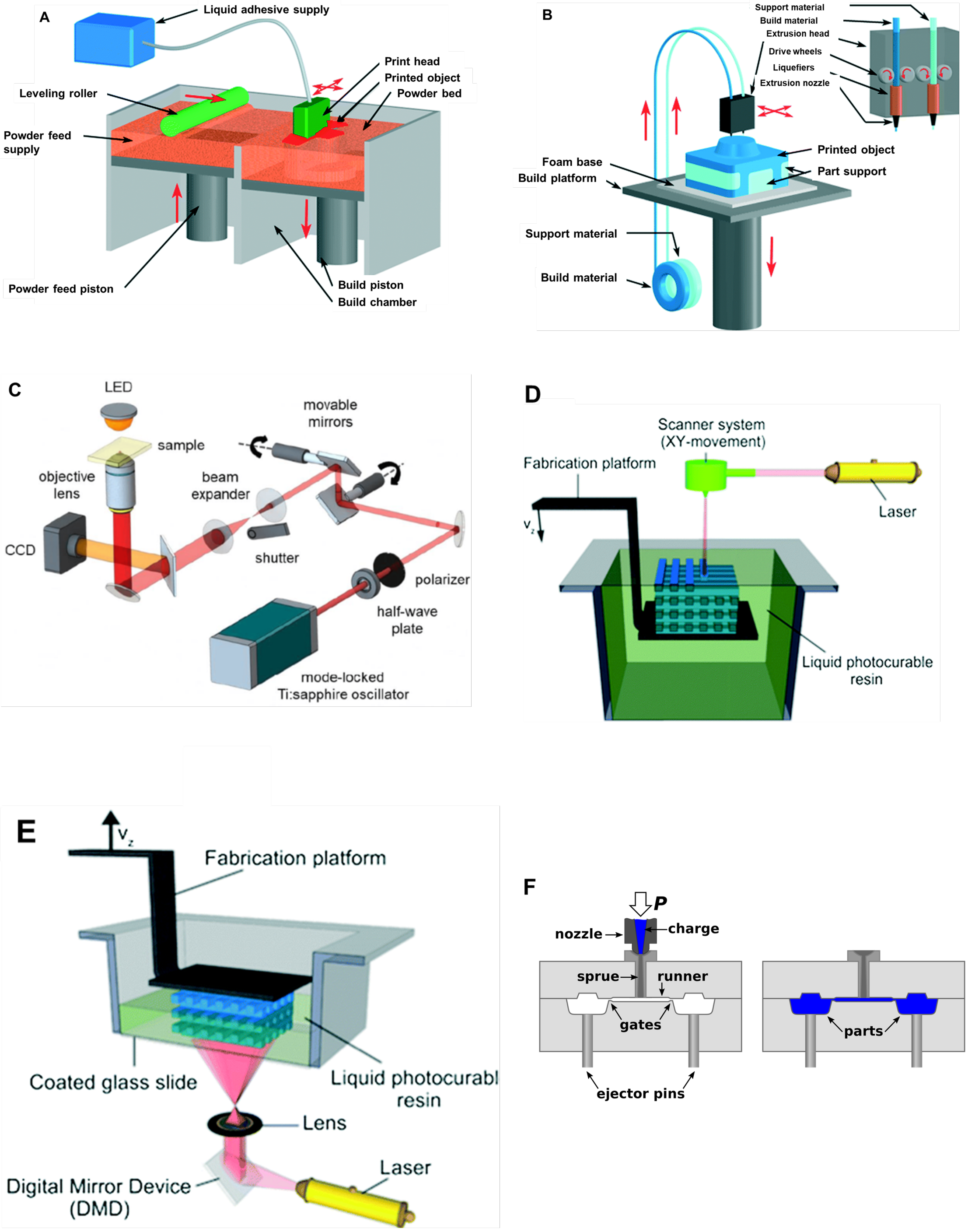

Figure 2.2: Different approaches for the fabrication of microfluidic devices. (A) Inkjet printing. The powder is spread evenly across the surface by the roller. Photopolymerizable ink is deposited on the powder at the desired place to bind the particles together. Excess powder functions as support to the printed object. (B) Fused deposition modeling. Thermoplastics are provided as a filament into the extrusion head. The materials is heated and extruded on the desired place, after which the material solidifies. (C) Two-photon polymerization. The femtosecond laser is focused by a lens and precisely controlled by a computer. The laser polymerizes the structure from the bottom of the resin. (D) Stereolithography: laser-scanning SL. The laser polymerizes a 2D layer from the top, after which the platform is lowered and a new layer can be build. (E) Digital light projector. The digital mirror devices focuses the laser to print a complete layer simultaneously. Afterwards, the platform rises and a new layer is build (F) Injection molding. A two part mold is connected together, after which the liquified material is injected. The material solidifies and is released from the mold[18, 32].

nels greater than 400 μm. The greatest advantage of i3DP printing is the ability to print highly complex build with multiple different materials [32].

2.3.1.2. Fused Deposition Modeling (FDM)

Fused deposition modeling (FDM) is one of the most widely used 3D printing technologies. The technology is based on the extrusion of thermoplastics through a high temperature nozzle [35]. The temperature can be controlled at the nozzle. To print thermoplastics or elastomers, the temperature is increased just above its melting point to let the material flow through the nozzle. After the melted material is deposited on the targeted area, it immediately solidifies. After a full layer is complete, the build platform is lowered and the whole process is repeated. The layer thickness and accuracy is based on the diameter of the nozzle. A visualization of FDM is shown in Fig. 2.2B.

FDM can be used for almost all types of thermoplastics and elastomers, which are also used in mass production techniques such as hot embossing or injection molding [32]. Additionally, several composite materials such as polymer composites can also be printed with FDM [36].

FDM is a cheap, easy to use and reliable 3D printing option. Moreover, due to the nature of printing, hardly any post-processing is required (besides support removal). However, the dimensional accuracy and surface finish is relatively poor for FDM 3D printing. Due to the layer by layer deposition, a staircase-like surface can be created, resulting in a rough surface. Moreover, the achievable dimensions are large compared to other additive manufacturing technologies such as stereolithography or i3DP [32].

2.3.1.3. Two-Photon Polymerization (2PP)

Two-photon polymerization (2PP) is based on curing of a photocurable resin with a near-infrared femtosecond laser. The main difference of 2PP and SLA is the usage of two photons simultaneously in 2PP, compared to a single photon in SLA. The focused laser scans the photosensitive resin from the bottom. Two photons are simultaneously absorbed by the molecules in the resin. This induces a photochemical reaction between the photo-initiator and cross-linking monomers [37]. After fabrication, the complete sample is immersed in a development solvent to remove unpolymerized materials [38]. A visualization of 2PP is shown in Fig. 2.2C. 2PP techniques are able to achieve a reproducible resolution of tens of nanometers [32]. The materials used in 2PP are similar to those used in conventional lithography (discussed later). Both negative and positive photoresists can be used. In negative photoresists, exposure to the photons results in cross-linking of the monomer chains. This makes the exposed areas insoluble in a development solvent. In positive photoresists, exposure to photons causes the polymeric chains to break, resulting in a soluble material, which can be removed with a development solvent.

2PP offers a high spatial resolution (below 100 nm), which the highest possible resolution at the moment of writing [32]. Similar to SLA, a wide range of materials can be used and post-processing is required to remove any uncured material. However, 2PP is an extremely time consuming process and expensive methods. Moreover, multimaterial printing is difficult to achieve. Thus, although 2PP offers the highest resolution of all 3D printing methods, its not considered to be the best fabrication method for microfluidic structures [32].

2.3.1.4. Stereolithography (SLA)

Stereolithography (SLA) is a 3D printing technique based on the polymerization of liquid curable materials using lasers. SLA can be divided into two different configurations: Laser-scanning stereolithography and digital light processing (DLP) (Fig. 2.2D & E) [32]. Laser-scanning SLA is the conventional setup for SLA. It polymerizes a photocurable resin using a ultraviolet (UV) laser which moves along a 2D surface. After completion of a full 2D layer, the substrate is lowered and the laser starts the polymerization of the next layer on top of the previous one. In between each layer, the surface is leveled to ensure a uniform layer. In laser-scanning SLA, the dimension of the print are restricted to the size of the bath and printer head. Moreover, the resin is prone to chemical reactions with surrounding air and waste products during polymerization [32].

In DLP 3D printing, the movable substrate is lowered in the resin bath and the print is created hanging from the substrate. The laser is located underneath the resin bath, which therefore requires a clear and transparent bottom and an anti-adhesive layer to prevent the print from sticking to the bottom. DLP utilizes a digital mirror device. This allows DLP to print a complete layer of resin material simultaneously [32]. Compared to laser-scanning SLA, this significantly reduces printing time, as the printing time is not dependent on the 2D size of the print [39]. Moreover, the printed layers are printed between the previous layer and the bottom of the resin bath, which allows the resin bath to be filled with a minimal amount of resin material. This also prevents exposure to the atmosphere, which limits oxygen inhibition in printed layers. To due to printing configuration, the printed part is limited to the size of the printer head and the allowed height of the printer head [40].

SLA printers offer a balance between performance, price and resolution [32]. The maximum resolution of the print is based on the printer and the resin of choice. Multiple printers are able to printer structures below 100 µm. Besides the required resolution, another issue with SLA printing of microfluidics is the removal of uncured resin. Low viscosity fluids are required to be able to be removed from the printed microchannels. Moreover, SLA printers are limited to the printed material in the resin bath. This prevents SLA printers to create prints with multiple materials simultaneously.

2.3.2. Injection Molding

Injection molding is a mass fabrication method which can be used for thermoplastics. Molds are divided into two parts which are compressed together. Molten material is injected in the mold and allowed to cool down. After cooling, the fabricated part is released from the mold (Fig. 2.2F). This method is especially useful for the mass production of complicated parts. The cost of high precision fabrication is limited to the master mold [18]. The temperature, pressure and injection rate must be precisely controlled to ensure product quality. A possible downside of this method is that changes cannot be made once the mold is fabricated. In 3D printing, minor changes can be made between individual parts by changing the model provided to the printer. In injection molding, changing the parts requires changing the master mold.

2.3.3. Soft Lithography

Soft lithography is a fabrication method which uses photolithography to produce microfluidic patterns for a wide range of materials, especially elastomers (PDMS) [18]. Photolithography utilizes UV light and photosensitive materials. A substrate material (often silicon wafer) is coated with a layer of photoresist material. A photomask containing the desired pattern is placed over the photoresist-coated substrate. After the substrate is exposed to UV light, the exposed area of the photoresist can be removed with a developing solution. The resulting patterned photoresist serves as a master for further fabrication. Subsequently, soft materials (often PDMS) can be poured on top of the obtained micro-patterned substrate. After the layer of PDMS is fully cured, the substrate material can be removed and the PDMS layer with the desired microfluidic pattern can be bonded to glass (or another layer of PDMS) [18, 41]. Alternatively, the master mold of the desired structure can be patterned on a substrate (such as silicon wafers). Poured and cured PDMS serves then as a negative mold of the desired structure (replica molding) [41]. This type of PDMS molds serve as a more durable, less fragile and less expensive alternative [42]. The micro-patterned substrate and the mold can be reused multiple times.

Photolithography is able to achieve high resolutions due to advanced lithography techniques. However, this fabrication process requires advanced materials such as photomasks, exposure systems and development tools. Moreover, the complete process is often performed in cleanroom facilities. The utilization of replica molding minimizes the usage of these tools and facilities, simplifying the process.

2.3.4. PDMS Molding

Additive manufacturing technologies and soft lithography can also be combined. The fabrication of molds using photolithography required specific facilities and is labor-intensive. Moreover, when molds require variation in channel heights, fabrication using photolithography become increasingly complex, requiring repetition of all steps named in Sec. 2.3.3 for the number of different channel heights [43]. Additive manufacturing is an attractive alternative for the prototyping and fabrication of PDMS molds. 3D printing techniques can be used to produce molds for soft lithography. Especially, SLA and DLP are used because of their high resolution, being able to print with a resolution of 5 µm for the most advanced printers [44].

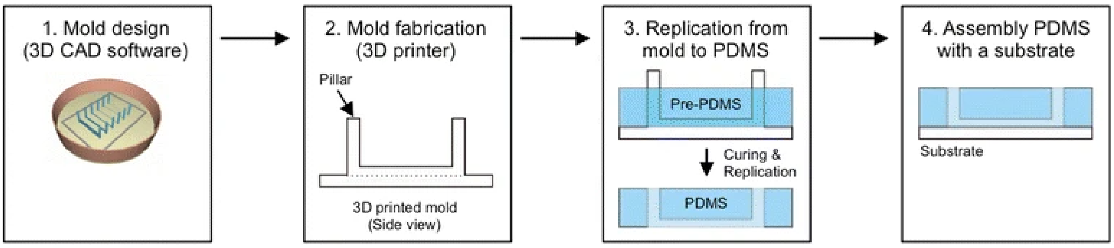

Figure 2.3: PDMS molding procedure. The desired mold is designed using CAD software and printed with a 3D printer. PDMS is poured into the mold and fully cured. The molds can be removed from the cured PDMS. Afterwards, the PDMS can be bonded to a substrate layer to finalize the microfluidic channel [43].

A general flowchart of the protocol of 3D printing molds for rapid prototyping of PDMS microfluidic devices is shown in Fig. 2.3. The mold is first designed in CAD software, after which it is 3D printed. The 3D printed mold can be covered in PDMS. After the PDMS is fully cured, the mold can be removed from the PDMS layer. To enclose the microfluidic channels at the bottom of the PDMS layer, the PDMS layer can be bonded to a substrate layer (often glass or PDMS) [43].

Although 3D printing accelerates the process of fabrication of PDMS microfluidics, it is also limited in some aspects [45]. First, the 3D printed molds are limited by the resolution of the printer. If printers cannot print accurate below 50 µm, the resulting microfluidic channels cannot include smaller dimension than 50 µm. The molds also suffer from surface roughness from the printer head. Although, this can be prevented by design and rotation of the parts. Last, 3D printing is limited in usable materials. Detailed additional information on the PDMS synthesis, PDMS surface activation, PDMS bonding and mold surface treatment is shown in App. A.

2.3.5. Comparative Analysis

The above mentioned fabrication methods all have their respective advantages and drawbacks. Depending on the needs of fabrication, one method is better suited than another. For mass-fabrication of thermoplastics, injection molding would be a suitable options, although this requires significant initial investments. Two-photon polymerization is the most accurate additive manufacturing technique, but is also very slow and expensive. Therefore, this method should only be chosen when extremely small features are required. Fused deposition modeling and inkjet printing can be used for the manufacturing of multi-materials parts and are relatively cheap. Tab. 2.1 lists the advantages and disadvantages of each fabrication method.

However, in this work, stereolithography through digital light processing and PDMS molding will be utilized. DLP offers high resolution and precision, being able to print complex structures below 100 µm. Simultaneously, printing times are low, being able to print complete OoC platforms within hours. Moreover, manufacturing OoC platforms through DLP is easy-to-use as it relies on a single step fabrication. This also makes DLP a perfect fabrication method for prototyping. Changes in geometry or dimensions can quickly be changed in CAD models and prints. Materials used in DLP printing include thermoplastics. For this work, transparent UV curable resins will be used in DLP printing. The surface finish of transparent 3D printed parts with DLP depends on the surface roughness of the printer head. This can be optimized by printing on smooth surfaces, such as glass or steel. Alternatively, additional liquid resin can be applied on the surface of the print and smoothened before curing.

Because of biocompatible properties of PDMS, PDMS molding was also utilized. PDMS allows for the fabrication of flexible, transparent and biocompatible OoC platforms. Simultaneously, easy fabrication allows for the possibility of quick changes in fabrication procedure.

The combination of making PDMS molds with DLP leverages the advantages of both additive manufacturing and PDMS molding. DLP can be used to fabricate detailed molds containing the desired micro-structure of the OoC platform, while PDMS provides the desired biocompatible and mechanical properties.

Table 2.1: Advantages and disadvantages of fabrication methods for OoC platforms

Fabrication method	Advantages	Disadvantages
Inkjet printing	- Multi-material - Low cost	- Extensive post-processing - Low resolution - Limited materials
Fused deposition modeling	- Low cost - Wide range of materials	- Slow - Low resolution
Stereolithography	- High resolution - Low cost - Fast	- Limited materials - Post-processing
Two-photon polymerization	- Very high resolution - Small features	- Slow - Expensive
Injection molding	- High precision - Mass production	- Limited materials - High initial costs
Soft lithography	- High resolution	- Limited materials
PDMS molding	- Flexible - Easy fabrication	- Small-scale - Requires mold fabrication

2.4. Vascularized Organoids-on-a-Chip

Organoids are three dimensional miniature versions of organs or tissue derived from human cells. Organoids can self-organize and differentiate into 3D cell cultures, resembling the morphology and function of their respective organs or tissue [4]. Organoids are widely used as models of disease development and have tremendous potential to be used in regenerative medicine and drug development [46]. The main limitation of achieving completely functional organoids *in vitro* is the lack of rational tissue size [3]. In the human body, most cells cannot survive if they are located further than 200 μm away from any blood vessel. The lack of proper vascularization limits the oxygen and nutrient supply and the removal of waste products [47, 48, 49]. Oxygen and nutrient supply are vital for growth and survival of cells, whereas waste removal is essential for survival as well [3]. However, vascularization can also be of vital importance for signaling pathways and tissue maturation, especially for the brain, which is one of the most densely vascularized organs in the human body, as it receives approximately 20% of all the cardiac output [48].

Currently, the only way to achieve vascularization in generated organoids is through transplantation [3, 46, 50]. When the organoids are transplanted *in vivo*, vascularization resembles that which occurs in the human body. Therefore, organoids will efficiently develop with complete function.

Micro control systems successfully mimic the regulation of tissue micro-environments. It can provide biochemical and mechanical forces to allow for proper vascular network construction [3]. Different microfabrication techniques successfully constructed *in vitro* vascular network models. The different techniques can be categorized in two groups: templating and self-organizing methods [49].

2.4.1. Templating

Templating models are advantageous because they can be immediately used after fabrication. However, due to the nature of templating models, the vasculature cannot dynamically adjust to the environment of the surrounding tissue [49]. Templating methods to obtain vasculature networks include hydrogel (needle) or sacrificial molding, assembly of patterned hydrogels and bioprinting [3, 46, 49].
The molding techniques involve the creation of 3D networks by casting 3D printed polymerized hydrogels around temporary molds or materials. These molds or materials are removed or dissolved, creating a 3D hollow channel network for vascular perfusion [3, 46]. Endothelial cells (EC) can be

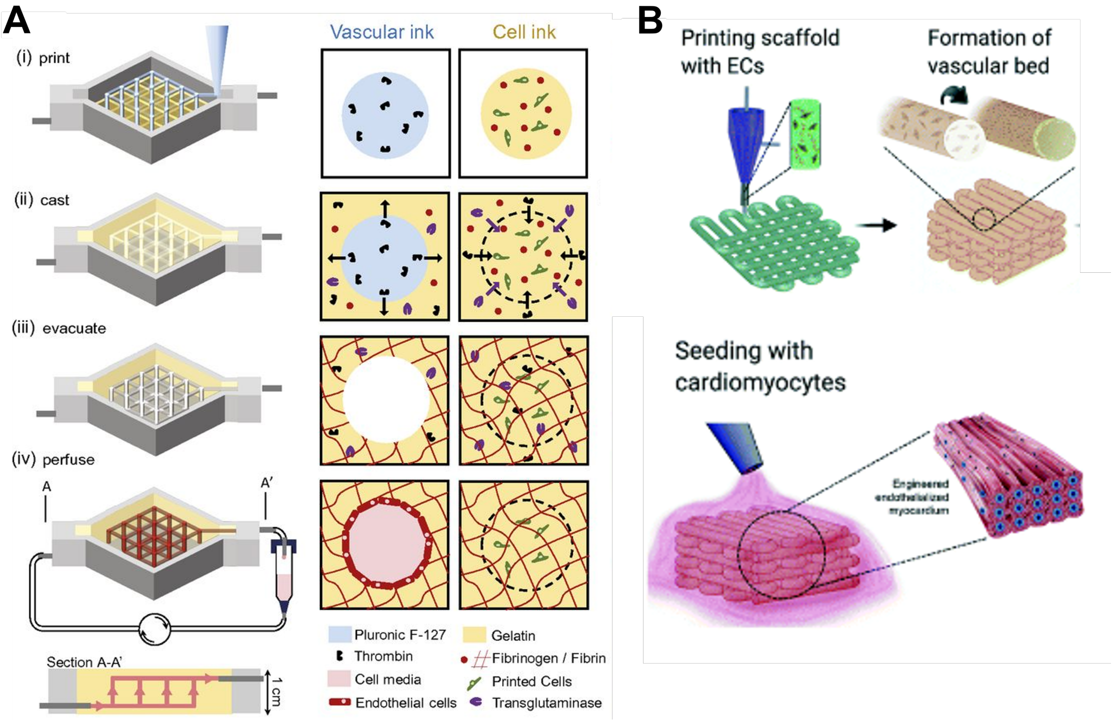

Figure 2.4: (A) Micro-molding of vascularization through simultaneous printing of sacrificial materials (vascular ink) and hydrogel (gelatin) constructs. The sacrificial material are removed later to obtain perfused networks [51]. (B) Vascular structures are fabricated through bioprinting methods by depositing cell-laden bioinks according to a pre-designed pattern. [46].

placed in the walls of these channels to create vascular layers (Fig. 2.4a.)
Vascularization can also be obtained in an additive manner. Through deposition of cell containing hydrogels layer-by-layer. Through printing in pre-designed patterns, using ECs and other required cells and molecules, vascularized tissue can be engineered (Fig.2.4b) [46]. The ECs gradually migrate towards the periphery of the printed microfibers to form an endothelial layer [3]. Printed scaffolds can also be further stabilized by encapsulation of hydrogels or through polymerization.

2.4.2. Self-Organizing

Self-organizing methods allow for spontaneous vascularization and vascular remodeling [49]. This is supported by micropatterning of endothelial cells, the supply of growth factors and co-culturing of supporting cells [49, 52, 53, 54]. Therefore, self-organizing methods better mimic *in vivo* physiological conditions compared to templating methods.
Self-organizing methods promote conditions through which vasculogenesis and angiogenesis can occur [46]. Vasculogenesis occurs in developing embryos to form the earliest form vascularization. *In vitro* models utilize microfluidics seeded with hydrogels containing ECs and other necessary cells and molecules. Hydrogels containing fibrin, fibroblast and ECs can be cultured in a central part of a microfluidic chip. Culture medium can be introduced in parallel placed channels separated by micro-pillars to support the further development of the vasculature [46]. This results in perfused vasculature networks in approximately seven days.
Angiogenesis occurs through the utilization of pre-existing vessels (created through vasculogenesis). Angiogenesis is initiated by the introduction of of ECs seeded in hydrogel layers. The incorporation of such hydrogels in microfluidic chips, allows for migration and lumen formation across the complete gel. To allow for perfusion of organoid, a successful approach includes the seeding of hydrogels with human umbilical vein endothelial cells (HUVECs) in hydrogels on opposite sides of a centrally-located organoid [46, 55]. Sprouting of vasculature from both sides spontaneously results in perfused organoids through angiogenesis (Fig. 2.5).

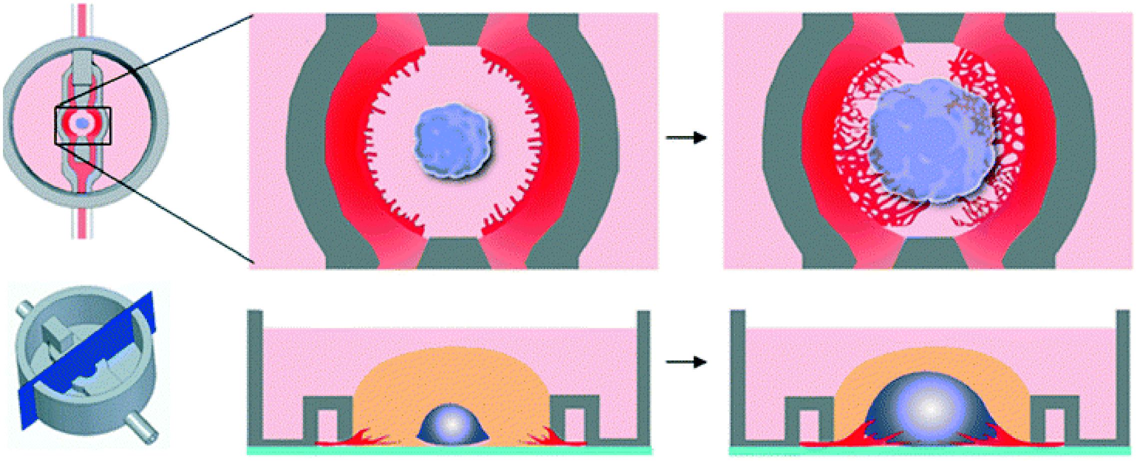

Figure 2.5: (Top) top view and (bottom) side view of angiogenesis in organoids. Hydrogels seeded with HUVECs (red) are located on either side of the organoid (blue). Grown vasculature sprouts from both sides of a centrally-located organoid. Angiogenesis spontaneously occurs in the organoid [55].

2.4.3. Shear Stress

Shear stress forces from fluid flow influence ECs significantly [56]. *In vivo*, ECs are exposed to tangential shear forces on the endothelial surface. This shear stress induces the secretion of biomolecular signals, leading to vascular remodeling and transcriptional gene expression [56]. Furthermore, shear stress has also been shown to increase cell attachment and pathological response [57].

In microfluidic devices, shear stress can be generated using a gradients of growth media in the media channels by applying a difference in pressure on both sides of the channel [56, 57]. This pressure difference can be created by applying a difference in injected volume of growth media on both sides. A gravity induced flow will be created within the micro channel. Within microfluidic devices, other forces such as inertial- and gravitational forces are small. This allows the shear stress to become a dominating factor within the micro-environment [57].

A microfluidic design using micro-pillars increases the shear stress levels. A pillar array is used to allow for communication between hydrogel- and growth media channels, while maintaining a well-defined micro-environment [57]. However, micro-pillars influence the shear stress levels in the micro-channels. First, the addition of microfluidic pillars reduces the channel width. This increase the fluid flow rate in this channel and therefore the shear stress on the periphery. The distance between the micro-pillars should be accurately determined. Small distances (less than 30 μm) provide a homogeneous shear stress, similar to the levels found in continuous channels [57]. Larger distances (more than 150 μm) lead to oscillation in shear stress levels along the channel. Therefore, to create increased shear stress levels in the micro-fluidic channels, pillar arrays are used with a spacing of approximately 100 μm.

2.4.4. Vascularization

The Vasculature-on-a-Chip (VoC) is created by the incorporation of human induced pluripotent stem cells (hiPSC) derived endothelial cells (EC) and vascular smooth muscle cells (VSMC) [58]. These hiPSC are generated from healthy individuals and patients. The hiPSC reflect the genetic background of the individuals from whom they are derived [59]. hiPSCs are human derived stem cells which have been reprogrammed to pluripotent stem cells. Pluripotent stem cells are similar to embryonic stem cells, because they are able to differentiate into different tissue types, depending on the chemical (growth factors) and mechanical (stresses) in their direct environment [60]. The following protocol to generate Vasculature-on-a-Chip is used by Arslan et al. (2023) and is representative for the VoC referred to in this work [61]. The ECs and VSMCs are prepared prior to injection in the OoC platform. The OoC platform used for VoC was a commercially available microfluidic chip (AIM Biotech) with a central gel channel and two media channels on opposite sides. hiPSC-ECs were combined with hiPSC-VSCMs, together with Endothelial Cell Growth Medium-2 (EGM-2) supplemented with thrombin and mixed with fibrinogen. EGM-2 is the cell growth medium necessary to maintain optimal environment and thrombin and fibrinogen are added to promote angiogenesis (formation of new blood vessels) [62, 63]. The

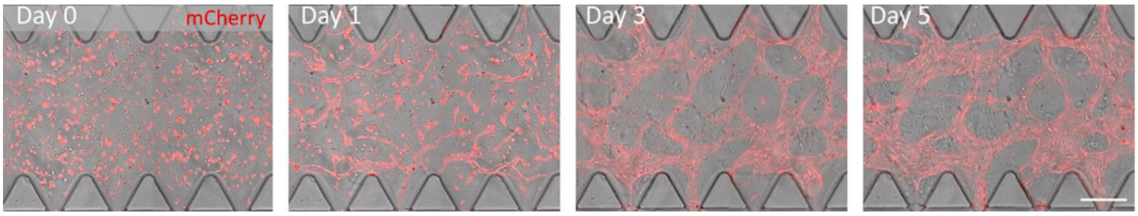

Figure 2.6: A visualization of the vasculature growth on day 0, 1, 3 and 5 on the OoC platform. In this setup, the media channels are located above and below the central channel. After approximately seven days, the vasculature has grown sufficiently and can be used for other applications [61].

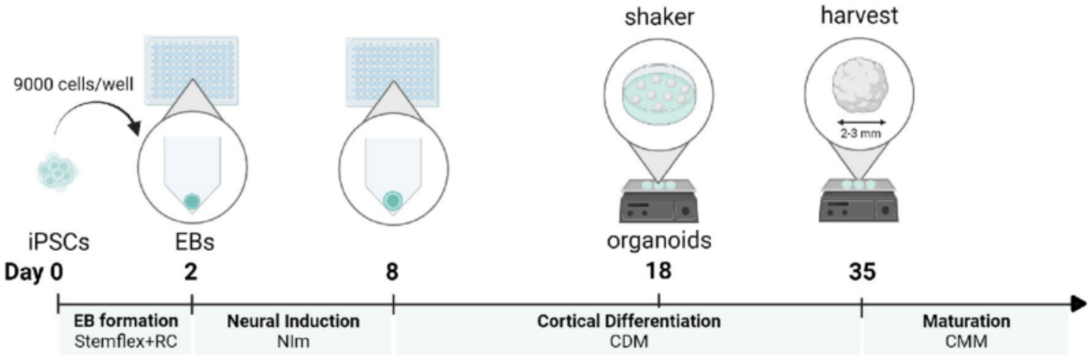

Figure 2.7: A visualization of the protocol for cortical organoids development. hiPSCs are loaded into 384 well-plates in which they form embryoid bodies (EB) in two days. Within six more days, neural induction will stimulate neural tissue growth. After 18 days, the differentiated organoids are transferred to dishes and paced in a shaker. After approximately 35 days, the organoids are fully developed and can be harvested [64].

cell/hydrogel mixture was loaded in the central channel of the OoC platform. EGM-2 supplemented with vascular endothelial growth factor (VEGF) was loaded in the media channels and refreshed daily. A detailed description of the protocol for VoC is described by Arslan et al. (2023) [61].

After approximately seven days, the vasculature has grown sufficiently. Fig. 2.6 shows the growth stages of vasculature on the OoC platform. In this OoC platform the media channels are located above and below the central channel (not shown). These media channels are used to provide growth medium and shear stress. The shear stress is generated by gravity-induced flow. A difference of injected medium volume on each side of the media channels (100 vs 50 µL) caused the medium to flow in the direction of lowest pressure [58]. This gravity-induced flow was re-established every 24 hours due to the media exchange.

2.4.5. Cortical Organoids

The growth of the cortical organoids is also based on hiPSCs. The cortical organoids grow form hiPSCs that self-aggregate into embryoid bodies and spontaneously acquire neuronal fate [64]. In this work, an example protocol for cortical organoids by Eigenhuis et al. (2023) is used. Approximately, 9.000 hiPSCs are seeded on the bottom of 384-well plates to accumulate into embryoid bodies (EB) within two days. Subsequently, using simple growth medium, a robust neural induction will stimulate the generation of neuroectoderm and neuroepithelial tissues within six days, which will develop into specific brain regions. After 18 days, the differentiated organoids are transferred to non-adherent dishes and placed in a shaker. The organoids will further grow until they have a diameter of 2-3 mm [64]. A overview of the cortical organoid growth protocol is shown in Fig. 2.7.

The generation of cortical organoids is a delicate and long process. Moreover, the applied methods have a low reproducibility and are very sensitive [64]. In this protocol, gentle handling of the growing organoid is required to prevent organoid damage. The differentiation medium is refreshed every 2-3 days, which must be done by very slow (4-5 seconds) injection with a pipette. After the organoid has reached a diameter of 2-3 mm and a height of maximally 200 µm, the organoid can be harvested for

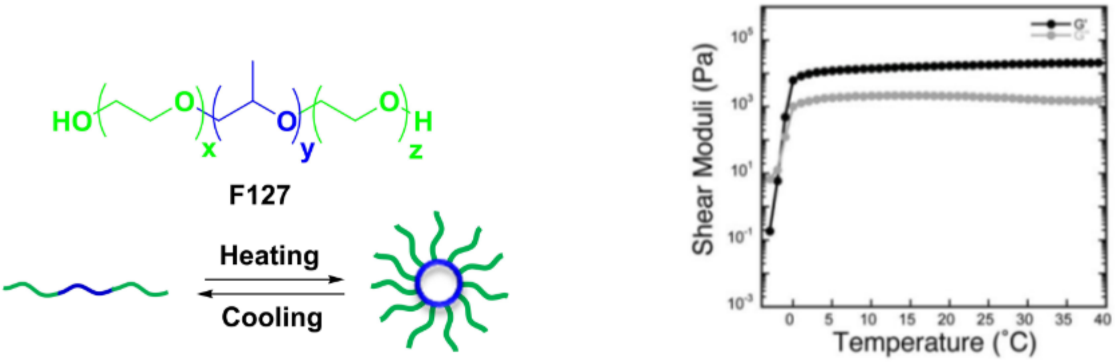

(a)

(b)

Figure 2.8: (a) Gelation principle of Pluronic F127 hydrogels. X = 65, Y = 99, Z = 65. Above the critical micelle temperature and critical micelle concentration, pluronic molecules will form micelle structures with the hydrophobic PPO blocks (blue) in the centre and the hydrophilic PEO blocks (green) at the edge [65]. (b) Gelation of Pluronic F127 hydrogels. When the storage modulus (G') exceeds the loss modulus (G"), Pluronic F127 solutions form hydrogels [66].

further use [64]. At this moment, it is important that the cortical organoids are perfused by vasculature to supply the cells at the inner part of the organoid with oxygen and nutrients. This will stimulate further development of the cortical organoid.

2.4.6. Barrier Requirements

The chemical and mechanical environments of the VoC and brain organoids differ significantly. As mentioned in Sec. 2.4.4, the VoC is grown in a microfluidic OoC platform. The media channels on each side of the central channel provide the needed shear stress and growth media. This creates a dynamic environment, which is refreshed daily. The vasculature growth time is approximately seven days. Meanwhile, the cortical organoids are grown in 384 well-plates, with growth media refreshed every 2-3 days. The environment of the organoids should remain static and calm, while the refreshment of growth media should be performed very gentle. The cortical organoid growth time untill maturation is 35 days.

To accommodate growth of both cell cultures on a single OoC platform, a transient barrier between both cell cultures is required. The transient barrier located in between the vascularized OoC platform and the growing cortical organoid should comply with several important requirements. The environment of the growing organoid should remain calm from the start of growth until vascular perfusion. To maintain this environment, the barrier placed in between should be non-permeable as well as be able to withstand the shear stress to which it is exposed from vascular hydrogel injection. The membrane should also be biocompatible and biodegradable to ensure that both cell cultures remain unharmed by the presence and removal of the barriers and its potential side-products. Moreover, since cell cultures are grown at 37°C to simulate human body environment, the barrier should remain stable at this temperature.

The growth time of both cell cultures and the fabrication of the OoC platform brings additional requirements. Due to geometric constraints of the designated channel, which is pre-fabricated on the OoC platform, the barrier should be injectable in the OoC platform. Additionally, the barrier should be transparent to aid in visualization on the already transparent OoC platform. Because cortical organoids have a growth period of more than 30 days and the vascular perfusion is not allowed to happen before the 35th day, the barrier should remain stable in aqueous environments at 37°C for more than the specified 35 days. After this period, the barrier should be able to be easily removed though, for example, thermoreversibility or chemical activation. Therefore, the barrier should provide a mean to control opening of the channel by external activation.

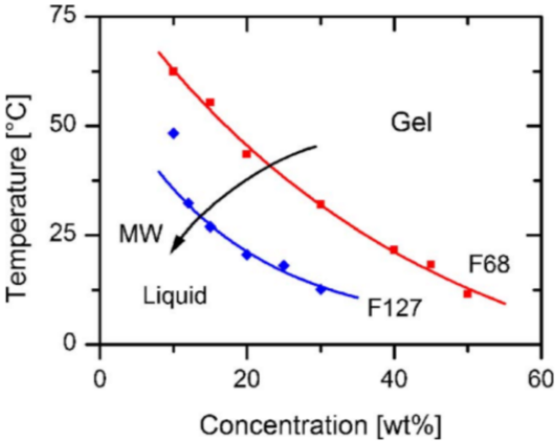

Figure 2.9: The gelation temperatures for Pluronic F127 and F68 hydrogels. The gelation temperatures are concentration dependent [8].

2.5. Material Investigated as a Barrier Between Cells: Pluronic F127

Pluronics are widely used and studied for a number of biomedical applications, including the generation of vasculature on a chip, encapsulation vehicles for drug delivery systems and post-surgery anti adhesion barriers. The most promising application is the usage of Pluronic F127 as sacrificial materials in templated vascularization generation and to form localized temporarily blockages by gel formation [8, 66]. The applications are discussed in the literature review (App. F).

Especially Pluronic F127 is extensively investigated for its application and (together with Pluronic F68) is the only FDA approved type of Pluronic [67]. Pluronics can be considered as a promising barrier option for OoC applications, as it could potentially comply to all above mentioned requirements. Pluronics form hydrogels when dissolved in aqueous media at body temperatures, while they can be easily flushed away at lower temperatures due to its thermoreversible properties [68]. Moreover, Pluronic F127 has many advantages including low toxicity, biologically inert, thermo-reversible properties and ease of use [69].

2.5.1. Properties

Pluronic F127 is a water-soluble, biocompatible poloxamer that consists of polyoxyethylene (PEO) and polyoxypropylene (PPO) with two 99-unit hydrophilic PEO blocks surrounding one 65-unit hydrophobic PPO block [70]. The gelation of Pluronic F127 is based on their amphiphilic structure. The PEO blocks are hydrophilic, while the PPO blocks are hydrophobic, which makes them self-assemble into micelles in aqueous solutions above the CMC and CMT [71]. The gelation principle is shown in Fig. 2.8. Pluronic F127 solutions undergo a phase transition which is both concentration and temperature dependent [68](Fig. 2.9). The sol-gel transition happens above the critical micelle concentration (CMC) and critical micelle temperature (CMT), where Pluronics form micelles, which lead to gelation.

The viscosity of Pluronic F127 hydrogels is dependent on the concentration, where higher concentrations of Pluronic result in a higher viscosity of the hydrogel, both in solvent and gel state[72]. The gelation temperature of Pluronic F127 can be adjusted by manipulating the concentration in deionized water, where a higher concentration results in a lower gelation temperature [73]. The gelation temperature is defined as the temperature when G' (storage modulus) exceeds the G" (loss modulus) (explained later) (Fig. 2.8b) [70].

A major drawback of the usage of Pluronic F127 hydrogels is the fast degradation rate in aqueous media at body temperature [67]. Pluronics are non-degradable materials and can be removed by dissolution in water. This also results in the relatively poor mechanical properties and dissolution in aqueous media which makes Pluronics suffer from a short persistence time *in vivo* [74, 75]. Therefore, chemically modified Pluronic polymers are studied to increase stability and integrity of the hydrogels.

2.5.2. Di-acrylated Pluronic F127

Pluronic F127 can be chemically modified to form terminally di-acrylated Pluronics. Di-acrylated Pluronic F127 was found to be the most suitable chemical modification as it complies to the previously mentioned barrier requirements (Sec. 2.4.6). Di-acrylated Pluronic F127 is chemically modified to contain acrylate terminal ends (instead of hydroxyl groups). This allows them to be photo-polymerized.

Di-acrylated Pluronic F127 (F127DA) hydrogels showed thermoreversible properties before photo-polymerization [76]. This allows the hydrogels to be injected in a liquid sate, form a gel in the micro-channels and be polymerized afterwards to increase stability and lower degradation rates. Fig.2.10a shows the degradation rates of F127 and F127DA hydrogels in Phosphate buffered saline (PBS) at 37°C [76]. It can be seen that normal Pluronic F127 hydrogels degrade completely within ten days. Simultaneously, F127DA hydrogels remain stable significantly longer. The mechanical strength (measured through elastic modulus using rheometry) of hydrogels for different UV cross-linking parameters was also tested. The polymerization of F127DA hydrogels can be modified by alternating photo-polymerization parameters. The strength of these hydrogels increased for higher UV intensities, longer irradiation times and higher concentrations of photo-initiators [76]. While testing for each of these parameters, the other parameters were kept constant. Moreover, lower concentrations of F127DA, required longer irradiation times to form stable polymerized hydrogels. These results suggest that strength, and potentially the degradation rates, of the hydrogels can be modified be adjusting UV irradiation parameters. Additionally, compared to normal Pluronic F127, F127DA has a lower gelation temperature and concentration, caused by the hydrophobic acrylate formation of Pluronic F127 terminal ends [77].

The acrylated end groups of the Pluronic molecules provided cross-linking possibilities between the Pluronic micelles [78]. These hydrogels still showed thermoreversible and biodegradable properties for lower concentrations [77, 79]. Without additional cross-linking monomers, the photo polymerization cross-linked the end cap micelle structures. This created covalent bonding between micelles, which improves mechanical behavior. To allow di-acrylated pluronic F127 to be removed from the barrier channel, it should be possible to wash the complete hydrogel out of the channels. Therefore, when these hydrogels are made through photo-polymerization into stable 3D structures, they can not be removed through thermoreversible properties anymore. This is one of the properties by which Pluronic F127 was chosen as a barrier option. Di Biase et al. (2011) found that di-acrylated pluronic F127 hydrogels could still exhibit thermoreversible properties after photo-polymerization [77]. This was only possible for hydrogels with a concentration below 15 wt% in combination with lower polymerization temperatures (Fig. **??**b). However, since the study from Lee et al. (2007) showed that lower concentration F127DA hydrogels already showed a significant decrease in degradation rates, these hydrogels could be very promising [76]. Therefore, the combined results of the degradation rates of the di-acrylated Pluronic F127 hydrogels and the results of Di Biase et al. (2011) suggest that thermoreversible, slow degrading di-acrylated hydrogels can be made by polymerizing micelle end caps.

Therefore, di-acrylated Pluronic F127 hydrogels are a promising option for the application as a barrier for vascularized organoids on a chip. The di-acrylated Pluronic F127 hydrogels shows slower degradation rates for similar concentrations, compared to conventional Pluronic F127 hydrogels. The mechanical properties of the hydrogels can be adjusted by alternating concentrations and photo-polymerization parameters. An extensive comparison of Pluronic F127 modification and results and applications of di-acrylated Pluronic F127 are shown in the literature review (App. F).

2.5.2.1. Chemical Modification

Di-acrylated Pluronic F127 is synthesized according to well established methods [76, 77, 80]. Dried Pluronic F127 molecules are dissolved in anhydrous methylene chloride. This solvent is used, since the presence of water in the solvent solution causes the Pluronic F127 molecules to form hydrogels due to the principles described in Sec. 2.5. Subsequently, triethylamine and acryloyl chloride are added drop wise under vigorous stirring. When the acryloyl chloride is added, it reacts with the hydroxyl groups at the terminal ends of the Pluronic F127 molecules. This reaction forms ester linkages between the acryloyl groups and the Pluronics. The hydrogen and chloride atoms from the Pluronic F127 and acryloyl chloride respectively form hydrogen chloride (HCl) molecules. Triethylamine is a base which is added as a capturing agent for the formed HCL. These molecules bind to the triethylamine and precipitate out of the solution. The reactions must be kept at a low temperature (below 5°C), while

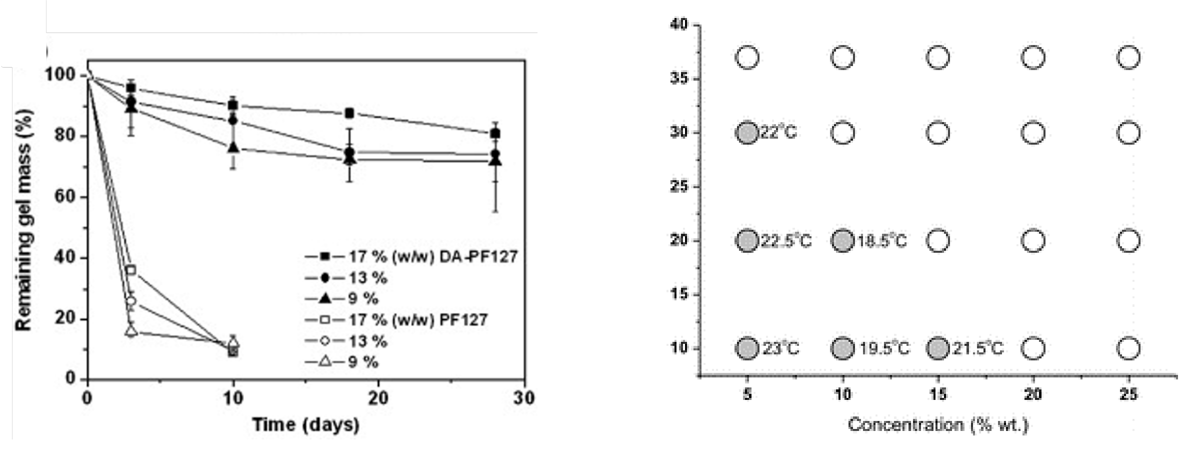

(a) (b)

Figure 2.10: (a) Degradation rates of normal and di-acrylated Pluronic F127 hydrogels with concentrations of 9, 13 and 17 wt% [76]. (b) Di-acrylated Pluronic F127 hydrogels which exhibit thermoreversible properties after photo-polymerization. Lower F127DA concentrations and/or lower polymerization temperatures cause the hydrogels to exhibit thermoreversible behavior [77]

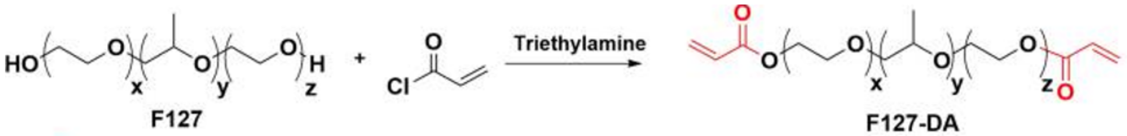

Figure 2.11: Schematic representation of the chemical modification of Pluronic F127 molecules into di-acrylated Pluronic F127. The Pluronic F127 molecules are dissolved in methylene chloride. The Pluronic F127 molecules react with acryloyl chloride and triethylamine to form di-acrylated Pluronic F127 [74].

acryloyl chloride must be added in a controlled and slow manner to prevent overheating of the reactions [81]. The di-acrylated Pluronic F127 molecules are precipitated in anhydrous diethyl ether, filtered and dried. This chemical process results in dried Pluronic F127DA molecules which can be further used. The chemical process is shown in Fig. 2.11.

2.5.3. Characterization: Rheometry

Characterization with rheometry enables the identification of the viscosity and gelation temperatures for hydrogels. Rheometers utilize a rotating plate to determine the rheology of fluids and solids. A parallel plate geometry used in rheometry is shown in Fig. 2.12a. The test sample is placed in between the two plates and squeezed to a pre-defined height.

2.5.3.1. Viscosity

Rheometers can be used to measure the viscosity of samples through rotational tests (Fig. 2.12b). Shear is applied on the sample in between the two plates. The bottom plate is stationary while the upper plate rotates parallel to the bottom plate. The shear stress (τ) is preset and is defined according to Eq. 2.1.

$$\tau = F/A \tag{2.1}$$

Where F is the applied shear force (in N) and A is the shear area on the sample (in m^2). While rotating, the shear rate on the sample is measured. The shear rate ($\dot{\gamma}$) is defined according to Eq. 2.2.

$$\dot{\gamma} = v/h \tag{2.2}$$

Where v is the velocity (in m/s) and h the shear gap (in m). The size of the gap is known, while the velocity is measured as the rotational speed. Based on the applied shear stress and the measured shear rate, the viscosity can be determined. The viscosity (η) is defined according to Eq. 2.3.

$$\eta = \tau/\dot{\gamma} \tag{2.3}$$

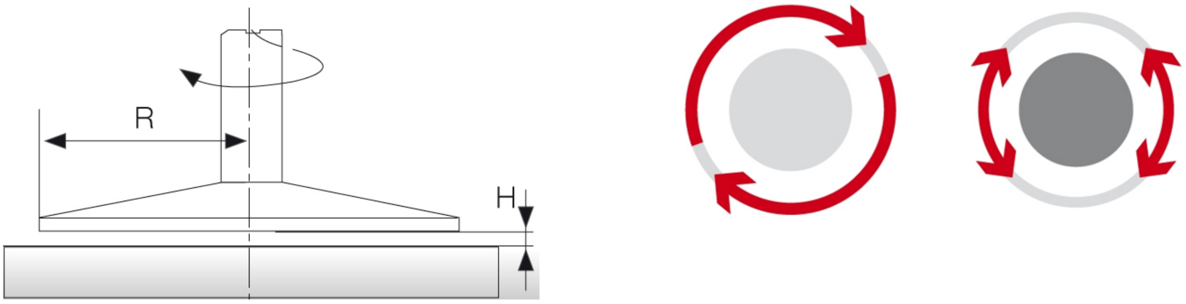

(a) **(b)**

Figure 2.12: (a) The parallel plate gemoetry of the rheometer. R is the radius of the plate (in this case 20 mm), H is the the height between the top and bottom plate (in this case 300 μm)(b) The measuring abilities of the rheometer. Continuous rotational testing (left) and rotational oscillation (right). [82].

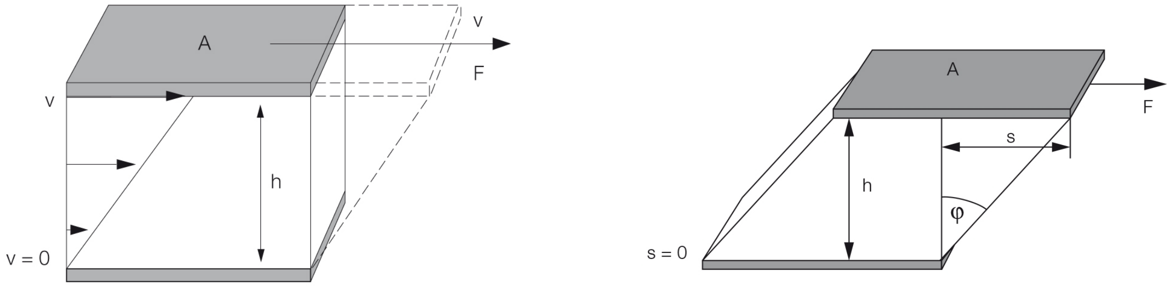

(a) **(b)**

Figure 2.13: (a) Calculation of shear stress and shear rate using the two-plates model with shear area A, gap width h, shear force F, and velocity v. (b) The parameters in oscillatory rheometry, with area (A), shear force (F), gap width (h), deflection paht (s) and deflection angle (δ) [82].

A visualization of all these parameters is shown in Fig. 2.13a.

2.5.3.2. Gelation Temperature

The gelation temperature of the hydrogels could be determined with a oscillatory temperature ramp on the parallel plate geometry. A predetermined shear stress is applied on the top plate as described in Sec. 2.5.3.1. The shear strain on the sample is measured during oscillatory rotation. Shear strain (γ) is defined according to Eq. 2.4.

$$\gamma = s/h \tag{2.4}$$

Were s is the deflection path (in m) and h is the height of the gap (in m). The parameters are shown in Fig. 2.13b .The shear strain is measured on the top plate and will result in a sine curve due to oscillation. Simultaneously, the shear stress (counter force) is measured on the bottom plate. For low strains, the shear stress diagram will also result in a sine curve, with the same frequency as the shear strain sine curve (Fig. 2.14a). For ideally elastic samples, there would be no time delay between these two sine curves. However, for viscoelastic behavior, a phase shift (δ) appears. For ideally elastic materials, this phase shift is zero degrees (δ = 0°). For viscoelastic materials, the material is in a fluid state if the phase shift is between 45° and 90°, with 90° representing ideally viscous flow behaviour [82]. Viscoelastic materials always take place between those maxima.

The complex shear modulus (G^*) describes the viscoelastic behaviour using the phase shift. The complex shear modulus is defined according to Eq. 2.5.

$$G^* = \tau_A/\gamma_A \tag{2.5}$$

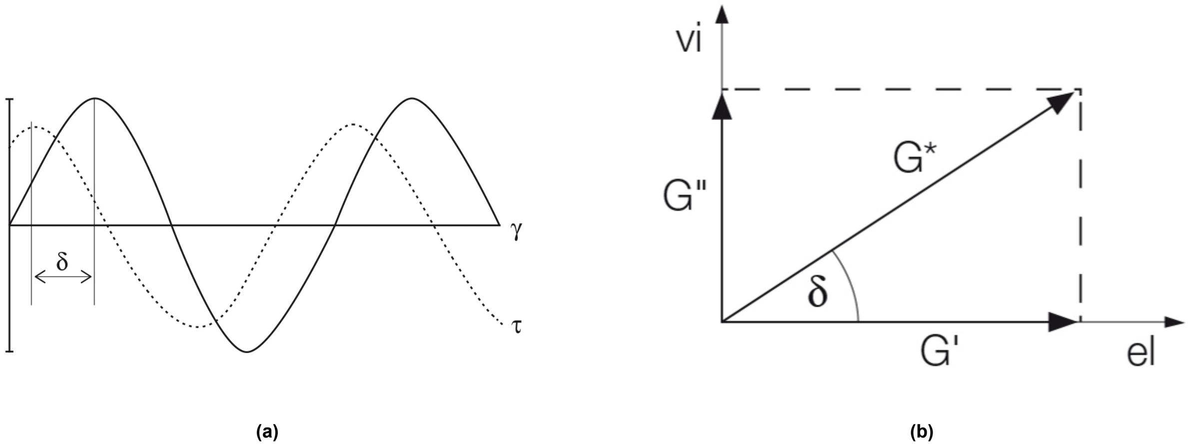

(a)

(b)

Figure 2.14: (a) The sine curves of shear strain (γ) and resulting shear stress (τ) versus time.(b) The complex modulus ($G*$) represented with a phase shift (δ) angle to determine the storage (G') and loss modulus (G"). [82].

Where τ_A is the amplitude of the shear stress and γ_A is the amplitude of the shear strain. The phase shift can be place below the complex modulus vector. Since the phase shift is always between 0° and 90°, the storage (G') and loss modulus (G") can be placed on the x- and y-axis, respectively (Fig. 2.14b). Here, the storage modulus represents the elastic behaviour and the loss modulus represents the viscous behaviour. Therefore, when the phase shift is small (G' > G"), the complex modulus represents viscoelastic solid (or gels). When the phase shift is large (G" > G'), the complex modulus represents viscoelastic liquids. By measuring the phase shift between the shear stress and shear strain in an oscillatory test, the storage- and loss modulus can be determined. The point at which the storage modulus exceeds the loss modulus is considered to be the point of gelation.

2.6. Research Plan

This project is guided by two important research questions:

How to develop an Organ-on-Chip platform for multi-cell culture with transient separation of a brain organoid and vascular network?

How can Pluronic F127 hydrogels be used as a transient barrier for vascularized Organoids-on-a-chip?

The first research question aims to explore possibilities to develop a biocompatible OoC platform for vascularized Organoids-on-a-chip. The second research question aims to find the optimal Pluronic F127 based hydrogels to be used as a transient barrier for vascularized Organoid-on-a-Chip. Therefore, the overall objective for this master thesis to fabricate a biocompatible OoC platform and to identify the optimal Pluronic F127 based hydrogel which can act as a transient barrier for vascularized Organoids-on-a-Chip.

For the development of a biocompatible OoC platform, three materials were proposed, including Moiin Tech Clear, Detax Freeprint Ortho (both photo-polymerizable resins) and PDMS. Moiin Tech Clear was chosen as a readily available material already tested for biocompatibility, Deatax Freeprint Ortho was chosen as a new photo-polymerizable resin with proven biocompatibility in literature and PDMS was chosen as an elastomer materials biocompatible with cortical Organoids and vasculature [7, 20, 28]. OoC platforms were made with all three materials, to determine to optimal way to fabricate OoC platforms for vascularized Organoids-on-a-Chip. The biocompatibility of these platforms remains to be determined.

For the development of Pluronic F127 based hydrogels, di-acrylated Pluronic F127 hydrogels show promising result to act as a transient barrier between vasculature and organoid growth. It was chosen to investigate the potential of di-acrylated Pluronic F127 hydrogels through several experiments. First, the hydrogels were synthesized based on present literature and tested for thermoreversible properties with different concentrations and photo-polymerization conditions. The results of several different papers were combined. Lee et al. (2007) demonstrated that di-acrylated Pluronic F127 hydrogel exhibit slow degradation rates in aqueous media, while Di Biase et al. (2011) demonstrated that di-acrylated Pluronic F127 hydrogels with lower concentrations and low polymerization temperature exhibit thermoreversible properties [76, 77]. Therefore, findings of these two papers were combined to test if di-acrylated Pluronic F127 based hydrogels can exhibit slow degradation rates in aqueous media while being thermoreversible simultaneously.

Furthermore, for both Pluronic F127 and di-acrylated Pluronic F127 hydrogels, the degradation rate in PBS at 37°C and the permeability rate in PBS at 37°C will be tested for several different concentrations. The mechanical properties of each hydrogel will be tested with rheometry and through differential scanning calorimetry (DSC). With rheometry, the elastic modulus, viscous modulus and viscosity of the hydrogels can be obtained, while DSC allows to find the micellation temperature and possible hysteresis patterns.

Based on the found properties in the characterization, the barrier channel on the OoC platform can be accurately modeled. After modeling the channel, the OoC platform will be 3D printed using digital light processing and it will be tested if the hydrogels do indeed remain within the channel. Finally, an optimal injection protocol will be formulated. This will included the optimal injection volumes, velocity, temperature and method.

Successfully execution of all steps should demonstrate the viability of (di-acrylated) Pluronic F127 based hydrogel to act as a transient barrier for Vascularized Organoids-on-a-Chip.

3

Materials and Methods

3.1. Organ-on-a-chip Platform for Vascularized Cortical Organoids

In this section, the design and fabrication process of all used OoC platforms is presented. All designs were made using Fusion 360 CAD software.

3.1.1. Design

In this work, three different microfluidic platform designs were used. The main design creates a OoC platform for Vascularized Organoids-on-a-Chip, while the injection testing and permeability testing designs were used in the characterization and injection of Pluronic F127 hydrogels.

3.1.1.1. Main Design

The OoC platform was originally designed by another member of the ECTM group [7]. It was designed in such a way to create a platform which combines the structural requirements for both the vascular and organoid cultures simultaneously. The designed OoC platform allows for the application of both cell protocols as described in Sec.2.4. The design was based on the properties of the culture platforms of both protocols. The design included an open-well chamber in the middle of the OoC platform used for organoid culturing. This open-well design replicates the wells used in 384-well plates. The central chamber divides the central vasculature gel channel used for vascularization culturing in two. This design was based on the platform used for vasculature culturing by [64]. The central channel in flanked by two media channels with a pillar-array placed in between. A barrier channel (called hydrogel channel) is placed in between the central chamber and the vasculature gel channel on both sides of the organoid chamber. These channels allow for the placement of a transient barrier in between the two cell cultures. An overview of the complete OoC platform is shown in Fig.3.1.

For the organoid culture, this design allows for direct and precise placement of an organoid in the central compartment as well as its easy removal. This design also allows for individual organoid seeding per chip, making it an ideal platform to study co-development of different cell-cultures at a single organoid level [55].

Dimensions: The dimension of the OoC platform are adjusted towards the imaging requirements and required volumes. The length of the platform was set to 25 mm, which is similar to the width of standard microscopic glass slides. This was kept the same to allow for imaging without changing the normal imaging workflow. The width of the platform was 16 mm. This width allowed for the incorporation of all required features, while allowing to print three platforms simultaneously. The thickness of the bottom plate was set to 0.17 mm. This value was chosen as a compromise between optimal imaging (thinner provides better visibility) and firmness (thicker provides more stability). To increase the optical imaging properties of the OoC platform, the bottom plate thickness can be reduces. However, this might results in breaking of the platform, as a thinner bottom plate makes the platform more fragile. The full dimensions of the OoC platform are shown in Tab. 3.1. The OoC platform was designed in such a way to incorporate all required features, while minimizing the used materials. This results in

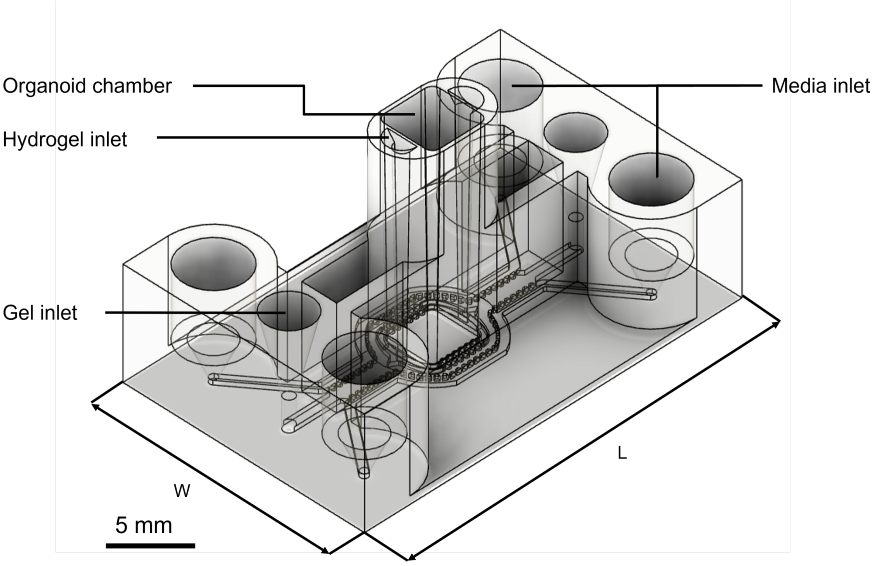

Figure 3.1: 3D visualization of the OoC platform for vascularized organoids on a chip. Media, gel and hydrogel inlets are similar on opposite sides. Parameters: Width of platform (W) and length of platform (L). Designed by [7].

Table 3.1: Dimension of OoC platform

Part of platform	Dimensions
Organoid chamber	V = 139.4 µl, h = 11.5 mm, w = 3.7 mm, l = 3.7 mm
Media inlets	V = 54.3 µl, d = 4 mm, h = 6 mm
Gel inlets	V = 14.2 µl, d = 3 mm, h = 6 mm
Hydrogel inlets	V = 5 µl
Media channels	W_m = 0.5 mm, h = 0.25 mm
Gel channel	W_{gel} = 0.43 mm, h = 0.25 mm
Hydrogel channel	W_h = 0.3 mm, L_h = 2.5 mm, h = 0.25 mm
Pillar array	W_g = 0.1 mm, L_1 = 0.3 mm, L_2 = 0.15 mm, h = 0.25 mm
Bottom plate	W = 16 mm, L = 25 mm, h = 0.17 mm

reduced 3D printing times.

The gel and media inlets were designed to fit the required volume as described in the vascularization-on-a-chip protocol [58]. The inlet volume of the gel channels was set to 14.2 µl, with a diameter of 3 mm to allow for optimal injection using pipettes. The inlet volume of the media channels was set to 54.3 µl, with a diameter of 4 mm. The volumes of the media inlets were much larger than the gel inlets to allow for the creation of a fluid flow through the media channels by creating a pressure difference. The central organoid chamber has a volume of 139.4 µl with a height of 11.5 mm. Therefore, this chamber is large enough to allow for sufficient media volume.

The microfluidic channel design is the most crucial part of the OoC platform. The design of the microfluidic channels is shown in Fig.3.2. The width of the media channels (W_m) and the dimensions of the pillar array (L_1, L_2, W_g) were identical to the dimension used in the vascularization-on-a-Chip protocol [58]. The pillars were placed in between each channel to confine the the vasculature gel, hydrogel and media in their respective channels. This is achieved through the surface tension generated by the vasculature gel and hydrogel. An increase in gap width might cause the vasculature gel or hydrogel to leak through the pillars into other areas of the OoC platform. A decrease in gap width reduces the shear stress generated by the fluid flow and reduces the cross-talk between two regions of the OoC platform. The height of the microfluidic channels was also kept identical to the vascularization protocol at 0.25 mm. This value was chosen as an optimal values as a decrease in channel height (< 0.3 mm)

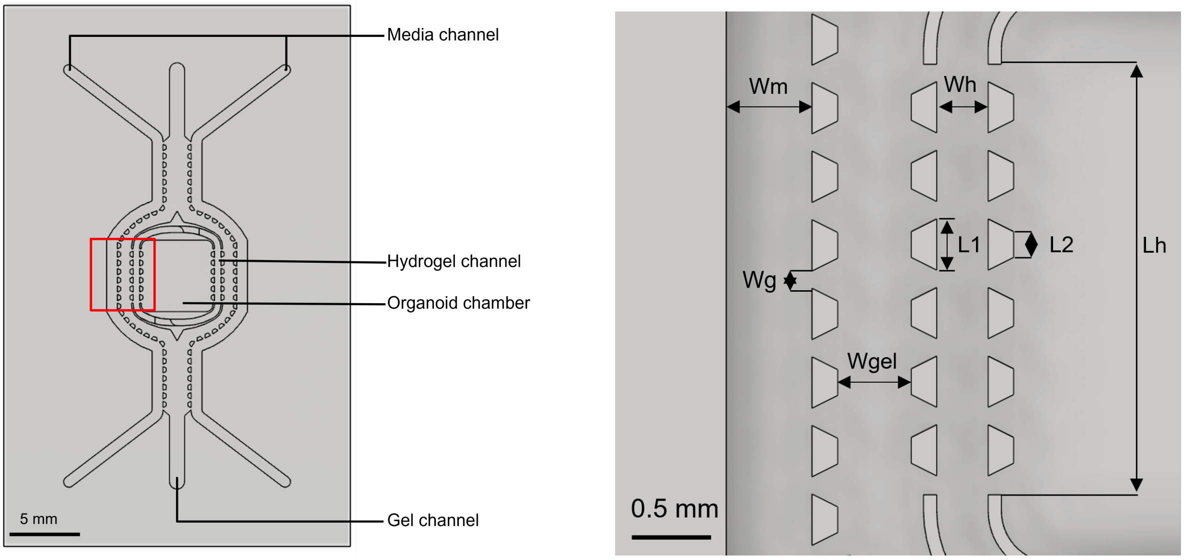

(a)

(b)

Figure 3.2: The microfluidic geometries of the OoC platform. (a) The full microfluidic channels. The organoid chamber is placed in the middle of the platform. The gel channels for vasculature growth is placed around the organoid chamber, with the membrane channel in between. The media channels are placed on the outside. The pillar arrays provides shear stress to the vasculature. (b) Enlarged image of the three adjacent channels. Geometry parameters: Width of media channel (W_m), width of gel channel (W_{gel}), width of hydrogel channel (W_h), gap width (W_g), length of hydrogel channel (L_h) outer width of pillars (L_1) and inner width of pillars (L_2).

causes all the ECs to extend along the axial direction of the flow path (i.e. channels don not form in z-direction). A channel height which is too small will inhibit vasculature growth all together [3].
The design of the barrier (hydrogel) channels allowed for a compartment to place a transient barrier to prevent cross-talk between the two cell cultures. The inlet of the hydrogel channel was placed vertically alongside the organoid chamber. The hydrogel channel is split into two distinct compartments. Each compartment needs to be filled through its own inlet. At the end of the hydrogel channel is an open extension of the channel. This allows for the removal of excess hydrogel when the channel needs to be opened. If the barrier channel is not filled, this compartment allows for cross-talk between the two cell-cultures. However, to achieve this, the channel should either be filled with gel for vasculature to grow or the organoid should be grown as wide as to fill the barrier channel. However, the second option blocks the organoid from being removed. Therefore, when the channel should be opened, additional vasculature gel for the vasculature to grow can be placed in this barrier channel. The width of the barrier channels was 0.3 mm and the gap size between the pillars was 0.1 mm. These values can be changed to optimized the containment of hydrogel in this channel.

3.1.1.2. Test Designs

To increase efficiency of used materials and reduce printing time, two different designs were made for permeability and injection testing. These designs only have a single barrier (hydrogel) channel and the required features for each test setup with as few additional structures as possible. This reduced the materials needed with 3D printing. Simultaneously, this method allowed to print twelve platforms at the same time, instead of three with the main design. To achieve this, the bottom plate had a width of 8 mm and a length of 12.5 mm.

Permeability Testing Platform: The platform designed to test for the permeability of hydrogels is shown in Fig.3.3. This platform included an organoid chamber, a central hydrogel channel and an empty channel at the opposite side of the organoid chamber. The organoid chamber is reduced in size to 107.82 µl. This reduced volume still allows to use the required volume of PBS (70 µl) but reduced printing time. The gel inlets are reduced to 6.45 µl as there was no need to create a fluid flow through volume differences. Therefore, the inlets were kept as small as possible. This inlet size with a diameter

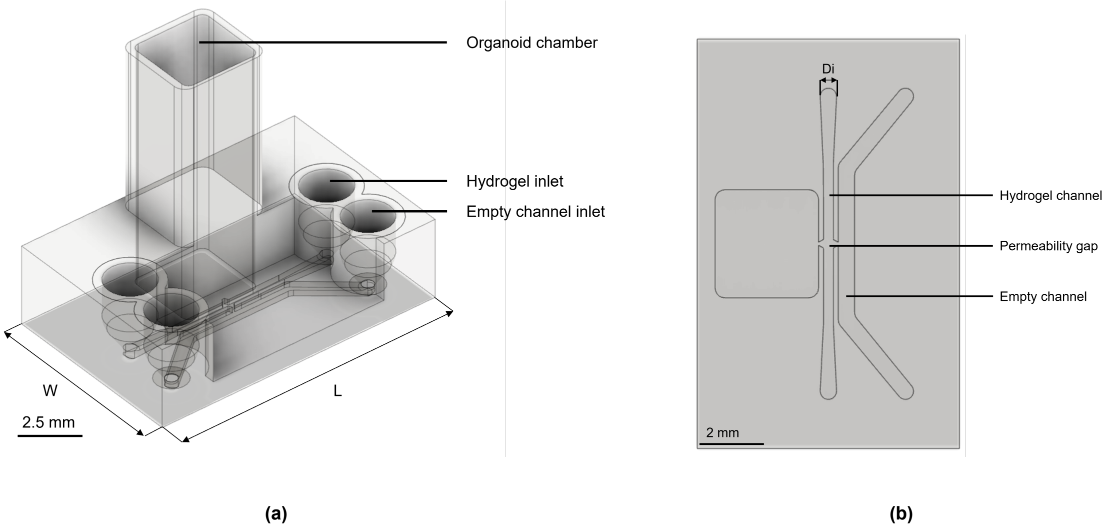

Figure 3.3: (a) 3D model of the 3D printed microfluidic platform for permeability testing. (b) Bottom plate of microfluidic platform for permeability testing. The geometries for the hydrogel channel and the organoid chamber are the same as the main OoC platform, except for the inlet diameter (Di), which has been increased to 0.5 mm. The empty channel has a width of 0.5 mm.

Table 3.2: Dimension of platform for permeability testing

Part of platform	Dimensions
Organoid chamber	V = 107.82 μl, h = 10.35 mm, w = 3.157 mm, l = 3.3 mm
Hydrogel inlets	V = 6.45 μl, d = 2 mm, h = 3 mm
Hydrogel channel	w = 0.3 - 0.5 mm, h = 0.25 mm
Empty channel	w = 0.5 mm, h = 0.25 mm
Pillar array	W_g = 0.1 mm, h = 0.25 mm
Bottom plate	W = 8 mm, L = 12.5 mm, h = 0.1 mm

of 2 mm allowed for a high accuracy with pipette injection, as the pipette could be pressed down on the inlet to create an air tight seal. When the hydrogels are injected, it is forced inside the channel. The hydrogel channel were similar in width to the main design, being 0.3 mm wide. However, at the side of the inlets, the width was increased to 0.5 mm. This creates a wider opening at the inlet, which improved injection. Additionally, the corners at the inlets were filleted to improve fluid flow through the channels. This was done to improve injection and simplify post-processing after 3D printing. Since, filleted corners simplified the removal of excess resin from the channels. All the dimensions of the platform for permeability testing are shown in Tab.3.2.
The number of gaps between the pillars in the pillar array was reduces to a single gap. This was done as this simplified the injection process and resulted in more successfully injected channels. Meanwhile, a single gap still allowed to test for the permeability of the hydrogels. The gap width remained the same at 0.1 mm.

Injection Testing Platform: The dimensions of the platform for injection testing were even further reduced. The platform used for injection testing is shown in Fig.3.4. The gel inlets were the same volume as the platform for permeability testing. The organoid chamber was completely removed, with only a gap for air inlet remaining. This was done as the hydrogel will be the first media to be injected in the OoC platform. Therefore, no additional structures are necessary to test for injection. The pillar array was identical to the pillar array in the main design. However, similar to the platform for permeability testing, the hydrogel channel was wider at the inlet sides (0.5 mm) and the corners were filleted.
In this design the dimensions of the pillar array can be adjusted towards the requirements needed to contain the hydrogel in its assigned channel. All the dimension are shown in Tab.3.3.

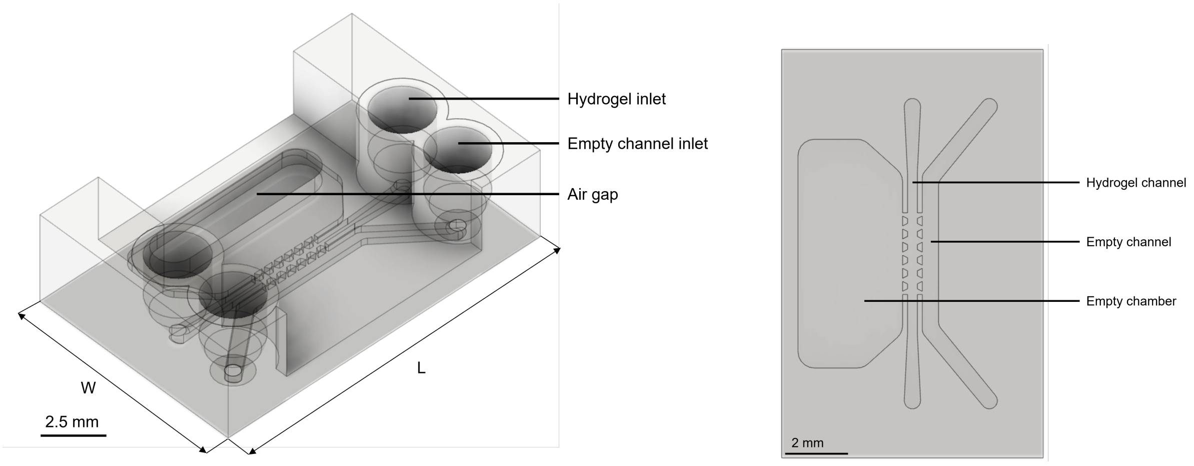

(a) (b)

Figure 3.4: (a) 3D model of the 3D printed microfluidic platform for injection testing. (b) Bottom plate of microfluidic platform for injection testing. The geometries for the hydrogel channels are the same as the main OoC platform, except for the inlet diameter (Di), which has been increased to 0.5 mm. The empty channel has a width of 0.5 mm.

Table 3.3: Dimension of platform for injection testing

Part of platform	**Dimensions**
Air gap	A = 8.5 mm^2, h = 0.6 mm
Hydrogel inlets	V = 6.45 µl, d = 2 mm, h = 3 mm
Hydrogel channel	w = 0.3 - 0.5 mm, h = 0.25 mm
Empty channel	w = 0.5 mm, h = 0.25 mm
Pillar array	W_g = 0.1 mm, h = 0.25 mm, L_1 = 0.3 mm, L_2 = 0.15 mm
Bottom plate	W = 8 mm, L = 12.5 mm, h = 0.1 mm

Table 3.4: Slice thickness and required accuracy of testing chip parts

Part of chip	**Required Accuracy**	**Slice Thickness** [µm]
Burn-in layer	High	50
Bottom plate	High	50
Microfluidic channel	High	50
Media in-/outlets (small)	Medium	50-100
Media in-/outlets (wide)	Low	100

3.1.2. Fabrication

Digital Light Processing (DLP) utilizes photo induced curing of photo-curable resins. These photo-curable resins consist of photo-polymers that undergo interactions and change their chemical and physical properties when exposed to light [83]. The resins consist of polymerizable monomers and photo initiators. Absorption of UV light by the photo-initiators create free radicals which induce polymerization of the polymerizable monomers [84].

For the fabrication of the microfluidic chips, Moiin Tech Clear was used as photo-curable resin. Moiin Tech Clear UV resin offers high spatial resolution, transparency and good mechanical properties. This is a photo-curable resin consisting of 98% methacrylate monomers and photo-initiators. This material polymerizes when exposed to 385 nm at 20-30°C due to UV light absorption. Therefore, this material is compatible with the available DLP Asiga Max X27 printer. Besides the fabrication of OoC platforms using Moiin Tech clear, Detax Freeprint Ortho resin was also tested as an alternative material. This resin has similar mechanical properties as Moiin Tech Clear and also polymerizes under UV exposure with a wavelength of 385 nm. However, this material is also marketed as biocompatible according to class IIa for medical devices[85]. Moreover, a study on cell viability of human gingival fibroblasts (GF1) showed that Detax Freeprint Ortho had a cell viability of more than 75% after 24 hours [28]. Therefore, the cytotoxic effect of this resin are considered minimal.

3.1.2.1. 3D Printing

The OoC platforms were designed with CAD modeling software Fusion 360 (Autodesk). The CAD models were exported as STL files and uploaded to the desktop attached to the Asiga 3D printer. The main design was printed three times on a single print, while the test designs were printed twelve times on a single print. This allowed for a maximum number of printed platforms on a single print allowed by the dimensions of the printer head (2.8 x 5.1 x 8cm). The STL files were uploaded in Asiga composer software and duplicated for the given number of times with a spacing between each chip of 0 mm. This created prints, with all platforms attached to each other in a single print.

The OoC platforms were fabricated using an Asiga Max X27 DLP printer (Fig. 3.5a). This 3D printer operates with a 385 nm UV laser curing specified UV resins. The printer has an XY-plane resolution of 27 µm. The resolution of the Z-plane (printing direction) can be adjusted by increasing or decreasing the slice thickness in the Asiga composer software, where a lower slice thickness increases the resolution of the printed part. However, an increase in resolution, and therefore increase in number of slices, also drastically increased printing time. Therefore, the optimal Z-plane printing accuracy was determined. Tab. 3.4 shows the distinctions of different parts of the platform and their required accuracy. The burn-in layer is required on all prints as attachment to the printer head. A lower thickness of the burn-in layer results in higher transparency of the bottom of the platform, but this also makes the platform more fragile and harder to remove from the printer head without damaging. The bottom-plate of the platforms and the microfluidic channels required a high accuracy. Therefore, the slice thickness of these parts of the platforms were set to 50µm. The optimal slice thickness and accuracy of the media inlets was also determined to be 50µm. The media inlets are very narrow at the bottom (300-500µm). A low accuracy in these parts could cause minor errors in the printed accuracy, which causes left-over resin the become stuck in these parts. Therefore, the optimal slice thickness and range was determined by printing multiple testing chips with varying slice thicknesses and ranges. Finally, the top part of the platform, including the media inlets, required a lower accuracy. Therefore, the slice thickness of these parts was set to 100µm.

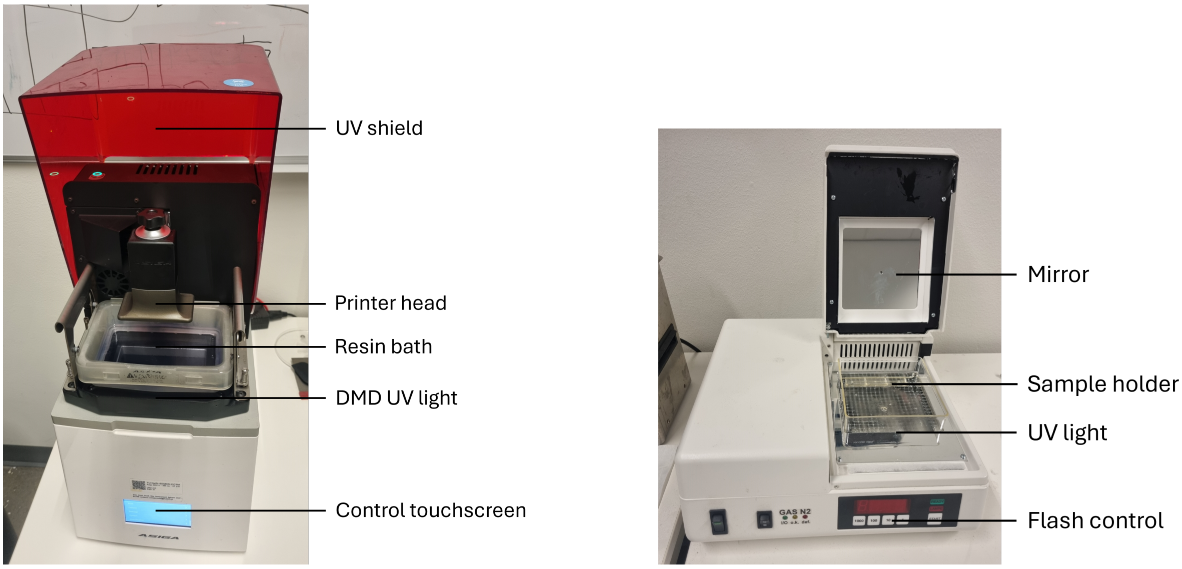

(a)

(b)

Figure 3.5: (a) The Asiga MAx X27 DLP printer. The printer head is lowered in the resin bath, after which the UV light source polymerizes the resin on the printer head. (b) The Otoflash G171 UV-flash device. The part is placed in the sample holder, after which the part is UV cured by the UV light. The mirror reflects UV to reach all sides of the part. The number of flashes per section can be adjusted in the flash control.

Post Processing: To prevent residual methacrylate monomers to remain in the channels, extensive post-processing is needed after printing. This is done, to remove uncured resin, since uncured monomers can be cytotoxic [27]. Therefore, a post-processing workflow was developed to remove uncured resin from the prints and confirm opening of all microfluidic channels. The following post-processing, which resulted repeatedly in opening of all microfluidic channels without uncured resin present, is listed below:

- Remove print from printer head using metal slider. Without applying too much force, force the metal slider between the print and the printer head and allow air to flow underneath the print. Repeat this step at all four sides of the print. The print will come loose of the printer head relatively easily. Applying too much force might damage the print.
- Clean the part in an ultrasonic bath (Emag emmi-30hc) filled with Isopropyl alcohol (IPA) for five minutes at room temperature. Make sure the openings of the print are facing down.
- Flush channels with deionized water, IPA and compressed air under low pressure.
- Repeat the previous two steps three times in total.
- Fully emerge the print in IPA at room temperature for one hour.
- Flush channels with compressed air using maximum pressure until no leftover resin is present in the channel.
- UV cure the print in UV-flash device (Otoflash G171 UV-flash device) under nitrogen flush at room temperature. Use three times 2000 flashes while turning the print between flashing sessions (Fig. 3.5b).

In this protocol, the part is fully emerged in IPA for one hour. This time can also be in-/decreased for simpler structures as long as all channels are opened. However, a prolonged exposure to IPA may negatively impact the mechanical properties and damage the print [86]. The amount of UV flashes can also be increased. However, a maximum of 2000 flashes per cycle was used to prevent overheating of the print.

Quality Control: Quality control of the printed platforms was performed through optical imaging using DinoXcope microscope (30x magnification) and testing of the channels using IPA. Fig. 3.6a shows the

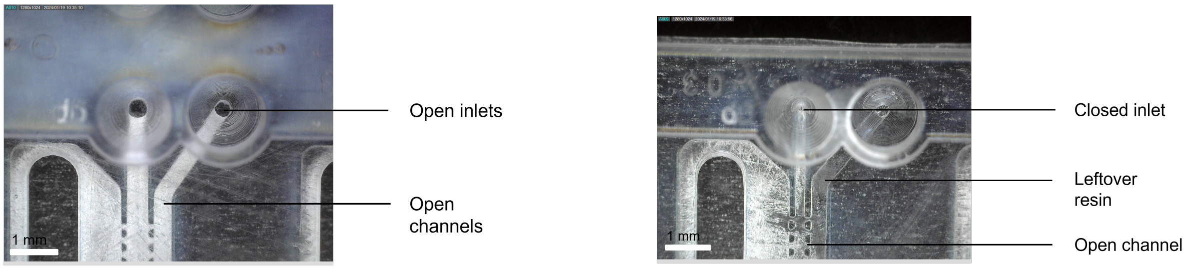

(a)

(b)

Figure 3.6: (a) Desired final state of a platform with open media inlets and open channels. (b) Unsuccessful platform with closed inlets and leftover resin present in the channels.

desired final state of microfluidic channels and inlets. It can clearly be seen that the inlets are open (indicated by the dark color) and that no leftover resin is present in the channels (indicated by the white color). Fig. 3.6b shows a printed platform which was unsuccessful. It can be seen that the inlets are not opened, which is caused by a too low resolution in the Z-plane in the printer (i.e. slice thickness was too high for the lower part of the inlet). Moreover, the dark color in the channels indicate that leftover resin is present within these channels. As a consequence of the unopened inlets, the resin could not be flushed out of these channels.

Additionally, to confirm open channels, IPA was flushed through the channels from each of the media inlets of the platform. Through this way it could be confirmed if all inlets and channels were opened, by visual determination if fluids could flow through all channels.

3.1.2.2. Detax Freeprint Ortho Initiator File Configuration

The material configuration was performed according to predefined guidelines by Asiga [87]. The Asiga 3D printer requires a material configuration initiator file to provide instruction for the Asiga composer software. The most important part of this file is the z-curing table, which describes the amount of energy needed to cure a slice to a specific thickness. The z-curing table was created by logarithmically increasing the exposure time to tiny droplets of resin material. The droplets were placed on a film of plastic (0.31 mm thick) provided by Asiga. Ideally, this test would be performed on a film of fluorinated ethylene propylene (FEP), which is the same material as the bottom of the used building trays. A syringe was used to deposit tiny droplets of uncured resin on this plastic film and the film was placed directly over the LED. The intensity of the LED was set to 7.03 mW/cm^2 and exposure time was logarithmically increased from 0.7 seconds to 100 seconds. After exposure, uncured resin was removed from the plastic film using IPA. For each exposure time, the thickness of the cured material was measured using a caliper and documented in the z-curing table. Exposure times below one second resulted in slice thicknesses of less than 100 µm. Therefore, it was especially important to include multiple measurements with low exposure times, as low exposure times result in a low cured thickness. Since, the previously described OoC platform depends on these small structures, accurate measurements in lower ranges of exposure time is of vital importance. Based on the LED intensity and the exposure time, the z-curing table could be made. This table consist of three columns being: required energy, thickness and intensity. The thickness and intensity result directly from the measurements, while the energy can be calculated by multiplying the intensity with the exposure time.

To obtain a print with correct dimensions in the XY-plane, the XY-growth and XY-shrinkage must be determined. XY-growth causes the perimeter of the part to grow, while XY-shrinkage causes the entire part to shrink. Based on the obtained z-curing table, the XY-shrinkage could be determined by printing a test structure with a step-design. The step-design used consisted of know distance between 5 mm and 30 mm with a spacing of 5 mm. After printing, the XY-dimensions of each step can be measured and compared to the theoretical dimensions. The obtained values were plotted against the theoretical values to obtained the XY-shrinkage (gradient) for the slice thickness with which the print was made. Furthermore, the XY-growth can by calculated by dividing the Y-intercept by the gradient, then dividing by two. This step was repeated for a slice thickness of 25, 50 and 100 µm. The obtained XY-shrinkage and XY-growth values were inserted in the XY-scaling table in the initiator file.

It is important that the initiator file is made with representative values for the desired printing dimen-

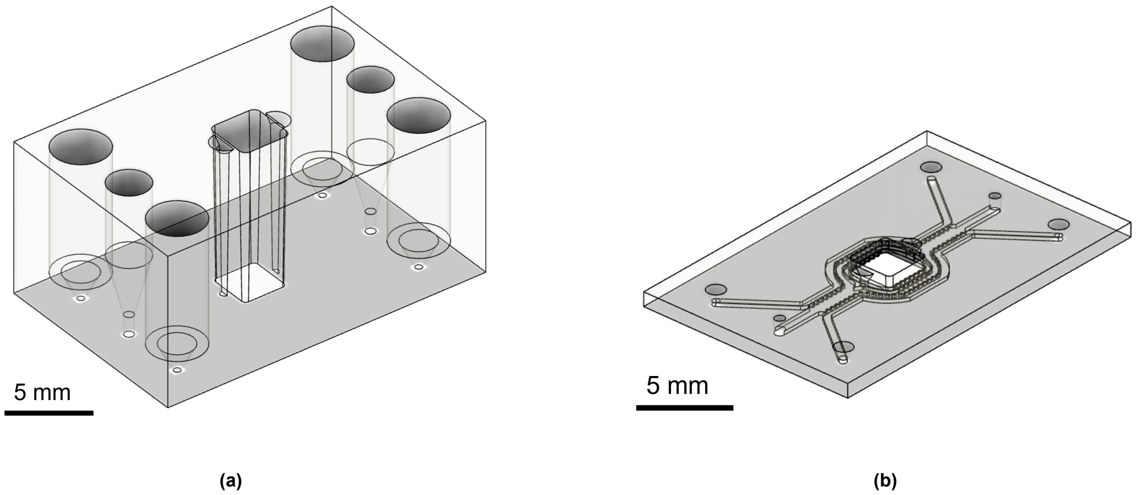

Figure 3.7: The split OoC platform. (a) Top layer of the mold, fully extruded to the height of the organoid chamber. (b) Bottom layer.

sions. If the required dimensions and slice thicknesses are below 100 µm, the configuration should be performed focusing on values within this range.
After the initiator file was complete, printing of OoC platforms using Detax Freeprint Ortho was tested using Asiga Universal- and UltraGloss building trays.

3.1.2.3. Polydimethylsiloxanes (PDMS) Molding

Besides fabrication of the OoC platform with DLP, the platforms were also fabricated using PDMS molding. PDMS allows for the fabrication of biocompatible, transparent and gas permeable OoC platforms. This is especially useful, since OoC platforms fabricated with thermoplastic material lack the latter property [19, 27].

Molds 3D Printing The dimensions of the OoC platform prevent the OoC platforms to be molded with a single mold. Therefore, the platforms was split into two layers, as this was the minimal amount of layers required to be able to mold the OoC platform. The platform was split at the top of the microfluidic channels. This results in a bottom layer containing the microfluidic channels and the bottom plate and a top layer containing the inlet- and organoid chamber- structures. When the platform was fabricated with DLP, the platform was designed in such a way to minimize the usage of materials and printing time. When the platform was fabricated using PDMS molding, this was considered less relevant. Therefore, the top layer was extruded over the full width and length. This was done as this simplifies the molding and demolding process of the PDMS platform. Simultaneously, the dimensions of the inlets and organoid chamber were kept similar to the dimension of the original platform. The layers are shown in Fig. 3.7.

The molds were designed by making the negative of the original layers (Fig. 3.7 with CAD modeling software Fusion 360. The designed molds were exported as STL files and 3D printed using the Asiga 3D printer. Initially, the molds were printed using Sunlu Black plant based resin and later with Moiin Tech Clear resin. Sunlu Black resin was chosen since transparency was not required, several molds were sacrificial and this resin was significantly cheaper compared to Moiin Tech Clear. The molds containing features of the microfluidic channel were printed with a slice thickness of 0.05 mm to be able to accurately print the small features present in the microfluidic channels. Other molds were printed with a slice thickness of 0.1 mm. Post processing of the molds was done similar to post-processing of OoC platforms printed with Moiin Tech Clear as described in Sec. 3.1.2.1.

After printing, the molds were silanized using Trichloro(1H,1H,2H,2H-perfluorooctyl)silane (Sigma-Aldrich) as a silanization agent. The molds were placed inside a desiccator together with several drops ($<$ 1 ml) of the silanization agent. A vacuum was created inside the desiccator and the molds were silanized overnight. This should result in silanization of all accessible surfaces.

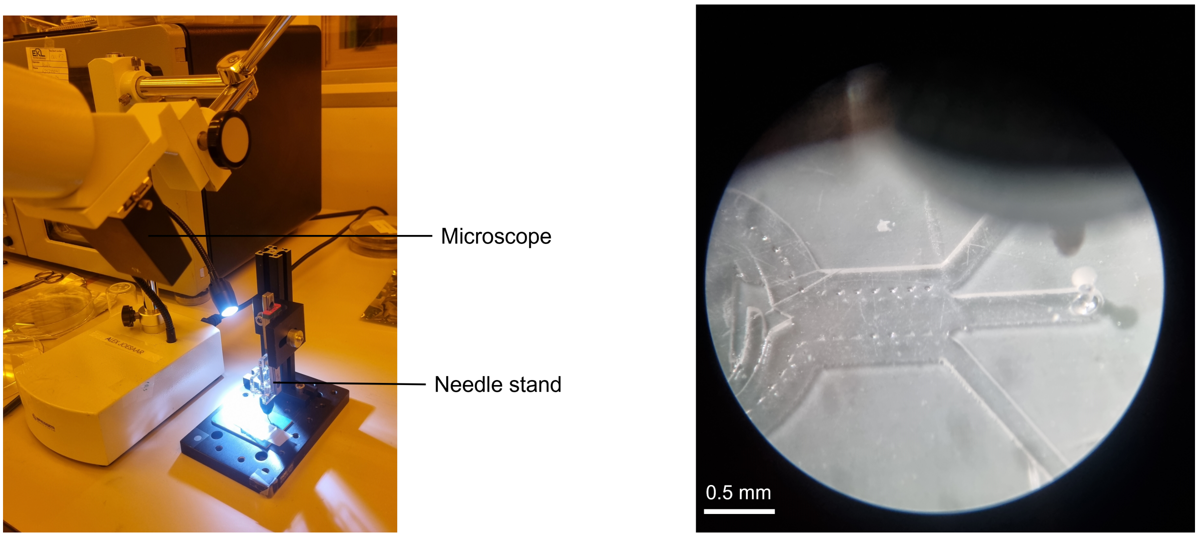

(a) (b)

Figure 3.8: Punching of PDMS layers. (a) The used setup. A microscope and lamp were used to accurately punch PDMS layers. The punching needle was located on a stand and could only move in the z-direction. (b) Close-up of punching hole with the microscope

PDMS was synthesized using a Sylgard 184 silicone elastomer kit. This kit consist of the elastomer base and curing agent. The PDMS was mixed with a ratio of 10:1 of elastomer base to curing agent. Mixing was done using a Thinky mixer (Are250) for 30 seconds at 500 revolutions-per-minute (RPM). Afterwards, defoaming of the mixture was done for 1 minute and 30 seconds at 2200 rpm.

The obtained PDMS was poured into the molds and degassed for 30 minutes using a created vacuum in a desiccator. After degassing, PDMS was cured at 80°C. Initially, the bottom molds were cured for two hours, while the exact curing time of the top molds made with Sunlu Black resin was determined by retrieving and demolding a sample every 30 minutes. Top molds made with Moiin Tech clear were cured at 80°C for four hours. After full curing, the obtained PDMS layers were demolded and covered with scotch tape to prevent surface contamination.

Some PDMS layers required punching to obtain the inlet structures of the original platform (discussed later). These layers were first perforated with a needle at the exact location using a microscope (40x magnification) (Fig. 3.8b). This was done to get an accurate perforation at the correct location which could easily be seen on the other side of the PDMS layer. Perforation was done with a needle bounded to a stand. The needle could only move in the z-direction, which guaranteed vertical holes (Fig. 3.8a). Initially, it was tested if the perforation of the PDMS layers was large enough for fluids to flow through. Later, PDMS layers were fully punched to acquire wider inlets. The initial perforation assisted in accurately punching the PDMS layers at the correct location. Punching was done using a microfluidic PDMS puncher with a outer diameter of 2 mm.

The obtained (and punched) PDMS layers were cleaned and bonded using oxygen plasma. Cleaning was done with IPA. Afterwards, the PDMS layers were rinsed with deionized water, blown dry with compressed nitrogen and covered with scotch tape [88]. The same parameters were used for PDMS-PDMS bonding as for PDMS-glass bonding. The PDMS layers were placed in a oxygen plasma chamber (Diener atto) with the bonding surfaces exposed. Pumping down pressure was set to 0.2 mbar. Afterwards, 100% oxygen was supplied in the chamber for 30 seconds. The plasma process was done for 20 seconds, at 0.25 mbar with a power of 40 W. After the plasma process. the PDMS layers were aligned and manual pressure was applied for one minute. After the layers adhered together, they were placed in an oven at 130°C for five minutes. The obtained boned PDMS layers were manually tested for delamination by applying a minimal amount of tensile force on the corners of either layer.

Fabrication Methods: To fabricate the OoC platform using PDMS molding, five different fabrication methods were used. This was done to determine the optimal fabrication method. The five methods are described below and shown in Fig. 3.10.

1. The first option for fabrication was done by molding the top and bottom layers of the OoC platform in individual negative molds. PDMS was added to these molds and fully cured. After curing, the PDMS was demolded. In this process, the top mold was sacrificial as at least one of the side walls needed to be broken for successful demolding. The PDMS layers were then bonded using oxygen plasma. Theoretically, this method was the most straightforward. However, due to the usage of two separate layers, this method was prone to misalignment and delamination. Additionally, the thick top layer caused the top molds to be sacrificial. This method is shown in Fig. 3.10A.
2. In the second option, the inlet pillars were 3D printed separately from the bottom plate. The lower ends of the pillars were extended and similar sized holes were placed in the bottom plate. This allowed the pillars to be placed at the correct location to prevent misalignment. The walls of the top mold were completely removed. Instead, the pillars and bottom plate were connected and placed in a petridish. The bottom mold was similar to the previous method. After mold fabrication, PDMS was poured in the molds and fully cured. Then pillars were removed from the PDMS layers and the obtained PDMS layers were demolded. The demolded PDMS layers were bonded using oxygen plasma. This method is similar to the previously mentioned method as it is still prone to misalignment of the two layers and delamination. However, due to separation of the pillars and the bottom plate, the materials were intended to be reusable. This method is shown in Fig. 3.10B.
3. The third fabrication option is based on punching inlet and outlet holes in the PDMS layers as described by [89]. In this fabrication method all the pillars (except the organoid chamber pillar) are removed from the mold. The bottom mold is the same as previously described. PDMS was poured in the molds and fully cured. After demolding, the PDMS layers were either bonded with oxygen plasma before or after punching of inlet holes. Once both layers were punched and bonded, the final combined PDMS platform was bonded to glass. Punching after bonding of the two layers might cause delamination of the two layers due to force needed to retrieve the puncher from the PDMS layers, while punching before bonding requires the layers to be aligned. This was done by using an alignment tool (3D printed). The alignment tool consisted of pillars on the correct place, to assist in alignment of the two layers. Because punching requires the be done through the full height of the layers, the bottom layer was inverted. This results in the microfluidic channels facing downwards and being exposed after bonding. Therefore, after bonding, the combined PDMS platform was bonded to a glass substrate. The full fabrication process is shown in Fig. 3.10C.
   Later, this option was further explored by molding the top and bottom layer simultaneously using only the bottom molds. Twelve bottom molds were placed together in a plastic tray. PDMS was poured over and fully cured. PDMS layers containing the microfluidic channels were cut out of the tray, inlet holes were punched in and the layer was bonded to glass.
4. Because of difficulties with demolding of the relatively large top layer, the fourth method of fabrication uses six individual smaller molds. Therefore, original OoC platform was extruded to an extend at which all layers would be made of flat surfaces. The splitting of the OoC platform is shown in Fig. 3.9. This design differs from the other top layers, as the sides at which the inlets are located are not fully extruded to the height of the organoid chamber. All the individual molds were fabricated using DLP. PDMS was poured in the molds and fully cured. After demolding, the PDMS layers were bonded using oxygen plasma, starting from the top. Alignment of the layers was done using a 3D printed alignment tool with inlet pillars at the correct locations. This method simplifies the demolding process of the PDMS layers. However, this methods is very vulnerable to delamination. The full fabrication process is shown in Fig. 3.10D
5. The fifth and last method combines fabrication through DLP and PDMS molding. The bottom layer was still molded similar to previously described methods. However, the top layer was fabricated using DLP, similar to the fabrication of the complete OoC platform as described in Sec. 3.1.2. Although, conventional approached to bond PDMS layers to thermoplastics depend on (3-Aminopropyl)triethoxysilane (APTES) treatment prior to oxygen bonding, the bonding in this method was performed solely with oxygen plasma treatment [90]. This method simplifies the fab-

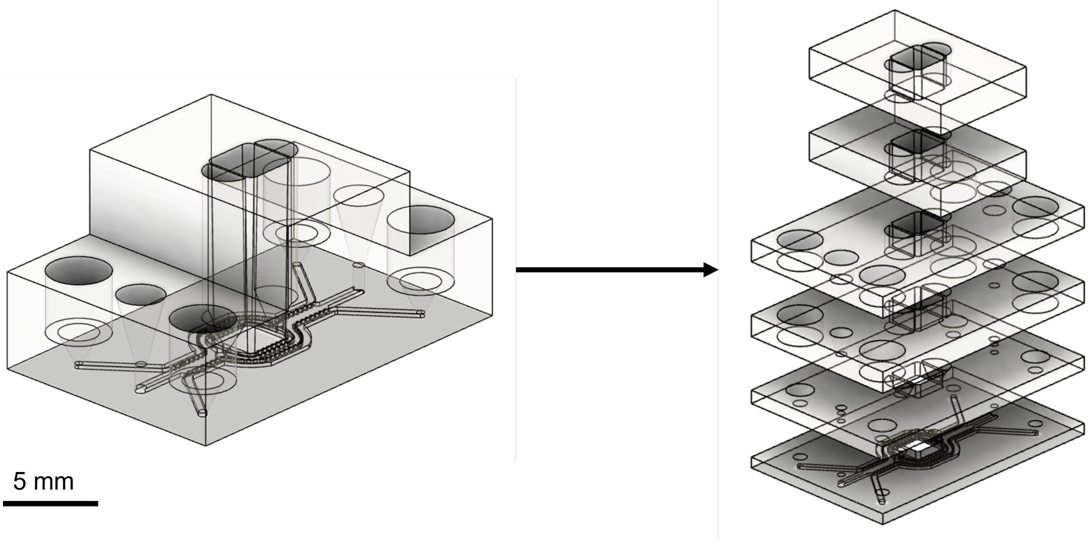

Figure 3.9: A visualization of splitting the OoC platform in six layers. The platform was fully extruded to the height of the organoid chamber in the middle part and extruded to the height of the inlets on the outer parts

rication of the top layer of the OoC platform, while the bottom layer still provides the advantages of PDMS, including gas-permeability. However, the bonding strength between PDMS and thermoplastics might be low and this method still suffers from difficult alignment. The full fabrication process is shown in Fig. 3.10E

3.1.2.4. Dimensional Accuracy

For the successfully 3D printed OoC platforms and fabricated PDMS layers, with open inlets and channels, the dimensional accuracy was determined. The accuracy was determined using a DinoXcope microscope (30x magnification) and Keyence vhx (100x and 1000x magnification). Using the DinoXcope microscope, the accuracy in the XY-plane was determined by measuring the gap size and channel width of successful printed platforms and PDMS layers. Additionally, with the Keyence vhx microscope, the accuracy of both the printed platforms and the DinoXcope microscope was determined. This was done to test if the DinoXcope microscope was accurate enough to determine dimensional accuracy of the OoC platforms. The investigated elements of printed platforms are shown in Fig. 3.11.

3.2. Biodegradable Barrier for Multi-Cells Culture of Vascular Networks and Cortical Organoids

The biodegradable barrier was made from Pluronic F127 based hydrogels. This included conventional Pluronic F127 and di-acrylated Pluronic F127 hydrogels.

3.2.1. Pluronic F127 Hydrogels

To test Pluronic F127 hydrogels as barrier option for vascularized cortical organoids-on-a-Chip, four different hydrogels were made with different concentrations of Pluronic F127. The concentrations included were 15, 20, 25 and 30 wt%. These four concentrations were chosen to systematically identify the difference in permeability, degradation and gelation temperature for differences in concentration. Lower concentrations have a gelation temperature which exceed 37°C [8]. Therefore, these were not included, as the gelation temperature is too high to be used in OoC applications. Concentrations above 30 wt% have a high viscosity and are injected through shear thinning behavior [8, 66]. Therefore, these concentrations were not included. The hydrogels were preferred to be injected in the microchip using a pipette, since this allowed for accurate control of the injected volume. Hydrogels which need to be injected through shear thinning behavior cannot be injected with a pipette, which drastically decreases the accuracy.

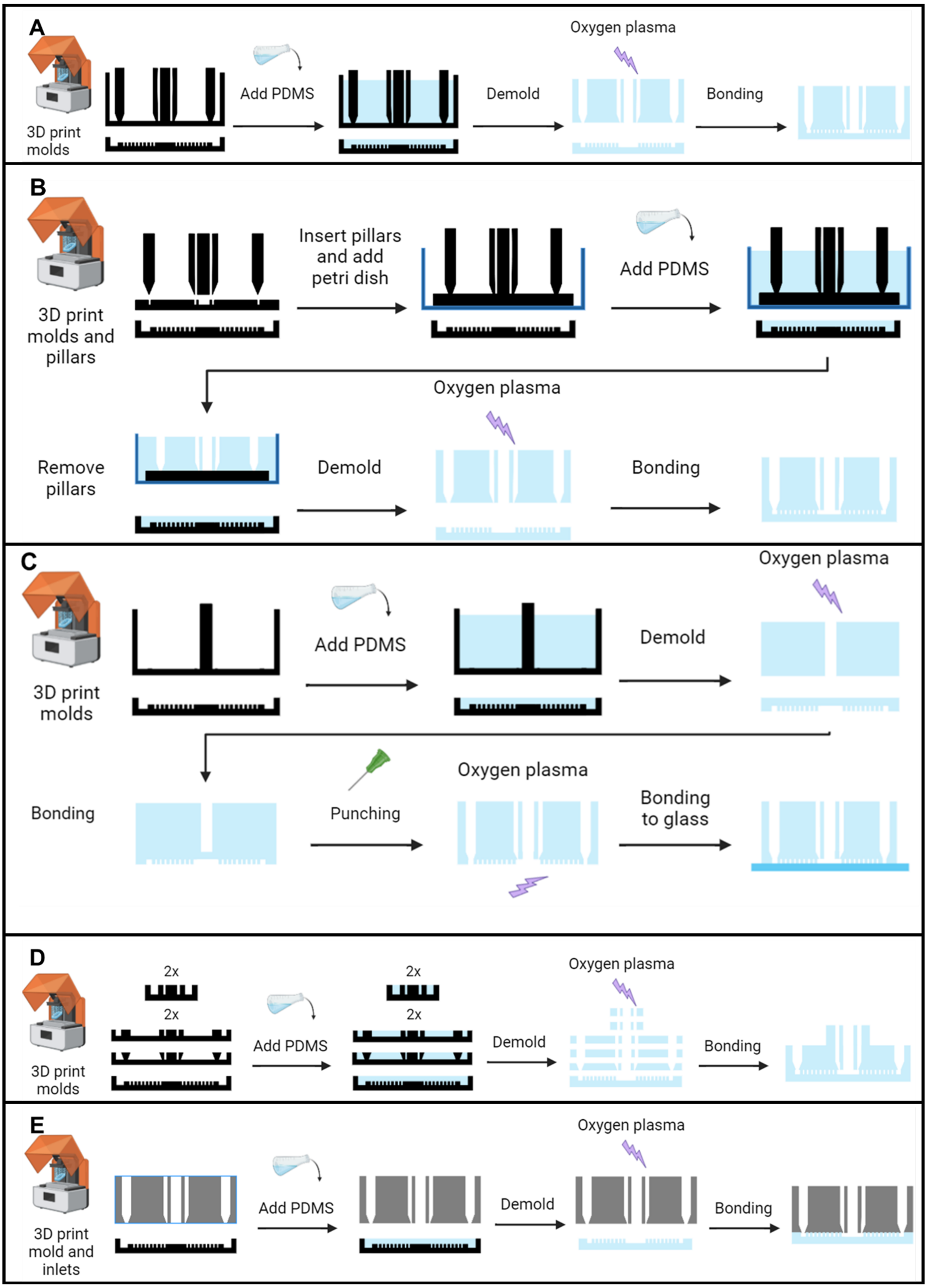

Figure 3.10: Five different fabrication processes using PDMS molding. (A) Top and bottom layer are 3D printed. PDMS is poured in the molds, fully cured, demolded and bonded using oxygen plasma. (B) Pillars and bottom plate are 3D printed separately. Pillars are inserted in the bottom plate and placed in a petridish. PDMS is poured in the molds and fully cured. Pillars are removed first after which PDMS layers are demolded and bonded using oxygen plasma. (C) Top mold consists of only a pillar for the organoid chamber. PDMS is poured in molds, fully cured, demolded and bonded with oxygen plasma. Inlets are punched in the bonded PDMS layer and punhced PDMS is bonded with glass using oxygen plasma. (D) OoC platfrom is split in six layers and negative molds are 3D printed. PDMS is poured in the molds, fully cured, demolded and bonded with oxygen plasma using an alignment tool. (E) PDMS is poured in bottom mold, fully cured and demolded. Top layers is fabricated using DLP 3D printing. Bottom PDMS layer and 3D printed top are bonded using oxygen plasma

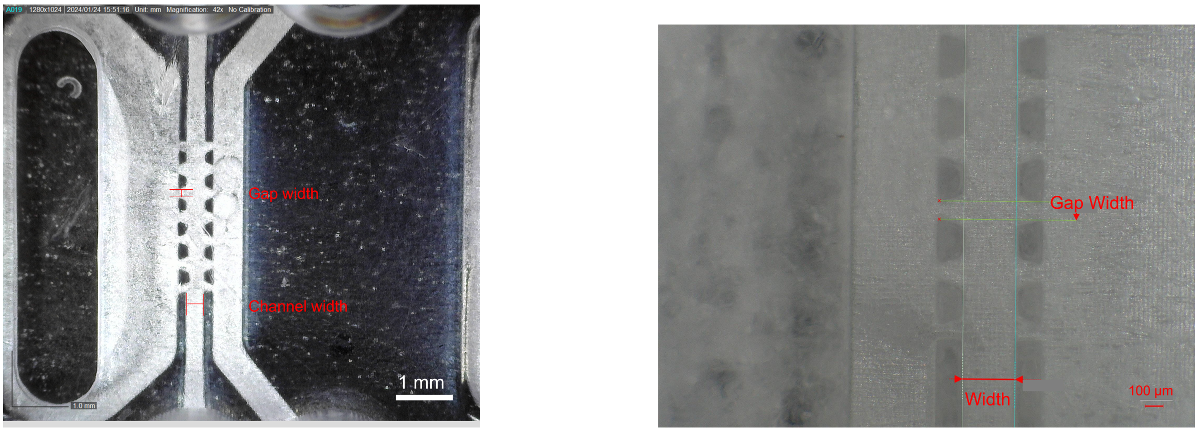

(a)

(b)

Figure 3.11: Determination of gap size and channel width of 3D printed OoC platforms using DinoXcope (a) and Keyence vhx (b) microscopes respectively. In this example, the DinoXcope and Keyence vhx microscope give a gap size of 0.145 mm and 0.1017 mm respectively.

3.2.1.1. Synthesis

The Pluronic F127 hydrogels were fabricated according to the cold method by dissolving Pluronic F127 powder (Sigma-Aldrich) in cold (4°C) deionized water [91]. Pluronic F127 solutions of four different weight percentages (15, 20, 25 and 30 wt%) were made. First, the desired weight percentage of deionized water was added to cleaned glass beakers. The glass beakers were placed in a ice bath made of deionized water and ice cubes, where the temperature remained below 4°C. The Pluronic F127 powder was added gradually while stirring using a magnetic stirrer until the desired weight fraction was reached. Additionally, the solutions were mixed using a vortex mixer (Fisherbrand ZX3) to prevent the formation of lumps. After mixing, the Pluronic F127 solutions were stored in the fridge at 4°C until further use.

3.2.2. Di-acrylated Pluronic F127 (F127DA) Hydrogels

Hydrogels made from di-acrylated Pluronic F127 (F127DA) should have a lower degradation rate compared to conventional Pluronic F127 hydrogels [76]. Therefore, di-acrylated Pluronic F127DA was synthesized to determine its effect on degradation rate.

3.2.2.1. Synthesis

Di-acrylated Pluronic F127 was synthesized according to the protocol by Lee et al. (2007) [76]. The synthesis was performed twice with a different precipitation ratio of methylene chloride to diethyl ether. The first time, the ratio was 1:2.5, the second time it was 1:5. The final synthesis protocol is described below. Pluronic F127, methylene chloride, triethylamine, acryloyl chloride and diethyler ether were all purchased from Sigma-aldrich.

The synthesis used 15 grams of Pluronic F127. The Pluronic F127 was dried for five hours at 50°C. The dried Pluronic F127 was dissolved in 100 ml of methylene chloride in a 500 ml round-bottomed flask while stirring using a magnetic stirrer at 800 rpm. 1.55 ml of triethylamine and 0.5 ml of acryloyl chloride (dropwise) were added. The mixture was again stirred for eight hours at a temperature below 4°C using an ice bath. Afterwards, the mixture was stirred for 18 hours at 20°C overnight. The obtained mixture was added dropwise, using a dropping funnel, in 500 ml of cold ($<$ 4°C) diethyl ether while stirring using a magnetic stirrer. The di-acrylated Pluronic F127 was allowed to precipitate for three hours and filtered using StonyLab filtration paper, with a pore size of 20 µm. Filtration was done twice and the filtration paper was washed afterwards with cold diethyl ether. The obtained residue on the filtration paper was retrieved of the filtration paper and dried for three days at 20°C.

Di-acrylated Pluronic F127 hydrogels were synthesized similar as conventional Pluronic F127 hydrogels as described in Sec. 3.2.1.1. Four different hydrogels were made with a concentration of 10, 15, 20 and 25 wt%. The used concentrations were lower compared to the conventional Pluronic F127 hydrogels, since the gelation temperature was found the be lower compared to conventional Pluronic F127 [77]. For the degradation testing of these hydrogels, the hydrogels were first photo-polymerized. To each hydrogel 0.2 wt% of photo-initiator was added. The used photo-initiator was 2-Hydroxy-4′-(2-hydroxyethoxy)-2-methylpropiophenone (Irgacure 2959) (Sigma-Aldrich). The hydrogels and the photo-initiator were mixed using a vortex mixer. The hydrogels with photo-initiator were placed in an oven at 30°C for ten minutes and afterwards exposed to UV light (225 mW/cm^2) for ten minutes.

3.2.2.2. Degree of Acrylation

The degree of acrylation of di-acrylated Pluronic F127 was determined using hydrogen-nuclear magnetic resonance (H-NMR) spectroscopy. H-NMR utilizes the magnetic properties of atomic nuclei possessing angular momentum to determine molecular structures [92].

Working Principle: The proton (H) has a spin quantum number of I = $\frac{1}{2}$. Therefore, it can only exist in two spin states, characterized by the magnetic number: $m = +\frac{1}{2}$ or $m = -\frac{1}{2}$. This make the proton a magnetic dipole [93]. In the absence of a magnetic field, both spin states have the same energy. In presence of a magnetic field, the protons align either with (lower energy) or against (higher energy) the magnetic field. Using short pulses of radio frequency, the protons can be excited towards a higher energy state. After the radio frequency pulse, the proton turns back to its original state and emits radio frequency pulses. The emitted radio frequency pulses are detected and transformed using a Fourier transform to a frequency-domain spectrum. The frequency needed to excite a proton into its higher energy state (resonance frequency) depends on the chemical environment of that proton, which causes the proton to be more or less affected by the magnetic field [93]. Therefore, based on the difference in resonance frequencies, the chemical environment of different protons can be determined. Using this principle, different chemical groups can be detected using H-NMR. Since the resonance frequencies are dependent on the applied magnetic field, the resonance frequencies are depicted as chemical shift in part per million (ppm) relative to a reference compound according to Eq. 3.1 [94]. This is done to avoid complications in comparisons between different H-NMR instruments.

$$\delta = \frac{v_{reference} - v_{sample}}{v_{ref}} * 10^6 (ppm) \tag{3.1}$$

Where δ is the chemical shift and $v_{reference}$ and v_{sample} are the resonance frequencies of the reference material and the sample respectively.

Protocol: To determine the degree of acrylation, 30 mg of the obtained di-acrylated Pluronic F127 was dissolved in 0.75 ml of deuterated chloroform (CDCL3). This solvent is used, since solvents containing hydrogen atoms will interfere with the obtained spectrum. The sample was loaded in a 400MHz Agilent NMR spectroscope. Te number of scans was set to 256, with a acquisition time of 2.5 seconds, a relaxation time of one second and a pulse width of 45 degrees. A pulse width of 45 degrees was used as this significantly lowers to total measuring time compared to 90 degrees, which gives the maximum signal [92]. Fig. 3.12 shows the molecular structure of di-acrylated Pluronic F127 and the chemical shift if different hydrogen nuclei in the NMR spectrum [95]. As discussed in Sec. 2.5, Pluronic F127 molecules consists of 65 PPO blocks. Every PPO blocks consists of propylene oxides with three hydrogen atoms on the outer carbon (shown as ”b” in Fig. 3.12). These hydrogen atoms show up in the spectrum at 1.1 ppm. Simultaneously, the protons of the vinyl groups on the terminal ends (”c”, ”d” and ”e”) show up at 5.8-6.4 ppm. Because the number of protons in each of those structures is known, the intensities of the spectrum can be compared to determine the degree of acrylation. The peak corresponding to the propylene oxide units resembles 195 protons (65 PPO blocks with three protons each). The peaks corresponding to the vinyl groups should resemble six protons (three on each terminal end). Based on the known value of the propylene oxide protons, the number of protons for the vinyl groups can be calculated. This resulting number can be compared to the desired number of six protons to determine the degree of acrylation. The degree of acrylation was calculated according to Eq. 3.2:

$$D_A = \frac{(Protons_{propyleneoxide} * I_{vinyl})/I_{propyleneoxide}}{Protons_{vinyl}} * 100 \tag{3.2}$$

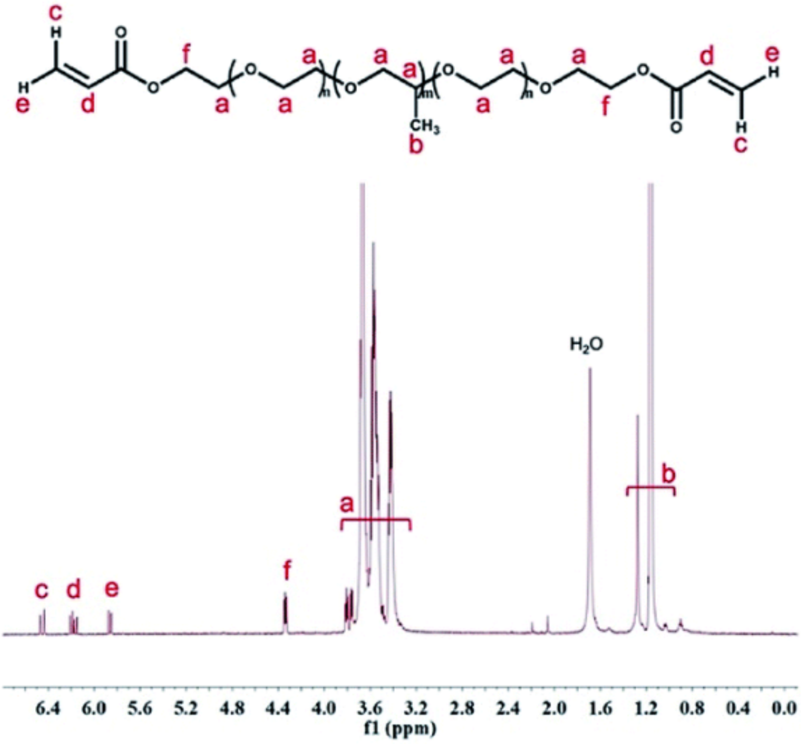

Figure 3.12: The molecular structure of di-acrylated Pluronic F127 and the NMR spectrum of this molecules with peaks corresponding to different protons. Horizontal axis: chemical shift in ppm. Vertical axis: Intensity of retrieved signal [95].

Where D_A is the degree of acrylation, I the intensity of the respective peaks in the NMR spectrum and protons the theoretical number of protons in each group.

3.2.2.3. Responsive Surface Methodology

The results from Lee et al. (2007) showed that di-acrylated Pluronic F127 hydrogel exhibit a lower degradation rate compared to conventional Pluronic F127 hydrogels [76]. Simultaneously, Di Biase et al. (2011) showed that di-acrylated Pluronic F127 hydrogels exhibit thermoreversible properties after photo-polymerization when photo-polymerization was performed at low temperatures [77]. However, both research groups used different a photo-initiator (concentration) and UV intensities. Therefore, it remains to be determined if di-acrylated Pluronic F127 hydrogels synthesized according to Lee et al. (2007) exhibit thermoreversible properties for low photo-polymerization times and temperature as well. To test the influence of photo-polymerization- time, temperature and photo-initiator concentrations on the degradation rate and thermoreversible properties of di-acrylated Pluronic F127 hydrogels, the responsive surface methodology was utilized as described by Boutry et al. (2010) [96]. The photo-initiator concentrations was between 0.1 wt% and 0.3 wt% with 0.2 wt% as center point. The temperature had a center point of 20°C and a range between 3°C and 30°C. Normally, 10°C would be the lower point in this method, but 3°C was chosen as a lower value as this simplified the protocol since hydrogels could simply be placed in the fridge. The polymerization times were between two and ten minutes, with five minutes as center point. Therefore, the center point include 0.2 wt% of photo-initiator, a temperature of 20°C and an UV exposure time of five minutes. The fractional factorial points are located according to the extreme values mentioned previously. Due to a lack of available di-acrylated Pluronic F127, the axial points were not used. Fig. 3.13 shows the Box-Wilson central composite design with center-, fractional factorial- and axial points.

After photo-initiator was added, the hydrogels were mixed using a vibrations shaker for two minutes and stored in aluminum foil until photo-polymerization. Each of the measurement corresponding to a center or fractional factorial point was performed three times. The degradation rate after seven days was used as a dependent variable and measured as described in Sec. 3.2.3.3.

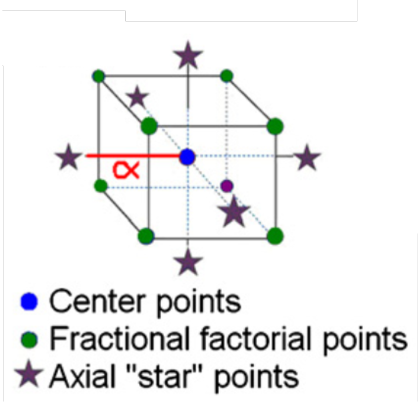

Figure 3.13: The Box-Wilson Central Composite Design including center- fractional factorial- and axial- points [96].

3.2.3. Characterization

The characterization of all hydrogels was performed through four different methods. The mechanical properties of the hydrogels were analyzed using rheometry and differential scanning calorimetry, as these methods are able to identify the mechanical properties with varying temperatures. To determine the viability of the hydrogels for the application as a transient barrier for vascularized cortical Organoids-on-a-Chip, the hydrogels were tested for their degradation- and permeability rate in PBS at 37°C.

3.2.3.1. Rheometry

The Pluronic F127 and F127DA hydrogels were all characterized using rheometry. Rheometry enables the identification of the viscosity and gelation temperatures for each hydrogels. The rheometer used was a TA Instruments AR-G2 with a parallel plate setup. The diameter of the plate was 40mm and gap size used between the rotor (top plate) and Peltier plate (bottom plate) was set to 300 µm. The Peltier plate is used to enable the cooling and heating of the samples. For the viscosity characterization of Pluronic F127 hydrogels, a rotational temperature ramp was used. The applied stress on the rheometer was kept constant at 10 Pa (for 15, 20 and 25wt%) and increased to 100 Pa for 20 wt%. This increase was done, since 10 Pa appeared to be too low for the rheometer to rotate the sample with a concentration of 30 wt%. While the rheometer was rotating, the temperature was increased with a rate of 8°C/min, from 0°C to 40°C. This gives the change in viscosity of the hydrogels with changing temperatures.

To test the gelation temperature of F127 hydrogels, an oscillatory temperature ramp was used. The shear stress was kept constant at 10 Pa, with a oscillation frequency of 1 Hz. Simultaneously, the temperature was increased with a rate of 8°/min. The temperature at which the storage modulus exceeds the loss modulus was considered to be the gelation temperature of that sample. An example is shown in Fig. 2.14b.

3.2.3.2. Differential Scanning Calorimetry (DSC)

Besides Rheometry, differential scanning calorimetry (DSC) was also used to determine the behavior of Pluronic F127 hydrogels with changes in temperature. A major difference compared with rheometry, is that DSC does not identify the gelation temperature of the hydrogels, but the micellation temperature [97]. The micellation temperature is significantly lower than the gelation temperature and indicates the temperature at which the Pluronic F127 unimers fold and aggregate into micelles. A further increase in temperature will result in a close packing of micelles, which causes a gel to form [97]. This micellation temperature is useful, as it indicate the temperature after which the viscosity of the hydrogels starts to increase. Therefore, this can be useful as an indicative temperature below which it is easiest to inject the hydrogels in the microfluidic platforms. DSC can also identify a possible hysteresis pattern in the micellation temperature.

DSC was performed in a TA instruments Q2000. For Pluronic F127, three different concentrations were analyzed, being 15,20 and 25 wt%. The concentration of 30 wt% was discarded as it was already found to be too difficult to inject. For di-acrylated Pluronic F127, four concentrations were measured, being

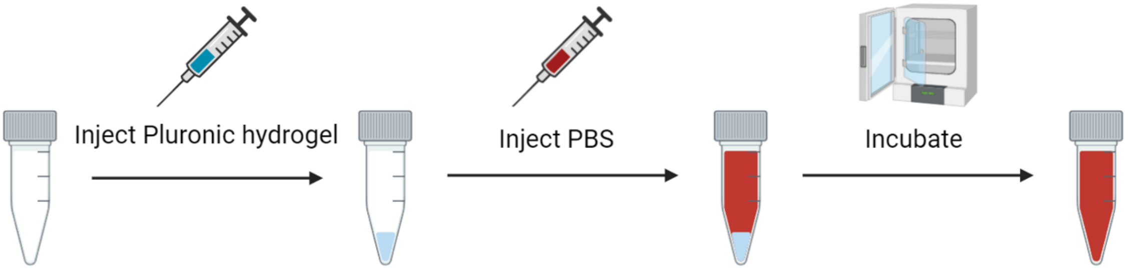

Figure 3.14: 0.3 ml of the Pluronic F127 based hydrogels were injected in 1.5 ml Eppendorf tubes. The hydrogels were allowed to form a hydrogel in the incubator at 37°C. Afterwards, 1.2 ml red colored PBS was injected on top of the hydrogel and placed back in the incubator. After several days, the hydrogel is completely dissolved into the surrounding PBS.

10, 15, 20 and 25 wt%. The samples were tested by comparing the heat flow through approximately 20 mg of hydrogel to a reference container filled with air. The samples were first kept isothermal at 40°C for two minutes, then the samples were cooled with 10°C/min to 0°C and kept at 0°C for two minutes. Finally, the samples were heated back to 40°C with 10°C/min and kept isothermal at 40°C for 2 minutes. The rate of cooling and heating was chosen as high heating rates results in sharper (and more distinctive) peaks in the final spectrum and it prevents influence of disturbance in the results.

3.2.3.3. Degradation Rate

As described in the literature review (App. F), the protocol for degradation testing differs significantly between research papers. Therefore, it was chosen to perform degradation testing uniformly for all samples using 1.5 ml Eppendorf tubes, where the remaining mass fraction was measured every two or three days. For all samples, the degradation rate was determined using 0.3 ml of hydrogel in 1.2 ml of PBS incubated at 37°C. The degradation testing will also include PBS refreshing to closely resemble the protocol used for the cortical organoid [64].

Degradation testing was done for three different concentrations of Pluronic F127 hydrogels (15, 20 and 25 wt%) and four concentrations of di-acrylated Pluronic F127 (10, 15, 20 and 25 wt%). The Pluronic F127 solutions were fabricated as described in Sec. 3.2.1 & 3.2.2. The di-acrylated Pluronic F127 hydrogels were mixed with 0.2 wt% of photo-initiator and photo-polymerized for five minutes at 20°C. 0.3 ml of the Pluronic hydrogels were injected at 4°C into 1.5 ml Eppendorf tubes. The Eppendorf tubes containing the Pluronic solutions were incubated at 37°C using an incubator (Binder CB-170 CO2/O2 Incubator) for 10 minutes to allow the Pluronic F127 solutions to form hydrogels. Subsequently, 1.2 ml of red colored (Dr. Oetker food colorant) PBS (pH 7.4, Sigma-Aldrich) was injected on top of the Pluronic hydrogels. The Eppendorf tubes were placed back in the incubator at 37°C. The PBS in the Eppendorf tubes was refreshed every 48 hours (or 72 hours over weekends). The remaining mass fraction (wet weight) of the Pluronic hydrogels was measured at every PBS refreshment moment. After a specific amount of time, the hydrogels were completed dissolved in the surrounding PBS. Every concentration was measured ten times for conventional Pluronic F127 and three times for di-acrylated Pluronic F127. The remaining mass fractions of the Pluronic hydrogels and the standard deviation was plotted against time. A schematic visualization of the degradation testing is shown in Fig. 3.14.

3.2.3.4. Permeability Rate

Permeability testing was done for three different concentrations of Pluronic F127 hydrogels (15, 20 and 25 wt%). 30 wt% was not used in degradation testing, since the viscosity of this concentration of hydrogel was too high. Therefore, the hydrogel could not be injected into the channels with a pipette anymore. The hydrogels were fabricated as described in Sec. 3.2.1 & 3.2.2. The hydrogels (4°C) were injected into the testing platform described in Sec. 3.1.1.2 using a pipette with 0.65 µl from both sides of the channels. This volume is slightly larger than half the volume of the channel. This causes the first injection to reach past the gap in the middle. The injection from the other side can be stopped when the channel is completely filled. Subsequently, the testing platforms were incubated at 37°C (Binder CB-170 CO2/O2 Incubator) for ten minutes to cause the Pluronic F127 solutions to form hydrogels. When hydrogels were formed in the channels, approximately 75 µl of red colored (Dr. Oetker food colorant)

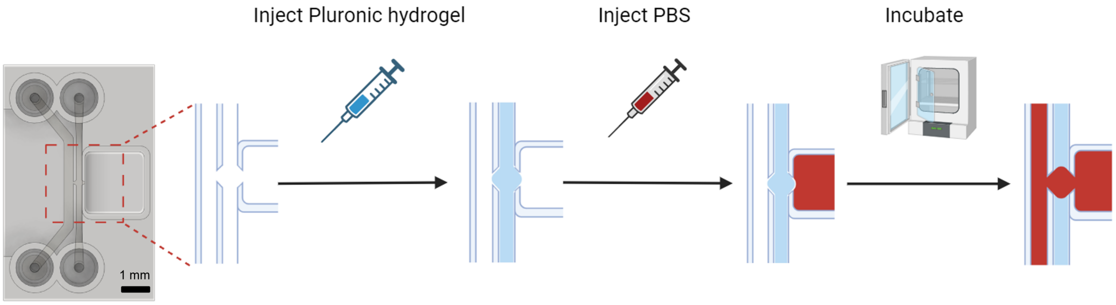

Figure 3.15: The testing platform was loaded with the Pluronic F127 hydrogel in the central channels. Afterwards the platform was incubated to allow the Pluronic solution to form hydrogels. The platform is injected with approximately 75 µl of red colored PBS. After several hours/days the red colored PBS can be found on the opposite side of the channel, indicating the permeation of the Pluronic F127 hydrogel.

PBS was injected in the central chamber. This volume was chosen as it is equal to the volume of culture media used in the cortical organoid protocol [64]. The percentage of remaining channels (not perfused by red PBS) was determined at numerous times, but at least every 24 hours (except over the weekend, due to access restrictions). Every 48 to 72 hours the PBS in the central chamber was refreshed. This was also done since the culture media of the cortical organoid is refreshed every 2/3 days [64]. For all three concentrations, the permeability test was performed with ten channels and the resulting percentage of remaining channels was plotted against time. A schematic visualization of the permeability testing is shown in Fig. 3.15.

3.3. Integration of biodegradable barrier on the OoC platform

To successfully integrated the synthesized hydrogels in the OoC platform, the channel geometry was modeled in COMSOL and injection testing was performed. The COMSOL model provided estimates on the injection velocity. Additionally, the influence of pillar shapes was determined on the breakthrough pressure (fluid pressure through the gaps of the pillar array) and velocity through the gaps of the pillars.

3.3.1. Simulation Model of Barrier Channel

COMSOL Multiphysics (version 5.1) was used to model the microfluidic barrier channel. This model was used to determine the optimal inlet flow rate to confine the hydrogel within its assigned channel and to determine the effect of pillar shape and gap size on the breakthrough pressure through the pillars. All simulations were performed based on obtained characteristic information of Pluronic F127 hydrogels with a concentration of 20 wt%. To determine the flow type in the simulation, the Reynolds number was calculated based on the obtained viscosity values from rheometry. The Reynolds number is defined as [98]:

$$Re = \frac{\rho_f V_{ch} D_h}{\mu} \tag{3.3}$$

Where Re is the Reynolds number, ρ_f is the fluid density in kg/m^3, V_{ch} is the velocity inside the channel in m/s, D_H is the hydraulic diameter in m and ρ is the viscosity in Pa. The hydraulic diameter for non-circular channels is defined as [99, 100]:

$$D_h = \frac{4A}{P} \tag{3.4}$$

Where A is the cross-sectional area in m^2 and P is the wetted perimeter in m. A Reynolds number below 1 resembles a creeping flow, where inertial forces are very small compared to inertial forces. A Reynolds number above 1 but below 2500 resembles a laminar flow. A flow with a higher Reynolds number is turbulent [101].

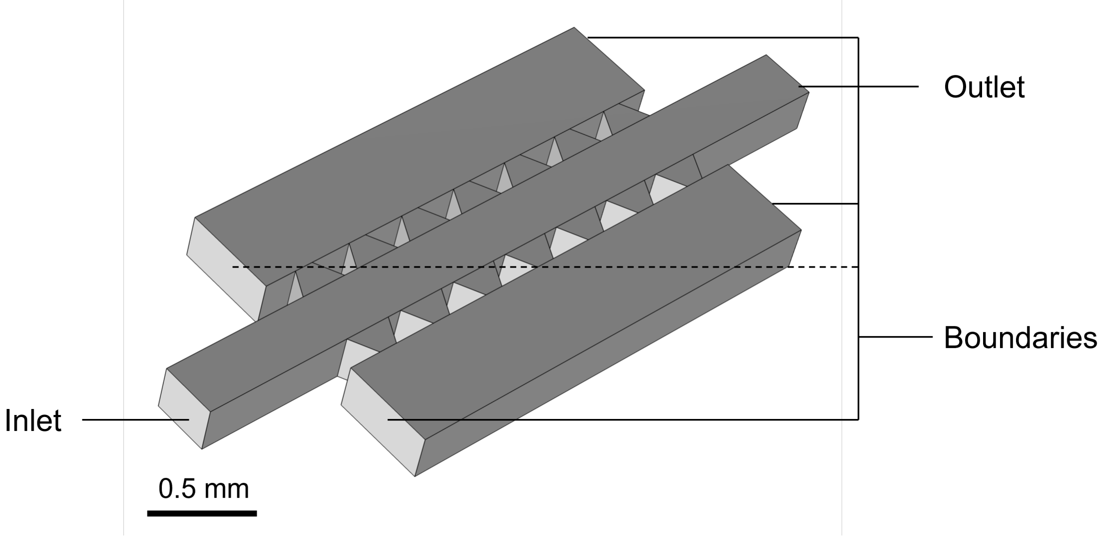

Figure 3.16: The COMSOL geometry used for simulations. The central channel has the same dimensions as the barrier channel on the OoC platform.

Fig. 3.16 shows the final geometry. The geometry has the same dimensions as the OoC injection platform described in Sec. 3.1.1.2. This means the the channel has a width of 300 μm, a height of 250 μm and a length of 2.5 mm. The gap width was set to 100 μm. The viscosity and density of the fluid were based on obtained values from rheometry and the fluid was simulated as stationary. The reference pressure was set to one atmosphere. Therefore, the outlet pressure was set to zero (as this is relative). In this way, the outlet pressure is one atmosphere and allows for outflow of fluids. The simulation was performed with both opened- and closed- boundaries. The open boundaries allow for fluid in- and outflow and have a relative pressure of zero (one atmosphere). Closed boundaries do not allow in- or outflow of fluids. Both tests were done to simulate injection testing in the OoC platform. Normally, injection would be done while all the other in- and outlets of the OoC platform are opened. However, to aid in injection, the other in- and outlets could also temporarily be closed off. All other wall conditions were set to anti-slip.

3.3.1.1. Injection Flow Rate

To estimate the injection flow rate at which the hydrogel is confined in the barrier channel, the inlet flow rate was used as a variable parameter initially set to 1 mm^3/s. The flow rate was included in a parametric sweep of the model ranging for 1 mm^3/s to 100 mm^3/s with steps of 10 mm^3/s. Therefore, the simulation was done for all flow rates in this parametric sweep. After the simulation, the maximum breakthrough pressure at the gaps of the pillar array was determined. If the hydrogel should not break through the gaps, the breakthrough pressure should not exceed the capillary pressure [102]. The capillary pressure for circular channels is given by the Youngs-Laplace equation [103]:

$$P_{cap} = \frac{4\gamma cos(\theta)}{d_p} \tag{3.5}$$

Where P_cap is the capillary pressure in Pa, γ is the surface tension in N/m, θ is the contact at a three phase boundary, where the fluid, the continuous phase and the OoC platform material intersect. This formula adjusted for capillary gaps and the assumption the the contact angle is the same on all side of the channels is [104]:

$$P_{cap} = \gamma(\frac{2}{h} + \frac{2}{w})cos(\theta) \tag{3.6}$$

Where w is the gap width and h the height of the channel, both in meters. The surface tension of Pluronic F127 hydrogels with a concentration of 20 wt% at room temperature was found in literature

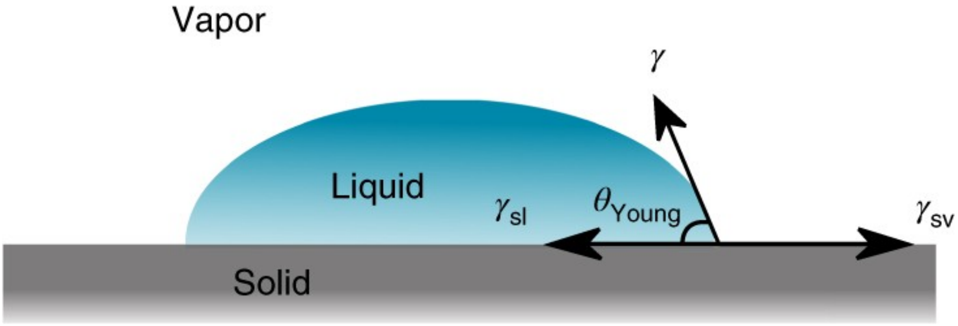

Figure 3.17: Three phase boundary contact angle of a fluid, with continuous phase and substrate material[108]

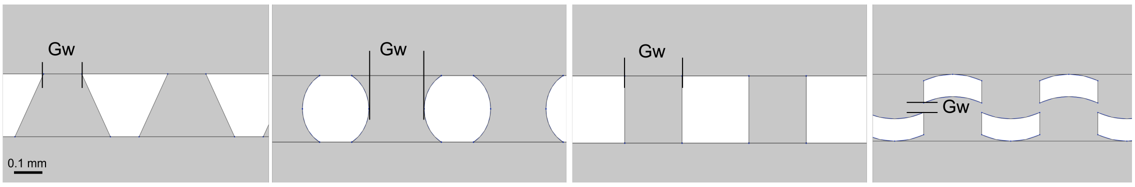

Figure 3.18: Different pillar geometries tested including triangles, circles, squares and curved. Grey = opened channels, White = pillars.

to be 40 mN/m [105, 106, 107]. The contact angle was determined as shown in Fig. 3.17. A droplet of 20 wt% Pluronic F127 hydrogel was placed on the surface of OoC platform fabrication with Moiin tech clear. The contact angle was determined optically and the average contact angle of six tests was used to determine the capillary pressure. In the used COMSOL simulations the flow rate for which the breakthrough pressure through the pillars did not exceed the capillary pressure could be determined. The injection velocity could then be estimated according to Eq. 3.7:

$$v_i = \frac{Q}{A} \tag{3.7}$$

Where v_i is the injection velocity in m/s, Q the flow rate in m^3/s and A the cross-sectional area of the injection device (syringe/pipette) in m^2.

3.3.1.2. Influence of Pillar Shape and Gap Width

The COMSOL model was also used to determine the influence of pillar shape and gap width. Four different pillar shapes were tested: triangles, squares, circles and curves (Fig. 3.18). The triangle shaped pillar are the same as used in the fabricated OoC platform as described in Sec. 3.1.1.1. Triangle pillar shapes are frequently used in vasculature on a chip [55, 99]. However, other research groups utilize other pillar shapes and gap widths compared to the OoC platform used in this work. Salmon et al. (2022) used triangular shapes but decreased the gap size to 50 µm [55], Nashimoto et al. (2017) used longer pillars [49], while Yu et al. (2024) also utilized just a single gap (capillary burst valve) [99]. Pisapia et al. (2022) and Tomecka et al. (2018) tested the effects of circular pillars in microfluidics [109, 110]. Last, Barbato et al. (2021) and Manneschi et al. (2016) used curved pillar arrays with smaller gap sizes for vascular mass transport [111, 112]. Squared pillars are not frequently used in vasculature on a chip, but still included in the simulation. The goal of changing the pillar array is to confine the hydrogel within the barrier channel. Most pillar arrays are used as they are more suitable for the growth of vasculature networks. Since this is not the case for this microfluidic channel, the squared pillars are included as comparison.

In this simulations the gap width was set to 25 µm as a parameter. This parameter was then included in a parametric sweep, similar to the inlet flow rate as described in Sec. 3.3.1.1. The maximum gap width was 150 µm, with interval steps of 25 µm. Based on these parameters, the breakthrough pressure for each pillar array could be determined for different gap widths and inlet flow rates. For the curved pillars, the gap width was not inputted as a parametric sweep. Instead, the gap width was set at 25 µm.

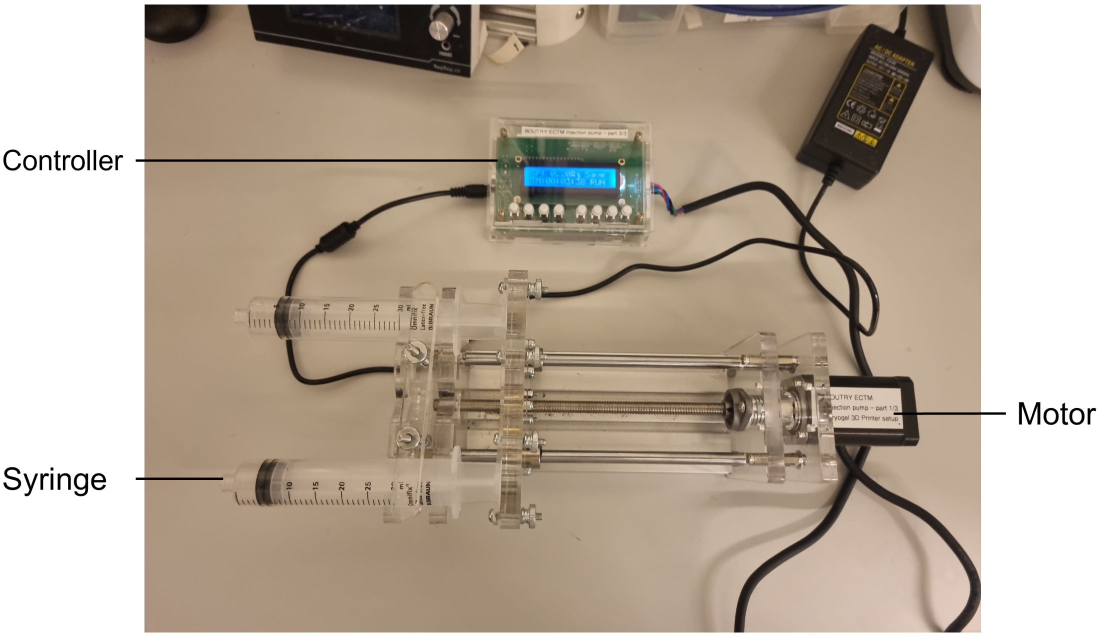

Figure 3.19: Injection pump used to achieve injection velocities in the range of 0.1 mm/s.

3.3.2. Injection Method

Injection testing was done to determine an optimal injection protocol for the Pluronic F127 hydrogels in the barrier channel. Five different parameters were tested: the injection method, temperature, volume, speed and number of gaps. All parameters were tested with a 20 wt% Pluronic F127 hydrogel using a mechanical pipette according to the forward pipetting technique [113]. In this method, uptake of liquid is done by pressing the button the first stop and discharge of the liquid is done by pressing down to the second stop.

Two different methods of injection were tested: gravitational and sealing. The gravitational injection method was done by injection of the hydrogel into the inlet chamber and allowing it to flow down through the channel. The sealing method was done by placing the tip of the pipette down into the inlet chamber and letting the weight of the pipette rest on the tip. This creates a seal between the cone shaped inlet chamber and pipette tip. Once injected, the hydrogel was forced down through the channel.

The injection temperature was tested for 4°C (below micellation and gelation temperature), room temperature (above micellation and below gelation temperature) and 30°C (above micellation and gelation temperature). To achieve these temperatures, hydrogels were placed in the fridge at 4°C or in the oven at 30°C. After the temperature was reached, the hydrogels were immediately used for injection testing. The volume of injection was tested by systematically increasing the injection volume from 0.5 μl to 1 μl. The injection speed was tested according to the obtained values from the COMSOL simulations. This was done using a velocity-controlled pump show in Fig. 3.19. This pump was able to achieve injection velocities as low as 0.1 mm/s. Last, the injection with a different number gaps was done for eight gaps (injection testing platform) and one gap (permeability testing platform).

4

Results

4.1. Organ-on-a-chip Platform for Vascularized Cortical Organoids

The fabrication of the OoC platform using DLP printing with the Moiin Tech Clear with the Asiga MAX 3D printer resulted in repeatedly similar printed structures. Below are the results from the configuration of Detax Freeprint Ortho, fabrication using PDMS molding and the dimensional accuracy of fabricated platforms with Moiin Tech Clear, Detax Freeprint Ortho and PDMS shown.

4.1.1. Detax Freeprint Ortho Initiator File Configuration

The configuration for Detax was successfully performed for curing thicknesses between 0.04 mm and 1.3 mm, resulting in a complete Z-curing table. The full Z-curing table is shown in App. B. The Z-curing table was uploaded in the initiator file, after which the step structure were printed for three different slice thicknesses. The resulting step structure printed with a slice thickness of 0.1 mm is shown in Fig. 4.1a. The XY-dimensions of the step structures were measured and plotted against the nominal values. The resulting XY-shrinkage (gradient) and XY-growth are shown in Tab. 4.1. It can be seen that the XY-shrinkage was 1 for a slice thickness of 0.1 mm and 0.99 for a slice thickness of 0.05 and 0.025 mm. This indicates that the printed step-structures had a minimal shrinkage compared to the nominal values. The average of the XY-shrinkage was used as the XY-scale in the initiator file. It should be noted that the smallest measured feature on the step-structure was 5 mm. Therefore, the step-structure used might not be representative for the small features used in the OoC platform.

After the configuration, the Detax Freeprint Orhto resin was first tested using Asiga Universal- and UltaGloss building trays. The UltaGloss building tray was used as it directly polishes the prints surfaces and provides clear and transparent parts [114]. The tested OoC platform for printing were the injection testing platforms as described in Sec.3.1.1.2.

4.1.1.1. UltraGloss Building Tray

3D printed platforms fabricated with Detax Freeprint Ortho with the same dimensions as used in printing with Moiin Tech Clear deformed under applied pressure from pressurized air. This required platforms made with Detax Freeprint Ortho to have a larger wall- (x2) and bottom layer (x3) thickness. Additionally, the viscosity of Detax Freeprint (1 Pa.s) is slightly higher compared to Moiin Tech clear (0.8 Pa.s) [115, 116]. Therefore, channel height was increased to allow for easier flushing of the channels. With a

Table 4.1: Detax Freeprint Ortho XY-shrinkage and XY-growth

	Slice Thickness [µm]			
	100	**50**	**25**	**Average**
XY-shrinkage	1	0.995	0.994	0.996
XY-growth	NA	0.007	0.014	NA

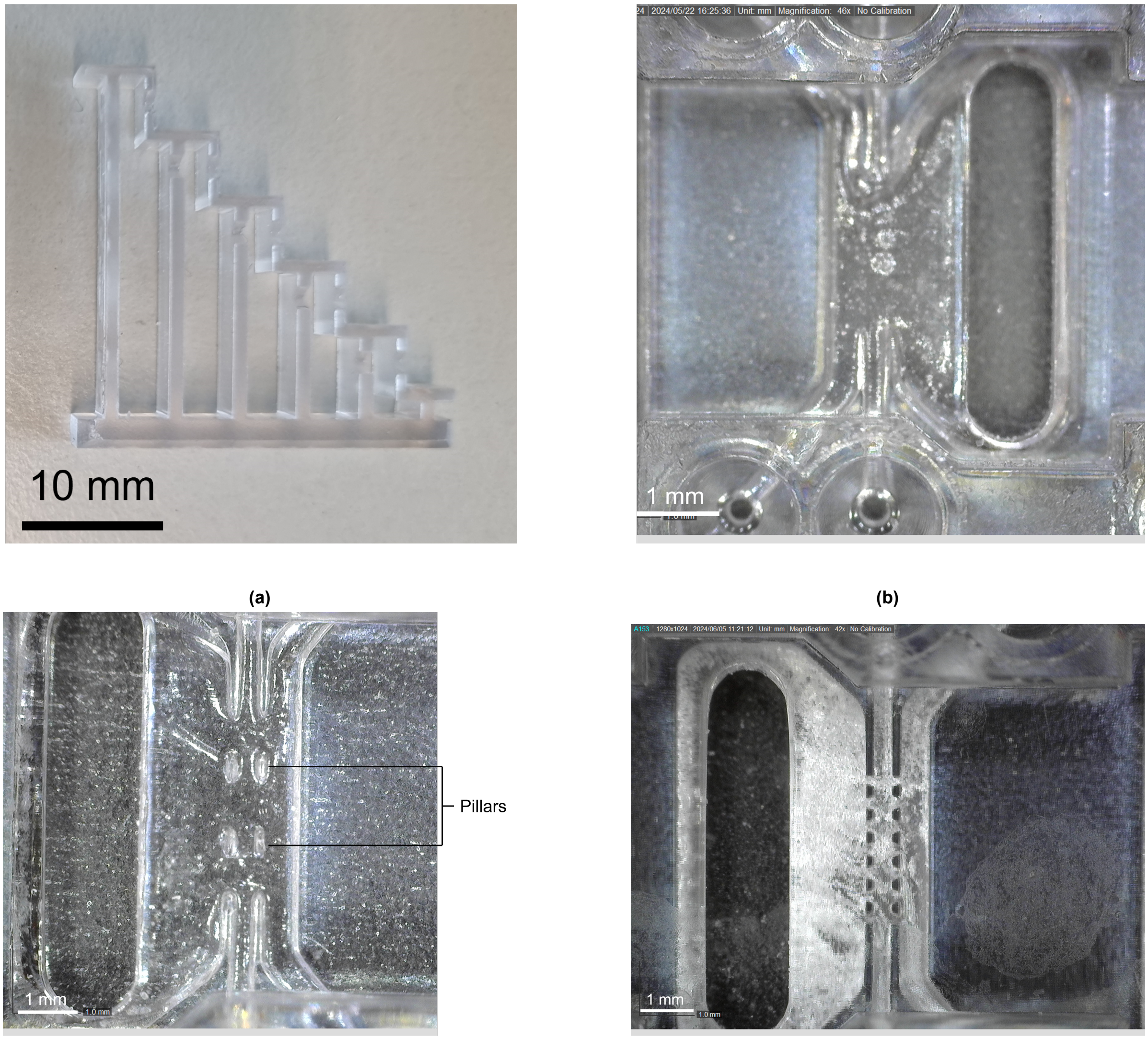

(a) **(b)** **(c)** **(d)**

Figure 4.1: (a) The hollow step structure printed with Detax Freeprint Ortho with at slice thickness of 0.1 mm. (b) Test print using Ultragloss building tray, with a channel height of 0.4 mm. (c) Test print using Ultragloss building tray, with a channel height of 0.4 mm and increased pillar size. (d) Test print using Universal building tray with channel height of 0.4 mm.

channel height of 0.4 mm (compared to the original 0.25 mm with Moiin Tech Clear), the channels could repeatedly be flushed and completely opened. Printing with the Asiga UltraGloss building tray resulted in improperly printed pillar arrays for normal pillars (Fig. 4.1b) and for enlarged pillars (Fig. 4.1c). It can be seen that the pillars are printed. However, they did not have the structure they should have. Printed pillars should have the structure shown in Fig. 4.1d, which are triangular shaped.

4.1.1.2. Universal Building Tray

3D printed platforms fabricated with Detax Freeprint Ortho were also tested in an Asiga Universal building tray. Fig. 4.1d shows the prints made with this building tray with a channel height of 0.4 mm. It can be seen that using this building tray, the small features of the platform are accurately printed. This worked repeatedly for channel height of 0.35 mm and higher. Printed platforms with the original 0.25 mm channel height were difficult to post-process, since significant amount of resin remained trapped in the channels.

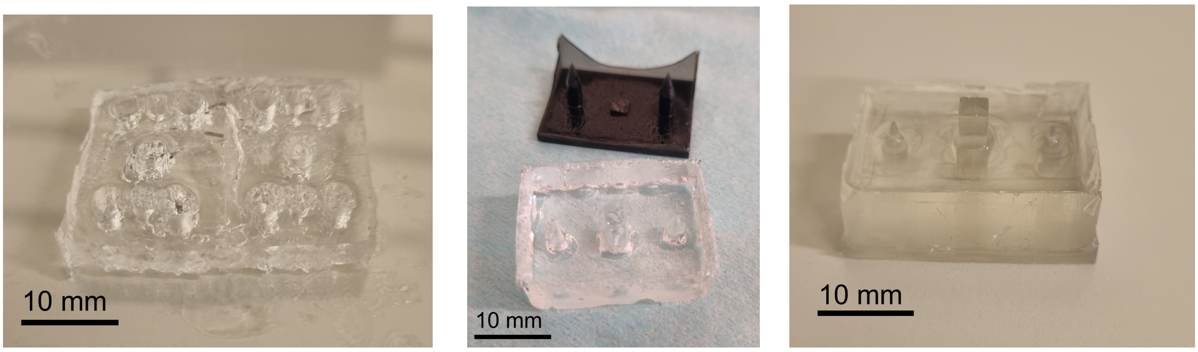

(a) (b) (c)

Figure 4.2: (a, b) demolded PDMS top layers using Sunlu Black molds. (c) PDMS top layer made with Moiin Tech clear molds.

4.1.2. PDMS Molding

PDMS molding was done with 3D printed molds made from Moiin Tech Clear. Initially, Sunlu Black resin was used, but molds made from this materials resulted in extremely sticky PDMS layers. The cure time for top layer molds was systematically increased by curing four at least four hours at 80°C, after which a mold was taken from the oven every 30 minutes and demolded. Even after eight hours of curing at 80°C and 35 hours at room temperature, the top layer molds were still sticky on the outside and hard to remove from the molds. Fig. 4.2a & b show demolded PDMS top layers. It can clearly be seen that the top layers are deformed and sticky on the outside. The deformation was caused by the fact that these layers had to be removed through excessive applied force. Moreover, all the top layer molds made with Sunlu Black were completely sacrificial. Not only did the outside walls needed to be broken off, the inside pillars also needed to be broken of from the bottom plate to completely demold the PDMS layer.

Fig. 4.2c shows a top layer of PDMS in a Moiin Tech clear mold where the outside walls were removed. It can be seen that this PDMS layer is fully cured and not sticky on the outside. Therefore, it was chosen to perform the PDMS fabrication with Moiin Tech Clear molds.

4.1.2.1. Fabrication Methods

The fabrication of the full OoC platform with PDMS was done using five different methods. Two methods were found to be optimal. This were method 1 and 3 as described in Sec. 3.1.2.3. Method 1 included separate molding of a top and bottom layer, which were bonded with oxygen plasma. Method 3 included punching of PDMS layers and bonding to glass. The results and findings of each method are discussed below.

1. The first option of fabrication was done by molding the top and bottom layer of the OoC platform and bonding those together using oxygen plasma. Using this method, the OoC platform was successfully fabricated as shown in Fig. 4.3a-c. Once the two layers were successfully bonded and aligned, the platform functioned as desired. Red-colored PBS was injected into the inlets, after which the PBS flowed through the channels. This process took several minutes to complete. Initially, the PBS stayed in the inlet, after which it proceeded to flow gradually through the channels (Fig. 4.3c). Please note that all the pillar arrays were fully opened, allowing the PBS to flow through all microfluidic channels. Although this method was successful, it is still prone to leakage and alignment errors. Leakage can be prevented by proper oxygen plasma bonding, while alignment can be improved using carefully designed alignment tools.
2. The second option utilized pillars which were separately printed from the bottom plate and outer walls. Although the demolding process of this method was significantly easier than other methods, the 3D printed molds remained sacrificial due to breaking of small pillar features in the bottom plate. The broken parts remained stuck in the bottom plate, which caused the bottom plate to be sacrificial as well. This could be prevented by increasing the smaller diameter of the pillars. However, this also compromises the desired inlet structure. Additionally, it was difficult to obtain the correct height of the top layer.

3. The third option was based on punching inlet holes in the top and bottom layer prior to bonding to glass. Initially, this was done by molding the top layer of the platform with a single pillar for the organoid chamber. The mold for the top layer was still sacrificial, as outer walls needed to be broken for successful demolding. Punching of the holes was done either prior to- or after bonding of the two PDMS layers. When punched prior to bonding, both layers needed to be accurately aligned, which could cause alignment errors. When punched after bonding, the bonded layers were very prone to delamination, since the force required to retrieve the puncher from the PDMS caused the layers to delaminate. After bonding and punching the layers were bonded to glass to seal of the microfluidic channels.
   Later, this option was changed by molding the top and bottom layer simultaneously using only the bottom molds in a plastic tray. The obtained PDMS layer could easily be cut out of the tray, after which inlet holes were punched in and the layers were bonded to glass. Bonding to glass repeatedly succeeded and was found to be stronger than PDMS-PDMS bonding with the bonding process used. Fig. 4.3d-f shows the successful fabricated microfluidic channels using this method. Compared to the first option, red-colored PBS flowed fast through the channels and completely filled everything within a few seconds (Fig.4.3f). Additionally, this using this method, the dimensions of the inlet chambers are different compared to the original OoC platforms. Where the original OoC platform contained inlet chamber which gradually decreased in diameter, OoC platforms fabricated using this method did not contain a decrease in diameter. Instead, the diameter was the same over the full height of the inlet chamber.
4. The fourth option was based on the division of the full OoC platform into six separate layers. This method was the least successful of all tried methods. Bonding of six separate layers made the OoC platform extremely prone to delamination and alignment errors. To overcome the latter, an alignment tool was used with inlet pillars on the correct place. However, numerous layers delaminated during fabrication. Moreover, printing six small layers without punching holes caused other difficulties. Because every mold had the exact inner dimensions, there was no room for shrinkage or deformation of the PDMS layers. It was found that many PDMS layers showed convex deformation at the interface of the PDMS and the molds. In other fabrication methods, the molds could be made wider and higher to create a margin for this. However, in this method this was not feasible. Therefore, the PDMS surface were not level at both sides, which caused difficulties with oxygen plasma bonding.
5. The last method included bonding of a DLP 3D printed top layer with a PDMS molded bottom layer. The fabrication of the top part was significantly easier than other methods as it did not have to be fabricated using PDMS molding. However, the alignment of the small inlets (0.3 mm) with the microfluidic channels was challenging. Moreover, the bonding between the 3D printed top part and PDMS molded bottom part was not strong and could easily be delaminated.

To summarize, two fabrication methods proved to be viable options for the fabrication of the OoC platform. Molding of the top and bottom layer with PDMS kept the original dimensions of the OoC platform intact but was prone to delamination. Molding of a single PDMS layer, punching holes and bonding to glass succeeded repeatedly, but had to compromise the original dimensions. Additional pictures of all fabrication methods are shown in App. C.

4.1.3. Dimensional Accuracy

For the successfully 3D printed OoC platforms and fabricated PDMS layers, with open inlets and channels, the dimensional accuracy was determined. To test if the DinoXcope microscope was accurate enough to determine the accuracy of manufactured OoC platforms, the gap width and width of four and six platforms respectively was compared with a Keyence VHX microscope. All platforms were printed with Moiin Tech Clear. The comparative results are shown in Tab. 4.2. It can be seen that the average measured values for both microscope have a neglectable difference. The average difference of measured gap width and channel width was 0.2 μm and 4.32 μm respectively. Therefore, the dimensional accuracy was continued with the DinoXcope microscope.

The dimensional accuracy was measured for 3D printed OoC platforms made with Moiin Tech clear and Detax Freeprint Ortho and molded PDMS layers. Tab. 4.3 shows the average measured values and percentage errors of the measured gap width and channel width. For a gap width of 100 μm

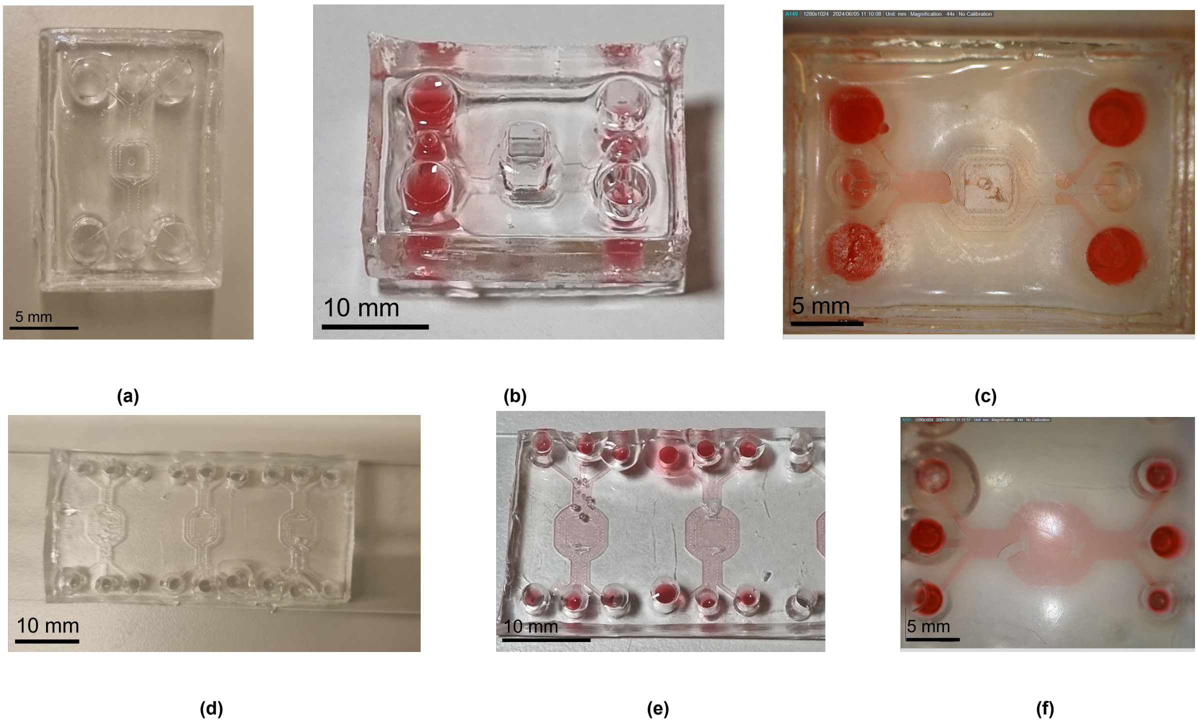

Figure 4.3: Successfully fabricated OoC platform using PDMS molding. (a) Top view of PDMS molded top and bottom layer. (b) Red-colored PBS injected in PDMS molded top and bottom layers. (c) Bottom view of gradual flow of red-colored PBS in PDMS molded top and bottom layers. (d) Top view of single PDMS molded layer bonded to glass. (e) Red-colored PBS injected in single PDMS molded layer. (f) Bottom view of completely filled microfluidic channels of single PDMS molded layer bonded to glass. The white unfilled areas are caused by deformations during bonding.

Table 4.2: Comparison of DinoXcope (x30) and Keyence vhx (x100) microscopes

Chip feature	**Theoretical value** [µm]	**Average measured value** [µm] [1]		**Average difference** [µm]	**Number of samples**
		DinoXscope	**Keyence vhx**		
Gap width	100	111.00 (8.04)	110.80 (4.06)	0.20	4
Width	300	282.33 (23.42)	286.65 (8.38)	4.32	6

[1] Standard deviation in brackets.

and a channel width of 300 µm all three fabrication methods showed similar results in accuracy. All measured gap widths were larger than the nominal values of 100 µm for all three methods, indicating that fabrication using DLP printing with the Asiga 3D printer with the parameters in the used initiator files has complications with printing smaller features than 100 µm. The measured channel widths of 300 µm had a deviation either above or below 300 µm for all three methods. Please note the difference in error between Tab. 4.2 and Tab. 4.3. The difference between theoretical values and measured values is smaller in Tab. 4.2. This difference was caused randomly, as six platforms were chosen randomly to determine the accuracy of the DinoXcope microscope with the Keyence microscope.

Beside the used gap width of 100 µm, two channels width a gap width of 80 µm and a single channel with a gap width of 50 µm were also tested. For either of these gap widths, the measured value was still above 100 µm. This support the previous statement about difficulties with printing features below 100 µm.

4.2. Biodegradable Barrier for Multi-Cells Culture of Vascular Networks and Cortical Organoids

Conventional and di-acrylated Pluronic F127 hydrogels were synthesized according to Sec. 3.2. Below are the results of synthesis and findings discussed.

Table 4.3: Dimensional accuracy of 3D printed chip with Moiin tech clear and molded PDMS with Sunlu black 3D printed molds tested with DinoXcope (x30)

Chip feature	**Theoretical value** [µm]	**Average measured value** [µm][1]	**Average percentage error** [%][1]	**Number of samples**
		Moiin Tech Clear 3D printed platform		
Gap width	100	128.52 (20.93)	28.52 (20.93)	21
Width	300	302.43 (37.19)	7.16 (10.04)	23
		Detax Freeprint Ortho 3D printed platform		
Gap width	100	123.5 (13.17)	23.5 (13.17)	12
Width	300	293.5 (30.63)	6.05 (8.33)	12
		Molded PDMS		
Gap width	100	132 (8.45)	32 (8.45)	8
Width	300	285 (13.08)	5.57 (3.46)	7

[1] Standard deviation in brackets.

4.2.1. Pluronic F127

Conventional Pluronic F127 hydrogels were made by measuring mass fractions of Pluronic F127 powder and dissolving in deionized water. This was done according to the cold method, where the powder was dissolved in water and mixed using a vortex mixer. It was found that simply storing the correct mass fractions of Pluronic F127 and deionized water in the fridge overnight resulted in complete dissolution as well. Although this is more time consuming, it is significantly less labor intensive. All Pluronic F127 hydrogels were made according to pre-defined weight percentages, with a scale accuracy of 0.1 mg.

4.2.2. Di-acrylated Pluronic F127 (F127DA)

The synthesis was performed twice, the second synthesis was performed to optimize the synthesizing steps. In the first synthesis, the yield of di-acrylated Pluronic F127 was 3.95 wt% with an amount of Pluronic F127 of 25 g (1.984 mmol). In the second synthesis, the amount for Pluronic F127 was lowered to 15 g (1.19 mmol). Moreover, the ratio of diethyl ether to solvent was increased and brought to a 1:5 ratio, which should increase precipitation. Filtration was done twice. The residue on the filter was retrieved and dried without vacuum at room temperature for three days. This resulted in 6 grams (0.470 mmol) of di-acrylated Pluronic F127. Therefore, the second synthesis resulted in a yield of 39.58 %. This is significantly higher than the yield of the first synthesis. However, both of these results are significantly lower than the yield of 80% found in literature [76].

The hydrogels were successfully produced by dissolving different amounts of di-acrylated Pluronic F127 in deionized water with the addition of photo-initiator.

4.2.2.1. Degree of Acrylation

The degree of acrylation was determined using H-NMR spectroscopy. Fig. 4.4 shows the obtained H-NMR spectrum of the synthesized di-acrylated Pluronic F127. The integration of the peak at a chemical shift of 1.1 ppm had a normalized intensity of 99.65 and the integration of all three peaks between 5.8 and 6.4 ppm had a normalized intensity of 1.74. The degree of acrylation was calculated by filling in Eq. 3.2:

$$D_A = \frac{(195 * 1.74)/99.65}{6} * 100 = 57\% \tag{4.1}$$

A degree of acrylation of 57% is lower than the obtained degree of acrylation of 98% in the followed protocol of Lee et al. (2007) [76].

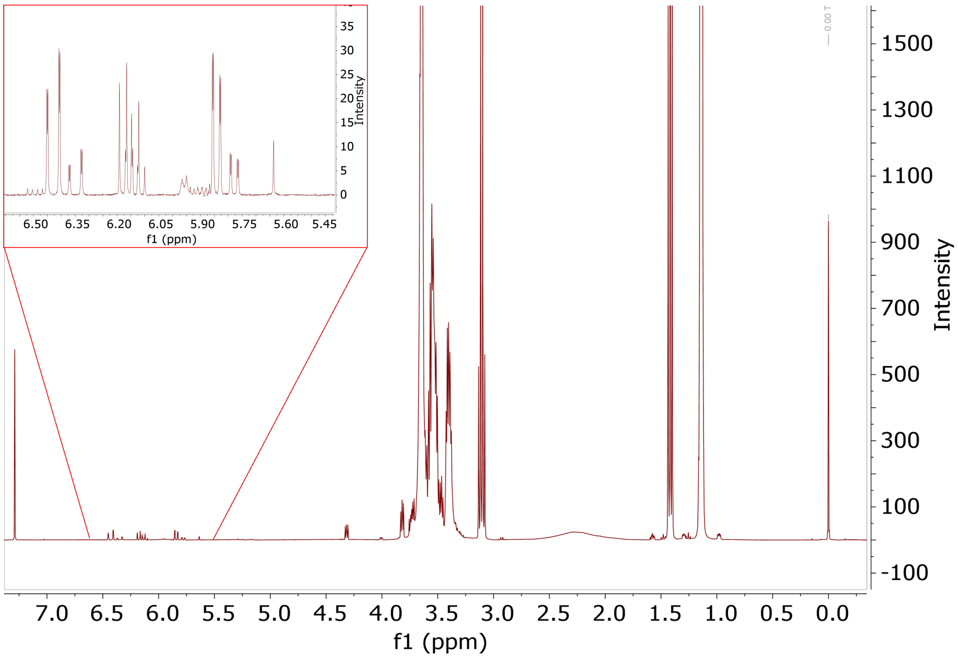

Figure 4.4: The obtained H-NMR spectrum of the synthesizes di-acrylated Pluronic F127. The peaks corresponding to the propylene oxide groups (5.8-6.4 ppm) are zoomed in.

4.2.3. Characterization

All the fabricated hydrogels were characterized using rheometry and differential scanning calorimetry. Additionally, the degradation rate of these hydrogels was determined by incubated in PBS at 37°C.

4.2.3.1. Rheometry

Rheometry was performed on Pluronic F127 and F127DA hydrogels to determine the gelation temperature of different concentrations. The results of four different concentrations (15, 20, 25 and 35 wt%) of Pluronic F127 hydrogels are shown in Fig. 4.5a-d. The results of four different concentrations (10, 15, 20, 25 wt%) of di-acrylated Pluronic F127 are shown in Fig. 4.5e-h. The gelation temperature decreases with increasing concentration. The gelation temperature of 15 wt% Pluronic F127 hydrogels is approximately 33°C, while the gelation temperature for 30 wt% is approximately 10°C. For all concentrations, the gelation temperature is clearly visible at the temperature at which the storage modulus exceeds the loss modulus.

The di-acrylated Pluronic F127 hydrogels with a concentration of 20 and 25 wt% showed similar results compared to the conventional Pluronic F127 hydrogels. However, the di-acrylated Pluronic F127 hydrogels with a concentration of 10 and 15 wt% did not form a gel in the used temperature range. Fig. 4.5e-f show that the storage modulus did not exceed the loss modulus at any given temperature. This indicates that the hydrogel remained in solvent state.

The viscosity of the same hydrogels were also measured using rheometry. The resulting viscosity over increasing temperature is shown in Fig. 4.6. It can be seen that the viscosity for F127 hydrogels (Fig. 4.6a) drastically increases after the gelation temperature, indicating that the hydrogel solutions have formed a stable gel. Especially, for the lower concentrations, the viscosity initially decreases with increasing temperature until the micellation temperature (discussed later). After this temperature the viscosity gradually increased until a fast increase after the gelation temperature. The lowest point of viscosity can be used as the injection temperature, as this temperature indicates the point of lowest viscosity and thus easiest injection. The exact micellation temperature is determined using differential scanning calorimetry. Additionally, it can bee seen that the viscosity increased with increasing concentration. The viscosity of 30 wt% F127 hydrogels is a tenfold higher than the viscosity of 15 wt% F127 hydrogels at 0°C. Therefore, lower concentrations are easier to inject at any given temperature. This indicates that for ease of use, the goal should be to find the lowest concentration hydrogel which is able to be used as a transient barrier for 35 days.

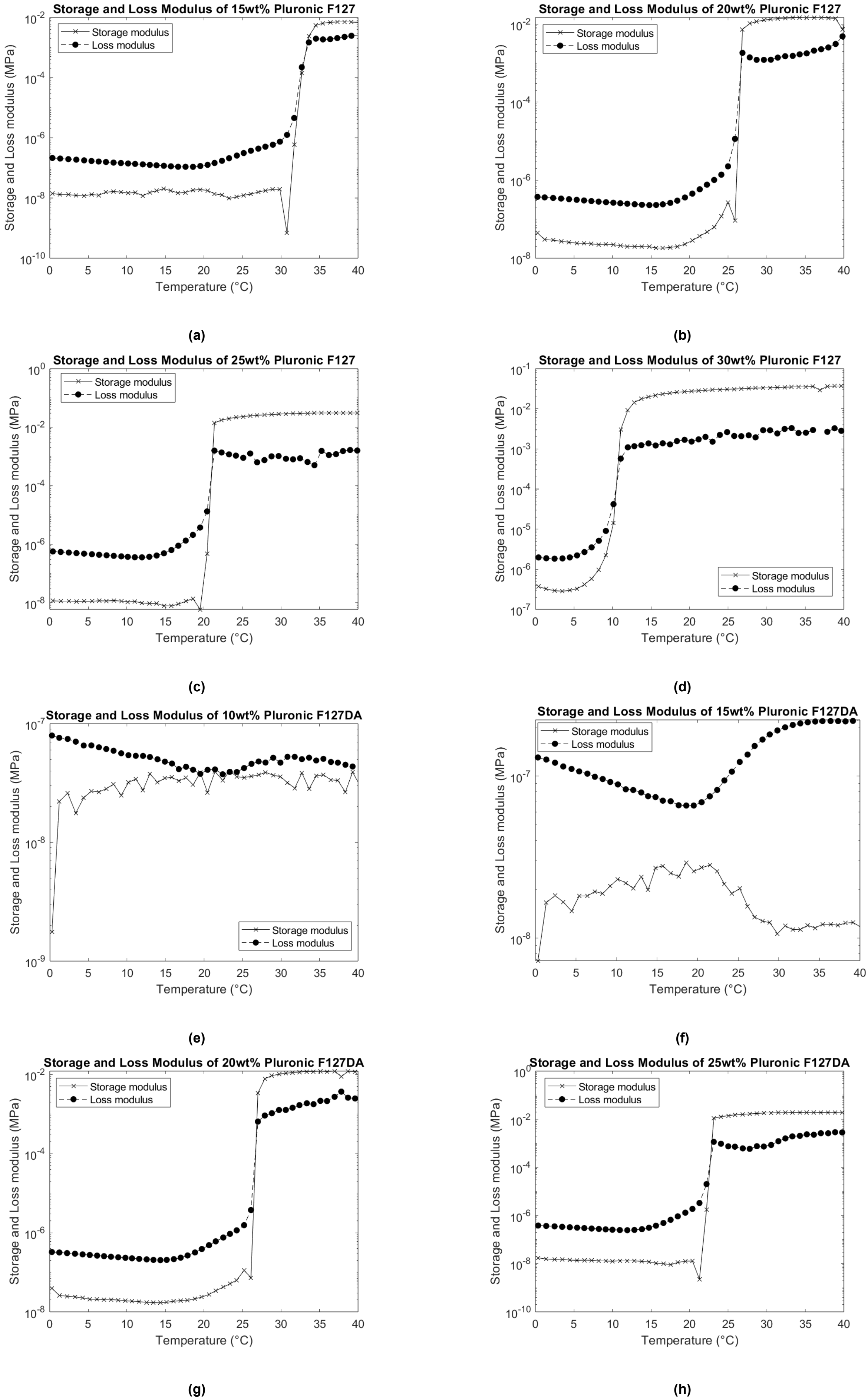

(a)

(b)

(c)

(d)

(e)

(f)

(g)

(h)

Figure 4.5: Storage and loss modulus of Pluronic F127 and F127DA hydrogels between 0 and 40 degrees with a concentration of (a) 15 wt% F127, (b) 20 wt% F127, (c) 25 wt% F127 ,(d) 30 wt% F127, (e) 10 wt% F127DA, (f) 15 wt% F127DA, (g) 20 wt% F127DA and (h) 25 wt% F127DA.

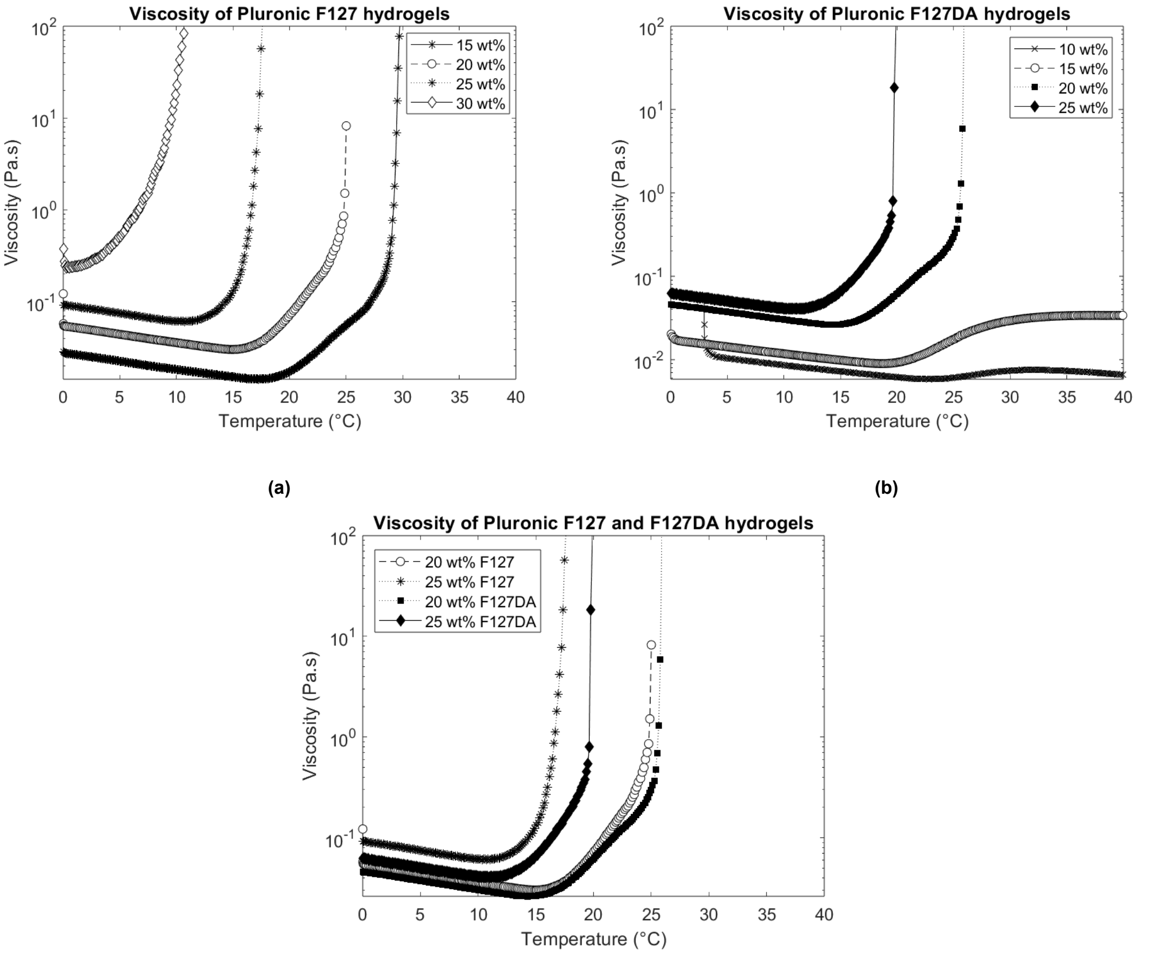

(a) (b)

(c)

Figure 4.6: (a) Viscosity of Pluronic F127 hydrogels with a concentration of 15 wt%, 20 wt%, 25 wt% and 30 wt%. (b) Viscosity of Pluronic F127DA hydrogels with a concentration of 10 wt%, 15 wt%, 20 wt% and 30 wt%. (c) Comparison of viscosity of F127 and F127DA hydrogels with a concentration of 20 wt% and 30 wt%.

For the F127DA hydrogels with a concentration of 20 or 25% the viscosity is similar to those found for Pluronic F127 hydrogels (Fig. 4.6c). After the gelation temperature, a fast increase in viscosity was observed for those hydrogels. For the F127DA hydrogels with a concentration of 10 and 15 wt% this was not the case. As indicated previously by the storage- and loss modulus, these hydrogels did not form a stable gel. This can also be seen in the viscosity in Fig. 4.6b. The viscosity of these hydrogels remains low for the used temperature range, indicating that the hydrogels remained in solvent state. However, it can be seen that there is a negative peak in the viscosity plot, which was coherent with the behavior of the other hydrogels.

4.2.3.2. Differential Scanning Calorimetry (DSC)

The exact micellation temperature (temperature of lowest viscosity) can accurately be found using DSC. DSC measures the heat flow through a sample. In Pluronic F127 hydrogels, a small and wide peak appears at the micellation temperature for a given concentration. This temperature indicates the point at which the Pluronic polymers fold, which requires heat. The DSC results of three concentrations of Pluronic F127 hydrogels are shown in Fig. 4.7. It can be seen that all three samples have both an exothermic (positive heat flow) and endothermic (negative heat flow) peak. The endothermic peaks indicate the micellation temperatures. The exothermic peaks indicate the point at which the Pluronic polymers unfold to their original state. All micellation temperatures are significantly lower than the gelation temperatures for a given concentration. The DSC results of three concentrations of di-acrylated

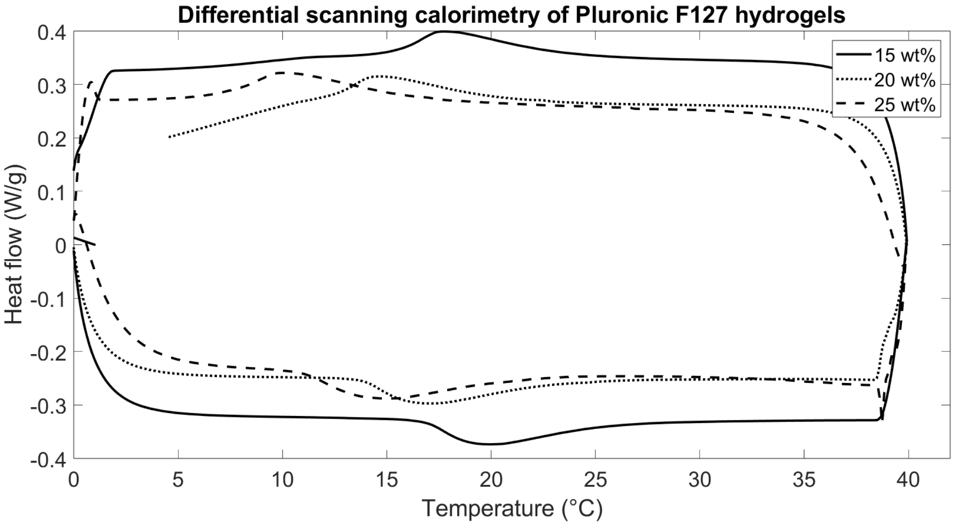

Figure 4.7: Differential scanning calorimetry of Pluronic F127 hydrogels with concentrations of 15, 20 and 25 wt%.

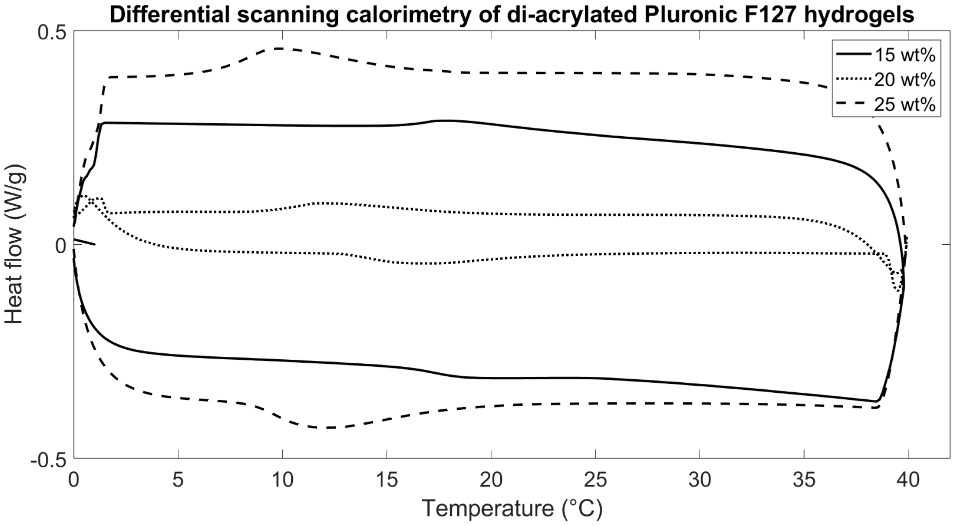

Figure 4.8: Differential scanning calorimetry of di-acrylated Pluronic F127 hydrogels with concentrations of 15, 20 and 25 wt%.

Pluronic F127 hydrogels are shown in Fig. 4.8. The results from the di-acrylated Pluronic F127 hydrogels are similar to those found for conventional Pluronic F127 hydrogels. However, it must be noted that all samples were tested three times, and for all shown samples only one sample gave results as shown. Other samples did not give a peak in the results or no representative results at all. Additionally, for the concentrations of 15 and 20 wt% of di-acrylated Pluronic F127 the shown peak is minimal.

The micellation- and gelation temperatures are shown in Fig. 4.9. Especially for lower concentrations, the micellation temperature is significantly lower than the gelation temperature. This indicate a increase in viscosity at a lower temperature than the gelation temperature. This is also confirmed in the viscosity plots, shown in Fig. 4.6. The di-acrylated Pluronic F127 hydrogels with a concentration of 10 and 15 wt% did not form a stable gel. However, the di-acrylated Pluronic F127 hydrogel with a concentration of 15wt% showed a minor peak in the DSC results, indicating that the Pluronic polymers do form micelles. If these results are compared with the results from the viscosity test, it can be seen that the temperatures of the peak and the lowest viscosity coincide. For example, for Pluronic F127 hydrogels, the peak in the DSC plot (Fig. 4.7) is at approximately 17°C. The lowest point of viscosity for this hydrogel is located at the same temperature (Fig. 4.6a).

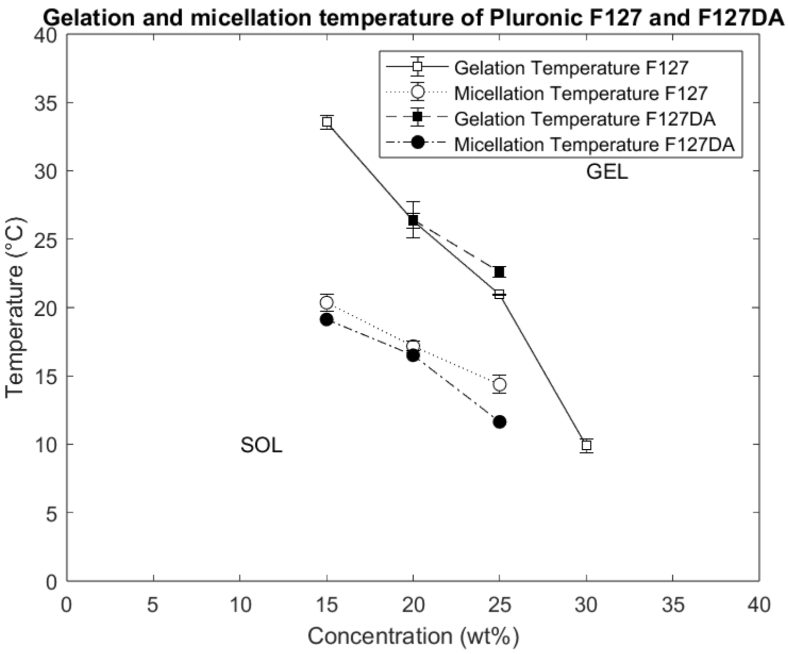

Figure 4.9: The Gelation and micellation temperatures of Pluronic F127 and F127DA hydrogels. The gelation temperatures of F127 and F127DA hydrogels are significantly higher than the micellation temperature for any given concentration. The gelation and micellation temperatures of F127DA hydrogels was found to be very similar to F127. F127DA hydrogels with a concentration of 15 wt% and lower did not form a gel in this temperature range.

Moreover, the DSC results also indicate a hysteresis pattern in the endothermic and exothermic peaks. For each concentration the temperature at which the polymers unfold (exothermic) is lower than the micellation temperature (endothermic). The exothermic peak indicate the temperature at which the hydrogels are at their lowest viscosity point again. Therefore, to remove hydrogels from the OoC platforms, the temperature should be lower than the exothermic peak for easiest removal.

4.2.3.3. Degradation Rate

The degradation rate of Pluronic F127 hydrogels was determined by injecting 0.3 ml of hydrogel and 1.2 ml of red colored PBS in Eppendorf tubes (Fig. 4.10). The hydrogel was injected first, allowed to form a stable hydrogel in an incubator and the PBS was injected afterwards. The Eppendorf tubes were placed in an incubator on 37°C. The degradation rate was determined by measuring the relative mass fraction of the hydrogels compared to the initial mass. The resulting degradation rates of Pluronic F127 hydrogels with a concentration of 15, 20 and 25 wt% and di-acrylated Pluronic F127 with a concentration of 10, 15, 20 and 25 wt% are shown in Fig. 4.11a and b respectively. At each indicated time point, the PBS in the Eppendorf tubes was refreshed. This was done every two or three days. From the results is visible that all hydrogel samples were completed degraded within ten days, where most of the samples were already fully degraded within seven days. Moreover, for the first five days, a large standard deviation is visible. This is caused by the significant differences in degradation of individual samples within the same concentration. Some samples were already fully degraded after two or five days, while other samples hardly showed any degradation at all. Last, higher concentration samples show a slower degradation rate compared to lower concentration samples. This is clearly visible at day two and five, where higher concentration samples perform better than the other concentrations. However, all concentrations degraded completely within ten days. No significant difference was found in the degradation rate between Pluronic F127 and F127DA. Both Pluronic hydrogels degraded within ten days. This suggests that a degree of acrylation of 57% is not enough to decrease the degradation rate of Pluronic F127 hydrogels.

4.2.3.4. Permeability Rate

Permeability testing was performed using 3D printer microfluidic chips, as discussed in Sec. 3.1.1.2. Three concentrations of Pluronic F127 hydrogels (15, 20 and 25 wt%) were injected in the central

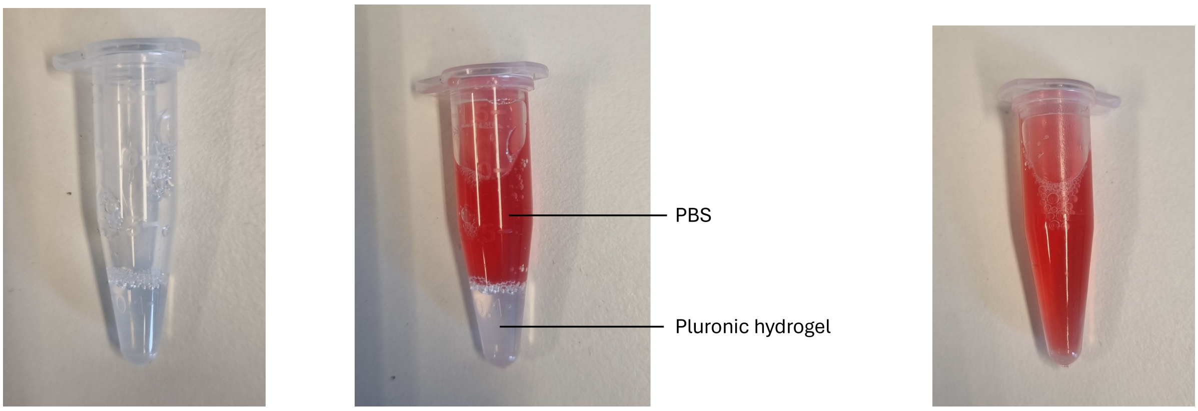

(a) **(b)** **(c)**

Figure 4.10: Degradation testing in Eppendorf tubes. (a) 0.3 ml of hydrogel is injected in an Eppendorf tube and allowed to form a gel in the incubator at 37°C. (B) Red-colored PBS is injected on top. (c) The hydrogel will degrade completely in the surrounding PBS

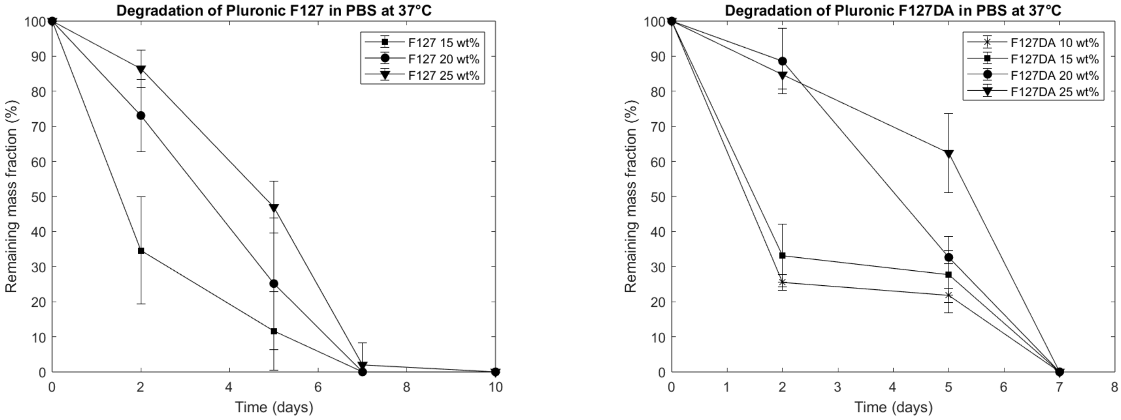

(a) **(b)**

Figure 4.11: (a) The degradation rate of three Pluronic F127 concentration (15, 20 and 25 wt%) in PBS at 37°C. (b) The degradation rate of four Pluronic F127DA concentration (10, 15, 20 and 25 wt%) in PBS at 37°C. The hydrogels with a higher concentration have a slower degradation rate.

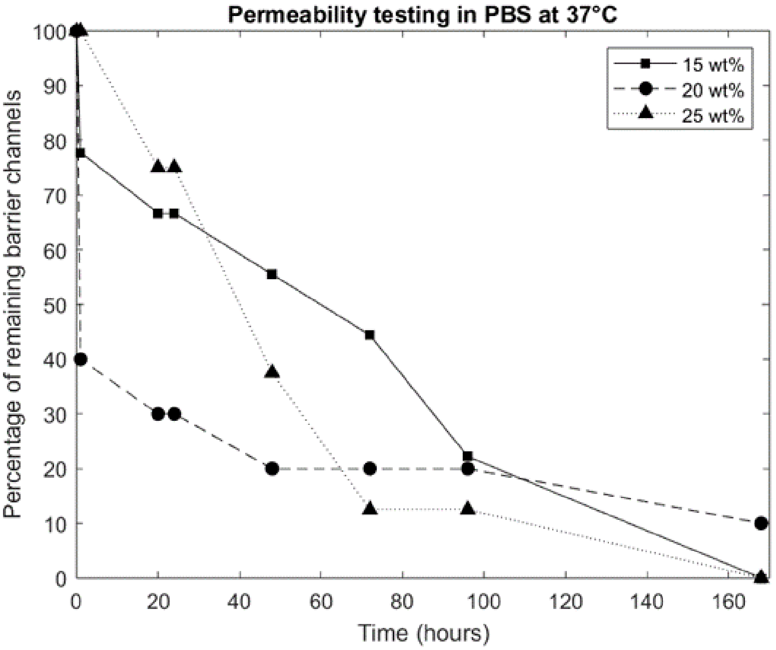

Figure 4.12: The permeability of four Pluronic F127 concentration (15, 20 and 25 wt%) in PBS at 37°C. The hydrogels with a lower concentration take longer until perfused. Nine, ten and eight channels were filled successfully for 15, 20 and 25 wt% respectively.

channel of these microchips at 4°C. For each concentrations, twelve channels were tried to fill. However, not all channels were successfully filled. Nine, ten and eight channels were filled successfully for 15, 20 and 25 wt% respectively. The hydrogels were allowed to form stable gels in the incubator, after which 70 µl of red colored PBS was injected in the organoid chamber. This volume is identical to the volume of growth media used by the vascularized brain organoid protocol [64]. The testing platforms were incubated in an incubator at 37°C The PBS was refreshed every two or three days. The hydrogels were considered to be perfused, when the red colored PBS was found in the empty channel on the other side of the hydrogel. The permeability rate of the hydrogels was determined by plotting the remaining percentage of non-perfused hydrogels. The results are shown in Fig. 4.12. It is visible that all (but one) channels were perfused within seven days (168 hours), where most of the channels were already perfused after four days (96 hours). Interestingly, the lower concentration samples showed fewer perfusion compared to the higher concentration samples. However, through the permeability testing, it was shown that Pluronic F127 hydrogels can effectively be used to temporarily block microfluidic channels. PBS from one side was effectively prevented from flowing to the other side.

4.3. Integration of Biodegradable Barrier on the OoC Platform

To successfully integrated the synthesized hydrogels in the OoC platform, the channel geometry was modeled in COMSOL and injection testing was performed.

4.3.1. Simulation Model of Barrier Channel

Based on the obtained viscosity values, a COMSOL model was developed to simulate the flow through the microfluidic channels. This was done to estimate the injection velocity needed to confine the hydrogel in the barrier channel. This injection velocity was further used in injection testing. Moreover, different pillar shapes were included in the simulation to determine the optimal pillar shape to confine the hydrogel in the barrier channel. For all simulations a Pluronic F127 hydrogels with a concentration of 20 wt% was used. At the lowest point, this hydrogel had a viscosity of 0.0302 Pa.s. The density was obtained by measuring the weight of 1 ml of 20 wt% Pluronic F127 hydrogel, which was 1.247 g. The flow speed was estimated at 1 mm/s. The Reynolds number can be obtained by filling in Eq. 3.3:

$$Re = \frac{1247 * 10^{-3} * 2.7 * 10^{-4}}{0.0302} = 1.126 * 10^{-2} \tag{4.2}$$

Where the hydraulic diameter was calculated using the dimensions of the microfluidic channel, which has a width of 300 μm and a height of 250 μm. The hydraulic diameter could then be calculated using Eq. 3.4:

$$D_h = \frac{4(3 * 10^{-4} * 2.5 * 10^{-4})}{2(3 * 10^{-4} + 2.5 * 10^{-4})} = 2.7 * 10^{-4} m \tag{4.3}$$

This gives a Reynolds number of $1.126 * 10^{-2}$, which makes it a creeping flow. This is a type of flow where the inertial forces are small compared to the viscous forces [101]. Using the Reynolds number, the viscosity and the density, the COMSOL simulation could be made.

Initially, the model was made with either open- or closed boundaries to simulate the flow in the microfluidic platform with open- or closed outlets. Fig. 4.13 shows the flow velocity in the microfluidic channels with open (a) and closed (b) boundaries. It can be seen that with open boundaries, the velocity is initially high, due to the inlet flow rate, but drops relatively fast, after which the velocity is low through the remaining of the channel. With closed boundaries, the velocity remains relatively high and rises again at the terminal end of the channel (Fig. 4.13a-b). This is caused by the fact that a stationary model in COMSOL assumes a fully filled environment. In the model with the closed boundaries, the fluid in the side channel could not flow away through the boundaries, which causes the pressure to build up everywhere in the microfluidic environment. It was found that the simulated maximum pressure in the simulation with closed boundaries was significantly higher compared to the maximum pressure in the open boundary simulation. When the direction of the velocity is plotted using surface arrows, it can be seen that in the closed boundary simulation, the velocity direction in the gaps at the terminal end is actually caused by fluid flowing back into the central channel, instead of the expected outflow (Fig. 4.13). Additionally, the arrow size is proportional to the velocity magnitude. In the simulation with open boundaries, the arrows direction is out of the boundaries, indicating that the open boundaries indeed allow for in- and outflow.

When injecting the hydrogel in the OoC platform with closed inlets, the air present in those channels should create an opposite pressure, containing the hydrogel in the channel. Since, with the used inputs this could not be accurately modeled, it was chosen to continue with the open boundary simulations.

4.3.1.1. Injection Flow Rate

The injection flow rate at which the hydrogel would be confined in the channel was estimated using the open boundary model. To estimate the injection flow rate, the capillary pressured needed to be calculated, which requires the contact angle between the fluid, the continuous phase and the OoC platform. This was obtained by placing a tiny droplet on the OoC platform and optically measuring the contact angle using the DinoXcope microscope as shown in Fig. 4.14. The average found contact angle of six tests was 36.31 degrees. Using the contact angle and the surface tension found in literature, the capillary pressure could be calculated using Eq. 3.6:

$$P_{cap} = 0.04(\frac{2}{2.5 * 10^{-4}} + \frac{2}{1 * 10^{-4}}) cos(36.31) = 902.52 Pa \tag{4.4}$$

Using the capillary pressure, the maximum inlet flow rate could be determined using the Comsol model. In the Comsol simulation, the inlet flow rate and gap widths were used as independent parameters. A parametric sweep was performed for inlet flow rates between 1 mm^3/s and 100 mm^3/s. Then, the maximum pressure through the gaps was determined. It was found that a breakthrough pressure of 902.52 Pa relates to an inlet flow rate of $3.17 * 10^{-8} m^3/s$. This estimate could be used to estimate the injection velocity. Ignoring any channel resistance, the inlet flow rate in the channel is similar to the flow rate in the syringe. The smallest available syringe had a diameter of 9.5 mm. Using this, the injection velocity could be estimated using Eq. 3.7:

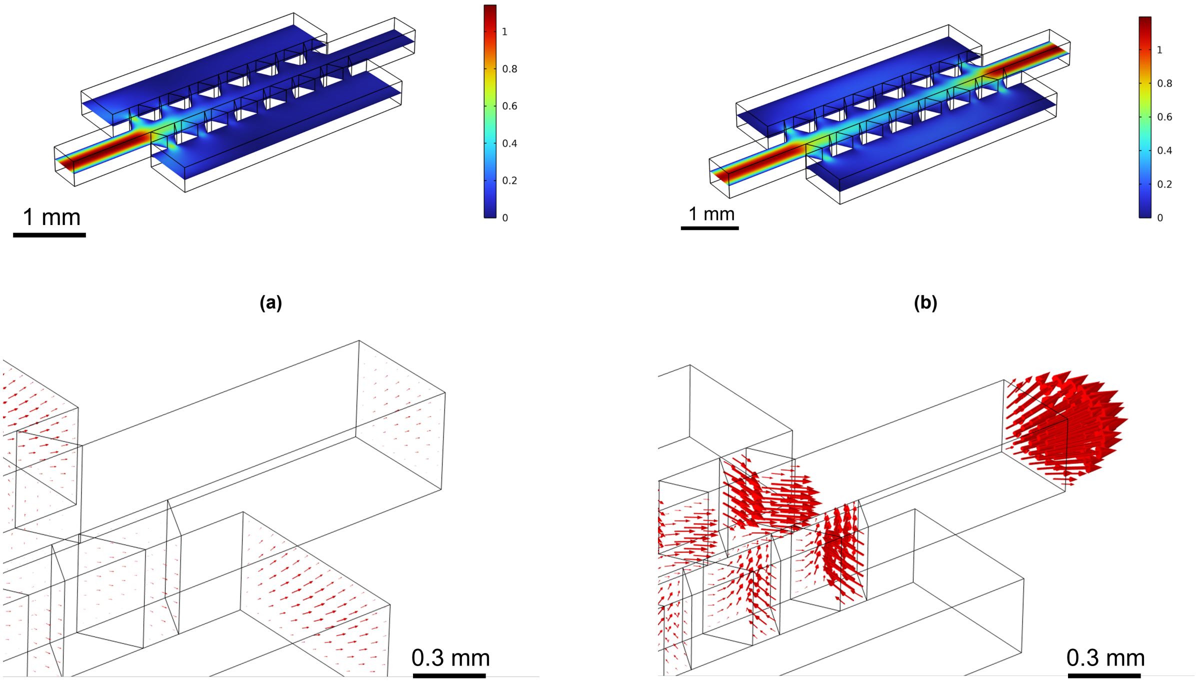

(a) (b) (c) (d)

Figure 4.13: Flow velocity simulation with open and closed boundaries with an inlet flow rate of $40 mm^3/s$ and a gap width of 100 µm. (a) Flow velocity (m/s) in microfluidic channel with open boundaries and (b) closed boundaries. (c) Surface arrow plot of indicating the direction of the flow in the microfluidic channel with open boundaries and (d) closed boundaries.

$$v_i = \frac{3.17 * 10^{-8}}{\pi(0.00475)^2} = 4.47 * 10^{-4} m/s = 0.447 mm/s \tag{4.5}$$

This injection velocity estimate was further used in Sec. 4.3.2.

4.3.1.2. Influence of Pillar Shape and Gap Width

The influence of pillar shape in breakthrough pressure through the pillars was determined for four different pillar shapes: triangles, circles, squares and curves. The maximum breakthrough pressure was determined using a cross-sectional slice at the gaps of the pillars. The inlet flow rate and gap width were used in a parametric sweep to determine the effect of those parameters on the maximum breakthrough pressure. Only for the curved pillar shape, the gap width was not used in the parametric sweep. Instead, the gap width was set to 0.25 mm. Using these parameters in a parametric sweep, a surface plot could be made to determine the influence. Fig. 4.15 shows the pressure in Pa for the circular shaped pillars with varying gap widths and inlet flow rates. It can be seen that the pressure through the gaps increases with an increasing gap width and flow rate. This suggests that a lower flow rate and gap width would easier confine the hydrogel in the barrier channel. The same was found for the velocity of the fluid through the pillars. Similar plots for maximum breakthrough pressure and maximum breakthrough velocity are shown in App. E. Interestingly, it was found that the breakthrough pressure and velocity increase with increasing gap width for the circular shaped pillars. However, for the triangular shaped pillars, the breakthrough pressure and velocity decreased with increasing gap width and for the square shaped pillars, the breakthrough pressure decreased with increasing gap width (same as circles) but the breakthrough velocity increased with increasing gap width (same as triangles). Fig. 4.16c and d show the breakthrough pressure and breakthrough velocity for triangular, circular and square shaped pillars. The triangular shaped pillars both have the highest breakthrough pressure and velocity, while the circular shaped pillars have the lowest breakthrough velocity and pressure. This difference is especially evident for gap widths below 50 µm. At gap width above 100 µm the breakthrough pressure

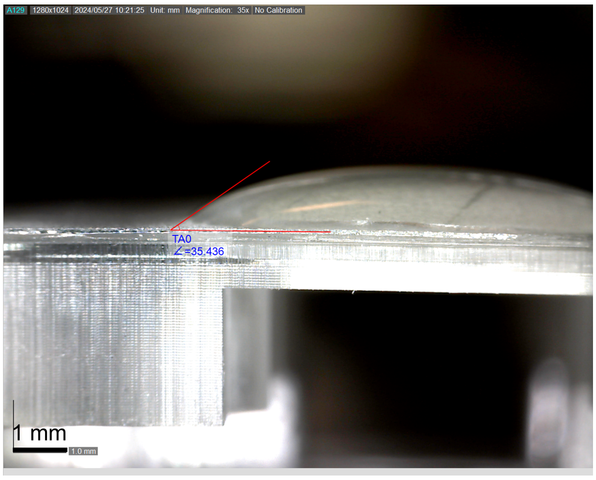

Figure 4.14: The permeability of four Pluronic F127 concentration (15, 20 and 25 wt%) in PBS at 37°C. The hydrogels with a lower concentration take longer until perfused.

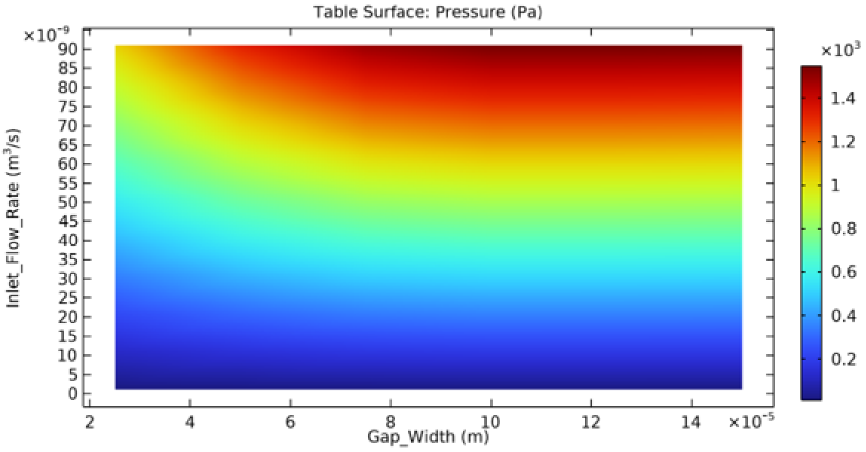

Figure 4.15: Maximum breakthrough pressure of circular shaped pillars with varying gap widths and inlet flow rates. The breakthrough pressure increases with an increasing gap width and inlet flow rate. This suggest that for circular shaped pillars a lower gap width and inlet flow rate can easier confine the hydrogels in the barrier channel.

and velocity for all pillar shapes approaches similar values. Therefore, for smaller gap widths, circular pillar shapes might actually perform better in confining the hydrogel in the channel.

Since, the used gap width of the OoC platform in this work is 100 µm, the maximum breakthrough pressure for this gap width was determined with varying inlet flow rate for three pillars shapes (triangles, circles and squares). Fig. 4.16a shows the results. It can be seen that the breakthrough pressure for any given inlet flow rate is highest for the triangle shaped pillars and lowest for the circular shaped pillars. This suggests that the triangular shaped pillars are the worst pillar shape of the three pillar shapes used in minimizing the breakthrough pressure. A higher breakthrough pressure might make it more difficult to confine the hydrogel within the channel. Furthermore, the maximum breakthrough pressure was also compared for a gap width of 25 µm (Fig. 4.16b). In this comparison, the curved shaped pillars were also included. It can be seen that for this gap width, the triangle pillar shape has a significantly higher breakthrough pressure compared to any of the other pillar shapes. Moreover, the circular shaped pillars perform similar compared to the curved shaped pillars. Combined results from both gap width suggest that circular shaped pillars are the best pillar shape to confine the hydrogel in the channel.

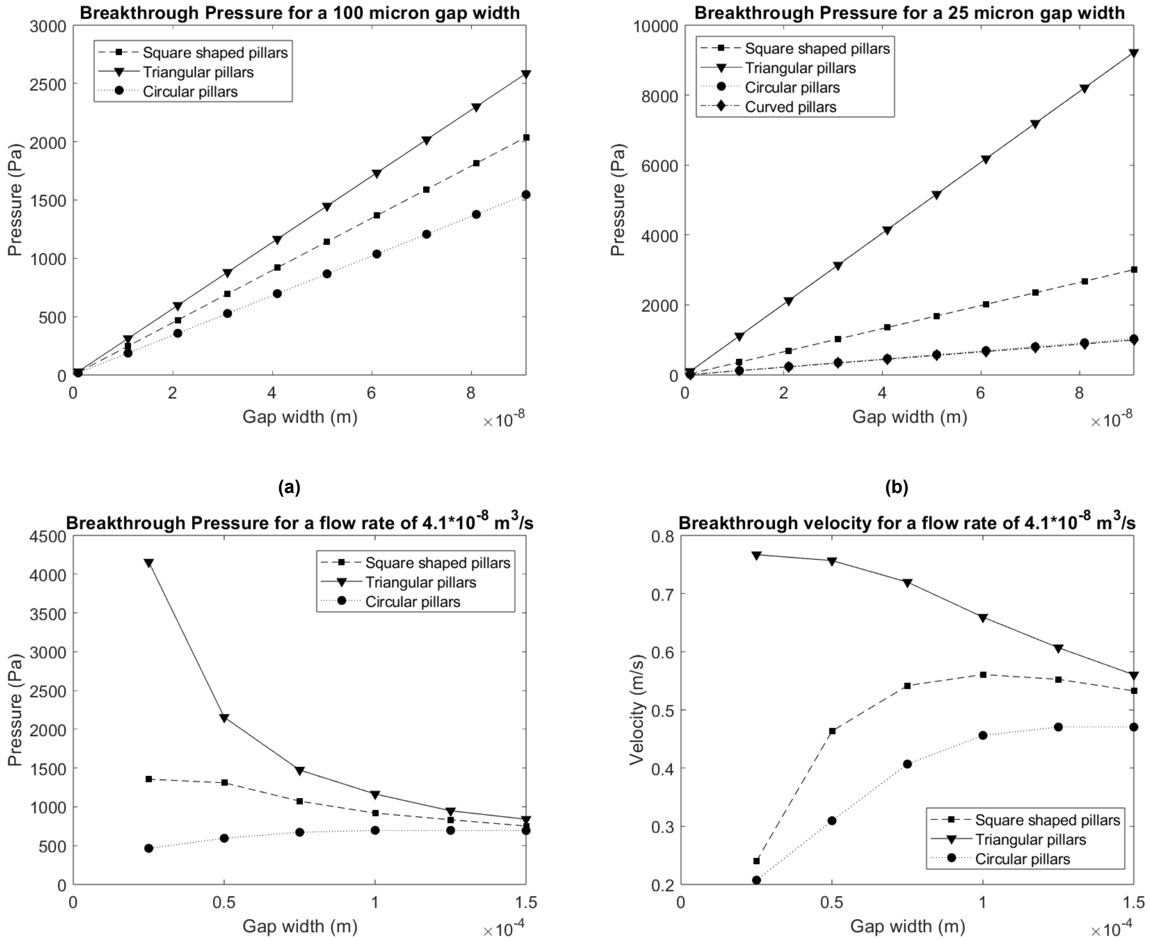

(a) (b)

(c) (d)

Figure 4.16: The maximum breakthrough pressure for (a) three different pillar shapes with a gap width of 0.1 mm and (b) four different pillar shapes with a gap with of 0.025 mm. (c) The breakthrough pressure and (d) breakthrough velocity of triangle- circular- and square shaped pillars for varying gap widths with a inlet flow rate of $40mm^3/s$.

4.3.2. Injection Method

To determine the optimal injection method of Pluronic F127 hydrogels, five different parameters were tested: injection methods, temperature, volume, velocity and the number of gaps. All the injection testing was done on the injection platform described in Sec. 3.1.1.2. Fig. 4.17 visualizes a half filled, successful filled and leaking channel.

First, it was tested if the hydrogels could flow through the channel based on gravitational force. The hydrogels were injected into the inlet chamber, after which they were allowed to flow. This was done for twelve different channels. In none of the twelve channels did the hydrogel flow through the channel. Instead, it remained in the inlet chambers. Afterwards, injection was tested using the sealing method. In this method, the weight of the pipette rests on the tip, which is placed in the inlet chamber. This creates a seal between the inlet chamber and the pipette tip. This method was also tested on twelve channels. In every channel, the hydrogels did flow through the channels. However, it was found that all channels broke through the pillars after the middle part of the channel was reached. In this method, any of the following parameters was not taken into account. Therefore, excessive pressure or volume might have caused the leakage.

The injection temperature was tested with three different temperatures: 4°C, room temperature (20°C) and 30°C. All temperatures were again tested on twelve channels. No significant difference was found on injection at 4°C and 20°C. To inject at 30°C, the hydrogels were loaded in a syringe and placed in an oven. A syringe was used as placing the mechanical pipettes in the oven was undesired. After the hydrogels formed stable gels, they were taken from the oven and injected in the channels. Because Pluronic F!27 hydrogels show shear thinning behavior, the hydrogels could flow through the channels [66]. However, due to the excessive force needed to achieve shear thinning behavior and the inaccurate injection volumes used in the syringe. The hydrogels filled the complete microfluidic platform after injection (i.e. leaked through all the gaps). Therefore, it was chosen to inject at room temperature, as this was the most convenient temperature no significant difference was found between room temperature and 4°C.

Injection volume was tested by systematically increasing the volume from 0.5 µl to 1 µl. Injection was done from both sides, as the initial injection method testing indicated that numerous channels leaked when filled from one side. It was found that 0.6 µl injected from both sides was the most successful volume for successful injection (Fig. 4.17b). Out of twelve channels tested, three were successfully filled, three had a gap remaining in the middle and six leaked. Although this sounds unsuccessful, the leakage in these channels were minimal (Fig. 4.17c).

Injection velocity was tested with according to the obtained Comsol results. This indicated that the injection velocity using syringes with a diameter of 9.5 mm at which the hydrogel is confined in the channel must be below 0.44 mm/s. This was tested using a controlled injection pump. Out of twelve tested channels, eight were successfully filled, three were half filled and only one leaked. However, it must be noted that injection still needed to be done from both sides. Injection with this injection velocity still caused leakage once the hydrogel filled more than half of the channel. These results indicate that the hydrogel can be confined in the channel using injection velocities below 0.5 mm/s for syringes with a diameter of 9.5 mm.

Last, the influence of the number of gaps was tested. To test this, the permeability testing platform as described in Sec. 3.1.1.2 was used. This platform consist of a central channel with a single gap on each side of 100 µm. Using this method eleven out of the twelve tested channel were successfully filled, while one leaked.

4.4. Setup of Responsive Surface Methodology Method for Future Investigation on Pluronic F127 Hydrogel Formulation

A full responsive surface methodology study to determine the effect of photo-polymerization time, temperature and photo-initiator concentrations on the remaining mass fractions was established. The initial parameter value chosen were based on the results of Lee et al. (2007) and Di Biase et al. (2011) [76, 77]. This study should be considered a preliminary attempt, to evaluate the aspects to be taken into account. The results from the RSM performed in this work were not representative due to the fact that

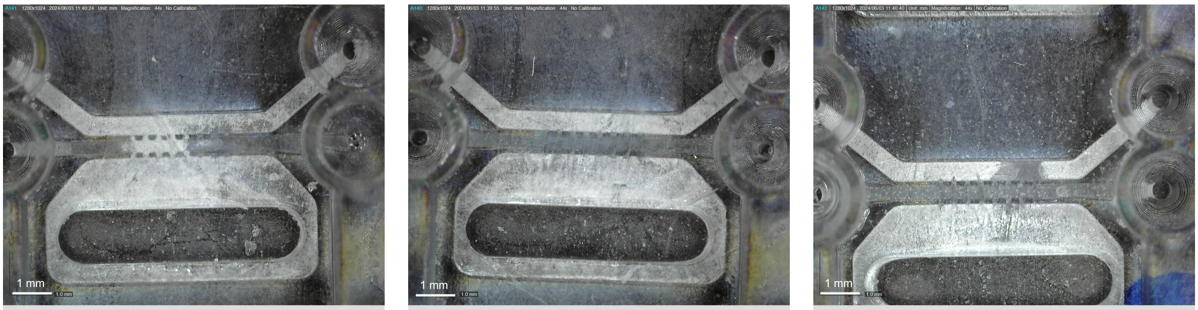

(a) (b) (c)

Figure 4.17: Injection testing of OoC platform. (a) Central channel only half filled. (b) Successfully filled channel. (c) Leaking channel.

hydrogels with a concentration of 10 and 15 wt% did not form a gel based on micellation in the used temperature range. Therefore, a detailed protocol to perform RSM and possible interpretations are discussed below.

4.4.1. Responsive Surface Methodology Protocol

RSM is a resourceful approach to determine the effect of different photo-polymerization parameters on the degradation rate and thermoreversible properties of di-acrylated Pluronic F127 hydrogels simultaneously. According to the findings from Lee et al. (2007) and Di Biase et al. (2011), di-acrylated Pluronic F127 hydrogels with low concentrations can exhibit a low degradation rate while being thermoreversible [76, 77]. Therefore, RSM should be used to determine the exact photo-polymerization conditions for which this is the case. The following protocol is based on the obtained findings from the previously mentioned studies and should be used for di-acrylated Pluronic F127 hydrogels with a concentration of 10 or 15 wt%. However, this protocol can be used for hydrogels with any concentration.

RSM is used to determine the effect of multiple different independent variables simultaneously. In this work, the independent variables were: photo-initiator concentration, photo-polymerization time and photo-polymerization temperature. For every variable, a center point is chosen to create the factorial points around as described in Sec. 3.2.2.3. In the following protocol the center point has a photo-initiator concentration (I_c) of 0.2 wt%, a photo-polymerization time t of 5 minutes and a photo-polymerization temperature T of 20°C. However, any other values for the independent variables can be chosen, as long as they are logical within the framework of this study. The fractional factorial points should be chosen on equal distance of the center point. This can be done by choosing $\Delta I_c = 0.1$, $\Delta t = 3$ and $\Delta T = 10$. This results in extreme values for the photo-initiator concentration of 0.1 and 0.3 wt%, for the photo-polymerization time of two and eight minutes and for the photo-polymerization temperature of 10°C and 30°C. These values will be used below but can also be changed. Additionally, the values in the protocol below are based in degradation testing of 0.3g, performed in triplets. For accurate measurement, it is more convenient to use larger volumes. Moreover, it is advised to use larger quantities in the mixing process to account for potential losses.

1. Prepare the desired hydrogels according to protocol and store in the fridge. Mixing in the following steps will be easier at temperatures below the gelation temperature.
2. Mix 0.0036g, 0.0018g and 0.0108g of photo-initiator with 3.6g, 0.9g and 3.6g of the desired hydrogel in 10ml glass vials to obtain hydrogels with a photo-initiator concentrations of 0.1, 0.2 and 0.3 wt% respectively. The volume of 0.2 wt% is lower as there is only one center point, compared to four fractional factorial points for the other concentrations. Cover the glass vials in aluminum foil and mix the hydrogels for two minutes on vibrating shaker.
3. Inject 0.3g of the mixed hydrogels into 1.5 ml Eppendorf tubes. For the hydrogels with a photo-initiator concentration of 0.1 and 0.3 wt%, this should result in twelve filled Eppendorf tubes. For the hydrogel with a photo-initiator concentration of 0.2 wt%, this should result in three filled Eppendorf tubes.

4. Place six of the twelve filled Eppendorf tubes in with a photo-initiator concentration of 0.1 and 0.3 wt% in an oven at 30°C for 15 minutes. Place the other six Eppendorf tubes in the fridge until they reached a temperature of 10°C. Keep the filled Eppendorf tubes with photo-initiator concentration at room temperature (20°C).
5. Photo-polymerize the Eppendorf tubes with the photo-initiator concentration of 0.2 wt% for five minutes at the desired intensity.
6. Photo-polymerize three from the six Eppendorf tubes from the oven (30°C) for two minutes and the other three for eight minutes. Do this for both photo-initiator concentrations (0.1 and 0.3 wt%).
7. Repeat step 6 for the filled Eppendorf tubes at 10°C.
8. At this point, thermoreversibility can be tested by placing all samples in the fridge at 4°C for ten minutes. For the samples showing thermoreversible behavior (i.e. liquefy), accurate thermoreversible behavior can be determined using oscillatory rheometry with a temperature ramp (Sec.2.5.3).
9. Place all sample in an incubator at 37°C and allow to form gels for ten minutes.
10. Fill all Eppendorf tubes with 1.2 ml of (red-colored) PBS. Refresh PBS by removing supernatant and injecting 1.2 ml of PBS every two/three days.
11. After seven days, remove supernatant and measure remaining weight (wet mass) or vacuum dry for twelve hours and measure remaining weight (dry mass). Compare the wet mass to the original wet mass of the hydrogels injected in the Eppendorf tubes or compare dry mass to the original di-acrylated Pluronic mass in the hydrogel.

Based on the obtained remaining mass fractions for all samples, a first order polynomial can be fitted using least squares regression according to:

$$y_i = \beta_0 + \beta_1 x_1 + \beta_2 x_2 + \beta_3 x_3 + \beta_{12} x_1 x_2 + \beta_{13} x_1 x_3 + \beta_{23} x_2 x_3 + \epsilon \tag{4.6}$$

Where y_i is the remaining mass fraction after seven days for di-acrylated Pluronic F127 hydrogels with a concentration of 10 and 15 wt%, x_1, x_2 and x_3 are the unit values for the independent variables: photo-initiator concentration, temperature and time, and β_i and ϵ are the variable estimates. The unit values can be related to real units by dividing the difference in variable values between the center point and the middle point by two. For the photo-initiator concentrations this will be 0.05 wt%: $\Delta I_c/2 = 0.05$. The polynomial can easily be fitted using Python (statsmodel OLS) or R. Based on the fitter polynomial, the direction of steepest ascend can be obtained by taking the partial derivatives. Based on the steepest ascend, a new center point for a new RSM model can be determined. Once the direction of steepest ascend changes, axial points should be added according to the Box-Wilson central composite design [96]. For a 3D model, these points are located 1.682 units away from the center point. Once, first order polynomials reach a plateau, it is beneficial to use higher order polynomials to account for curvature in the polynomial plot. The second order polynomial looks as follows:

$$y_i = \beta_0 + \beta_1 x_1 + \beta_2 x_2 + \beta_3 x_3 + \beta_{11} x_1^2 + \beta_{22} x_2^2 + \beta_{33} x_3^2 + \beta_{12} x_1 x_2 + \beta_{13} x_1 x_3 + \beta_{23} x_2 x_3 + \epsilon \tag{4.7}$$

The polynomial can be interpreted similarly as the first order polynomial. Eventually, this approach should lead to the optimal photo-polymerization parameter values for the remaining mass fraction after seven days. However, since thermoreversibility is considered equally important, the RSM can be stopped once the hydrogels do not exhibit thermoreversible properties anymore to obtain the photo-polymerization parameter values for which the remaining mass fraction is highest while exhibiting thermoreversible properties.

4.4.2. Responsive Surface Methodology Results

The effect of photo-polymerization time, temperature and photo-initiator concentration on remaining mass fraction was determined using responsive surface methodology. The remaining mass fraction for di-acrylated Pluronic F127 hydrogels after seven days was used as a dependent variable in the responsive surface methodology. The resulting mass fractions are shown in App. D. It should be noted that numerous samples had a remaining mass fraction of 0%. Due to the fact that hydrogels with a concentration of 10 and 15 wt% did not form a hydrogels below 40°C, the remaining mass fraction completely depends on polymerization. It was found that several samples formed lumps after photo-polymerization, indicating that 3D network structures have formed and captured water. However, based on the obtained results, no correlation can be found for the photo-polymerization time, temperature and photo-initiator concentrations. Therefore, the resulting mass fractions are not representative to determine the effect of photo-polymerization on the remaining mass fraction and thermoreversibility of these hydrogels.

However, the results from this preliminary study indicated that it is possible to photo-polymerize di-acrylated Pluronic F127 hydrogels. Several samples showed lump formation even without gel formation. This indicate successful polymerization.

4.5. Future Perspectives and Implications of Biocompatibility Testing Outcomes

Biocompatibility testing of the fabrication materials of the OoC platform and (di-acrylated) Pluronic F127 hydrogels will be performed with the cortical organoid cultures [64]. To test for biocompatability of the fabrication materials, a 9-well plate was designed using CAD software Fusion 360. The wells in the 9-well plate had the same dimensions as the dimensions of the organoid chambers on the OoC platform. Fabrication of these well plates was done with Moiin Tech Clear, Detax Freeprint Ortho and PDMS. The fabrication with Moiin Tech Clear and Detax Freeprint Ortho was done as described in 3.1.2. The fabrication of the 9-well plates from PDMS was done by 3D printing a negative mold of the 9-well plates with Moiin Tech Clear. PDMS was poured in the molds, fully cured and demolded.

The 9-well plates fabricated with DLP 3D printing, suffer from surface roughness due to the surface roughness of the printer head. Since, imaging of cells is performed from the bottom, the transparency of the 9-well plates needed to be enhanced. This was done manually by placing tiny drops of uncured resin on a glass slide (Fig. 4.18a), placing the 9-well plates on top and compressing the 9-well plates down using another glass slides bonded together with tape (Fig. 4.18b). The uncured resin was cured using an UV-flash device (Otoflash G171 UV-flash device) with 500 flashes. Due to the smooth surface finish of glass, the cured resin in between the glass and the 9-well plates obtained a smooth surface finish with increased transparency. The difference in transparency is shown in Fig. 4.18a,b.

Biocompatibility test will be performed on the fabricated 9 well-plates through live/dead staining of cortical organoid cells. Additionally, Pluronic F127 and di-acrylated Pluronic F127 will be tested both in solvent and gel state. In the gel state, (di-acrylated) Pluronic F127 hydrogels will be placed on the side walls of the wells in the 9-well plates, cortical organoid cells will come in contact with the (di-acrylated) Pluronic F127 hydrogels. The (di-acrylated) Pluronic F127 hydrogels will be tested in solvent state through dissolution in the used growth media. This growth media containing (di-acrylated) Pluronic F127, will be supplied to the cortical organoid cultures similar as done in the protocol described in Sec. 2.4.5.

The results from the biocompatibility test were not retrieved within the timeframe of this report. Therefore, possible outcomes will be discussed.

4.5.0.1. 3D Printed Well-plates

The optimal results will include a high cell viability, proliferation and differentiation. This would indicate that the organoid grow in a similar manner as they would in normally used protocols [64]. However, a low cell viability might be caused by leaching monomer from the methacrylate resins as discussed in Sec. 2.3.1.4. This suggest that the 3D printed 9 well-plates are not properly post-processed. Additional UV curing or thermal treatment might improve the biocompatibility and reduce leaching of cytotoxic monomers [44]. Additionally, possible abnormal growth of cortical organoids might be caused by a sub optimal surface finish in the 9 well-plates. The 9 well-plates fabricated with DLP 3D printing can suffer from surface roughness. This can be overcome by using printer heads and resin baths with a smoother finish (discussed later) [27].

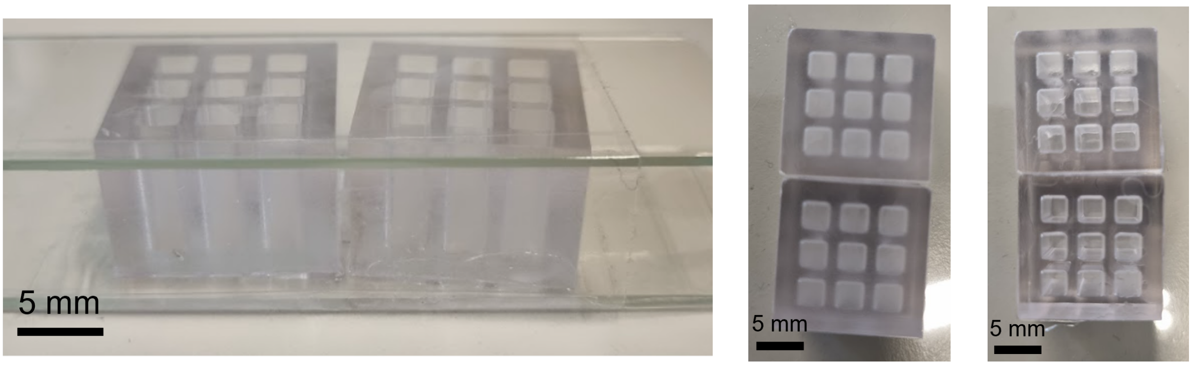

(a) (b) (c)

Figure 4.18: Enhancement of transparency of 9-well plate made with Detax Freeprint Ortho. (a) The 3D printed 9-well plates are compressed between two glass slides with a few drops of uncured resin in between the bottom and the glass slide. (b) Transparency before enhancement. (c) Transparency after enhancement.

4.5.0.2. PDMS Molded Well-Plates

Biocompatibility of PDMS molded 9 well-plates is expected due to the proven biocompatibilty of PDMS [20]. However, potential low cell viability or proliferation can be caused by several factors. First, as mentioned previously, uncured PDMS at the interface of the molds has been as problem. PDMS molding with methacrylate based resin exhibited a PDMS cure inhibition to a lesser degree. However, leaching of PDMS might still happen. If this happens, several things can be done. First, the PDMS curing times can be increased to decrease uncured PDMS. Secondly, the molds can be fabricated from different materials which do not inhibit PDMS curing. Besides uncured PDMS, surface roughness or deformations in PDMS might cause stress in the organoid cell cultures. This could also lead to a lower cell viability or proliferation. It was found that the PDMS 9 well-plates were difficult to demold due to a very thin layer in between each well. To improve this, the PDMS molds must be designed with an increased spacing between each well. This should result in easier demolding and less deformation in the final PDMS 9 well-plate.

4.5.0.3. Pluronic F127 and F127DA

Biocompatibility of normal Pluronic F127 hydrogels is also expected due to FDA approval for various medical application as discussed in Sec. 2.5. However, cell viability and proliferation might be reduced due to structural changes or interaction with Pluronic F127 polymers. It might be possible that the mechanical structure of Pluronic F127 hydrogels inhibit organoid development. This can be tested by exposing the organoid to Pluronic F127 solutions in liquid and gel state. Moreover, high concentrations of Pluronic F127 might inhibit organoid growth due to interactions of the Pluronic F127 polymers with the organoid cells.

For di-acrylated Pluronic F127, biocompatibility is not established. Residual unreacted acrylate groups or improperly cross-linked acrylates might be cytotoxic, similar to leaching metachrylate groups from the 3D printed 9 well-plates. This might significantly inhibit cell growth. When this is the results, this indicates that di-acrylated Pluronic F127 can only be used in a fully cross-linked state. This in turn complicates the process described in Sec. 4.4.1. Finding an optimal hydrogel by altering photo-polymerization parameters suggest that some samples in the RSM are not fully cross-linked. If an optimal hydrogel photo-polymerization protocol is found, it must be established if these hydrogels in particular are biocompatible.

If all of the Pluronic F127 hydrogels are found to be not biocompatible with the cortical organoid culture, the application of Pluronic F127 hydrogels as a transient barrier for vascularized Organoids-on-a-Chip will not be possible. Therefore, biocompatibility tests are performed to make sure Pluronic F127 hydrogels are biocompatible with the cortical organoid cultures. Biocompatibility of Pluronic F127 hydrogels is expected due to its proven biocompatiblity and usage in medical applications as discussed in App. F.

5

Discussion and Future Recommendations

5.1. Organ-on-a-Chip platform

Fabrication of the OoC platform was done with three different materials: Moiin Tech Clear, Detax Freeprint Ortho and PDMS. Fabrication using DLP 3D printing resulted in repeatedly similar printed structure. However, numerous things can still be improved to optimize the fabrication of the OoC platform.

5.1.1. Detax Freeprint Ortho Initiator File Configuration

Detax Freeprint Ortho was chosen as a new material because of the proven biocompatibility in literature [28]. Using the Universal building tray from Asiga, OoC platforms made with Detax Freeprint Ortho showed similar dimensional results compared to Moiin Tech clear. However, structures below 100 µm were still not able to be produced. The step structure used to determine the XY-shrinkage of this material utilized values above 5 mm. The measured dimensions of the step structures were shown to be very similar to the nominal dimension, To improve the printing of smaller dimensions, it might by usefull to print step-structures with smaller dimensions, especially in the desired range. Therefore, step structure with dimensions in between 50 µm and 250 µm should be used. Printing these structures and comparing the printed and nominal dimensions should result in XY-shrinkage values corresponding to these dimension. Loading these XY-shrinkage values in the initiator file might improve the dimensional accuracy for smaller structures.

It was found the 3D printing with the UltraGloss building tray did not results in accurately printed OoC platforms. The smaller features of the OoC platform were not printed accurately. The transparency was found to be improved using this building tray, but since it was not possible to print small features, this option was discarded. With the current printing parameters and post-processing steps it is therefore not desired to print OoC platform with this building tray.

The repeatedly accurately produced OoC platforms were printed with a channel height of 0.4 mm, while original channel height was 0.25 mm. Printing with Detax Freeprint Ortho with a channel height of 0.25 mm often resulted in opened channels with the post-processing steps used as described in Sec. 3.1.2.1. Since, it has been shown that it is possible to accurately print small features, the post-processing should now be optimized to print with smaller channel heights. This might include longer exposure to ultrasound bath or IPA. The ultrasound bath releases uncured resin from the channels. It might also be beneficial to increase to number of cycles in the ultrasound bath, with flushing with compressed air in between each cycle.

Thin layers of OoC platforms printed with Detax Freeprint Ortho were found to deform under the pressure from the pressurized air. This can be explained through the significantly lower flexural modulus of Detax Freeprint Ortho (1700 MPa) compared to Moiin Tech clear (2500 MPa) [115, 116]. Therefore, it was required to increase the thickness of thin layers of the OoC platform. No significant effect on transparency was found with an increased bottom layer thickness. Therefore, increasing thin layers is seen as a viable solution to the problem of deformation.

The optical transparency was enhanced using tiny droplets of uncured resin. By placing these droplets on the 3D printed OoC platforms surface, compressing the resin in between glass slides and curing it, the transparency was enhanced. Low optical transparency in DLP 3D printing is influenced by the building tray and the printer head. Light scattering, caused by scratches or deformations in the building tray, might occur and influence the optical transparency. Similarly, the surface roughness of the printer head can cause light scattering as well as an uneven surface finish of the printed part [27]. The optical transparency might be improved by changing the building tray or printer head. Fritschen et al. (2022) used highly polished steel printer heads and siliconized glass Petri dishes as building trays. This results in a significantly improved optical transparency. Therefore, to increase the transparency of the OoC platforms, changing any of these printer features could improve the optical transparency instantly.

5.1.2. PDMS Molding

The OoC platform was successfully fabricated using PDMS molding. Two different methods proved to be feasible options for the fabrication with PDMS. The first successful option included molding of the top and bottom layer of the OoC platform separately and bonding them using oxygen plasma. Although this method proved to be feasible, it was still prone to delamination and misalignment. Misalignment can be prevented by accurately aligning the two layers using microscopes and alignment tools. Delamination is harder to prevent. With the used oxygen plasma parameters as described in Sec. 3.1.2.3, PDMS-PDMS bonding did not succeed repeatedly. It was found that curvature in the PDMS surface and surface contamination drastically lowered the success of oxygen plasma bonding. Curvature in the PDMS layers can be prevented by increasing mold size. The initial molds were designed as exactly the negative of the fabricated structure. Therefore, the PDMS poured in the mold should be exactly leveled at the top surface of the mold. Excess PDMS caused convex curvature on the top of the layer, while too little PDMS caused convex curvatures. By increasing the molds width and height, this curvature can be prevented (to be above important features). If the molds are wide enough, the PDMS surface above the microfluidic channels will be flat, improving the bonding quality. Additionally, this prevents the creation of delamination points. In this work, the top and bottom molds were equally wide, creating vulnerable points at all corners. A wider bottom layer prevents this.

The second successful option was based on PDMS-glass bonding. This method proved to be repeatedly successful. Moreover, because the complete OoC platform can be molded simultaneously, with multiple platforms in a single tray, it was also a more efficient approach. The molded top layers were found to be sacrificial for every tried method. Therefore, molding of PDMS OoC platforms required printing of new molds for every platform. The molds made with this method did not have the original inlet structures of the OoC platform. Instead, the inlet chambers were punched in the PDMS layer. Therefore, if it is required that the inlet chambers remain their original structure, this is not a feasible method.

It was found that the flow rate of PBS differed significantly between these two fabricated OoC platforms. PBS injected in the PDMS-PDMS bonded platform propagated very slowly through the microfluidic channels. Simultaneously, the same injected PDMS filled all the microfluidic channels of the PDMS-glass bonded OoC platform instantly. This can be explained through the hydrophobic nature and surface roughness of PDMS [117, 118]. The hydrophilic surface of glass reduces the resistance to flow. Moreover, glass has a smoother surface than molded PDMS, allowing for fast fluid flow.

The other three methods tried were found to be unsuccessful. Using separately printed inlet pillars should prevent the top molds from being sacrificial. However, due to the small dimensions of the inlet channels, the pillars broke and were still sacrificial. This can be prevented by making the pillars (and therefore the inlet chambers) bigger. Alternatively, other materials might be used to prevent breaking.

Bonding of six individual layers was found to be extremely prone do delamination. As previously mentioned, bonding was difficult for PDMS layers with a curved surface. Because the molds in this method required to have the exact dimensions of their respective layer, all PDMS layers were found to be curved. This made successful bonding extremely challenging. This can be prevented by increasing the mold width and height. However, with an additional height, punching of the PDMS layers become

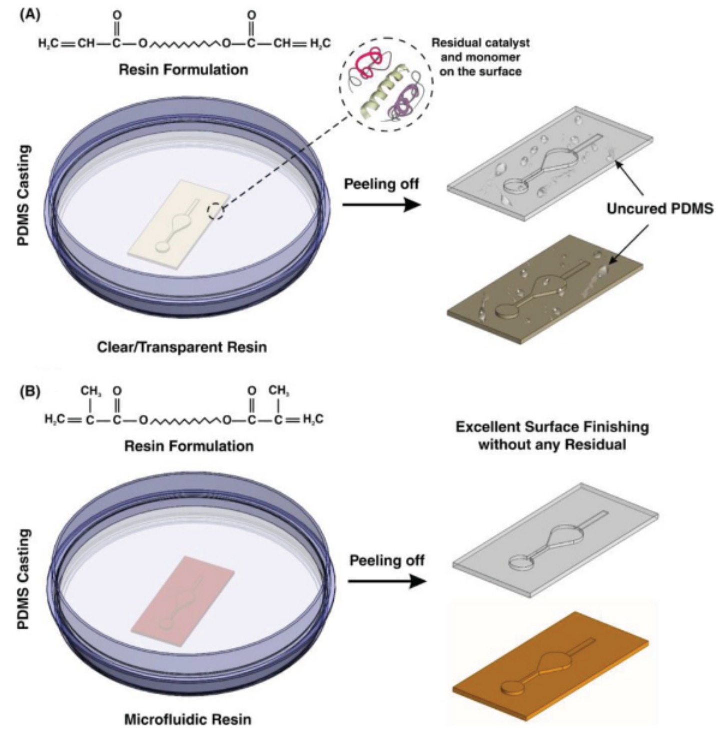

Figure 5.1: PDMS molding with acrylate (A) and methacrylate (B) resins. Methacrylate resins provide an improved surface finish of molded PDMS layers [120].

necessary. If the pillar structures are also increased in height, the PDMS layers will still form curved surfaces. Since other methods proved to be easier and more successful, this method is not considered a feasible option for the fabrication of OoC platforms.

In the final method, the objective was to bond a 3D printed top layer to a PDMS molded bottom layer. The bonding between these two layers was found to be very poor. This was expected beforehand due to differences in materials (acrylates and silicone). However, this method might still be feasible by using double sides pressure sensitive adhesive (PSA) tapes [90, 119]. These tape have an acrylate adhesive on one side of a carrier tape and a silicone adhesive on the other side. Using PSA, the PDMS molded bottom layer can be bonded with the 3D printed top layer. However, after bonding cutting the PSA is required to open in the inlet channels. If bonding with PSA proves to be feasible, this method might be the most efficient. The 3D printed top part can be fabricated with the original dimensions of the OoC platform. Therefore, the top layer will not be fabricated using PDMS molding, which make the sacrificial molds obsolete. Simultaneously, the PDMS molded bottom layer provides the advantages of PDMS, such as gas-permeability and biocompatibility [19].

Initially, molds were 3D printed using Sunlu black resin. However, after substantial curing times at 80°C, all surfaces which came in contact with the mold materials were uncured. After changing to Moiin Tech Clear this problem was minimized. This is also found in literature. Sunlu black resin is based on photo-polymerization of acrylate monomers, whereas Moiin Tech Clear is based on photo-polymerization of methacrylate monomers. Methacrylate based resins demonstrate improved performance in providing a smooth surface finish of PDMS without any residual materials [120]. Fig. 5.1 illustrates the difference between the two resin materials. The presence of unreacted monomers in the resin prevents the complete curing of PDMS. Methacrylate resins have a higher degree of cross-linking and do not inhibit PDMS curing. Alternatively, extensive post-processing might prevent PDMS curing inhibition. Additional UV curing further polymerizes uncured resin, limiting the risk of leaching uncured monomers. Simultaneously, thermal treatment allows for vaporizing of remaining photo-initiator and promotes recombination of photo-initiator fragments [44].

The used oxygen plasma input parameters were considered optimal, as they coincide with the optimal values of oxygen plasma as described in Sec. A.0.0.3. However, optimal conditions might differ between different oxygen plasma chambers. Bonding of PDMS-glass showed to be repeatedly successful. However, PDMS-PDMS bonding did not. The oxygen plasma input parameters should be further optimized by systematically changing input parameters and measuring the resulting bonding strength [121].

5.2. Biodegradable Barrier for Multi-Cells Culture of Vascular Networks and Cortical Organoids

The synthesis of di-acrylated Pluronic F127 resulted in a yield of 39%. This is significantly lower than the yield of 80% found in the followed protocol from Lee et al. (2007) [76]. Two plausible causes for the low yield were identified. First, the solubility when precipitating in diethyl ether can be decreased. In the first attempt, the yield was only 3.96%. In this synthesis, the ratio of methylene chloride to diethyl ether approximately 1:3. The second synthesis used at ratio of methylene chloride to diethyl ether of 1:5. Further increasing this ratio by increasing the volume of diethyl ether for precipitation causes a lower solubility of di-acrylated Pluronic F127, which in turn should results in more precipitation. Secondly, the filtration step can significantly influence the yield. In the second synthesis attempt, the precipitation was filtered twice. After filtering, the diethyl ether with precipitation turned slightly transparent, indicating that the precipitated di-acrylated Pluronic F127 was filtered out. However, additional filtration steps might increase the yield. Additionally, using filtration paper with smaller pores sizes might also increase the yield.

The degree of acrylation was found the be 57%. This is also significantly lower than the 98% found in the followed protocol of Lee et al. (2007) [76]. Several factors might have caused the low degree of acrylation obtained. First, the acryloyl chloride might have been added too quickly to the reaction. In the used synthesis, the acryloyl chloride was added dropwise using a syringe. This took approximately fifteen minutes. Too fast addition of acryloyl chloride might cause the reaction to heat up and cause undesired by products [81]. Moreover, acryloyl chloride reacts heavily with moisture. Therefore, too fast addition might cause acryloyl chloride to react with any present moisture instead of the Pluronic F127 molecules. Therefore, it might be suitable to use a dropping funnel for the addition of acryloyl chloride to increase the addition time. Moreover, dissolving acryloyl chloride in methylene chloride before the reaction prevents it from reacting with moisture while being added to the reaction [80].

Besides the addition of acyrloyl chloride, the reaction might also be carried out longer. In the followed synthesis, the reaction was stirred for eight hours at 4°C and 16 hours at 20°C. Which results in a total reaction time of 24 hours. Other protocols using reaction times of 48 hours [122] or even 72 hours [95]. A longer reaction time might increase the degree of acrylation.

Alternatively, other protocols can be followed for the synthesis of di-acrylated Pluronic F127. A well know alternative synthesis by Cellesi et al. (2002) used dried Pluronic F127 dissolved in toluene [80]. Pluronic is dried using a Soxhlet extractor filled with activated molecular sieves. Afterwards, triethylamine and acryloyl chloride are added similar to the synthesis in this work. Precipitated triethylammonium was filtered out and the solvent was evaporated in a rotary evaporator. The resulting oil was dissolved in methylene chloride, washed with water, dried with sodium sulfate and precipitated in cold diethyl ether. This synthesis is significantly more extensive than the synthesis in this work. Additionally, this synthesis filtered away the precipitated triethylammonium from the methylene chloride before precipitation in diethyl ether. This can be a useful step to add in the synthesis of this work, since the methyl groups of triethylamine might influence the NMR spectrum of the obtained di-acrylated Pluronic. The methyl groups of triehtylamine are located at the same chemical shift as the methyl groups from the Pluronic PPO groups [123]. Therefore, triethylamine might interfere with the calculations of the degree of acrylation.

Besides triethylamine, diethyl ether might also influence the obtained NMR spectrum. Fig. 5.2 shows two peaks identified in the obtained NMR spectrum with a chemical of 1.4 and 3.1 ppm. These peaks do not correspond to di-acrylated Pluronic F127 [74, 95]. However, these peaks correspond to the location where the peaks for diethyl ether are located [124]. The possibility that diethyl ether was still present can be further explained through peak splitting. In Fig. 5.2, the peak at 1.4 ppm is split in three,

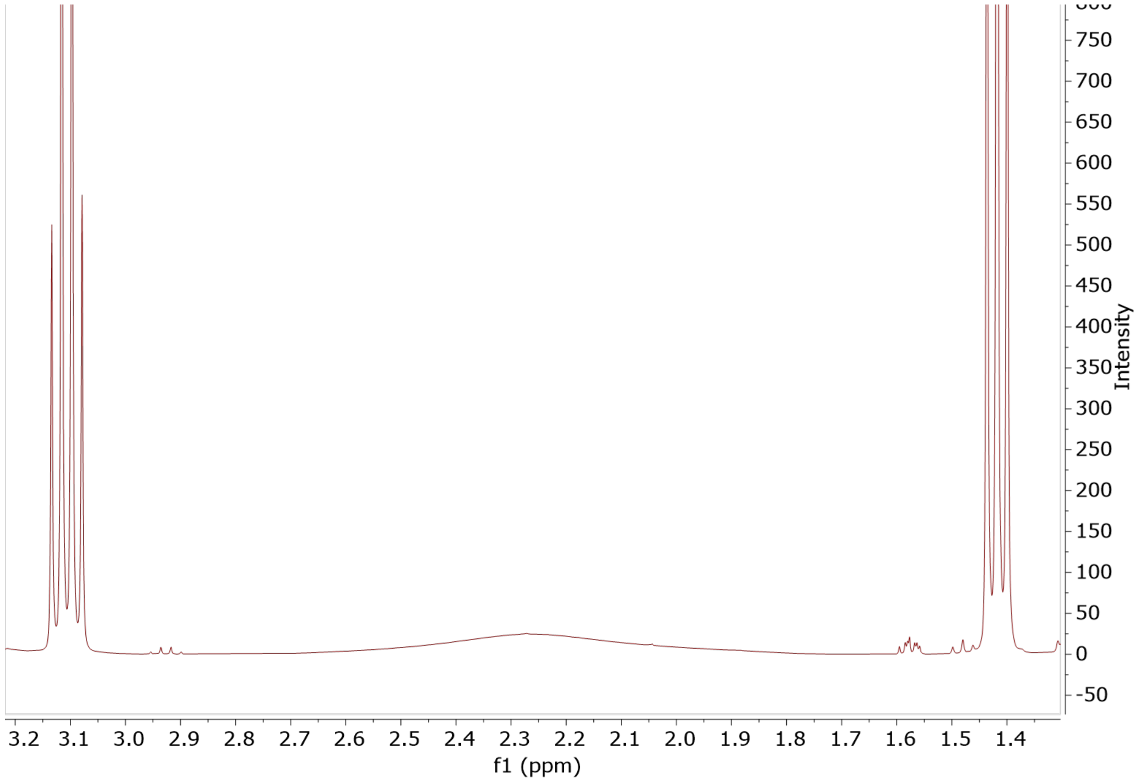

Figure 5.2: NRM spectrum of di-acrylated Pluronic F127 between 1.4 and 3.1 ppm

indicating that the adjacent carbon atom is bonded with two hydrogen atoms. Simultaneously, the peak at 3.1 ppm is split in four, indicating that the adjacent carbon atom is bonded with three hydrogen atoms. Both findings correspond to the chemical formula of diethyl ether, which has two ethyl groups bound to an oxygen atom. Taking into account that in the second synthesis, the drying step was not performed under vacuum, the presence of diethyl ether can be possible. However, to make sure that it was diethyl ether, NMR should be done again. In following syntheses, the drying step should be performed under vacuum while covering the obtained di-acrylated Pluronic F127 with aluminum foil to prevent it from being pumped out.

5.2.1. Characterization

Rheometry was found to be an accurate characterization method to determine the gelation temperature and viscosity of Pluronic F127 hydrogels. It was found that all tested Pluronic F127 hydrogels had a gelation temperature similar to what is found in literature [8]. This indicates that the synthesis of Pluronic F127 hydrogels went according to plan. Hydrogels made from the synthesized di-acrylated Pluronic F127 did only form a gel for concentrations above 20 wt% in the temperature range used. The obtained gelation temperature were similar to those of the same concentration of conventional Pluronic F127 hydrogels. In literature it was found that gelation temperatures of di-acrylated Pluronic F127 hydrogels should be significantly lower compared to conventional Pluronic F127 hydrogels [77]. Moreover, lower concentrations (10 and 15 wt%) of di-acrylated Pluronic F127 hydrogels did not form a gel in the used temperature range, where this should have happened. Considering the previously discussed findings, interference of other substance with the gelation temperature is very plausible. For example, diethyl ether acts as a solvent for Pluronic F127. If diethyl ether was still present, it can have lowered the gelation temperature because it reduces the interaction of Pluronic F127 with water.

DSC was found to be a less useful method for characterization of Pluronic F127 hydrogels. From numerous samples tested no representative results were obtained. Moreover, from the obtained results, the obtained peaks were often not distinct. The peaks in the DSC results corresponded to the micellation temperature of Pluronic F127 hydrogels. Since this temperature can also be found using viscosity testing with a rheometer, rheometry was found to be more useful. However, the obtained micellation

temperatures are similar to those found in literature [97].
Problems with the DSC results could be caused by several factors. First, numerous samples showed bubble formation after injection. Samples in DSC should be degassed as bubbles significantly influence the thermal results due to expansion. Moreover, to determine heat flow peaks for protein folding (micellation), a high concentration of that protein is needed to obtain distinctive peaks. Last, samples must be pure to prevent influence of other molecules in the heat flow results [125].

The degradation testing indicated that all Pluronic F127 hydrogels were fully degraded within ten days. This is similar to what is found in literature for these hydrogels [76]. However, di-acrylated Pluronic F127 hydrogels showed similar degradation rates. In literature it was found that di-acrylated Pluronic F127 hydrogels had significantly lower degradation rates after photo-polymerization [76, 122, 126]. The di-acrylated Pluronic F127 hydrogels in these studies had significantly higher degrees of acrylation. Therefore, these results suggest that a degree of acrylation of 57% is too low to significantly lower the degradation rate of Pluronic F127 hydrogels.

In all the degradation tests done, the wet weight was used to determine the loss in mass fraction. This was considered a viable option as the wet weight corresponds to degradation of the complete hydrogel. Since the goal of the degradation testing was to find the degradation of the hydrogels, the wet weight can be used as an indicative parameter. However, to accurately determine the degradation of Pluronic F127 polymers in aqueous solutions, the dry weight can be measured. This should simultaneously lower the significant standard deviation found in measuring wet weight.

The permeability testing results showed that injected Pluronic F127 hydrogels in microfluidic channels were perfused by surrounding PBS within seven days as well. Therefore, these results compare to the results found in the degradation testing. However, in the permeability testing, lower concentration hydrogels performed better than higher concentrations. This is probably caused by the fact that higher concentrations were more viscous. This caused these hydrogels to be harder to inject without bubble formation. A significant amount of bubbles in the hydrogels might have cause a lower permeability time. To overcome this, the pipetting technique used can be adjusted (discussed later).

However, none of the used Pluronic F127 hydrogels were stable for the 35 days needed for cortical organoid growth [64]. Therefore, synthesis of di-acrylated Pluronic F127 should be done to obtain a higher degree of acrylation. This might results in a lower degradation rate and a longer time before perfusion. Alternatively, additional Pluronic F127 hydrogels can be loaded in the barrier channel when needed. By lowering the temperature, the Pluronic F127 hydrogels become liquid, which allows for addition of more hydrogel in the channel. Through this manner, 35 days can be reached by step-wise addition of hydrogels.

A full responsive surface methodology study to determine the effect of photo-polymerization time, temperature and photo-initiator concentrations on the remaining mass fractions was established. This study should be considered a preliminary attempt, to evaluate the aspects to be taken into account. The results from the RSM performed in this work were not representative due to the fact that hydrogels with a concentration of 10 and 15 wt% did not form a gel based on micellation in the used temperature range. It was found the several samples showed lump formation, indicating that photo-polymerization resulted in the formation of 3D networks. However, to accurately determine the influence of photo-polymerization, RSM should be performed again. This can be done with the current degree of acrylation for hydrogels which did form a stable gel (20 and 25 wt%). Alternatively, the synthesis should be done again to obtained di-acrylated Pluronic F127 with a high degree of acrylation. In that case, hydrogel concentrations of 10 and 15 wt% can be used as done in this work.

However, the permeability results indicated that Pluronic F127 hydrogels can successfully act as a barrier to surrounding aqueous media. Moreover, di-acrylated Pluronic F127 was successfully synthesized. However, to improve the previously mentioned results, the degree of acrylation should be higher. With this in mind, These results paved the way for future successful research on Pluronic F127 as a transient barrier.

5.3. Integration of biodegradable barrier on the OoC platform

The breakthrough pressure and velocity through the gaps between the pillars was determined using COMSOL. It appeared that triangular pillar shapes caused the highest breakthrough pressure and velocity for any given gap width and inlet flow rate. Similarly, circular shaped pillars had the lowest breakthrough pressure and velocity for any given gap width and inlet flow rate. This might indicate that circular shaped pillars will perform better in confining the hydrogel in the channel. This especially illustrated for the lower gap width. With triangular shaped pillars, the breakthrough pressure and velocity increased with decreasing gap width, while for circular shaped pillars, both decreased. Similar results were found by [7], who determined that stadium shaped pillars and rectangular pillars had the lowest breakthrough velocity through the pillars. Although his model used a laminar flow with different input values, the similarity in results indicate the circular shaped (circle or stadium) pillars lower the leakage of fluid through the pillar array.

The triangular shaped pillars were chosen as design based on currently used microfluidic platforms for vasculature-on-a-chip [7, 58]. Triangular shaped pillars will cause an increase in shear stress, which is required for the formation of vasculature. However, in the OoC platform described in Sec. 3.1.1.1, only the outer two pillar arrays are required to have this feature. Since that is the place were a growth media gradient is supplied. The pillar array on the edge of the organoid chamber has a sole purpose to confine the hydrogel in the barrier channel, while being able to be perfused by formed vasculature. This suggest that a promising next step would be to lower the gap width between the pillars in the barrier channel and make the shape of the pillars circular. However, the minimal gap width should be large enough to allow for vasculature to perfuse through the barrier channel.

Additionally, square shaped- and curved pillars were tested using COMSOL. The square shaped pillar performed in between the triangular and circular pillar, while the curved pillars performed similar to the circular pillars. Other pillar shapes can also be tested to find the optimal shape to confine the hydrogel in the channel. Especially the curved pillars can be altered in width, radius, gap width and orientation [112]. Additionally, the pillar can be made wider and the number of gaps can be reduced. Yu et al. (2024) utilized capillary burst valves to create vasculature on a chip [99]. This indicates that a minimal number of gaps is required to allow for perfusion of vasculature. Simultaneously, a lower number of gaps simplifies the injection protocol as shown in Sec. 4.3.2 for the permeability testing platform.

The inlet flow rate for which the hydrogel is confined in the channel was estimated using COMSOL. It must be stressed that the used calculations and obtained results are based on estimates with several assumptions. To determine the capillary pressure, it was assumed that the contact angle of the hydrogel with the OoC platform materials was the same everywhere. Moreover, after obtaining the inlet flow rate, any resistance in the channels was neglected. Therefore, the injection velocity in the syringe was determined based on the inlet flow rate in the channel. In reality, the inlet flow rate in the syringe could be higher, due to resistance in the inlet channels. This would allow for a higher injection velocity.

5.3.1. Injection

Injection testing of 20 wt% Pluronic F127 hydrogels was done to determine the influence of five parameters (injection method, temperature, volume, velocity and number of gaps) on the accuracy of injection. First, it must be stressed that all injection testing was done according to the forward pipetting technique. For highly viscous fluids, the reverse pipetting technique might greatly improve the injection results. In this technique, the pipette is first pressed down to the second stop to inject the fluid into the the tip. For extrusion out of the tip, the pipette is pressed down to the first stop. With this technique, a residue remains in the tip and prevents bubble formation [113]. In forward pipetting, the complete volume in the tip is pressed out. For viscous fluids, the often results in the formation of bubbles, which decreases the accuracy of injection. The results from permeability testing indicated that lower concentration hydrogels performed better than higher concentration hydrogels. This might be caused by the presence of bubbles in the injected hydrogel. Reverse pipetting might solve this problem and provide more accurate results.

The results from injection testing provided optimal conditions for the injection of 20 wt% Pluronic F127 hydrogels. First, it was found that injection was most accurate by creating a seal between the pipette and the inlet chamber. This forced the hydrogel in the channel. When the hydrogel was injected without a sealing in the inlet chamber, the hydrogel did not propagate through the channels. Second, to accurately inject the hydrogel, the temperature must be below the gelation temperature. Pluronic hydrogels shows shear thinning behavior, which allows them to be injected above the gelation temperature. However, this method was found the be inaccurate for the channel volume used. The optimal injection volume was found to be 0.6 µl injected from both sides. Injection from one side increased the chance of leaking, while using lower or higher volume caused incomplete filling or leaking respectively. The injection velocity was estimated to be 0.5 mm/s. Using this injection velocity, the channels could successfully be filled. Although this was used as an estimate, these results indicate that very low injection velocity increase the chance of successfully filled channels. Combining all findings, the most optimal injection method would include injection of 0.6 µl from both sides below the gelation temperature at very low injection velocities while creating a seal between the pipette and the inlet chamber.

Simultaneously, the influence of the number of gaps was determined. It was shown that with only a single gap, the rate of successfully filled channels drastically increased. These results can be combined with the results from the COMSOL simulations to indicate that a decrease in number of gaps and decrease in gap width will significantly improve the chance of successfully filled channels. This would imply a modification of the original design, which shall be agreed with the biology counterparts of the project.

Although many channels leaked during injection, minor leakage might not necessarily be a problem, especially, if the results biocompatibility testing indicate that (di-acrylated) Pluronic F127 is biocompatible. In that case, minor leakage can be flushed away when the vasculature hydrogel is loaded in the OoC platform.

6

Conclusion

This Master's Thesis project aimed to develop a biocompatible Organ-on-a-Chip platform for vascularized Organoids-on-a-Chip with Pluronic F127 hydrogels as a transient barrier. It was shown that microfluidic platforms could be accurately fabricated with Detax Freeprint Ortho using digital light processing. This material was chosen because of its proven biocompatibiltiy in literature [28]. Besides, it was shown that the designed OoC platforms could be fabricated with PDMS. Two fabrication methods were shown to be feasible option to acquire repeatable fabrication of these platforms. The OoC platforms could be fabricated both by bonding of two separate PDMS layers as well as through bonding of a PDMS layer containing the microfluidic channels with glass. The optimal choice of fabrication depends on the desired features of the final OoC platform.

Simultaneously, the synthesis and characterization of several Pluronic F127 and di-acrylated Pluronic F127 hydrogels was done. It was shown that Pluronic F127 hydrogels could be injected in the microfluidic channels under the correct injection parameters. Moreover, through permeability testing, it was shown that Pluronic F127 hydrogels could serve as a transient barrier between two adjacent microfluidic channel. Aqueous media was effectively stopped from flowing through the hydrogel for seven days. To extend this period, di-acrylated Pluronic F127 hydrogels were synthesized. Due to a low degree of acrylation, it was found to be not currently possible to significantly extend this period. However, results coming from the di-acrylated Pluronic F127 indicate that it can be possible to achieve this goal through repetition and refinement of the synthesis process.

Future directions for the application of Pluronic F127 hydrogels in vascularized Organoids-on-a-Chip include improved synthesis of di-acrylated Pluronic F127 and several adjustments to the OoC platform. By changing the pillar shape to circles and reducing the gap size, the hydrogels could be confined easier in the microfluidic channels. Moreover, several improvements to the synthesis of di-acrylated Pluronic F127 were proposed to increase the degree of acrylation. This might decrease the degradation rate of di-acrylated Pluronic F127 hydrogels in aqueous media. Additionally, a protocol was proposed to find the optimal photo-polymerization parameters which influence the degradation rate and thermoreversible properties of di-acrylated Pluronic F127 hydrogels.

Combining all the results and future directions, this work effectively contributed to the future development of vascularized Organoid-on-a-Chip.

References

[1] Leung, C. M., de Haan, P., Ronaldson-Bouchard, K., Kim, G.-A., Ko, J., Rho, H. S., Chen, Z., Habibovic, P., Jeon, N. L., Takayama, S., Shuler, M. L., Vunjak-Novakovic, G., Frey, O., Verpoorte, E., & Toh, Y.-C. (2022). A guide to the organ-on-a-chip. *Nature Reviews Methods Primers*, *2*, 33.

[2] Lee, K. S., & Ram, R. J. (2009). Plastic–pdms bonding for high pressure hydrolytically stable active microfluidics. *Lab on a Chip*, *9*, 1618.

[3] Zhao, X., Xu, Z., Xiao, L., Shi, T., Xiao, H., Wang, Y., Li, Y., Xue, F., & Zeng, W. (2021). Review on the vascularization of organoids and organoids-on-a-chip. *Frontiers in Bioengineering and Biotechnology*, *9*.

[4] Yang, S., Hu, H., Kung, H., Zou, R., Dai, Y., Hu, Y., Wang, T., Lv, T., Yu, J., & Li, F. (2023). Organoids: The current status and biomedical applications. *MedComm*, *4*.

[5] Qian, X., Song, H., & Ming, G.-l. (2019). Brain organoids: Advances, applications and challenges. *Development*, *146*.

[6] Kim, M. R., & Park, T. G. (2002). Temperature-responsive and degradable hyaluronic acid/-pluronic composite hydrogels for controlled release of human growth hormone. *Journal of Controlled Release*, *80*, 69–77.

[7] Kahler, F. (2024). Organ-on-chip platform with transient membrane for vascularisation of brain organoids.

[8] Stoeber, B., Hu, C.-M. J., Liepmann, D., & Muller, S. J. (2006). Passive flow control in microdevices using thermally responsive polymer solutions. *Physics of Fluids*, *18*.

[9] Sahlgren, C., Meinander, A., Zhang, H., Cheng, F., Preis, M., Xu, C., Salminen, T. A., Toivola, D., Abankwa, D., Rosling, A., Karaman, D. Ş., Salo□Ahen, O. M. H., Österbacka, R., Eriksson, J. E., Willför, S., Petre, I., Peltonen, J., Leino, R., Johnson, M., … Sandler, N. (2017). Tailored approaches in drug development and diagnostics: From molecular design to biological model systems. *Advanced Healthcare Materials*, *6*.

[10] Lee, S.-R., Hyung, S., Bang, S., Lee, Y., Ko, J., Lee, S., Kim, H. J., & Jeon, N. L. (2019). Modeling neural circuit, blood–brain barrier, and myelination on a microfluidic 96 well plate. *Biofabrication*, *11*, 035013.

[11] Shahin□Shamsabadi, A., & Selvaganapathy, P. R. (2020). A 3d self□assembled in vitro model to simulate direct and indirect interactions between adipocytes and skeletal muscle cells. *Advanced Biosystems*, *4*.

[12] Wu, Q., Liu, J., Wang, X., Feng, L., Wu, J., Zhu, X., Wen, W., & Gong, X. (2020). Organ-on-a-chip: Recent breakthroughs and future prospects. *BioMedical Engineering OnLine*, *19*, 9.

[13] Al-Lamki, R. S., Bradley, J. R., & Pober, J. S. (2017). Human organ culture: Updating the approach to bridge the gap from in vitro to in vivo in inflammation, cancer, and stem cell biology. *Frontiers in Medicine*, *4*.

[14] Park, J., Lee, B. K., Jeong, G. S., Hyun, J. K., Lee, C. J., & Lee, S.-H. (2015). Three-dimensional brain-on-a-chip with an interstitial level of flow and its application as an in vitro model of alzheimer's disease. *Lab on a Chip*, *15*, 141–150.

[15] McAleer, C. W., Long, C. J., Elbrecht, D., Sasserath, T., Bridges, L. R., Rumsey, J. W., Martin, C., Schnepper, M., Wang, Y., Schuler, F., Roth, A. B., Funk, C., Shuler, M. L., & Hickman, J. J. (2019). Multi-organ system for the evaluation of efficacy and off-target toxicity of anticancer therapeutics. *Science Translational Medicine*, *11*.

[16] Pavlovic, M. (2015). What are biomaterials? Springer International Publishing.

[17] Kaushik, P., Kaushik, M., Jacob, S., & Parvez, S. (2022). Multiorgans-on-a-chip for personalized medicine. Springer Nature Singapore.

[18] Tajeddin, A., & Mustafaoglu, N. (2021). Design and fabrication of organ-on-chips: Promises and challenges. *Micromachines*, *12*, 1443.

[19] Nahak, B. K., Mishra, A., Preetam, S., & Tiwari, A. (2022). Advances in organ-on-a-chip materials and devices. *ACS Applied Bio Materials*, *5*, 3576–3607.

[20] Wang, Y., Wang, L., Guo, Y., Zhu, Y., & Qin, J. (2018). Engineering stem cell-derived 3d brain organoids in a perfusable organ-on-a-chip system. *RSC Advances*, *8*, 1677–1685.

[21] Zhang, W., Zhang, Y. S., Bakht, S. M., Aleman, J., Shin, S. R., Yue, K., Sica, M., Ribas, J., Duchamp, M., Ju, J., Sadeghian, R. B., Kim, D., Dokmeci, M. R., Atala, A., & Khademhosseini, A. (2016). Elastomeric free-form blood vessels for interconnecting organs on chip systems. *Lab on a Chip*, *16*, 1579–1586.

[22] Toepke, M. W., & Beebe, D. J. (2006). Pdms absorption of small molecules and consequences in microfluidic applications. *Lab on a Chip*, *6*, 1484.

[23] Regehr, K. J., Domenech, M., Koepsel, J. T., Carver, K. C., Ellison-Zelski, S. J., Murphy, W. L., Schuler, L. A., Alarid, E. T., & Beebe, D. J. (2009). Biological implications of polydimethylsiloxane-based microfluidic cell culture. *Lab on a Chip*, *9*, 2132.

[24] Essaouiba, A., Okitsu, T., Kinoshita, R., Jellali, R., Shinohara, M., Danoy, M., Legallais, C., Sakai, Y., & Leclerc, E. (2020). Development of a pancreas-liver organ-on-chip coculture model for organ-to-organ interaction studies. *Biochemical Engineering Journal*, *164*, 107783.

[25] Aalto-Korte, K. (2020). Acrylic resins. Springer International Publishing.

[26] Bayraktar, G., Guvener, B., Bural, C., & Uresin, Y. (2006). Influence of polymerization method, curing process, and length of time of storage in water on the residual methyl methacrylate content in dental acrylic resins. *Journal of Biomedical Materials Research Part B: Applied Biomaterials*, *76B*, 340–345.

[27] Fritschen, A., Bell, A. K., Königstein, I., Stühn, L., Stark, R. W., & Blaeser, A. (2022). Investigation and comparison of resin materials in transparent dlp-printing for application in cell culture and organs-on-a-chip. *Biomaterials Science*, *10*, 1981–1994.

[28] Bürgers, R., Schubert, A., Müller, J., Krohn, S., Rödiger, M., Leha, A., & Wassmann, T. (2022). Cytotoxicity of 3d□printed, milled, and conventional oral splint resins to l929 cells and human gingival fibroblasts. *Clinical and Experimental Dental Research*, *8*, 650–657.

[29] Guttridge, C., Shannon, A., O'Sullivan, A., O'Sullivan, K. J., & O'Sullivan, L. W. (2022). Biocompatible 3d printing resins for medical applications: A review of marketed intended use, biocompatibility certification, and post-processing guidance. *Annals of 3D Printed Medicine*, *5*, 100044.

[30] Zhang, X., Li, L., & Luo, C. (2016). Gel integration for microfluidic applications. *Lab on a Chip*, *16*, 1757–1776.

[31] Haq, M. R., Kim, Y. K., Kim, J., Ju, J., & Kim, S.-m. (2019). Fabrication of all glass microfluidic device with superior chemical and mechanical resistances by glass molding with vitreous carbon mold. *Journal of Micromechanics and Microengineering*, *29*, 075010.

[32] Waheed, S., Cabot, J. M., Macdonald, N. P., Lewis, T., Guijt, R. M., Paull, B., & Breadmore, M. C. (2016). 3d printed microfluidic devices: Enablers and barriers. *Lab on a Chip*, *16*, 1993–2013.

[33] Nielsen, A. V., Beauchamp, M. J., Nordin, G. P., & Woolley, A. T. (2020). 3d printed microfluidics. *Annual Review of Analytical Chemistry*, *13*, 45–65.

[34] de Gans, B.-J., Duineveld, P., & Schubert, U. (2004). Inkjet printing of polymers: State of the art and future developments. *Advanced Materials*, *16*, 203–213.

[35] Pham, D., & Gault, R. (1998). A comparison of rapid prototyping technologies. *International Journal of Machine Tools and Manufacture*, *38*, 1257–1287.

[36] Zhong, W., Li, F., Zhang, Z., Song, L., & Li, Z. (2001). Short fiber reinforced composites for fused deposition modeling. *Materials Science and Engineering: A*, *301*, 125–130.

[37] Maruo, S., & Kawata, S. (1997). Two-photon-absorbed photopolymerization for three-dimensional microfabrication. *Proceedings IEEE The Tenth Annual International Workshop on Micro Electro*

Mechanical Systems. An Investigation of Micro Structures, Sensors, Actuators, Machines and Robots, 169–174.

[38] Otuka, A. J. G., Tomazio, N. B., Paula, K. T., & Mendonça, C. R. (2021). Two-photon polymerization: Functionalized microstructures, micro-resonators, and bio-scaffolds. *Polymers*, *13*, 1994.

[39] Sun, C., Fang, N., Wu, D., & Zhang, X. (2005). Projection micro-stereolithography using digital micro-mirror dynamic mask. *Sensors and Actuators A: Physical*, *121*, 113–120.

[40] Zheng, X., Deotte, J., Alonso, M. P., Farquar, G. R., Weisgraber, T. H., Gemberling, S., Lee, H., Fang, N., & Spadaccini, C. M. (2012). Design and optimization of a light-emitting diode projection micro-stereolithography three-dimensional manufacturing system. *Review of Scientific Instruments*, *83*.

[41] Bhatia, S. N., & Ingber, D. E. (2014). Microfluidic organs-on-chips. *Nature Biotechnology*, *32*, 760–772.

[42] Ansari, A., Trehan, R., Watson, C., & Senyo, S. (2021). Increasing silicone mold longevity: A review of surface modification techniques for pdms-pdms double casting. *Soft Materials*, *19*, 388–399.

[43] Kamei, K.-i., Mashimo, Y., Koyama, Y., Fockenberg, C., Nakashima, M., Nakajima, M., Li, J., & Chen, Y. (2015). 3d printing of soft lithography mold for rapid production of polydimethylsiloxane-based microfluidic devices for cell stimulation with concentration gradients. *Biomedical Microdevices*, *17*, 36.

[44] Venzac, B., Deng, S., Mahmoud, Z., Lenferink, A., Costa, A., Bray, F., Otto, C., Rolando, C., & Gac, S. L. (2021). Pdms curing inhibition on 3d-printed molds: Why? also, how to avoid it? *Analytical Chemistry*, *93*, 7180–7187.

[45] Glick, C. C., Srimongkol, M. T., Schwartz, A. J., Zhuang, W. S., Lin, J. C., Warren, R. H., Tekell, D. R., Satamalee, P. A., & Lin, L. (2016). Rapid assembly of multilayer microfluidic structures via 3d-printed transfer molding and bonding. *Microsystems Nanoengineering*, *2*, 16063.

[46] Zhang, S., Wan, Z., & Kamm, R. D. (2021). Vascularized organoids on a chip: Strategies for engineering organoids with functional vasculature. *Lab on a Chip*, *21*, 473–488.

[47] Auger, F. A., Gibot, L., & Lacroix, D. (2013). The pivotal role of vascularization in tissue engineering. *Annual Review of Biomedical Engineering*, *15*, 177–200.

[48] LaMontagne, E., Muotri, A. R., & Engler, A. J. (2022). Recent advancements and future requirements in vascularization of cortical organoids. *Frontiers in Bioengineering and Biotechnology*, *10*.

[49] Nashimoto, Y., Hayashi, T., Kunita, I., Nakamasu, A., Torisawa, Y.-s., Nakayama, M., Takigawa-Imamura, H., Kotera, H., Nishiyama, K., Miura, T., & Yokokawa, R. (2017). Integrating perfusable vascular networks with a three-dimensional tissue in a microfluidic device. *Integrative Biology*, *9*, 506–518.

[50] Grebenyuk, S., & Ranga, A. (2019). Engineering organoid vascularization. *Frontiers in Bioengineering and Biotechnology*, *7*.

[51] Kolesky, D. B., Homan, K. A., Skylar-Scott, M. A., & Lewis, J. A. (2016). Three-dimensional bioprinting of thick vascularized tissues. *Proceedings of the National Academy of Sciences*, *113*, 3179–3184.

[52] Culver, J. C., Hoffmann, J. C., Poché, R. A., Slater, J. H., West, J. L., & Dickinson, M. E. (2012). Three□dimensional biomimetic patterning in hydrogels to guide cellular organization. *Advanced Materials*, *24*, 2344–2348.

[53] Kim, S., Lee, H., Chung, M., & Jeon, N. L. (2013). Engineering of functional, perfusable 3d microvascular networks on a chip. *Lab on a Chip*, *13*, 1489.

[54] Song, J. W., & Munn, L. L. (2011). Fluid forces control endothelial sprouting. *Proceedings of the National Academy of Sciences*, *108*, 15342–15347.

[55] Salmon, I., Grebenyuk, S., Fattah, A. R. A., Rustandi, G., Pilkington, T., Verfaillie, C., & Ranga, A. (2022). Engineering neurovascular organoids with 3d printed microfluidic chips. *Lab on a Chip*, *22*, 1615–1629.

[56] Kim, S., Kim, W., Lim, S., & Jeon, J. (2017). Vasculature-on-a-chip for in vitro disease models. *Bioengineering*, *4*, 8.

[57] Kim, T. H., Lee, J. M., Ahrberg, C. D., & Chung, B. G. (2018). Development of the microfluidic device to regulate shear stress gradients. *BioChip Journal*, *12*, 294–303.

[58] Cuenca, M. V., Cochrane, A., van den Hil, F. E., de Vries, A. A., Oberstein, S. A. L., Mummery, C. L., & Orlova, V. V. (2021). Engineered 3d vessel-on-chip using hipsc-derived endothelial- and vascular smooth muscle cells. *Stem Cell Reports*, *16*, 2159–2168.

[59] Samuel, R., Duda, D. G., Fukumura, D., & Jain, R. K. (2015). Vascular diseases await translation of blood vessels engineered from stem cells. *Science Translational Medicine*, *7*.

[60] Hoffman, G. E., Schrode, N., Flaherty, E., & Brennand, K. J. (2019). New considerations for hipsc-based models of neuropsychiatric disorders. *Molecular Psychiatry*, *24*, 49–66.

[61] Arslan, U., Brescia, M., Meraviglia, V., Nahon, D. M., van Helden, R. W., Stein, J. M., van den Hil, F. E., van Meer, B. J., Cuenca, M. V., Mummery, C. L., & Orlova, V. V. (2023). Vascularized hipsc-derived 3d cardiac microtissue on chip. *Stem Cell Reports*, *18*, 1394–1404.

[62] Lin, C.-H., Lee, S.-Y., & Lin, Y.-M. (2016). Plasma treatment in conjunction with egm-2 medium increases endothelial and osteogenic marker expressions of bone marrow mesenchymal stem cells. *Journal of Materials Science*, *51*, 9145–9154.

[63] Staton, C. A., Brown, N. J., & Lewis, C. E. (2003). The role of fibrinogen and related fragments in tumour angiogenesis and metastasis. *Expert Opinion on Biological Therapy*, *3*, 1105–1120.

[64] Eigenhuis, K. N., Somsen, H. B., van der Kroeg, M., Smeenk, H., Korporaal, A. L., Kushner, S. A., de Vrij, F. M. S., & van den Berg, D. L. C. (2023). A simplified protocol for the generation of cortical brain organoids. *Frontiers in Cellular Neuroscience*, *17*.

[65] Li, S., Yang, C., Li, J., Zhang, C., Zhu, L., Song, Y., Guo, Y., Wang, R., Gan, D., Shi, J., Ma, P., Gao, F., & Su, H. (2023). Progress in pluronic f127 derivatives for application in wound healing and repair. *International Journal of Nanomedicine*, *Volume 18*, 4485–4505.

[66] Kolesky, D. B., Truby, R. L., Gladman, A. S., Busbee, T. A., Homan, K. A., & Lewis, J. A. (2014). 3d bioprinting of vascularized, heterogeneous cell□laden tissue constructs. *Advanced Materials*, *26*, 3124–3130.

[67] Lippens, E., Swennen, I., Gironès, J., Declercq, H., Vertenten, G., Vlaminck, L., Gasthuys, F., Schacht, E., & Cornelissen, R. (2013). Cell survival and proliferation after encapsulation in a chemically modified pluronic® f127 hydrogel. *Journal of Biomaterials Applications*, *27*, 828–839.

[68] Wu, W., DeConinck, A., & Lewis, J. A. (2011). Omnidirectional printing of 3d microvascular networks. *Advanced Materials*, *23*.

[69] Shamma, R. N., Sayed, R. H., Madry, H., Sayed, N. S. E., & Cucchiarini, M. (2022). Triblock copolymer bioinks in hydrogel three-dimensional printing for regenerative medicine: A focus on pluronic f127. *Tissue Engineering Part B: Reviews*, *28*, 451–463.

[70] Yap, L.-S., & Yang, M.-C. (2016). Evaluation of hydrogel composing of pluronic f127 and carboxymethyl hexanoyl chitosan as injectable scaffold for tissue engineering applications. *Colloids and Surfaces B: Biointerfaces*, *146*, 204–211.

[71] Shirwaiker, R., Purser, M., & Wysk, R. (2014). Scaffolding hydrogels for rapid prototyping based tissue engineering. Elsevier.

[72] Lenaerts, V., Triqueneaux, C., Quartern, M., Rieg-Falson, F., & Couvreur, P. (1987). Temperature-dependent rheological behavior of pluronic f-127 aqueous solutions. *International Journal of Pharmaceutics*, *39*, 121–127.

[73] Gioffredi, E., Boffito, M., Calzone, S., Giannitelli, S. M., Rainer, A., Trombetta, M., Mozetic, P., & Chiono, V. (2016). Pluronic f127 hydrogel characterization and biofabrication in cellularized constructs for tissue engineering applications. *Procedia CIRP*, *49*, 125–132.

[74] Camana, G., Tavano, M., Li, M., Castiglione, F., Rossi, F., & Cellesi, F. (2023). Design of functional pluronic-based precursors for tailoring hydrogel thermoresponsiveness and cell-adhesive properties. *Materials*, *16*, 2749.

[75] Zhang, Z., Ni, J., Chen, L., Yu, L., Xu, J., & Ding, J. (2011). Biodegradable and thermoreversible pcla–peg–pcla hydrogel as a barrier for prevention of post-operative adhesion. *Biomaterials*, *32*, 4725–4736.

[76] Lee, S.-Y., & Tae, G. (2007). Formulation and in vitro characterization of an in situ gelable, photo-polymerizable pluronic hydrogel suitable for injection. *Journal of Controlled Release*, *119*, 313–319.

[77] Biase, M. D., de Leonardis, P., Castelletto, V., Hamley, I. W., Derby, B., & Tirelli, N. (2011). Photopolymerization of pluronic f127 diacrylate: A colloid-templated polymerization. *Soft Matter*, *7*, 4928.

[78] Bhusari, S., Hoffman, M., Herbeck-Engel, P., Sankaran, S., Wilhelm, M., & Campo, A. D. (2023). Rheological behavior of pluronic/pluronic diacrylate hydrogels used for bacteria encapsulation in living materials. *bioRxiv*.

[79] Lee, J. B., Chun, K. W., Yoon, J. J., & Park, T. G. (2004). Controlling degradation of acid□hydrolyzable pluronic hydrogels by physical entrapment of poly(lactic acid□ co □glycolic acid) microspheres. *Macromolecular Bioscience*, *4*, 957–962.

[80] Cellesi, F., Tirelli, N., & Hubbell, J. A. (2002). Materials for cell encapsulation via a new tandem approach combining reverse thermal gelation and covalent crosslinking. *Macromolecular Chemistry and Physics*, *203*, 1466–1472.

[81] Salaklang, J., Maes, V., Conradi, M., Dams, R., & Junkers, T. (2018). Direct synthesis of acrylate monomers in heterogeneous continuous flow processes. *Reaction Chemistry Engineering*, *3*, 41–47.

[82] Paar, A. (2010). Basics of rheology.

[83] Ho, C. M. B., Ng, S. H., Li, K. H. H., & Yoon, Y.-J. (2015). 3d printed microfluidics for biological applications. *Lab on a Chip*, *15*, 3627–3637.

[84] Ligon, S. C., Husár, B., Wutzel, H., Holman, R., & Liska, R. (2014). Strategies to reduce oxygen inhibition in photoinduced polymerization. *Chemical Reviews*, *114*, 557–589.

[85] SchoutenDental. (2024). Freeprint® ortho 3d print resin voor orthodontische basis componenten.

[86] Chen, X., Ashcroft, I., Tuck, C., He, Y., Hague, R., & Wildman, R. (2017). An investigation into the depth and time dependent behavior of uv cured 3d ink jet printed objects. *Journal of Materials Research*, *32*, 1407–1420.

[87] Asiga. (2024a). *Asiga material configutation file creation*.

[88] Facility, H. M. S. M. C. (2015, December). Procedures for bonding pdms.

[89] Akther, F., Yakob, S. B., Nguyen, N.-T., & Ta, H. T. (2020). Surface modification techniques for endothelial cell seeding in pdms microfluidic devices. *Biosensors*, *10*, 182.

[90] Li, Y., Wang, X., Wang, Y., & Fan, Y. (2023). Low-cost hybrid bonding between thermoplastics and pdms with differential adhesive tape for microfluidic devices. *Journal of Materials Science: Materials in Electronics*, *34*, 565.

[91] Jalaal, M., Cottrell, G., Balmforth, N., & Stoeber, B. (2017). On the rheology of pluronic f127 aqueous solutions. *Journal of Rheology*, *61*, 139–146.

[92] University, M. S. (2019, August). Basic practical nmr concepts: A guide for the modern laboratory.

[93] Günther, H. (2013, June). *Nmr spectroscopy* (Vol. 3). WIley.

[94] Smirnov, S., & McCarty, J. (2024). Chemical shift in units of hz and ppm.

[95] Chen, M., Li, C., Nie, F., Liu, X., Pipinos, I. I., & Li, X. (2020). Synthesis and characterization of a hyaluronic acid-based hydrogel with antioxidative and thermosensitive properties. *RSC Advances*, *10*, 33851–33860.

[96] Boutry, C. M., Kiran, R., Umbrecht, F., & Hierold, C. (2010). Processing and quantitative analysis of biodegradable polymers (plla and pcl) thermal bonding. *Journal of Micromechanics and Microengineering*, *20*, 085006.

[97] Barba, A. A., d'Amore, M., Grassi, M., Chirico, S., Lamberti, G., & Titomanlio, G. (2009). Investigation of pluronic© f127–water solutions phase transitions by dsc and dielectric spectroscopy. *Journal of Applied Polymer Science*, *114*, 688–695.

[98] Sahar, A. M., Wissink, J., Mahmoud, M. M., Karayiannis, T. G., & Ishak, M. S. A. (2017). Effect of hydraulic diameter and aspect ratio on single phase flow and heat transfer in a rectangular microchannel. *Applied Thermal Engineering*, *115*, 793–814.

[99] Yu, T., Yang, Q., Peng, B., Gu, Z., & Zhu, D. (2024). Vascularized organoid-on-a-chip: Design, imaging, and analysis. *Angiogenesis*, *27*, 147–172.

[100] Wei, M., Cheng, N.-S., & Lu, Y. (2023). Revisiting the concept of hydraulic radius. *Journal of Hydrology*, *625*, 130134.

[101] Stringer, R., Zang, J., & Hillis, A. (2014). Unsteady rans computations of flow around a circular cylinder for a wide range of reynolds numbers. *Ocean Engineering*, *87*, 1–9.

[102] Li, S., Xu, J., Wang, Y., & Luo, G. (2009). A new interfacial tension measurement method through a pore array micro-structured device. *Journal of Colloid and Interface Science*, *331*, 127–131.

[103] Vladisavljević, G. T. (2018). Fabrication of nanoemulsions by membrane emulsification. Elsevier.

[104] Olanrewaju, A., Beaugrand, M., Yafia, M., & Juncker, D. (2018). Capillary microfluidics in microchannels: From microfluidic networks to capillaric circuits. *Lab on a Chip*, *18*, 2323–2347.

[105] Ruxandra, L. A., Anghel, D., & Stinga, G. (2016). Physicochemical studies on ketoprofen encapsulated in pluronic f127 nanomicelles for drug applications. *ACADEMIA ROMÂNĂ*.

[106] İspir, E., İnal, M., Gök, Z. G., & Yiğitoğlu, M. (2024). Synthesis, characterization and in vitro release analysis of pluronic f127 copolymer micelles containing quercetin as a hydrophobic drug. *Polymer Bulletin*, *81*, 6801–6822.

[107] Zhang, Y., & Lam, Y. (2007). Controlled synthesis and association behavior of graft pluronic in aqueous solutions. *Journal of Colloid and Interface Science*, *306*, 398–404.

[108] Huhtamäki, T., Tian, X., Korhonen, J. T., & Ras, R. H. A. (2018). Surface-wetting characterization using contact-angle measurements. *Nature Protocols*, *13*, 1521–1538.

[109] Pisapia, F., Balachandran, W., & Rasekh, M. (2022). Organ-on-a-chip: Design and simulation of various microfluidic channel geometries for the influence of fluid dynamic parameters. *Applied Sciences*, *12*, 3829.

[110] Tomecka, E., Zukowski, K., Jastrzebska, E., Chudy, M., & Brzozka, Z. (2018). Microsystem with micropillar array for three- (gel-embaded) and two-dimensional cardiac cell culture. *Sensors and Actuators B: Chemical*, *254*, 973–983.

[111] Barbato, M. G., Pereira, R. C., Mollica, H., Palange, A., Ferreira, M., & Decuzzi, P. (2021). A permeable on-chip microvasculature for assessing the transport of macromolecules and polymeric nanoconstructs. *Journal of Colloid and Interface Science*, *594*, 409–423.

[112] Manneschi, C., Pereira, R. C., Marinaro, G., Bosca, A., Francardi, M., & Decuzzi, P. (2016). A microfluidic platform with permeable walls for the analysis of vascular and extravascular mass transport. *Microfluidics and Nanofluidics*, *20*, 113.

[113] Ewald, K. (2015, May). Impact of pipetting techniques on precision and accuracy.

[114] Asiga. (2024b). Ultragloss™.

[115] Detax. (2024). Freeprint® ortho.

[116] Moiin. (2024). Moiin tech clear.

[117] Kaneda, S., Ono, K., Fukuba, T., Nojima, T., Yamamoto, T., & Fujii, T. (2012). Modification of the glass surface property in pdms-glass hybrid microfluidic devices. *Analytical Sciences*, *28*, 39–44.

[118] Kim, Y.-M., Kim, W.-S., Lee, S.-H., & Baek, J.-Y. (2005). Effects of surface roughness on the flow characteristics in pdms microchannels. *2005 3rd IEEE/EMBS Special Topic Conference on Microtechnology in Medicine and Biology*, 292–295.

[119] Hassanpour-Tamrin, S., Sanati-Nezhad, A., & Sen, A. (2021). A simple and low-cost approach for irreversible bonding of polymethylmethacrylate and polydimethylsiloxane at room temperature for high-pressure hybrid microfluidics. *Scientific Reports*, *11*, 4821.

[120] Bazaz, S. R., Kashaninejad, N., Azadi, S., Patel, K., Asadnia, M., Jin, D., & Warkiani, M. E. (2019). Rapid softlithography using 3d□printed molds. *Advanced Materials Technologies*, *4*.

[121] Borók, A., Laboda, K., & Bonyár, A. (2021). Pdms bonding technologies for microfluidic applications: A review. *Biosensors*, *11*, 292.

[122] Lee, J. B., Yoon, J. J., Lee, D. S., & Park, T. G. (2004). Photo-crosslinkable, thermo-sensitive and biodegradable pluronic hydrogels for sustained release of protein. *JOURNAL OF BIOMATERIALS SCIENCE-POLYMER EDITION*, *15*, 1571–1583.

[123] chemicalbook. (2017). Triethylamine(121-44-8) 1h nmr.

[124] ChemicalBook. (2017). Diethyl ether(60-29-7) 1h nmr.

[125] Cooper, A., & Johnson, C. M. (1994). Differential scanning calorimetry. Humana Press.

[126] Yoon, J. J., Chung, H. J., & Park, T. G. (2007). Photo□crosslinkable and biodegradable pluronic/heparin hydrogels for local and sustained delivery of angiogenic growth factor. *Journal of Biomedical Materials Research Part A*, *83A*, 597–605.

[127] Lisensky, G. C., Campbell, D. J., Beckman, K. J., Calderon, C. E., Doolan, P. W., Ottosen, R. M., & Ellis, A. B. (1999). Replication and compression of surface structures with polydimethylsiloxane elastomer. *Journal of Chemical Education*, *76*, 537.

[128] Comina, G., Suska, A., & Filippini, D. (2014). Pdms lab-on-a-chip fabrication using 3d printed templates. *Lab Chip*, *14*, 424–430.

[129] Chan, H. N., Chen, Y., Shu, Y., Chen, Y., Tian, Q., & Wu, H. (2015). Direct, one-step molding of 3d-printed structures for convenient fabrication of truly 3d pdms microfluidic chips. *Microfluidics and Nanofluidics*, *19*, 9–18.

[130] Waheed, S., Cabot, J. M., Macdonald, N. P., Kalsoom, U., Farajikhah, S., Innis, P. C., Nesterenko, P. N., Lewis, T. W., Breadmore, M. C., & Paull, B. (2017). Enhanced physicochemical properties of polydimethylsiloxane based microfluidic devices and thin films by incorporating synthetic micro-diamond. *Scientific Reports*, *7*, 15109.

[131] Boccafoschi, F., Fusaro, L., & Cannas, M. (2018). Immobilization of peptides on cardiovascular stent. Elsevier.

[132] Hillborg, H., & Gedde, U. (1998). Hydrophobicity recovery of polydimethylsiloxane after exposure to corona discharges. *Polymer*, *39*, 1991–1998.

[133] Plasma, H. (2024). Pdms bonding (microfluidics).

[134] Bhattacharya, S., Datta, A., Berg, J., & Gangopadhyay, S. (2005). Studies on surface wettability of poly(dimethyl) siloxane (pdms) and glass under oxygen-plasma treatment and correlation with bond strength. *Journal of Microelectromechanical Systems*, *14*, 590–597.

[135] Clarson, S., & Semlyen, J. (1993). *Siloxane polymers*. Prentice Hall.

[136] Yang, C., Wang, W., & Li, Z. (2009). Optimization of corona-triggered pdms-pdms bonding method. *2009 4th IEEE International Conference on Nano/Micro Engineered and Molecular Systems*, 319–322.

[137] Eddings, M. A., Johnson, M. A., & Gale, B. K. (2008). Determining the optimal pdms–pdms bonding technique for microfluidic devices. *Journal of Micromechanics and Microengineering*, *18*, 067001.

A

PDMS Synthesis

A.0.0.1. PDMS Curing

PDMS is a colorless, transparent elastomer which can be fabricated using a base and curing agent. Both the base and the curing agent contain siloxane oligomers. The siloxane oligomers in the base contain vinyl terminated groups, while the curing agent contains cross-linking oligomers with at least three silicon-hydride bonds [127]. The base also includes a platinum-based (Pt-based) catalyst which cures the elastomers through cross-linking. When both the base and the curing agent are mixed together, the the Pt-based catalyst increase the rate at which the Silicon-Hydrogen (Si-H) bonds of the curing agent bond with the reactive double bonds in the base. This causes the two oligomers to cross-link. Cross-linking happens at room temperature but can be accelerated at higher temperatures. Due to multiple reaction sided on the curing agent oligomer, a three dimensional cross-linked elastomer is formed [127]. Fig. A.1 shows the complete reaction scheme. The ratio of base to curing agent defines the properties of the cured elastomer. An increase in curing agent results in a more rigid elastomer.

A.0.0.2. Surface Treatment

PDMS curing can be inhibited by many available UV curing resin, as PDMS strongly adheres to these molds [44]. Several chemical groups, including vinyl, maleate, fumerate and tri-organophosphite, can inhibit PDMS curing due to their strong affinity for the Pt-based catalyst found in the PDMS base. Moreover, unreacted monomers and phospine-oxide photoinitiators in 3D printed molds can inhibit the catalyst [44].

Therefore, 3D printed molds using UV curable resins require surface treatment to prevent the inhibition of PDMS curing. After 3D printing, any residual uncured resin should be removed from the print using isopropylalcohol (IPA). When the majority of uncured resin is removed, the 3D printed parts should be post cured using UV to further polymerize any uncured monomers. This reduces the risk of monomer leaching in a later stage. Subsequently, the mold can be thermally treated, which vaporizes any remaining photo-initiator which could remain in the 3D print. This is especially valid for resins containing phosphine-oxide based photo-initiators [44].

Besides UV post curing and thermal treatments, the mold surface can also be treated with solvents, sonication, silanization or coatings [128, 129]. On photo-lithography molds, silanization of the surface of the molds is done to provide a hydrophobic fluorinated monolayer on the mold surface. This prevents PDMS from sticking to the molds, which makes it easy to be removed [129, 130]. Silanization attaches organosilyl groups to surfaces which are rich in hydroxyl groups, such as silicon wafers and glass [131]. Other studies show that silanization is not required to prevent PDMS from sticking to 3D printed molds, because of the absence of hydroxyl groups [120].

A.0.0.3. PDMS Bonding

PDMS bonding is referred to as the creation of an irreversible chemical bond between activated PDMS and substrate layers [121]. For microfluidic applications, a strong bond is required, especially for applications with a high pressure or flow rate. Therefore, several bonding techniques will be discussed.

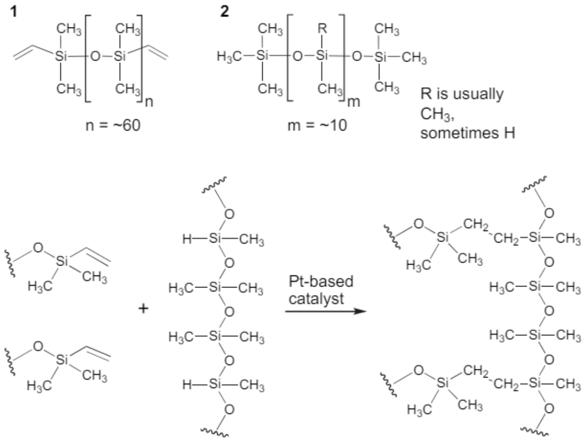

Figure A.1: PDMS elastomer reaction. (1) The base, containing vinyl terminated end groups. (2) the curing agent, containing at least three Si-H bonds per oligomer. Underneath: the chemical reaction leading to PDMS elastomers. The base oligomers binds to the Si-H bonds on the curing agent oligomers to form three dimensional elastomers. The reaction is accelerated by a Pt-based catalyst [127].

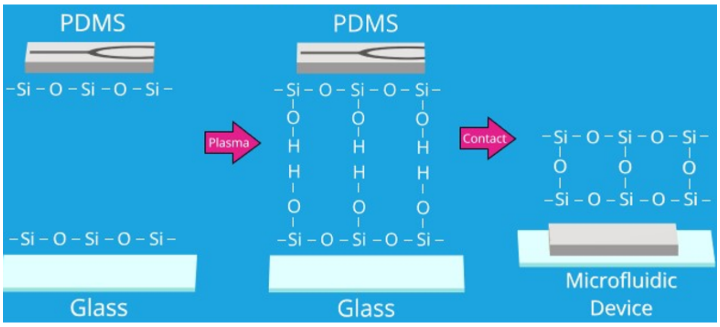

Figure A.2: Visualization of the surface activation with oxygen plasma. Upon exposure to oxygen plasma, silanol groups (Si-OH) groups are formed on the surface. These silanol groups form covalent bonds with other activated surfaces. This creates an irreversible bond between two activated layers [133].

Surface activation by oxygen plasma: The aim of surface activation is the removal of contaminants and the creation of reactive chemical groups for covalent bonding. As explained in Sec. A.0.0.1, silicon-based materials can bond through the silanol groups (Si-OH). Through surface activation, the unreactive methyl groups (-CH3) can be replaced by silanol groups. These silanol groups can form covalent bonds with other silanol groups on other activated surfaces [121]. Fig. A.2 visualizes the process of surface activation and bonding. The exposure to plasma treatment makes the surface hydrophilic. However, after exposure to ambient conditions, the treated surface quickly regains it hydrophobicity. Deformation of the treated surface speeds up this process. Therefore, it is important that treated PDMS surfaces are handled with great care during bonding and alignment [132].

The increased concentration of hydroxyl groups and surface oxidation of PDMS can also change the surface properties significantly. This can happen due to increase cross-linking or degradation of the cross-linked network. The extend to which this happens depend on the experimental conditions of the oxygen plasma treatment (power, pressure, exposure time, etc.) [121]. Therefore, the oxygen plasma parameters need to be optimized to create a strong bond between two activated surfaces.

Bhattacharya et al. (2005) studied the effects of chamber pressure, power and exposure time for oxygen plasma bonding of PDMS-glass and PDMS-PDMS [134]. Fig. A.3 shows the results of these three parameters for PDMS-glass bonding. They tested the effects of these parameters on bonding strength and contact angle. In this context, contact angle refers to the angle of water droplets with the surface of the treated PDMS layer. A high contact angle ($> 90°$) means that the surface is very hydrophobic, causing water to from droplets on the surface of the PDMS layer. A low contact angle ($< 20°$) means

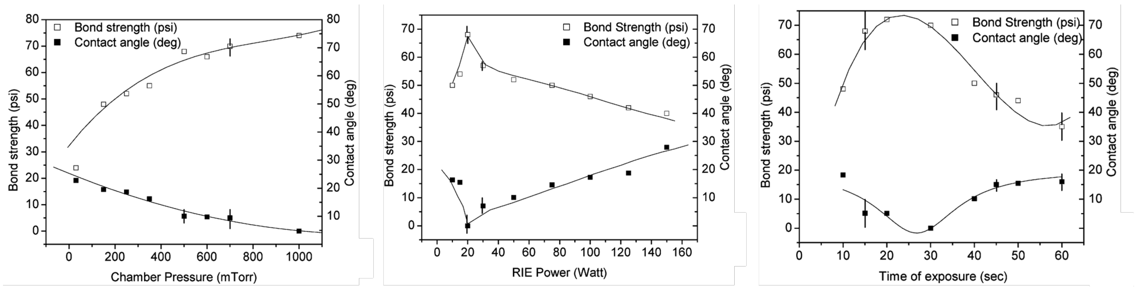

Figure A.3: The effects of chamber pressure, power and exposure time of oxygen plasma on bonding strength between PDMS and glass and contacts angle of DI water. The bonding strength increases with an increase in chamber presser. Initially, the bonding strength also increase with an increase in power and exposure time. However, the bonding strength peaks for these parameters, after which the bonding strength decreases with an increase in power and exposure time [134].

that the surface is hydrophilic, causing water to spread out over the surface, which creates a low contact angle. In Fig. A.3 can be seen that an increase in chamber pressure creates a stronger bonding between PDMS and glass. A chamber pressure below 100 mTorr (0.13 mbar) causes the plasma etching to become highly directional and anisotropic [134]. This could cause the decrease in bond strength below this value. The etching power show an interesting effect on bonding strength. Initially, the bonding strength rises and peaks at approximately 20W. After this peak, an increase in power causes the bonding strength to decrease. This is caused by damage of the Si-C backbone found in PDMS, which has a lower dissociation energy than the Si-O-Si bonds [135]. The exposure time shows a similar trend. Initially, an increase in exposure time result in an increase in bonding strength. This increase peaks at approximately 20 seconds, after which the bonding strength decreases with an increase in exposure time.
For PDMS-PDMS bonding, a similar trend was observed compared to PDMS-glass bonding [134]. However, for optimal bonding, the influence of these parameters on bonding strength need to be optimized individually.

Surface activation by corona treatment: Similar to oxygen plasma treatment, corona treatment also utilize plasma to create surface activation. Corona treatment exploits a handheld device which creates a high voltage across an electrode. The high voltage ionizes the surrounding air, creating a localized plasma [121]. Compared to the previously described oxygen plasma, which is performed in a closed environment, corona treatment does not require expensive equipment (no need for a vacuum system). Moreover, the device is portable and easy to use. However, the actual plasma treatment is hard to precisely control. The distance, movement speed and treatment time are all treatment parameters which can create variation in the treatment process [136].

Chemical gluing: To bond PDMS with other materials (not glass or silicon-based materials), functional groups should be on both materials or only on the target substrate. The process through which molecular monolayers are anchored on the surface of terminal functional groups is called chemical gluing [121]. The bonding of PDMS to these materials, such as thermoplastics, utilizes silane coupling agents. During surface treatment (oxygen plasma or corona treatment), the carbon-backbone of thermoplastic materials can be broken. The free carbon atoms react with the silicon of the silane coupling agents. This creates a surface with Si-O-C bonds [2]. Finally, the coupling agents bind the Si-OH groups on the activated PDMS surface to create an irreversible bond.

Partial curing: Besides the above listed bonding techniques, two PDMS layers can also be bonded by the additional of microscopic layers of PDMS or through partial curing of those PDMS layers. Instead of fully curing molded PDMS layers, PDMS layers can be partially cured (low curing duration) prior to bonding. The partially cured PDMS layers can be aligned and bonded together through an applied pressure and allowed to fully cure after bonding. This results in a higher bonding strength compared to the bonding methods described above [137]. This methods is cheaper and easier to perform compared to above mentioned bonding methods. However, partial curing of PDMS layers might cause the microfluidic layers in the PDMS to deform or collapse. Therefore, for microfluidic device with fragile components, this method might not be ideal.

B

Detax Freeprint Ortho initiator file

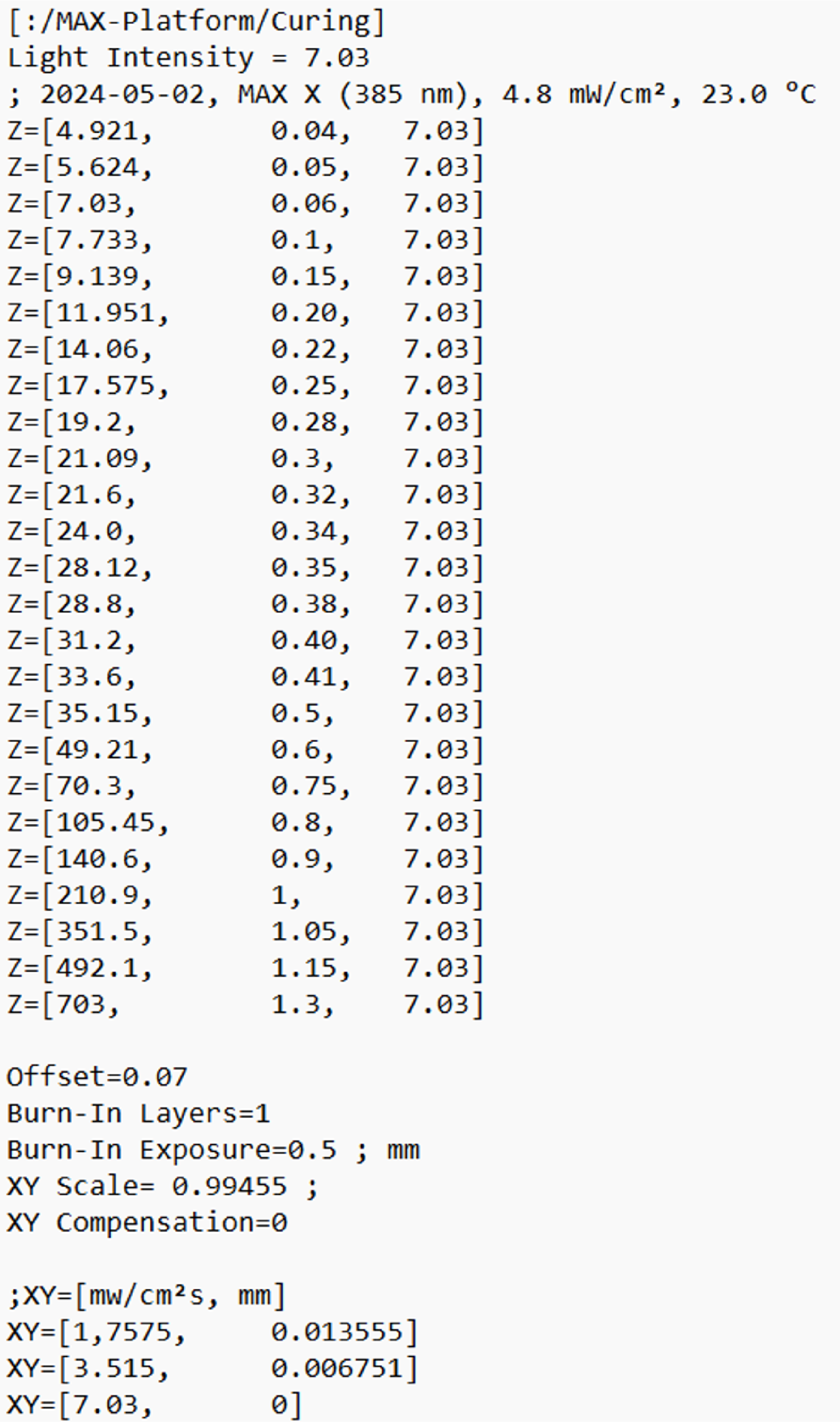

```
[:/MAX-Platform/Curing]
Light Intensity = 7.03
; 2024-05-02, MAX X (385 nm), 4.8 mW/cm², 23.0 °C
Z=[4.921,       0.04,   7.03]
Z=[5.624,       0.05,   7.03]
Z=[7.03,        0.06,   7.03]
Z=[7.733,       0.1,    7.03]
Z=[9.139,       0.15,   7.03]
Z=[11.951,      0.20,   7.03]
Z=[14.06,       0.22,   7.03]
Z=[17.575,      0.25,   7.03]
Z=[19.2,        0.28,   7.03]
Z=[21.09,       0.3,    7.03]
Z=[21.6,        0.32,   7.03]
Z=[24.0,        0.34,   7.03]
Z=[28.12,       0.35,   7.03]
Z=[28.8,        0.38,   7.03]
Z=[31.2,        0.40,   7.03]
Z=[33.6,        0.41,   7.03]
Z=[35.15,       0.5,    7.03]
Z=[49.21,       0.6,    7.03]
Z=[70.3,        0.75,   7.03]
Z=[105.45,      0.8,    7.03]
Z=[140.6,       0.9,    7.03]
Z=[210.9,       1,      7.03]
Z=[351.5,       1.05,   7.03]
Z=[492.1,       1.15,   7.03]
Z=[703,         1.3,    7.03]

Offset=0.07
Burn-In Layers=1
Burn-In Exposure=0.5 ; mm
XY Scale= 0.99455 ;
XY Compensation=0

;XY=[mw/cm²s, mm]
XY=[1,7575,     0.013555]
XY=[3.515,      0.006751]
XY=[7.03,       0]
```

Figure B.1: The most important parameters of the initiator file for Detax Freeprint Ortho including the Z-curing table and the XY-scaling table

C

PDMS molding pictures

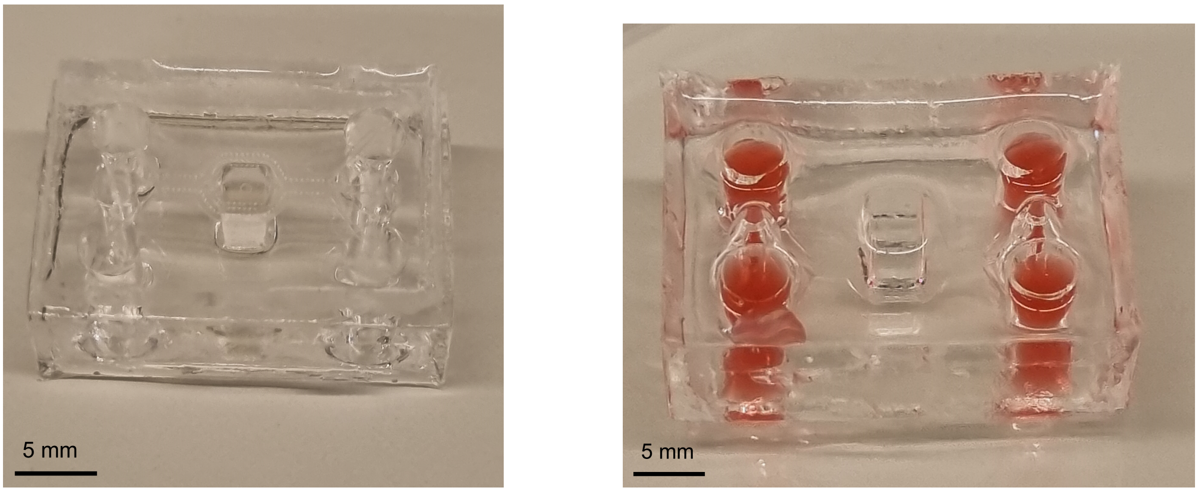

(a)

(b)

Figure C.1: PDMS fabrication pictures of bonding of top and bottom layer. (a) Bottom view of bonded layers. (b) Top view with red-colored PBS injected.

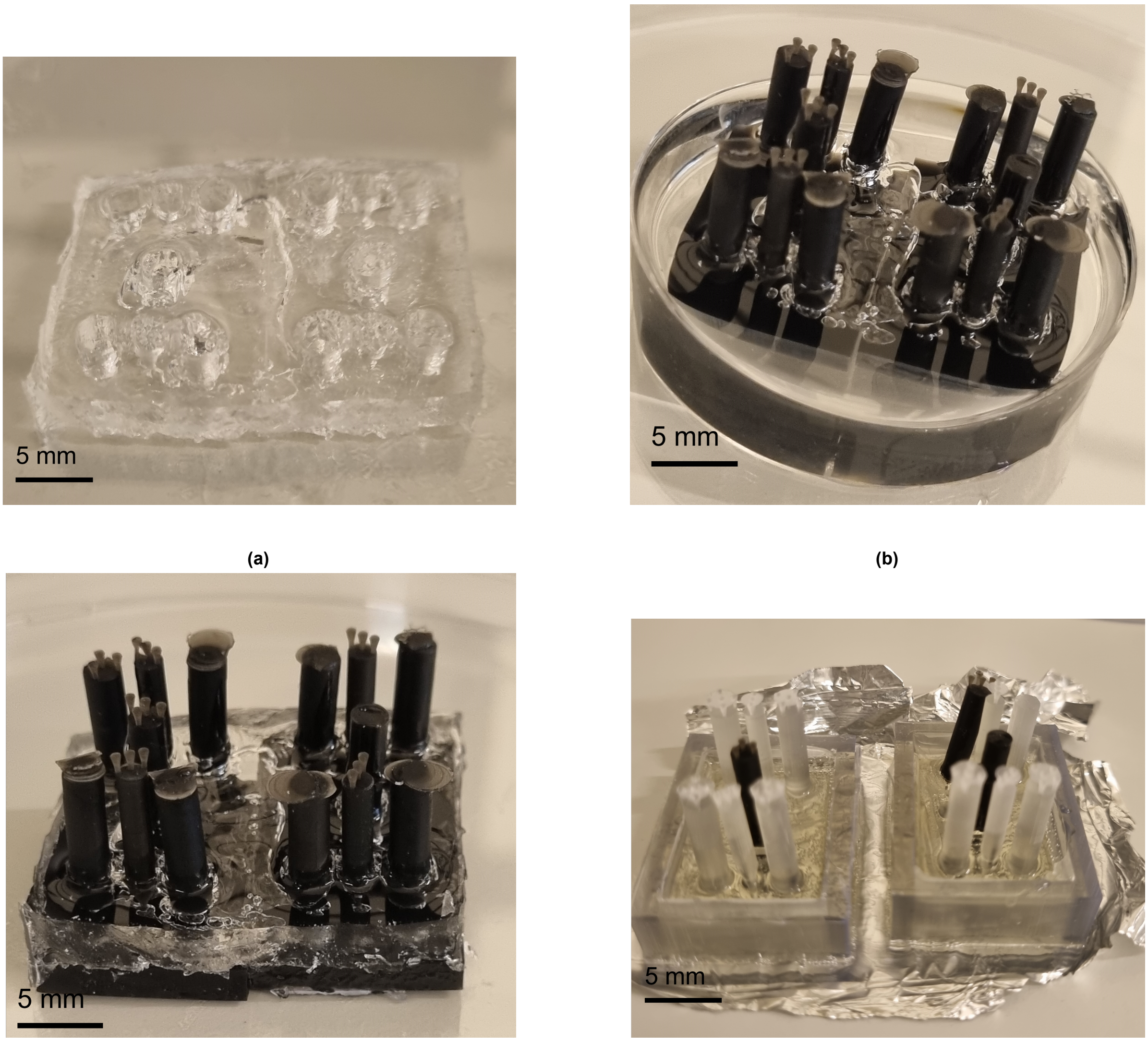

(a)

(b)

(c)

(d)

Figure C.2: PDMS fabrication pictures of separately printed pillars. (a) Demolded PDMS. (b) PDMS after curing in plastic Petri dish. (c) Petri dish removed and PDMS cut along the edge of the mold. (d) Petri dish replaced with 3D printed casing.

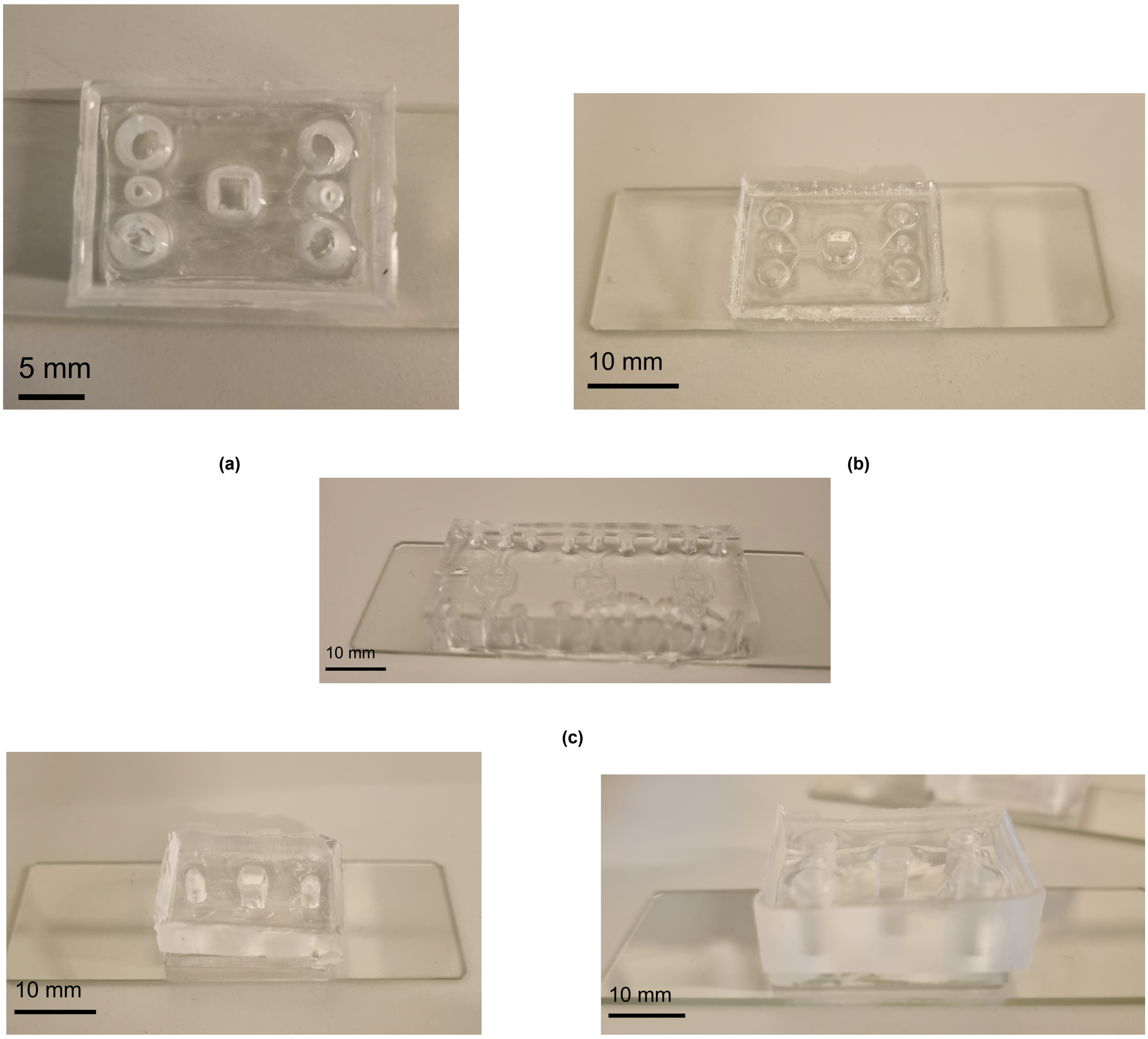

(a)

(b)

(c)

(d)

(e)

Figure C.3: PDMS molding pictures of punched PDMS bonded to glass. (a) Top view. (b) Side view of thin single layer with microfluidic channels. (c) Side view of single layer, with three platforms fabricated simultaneously. (d) Side view of thick layer without inlet punching. (d) Side view of additional microfluidic layer and top layer molded seperately, then bonded to glass.

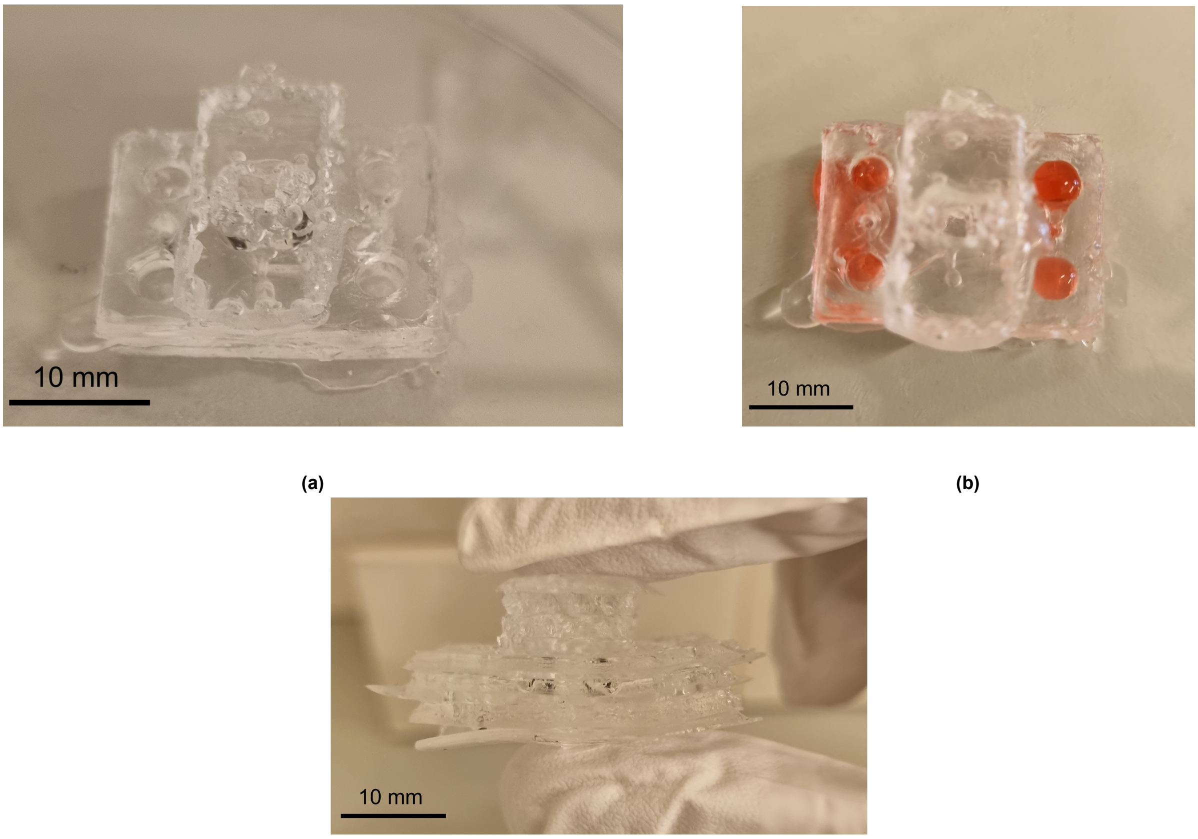

(a)

(b)

(c)

Figure C.4: PDMS molding pictures of multiple layer stacking. (a) Top view of bonded layers. (b) Top view of bonded layers with red-colored PBS injected. (c) Side view of bonded layers.

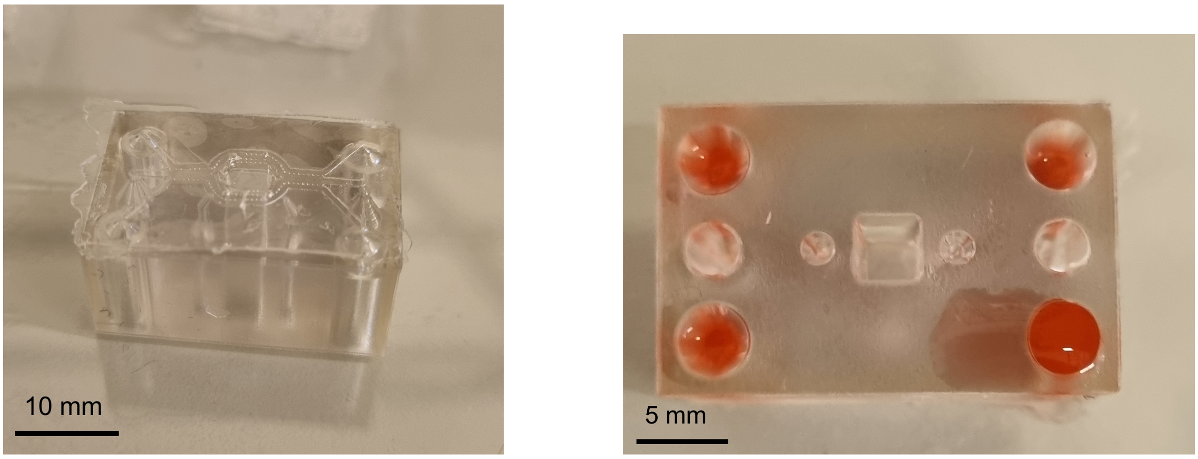

(a)

(b)

Figure C.5: PDMS molding pictures of 3D printed top layer. (a) Bottom view of bonded PDMS layer to 3D printed top layer. (b) Top view of 3D printed top layer with red-colored PBS injected

D

RSM resulting mass fractions

The effect of photo-polymerization time, temperature and photo-initiator concentration on remaining mass fraction was determined using responsive surface methodology. The remaining mass fraction for di-acrylated Pluronic F127 hydrogels after seven days was used as a dependent variable in the responsive surface methodology and are shown in Tab. D.1. The photo-polymerization time and temperature were set between two and ten minutes and 3°C and 30°C respectively. The photo-initiator concentration was initially set between 0.1 wt% and 0.3 wt%. However, the middle point for 10 wt% came out as 0.9 wt% (instead of 0.2 wt%) and the high fractional point for 15 wt% came out as 0.6 wt% (instead of 0.3 wt%).

Many of the samples were completely degraded after seven days, as indicated by the resulting mass fractions of 0%. Most other samples had a small remaining mass fraction after seven days, with mass fractions between 3.14 and 21.71%. Because the hydrogels concentrations used did not form gels based on micellation, the gel formation was completely dependent on photo-polymerization of 3D structures. For the samples with 0.3 wt% and 10 minutes of photo-polymerization, this was already found after photo-polymerization. These samples showed lump formation in the hydrogel solution after photo-polymerization.Interestingly, the middle-point sample of the hydrogels with a concentration of 15 wt% had a remaining mass fraction of 76.88%. This sample initially showed swelling behavior after two days, in which the mass fraction grew to 130%. This can be explained through additional uptake of water. Due to the fact that the wet mass fraction was used, the hydrogel masses can actually increase. If the dry mass fraction was used, the remaining mass fraction of this (and all other) samples would be significantly lower.

Because the hydrogels with a concentration of 10 and 15 wt% did not form a hydrogel, the results below are not representative to determine the photo-polymerization effects on the remaining mass fraction and thermoreversibility.

Table D.1: Remaining mass fraction responsive surface methodology

Photo-initiator concentration	0.1 wt%				0.2 wt %	0.3 wt%			
Time	2 min		10 min		5 min	2 min		10 min	
Temperature	3°C	30°C	3°C	30°C	20°C	3°C	30°C	3°C	30°C
10 wt%									
Mass fraction	**0**	**0**	**0**	**3.14**	**14.91**	**0**	**0**	**8.28**	**17.01**
15 wt%									
Mass fraction	**0**	**0**	**0**	**0**	**76.88**	**0**	**21.71**	**15.21**	**0**

E

Comsol simulation results

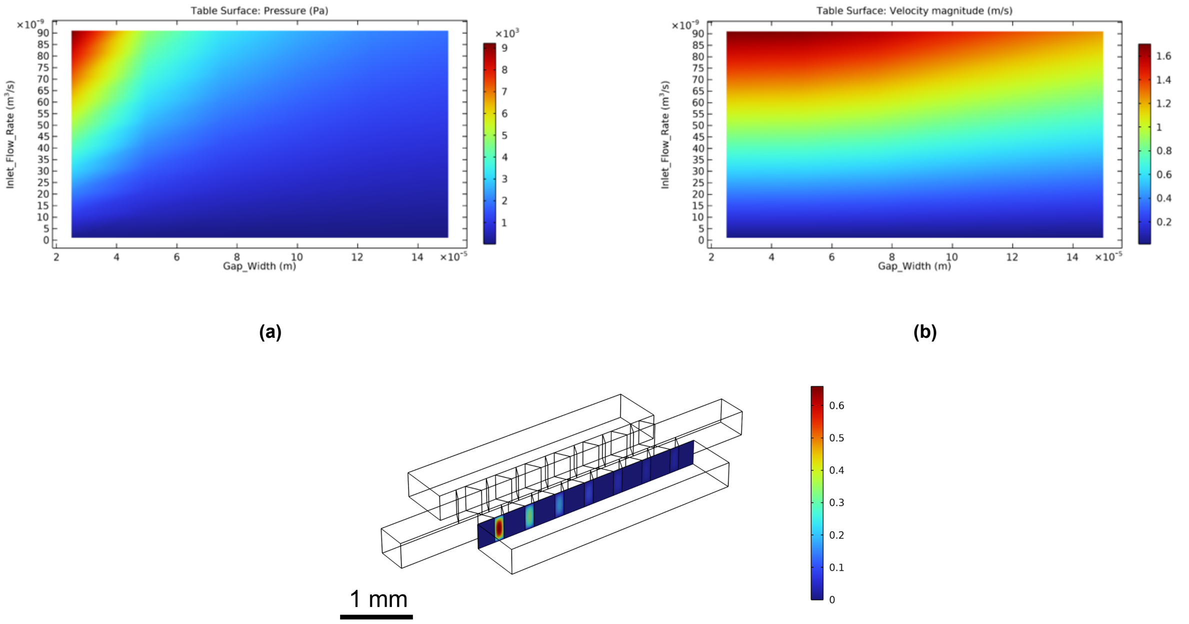

(a) (b)

(c)

Figure E.1: Breakthrough pressure (Pa) (a) and velocity (m/s) (b) of triangular shaped pillars. (c) Representative image of cut slice where pressure and velocity are determined

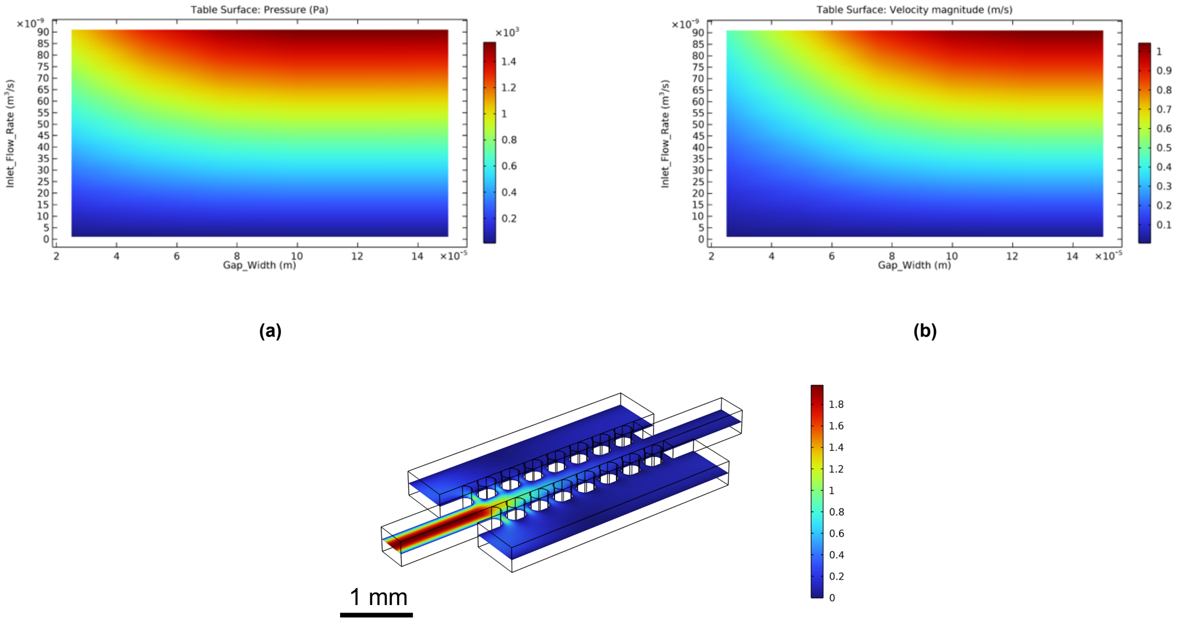

(a) (b)

(c)

Figure E.2: Breakthrough pressure (Pa) (a) and velocity (m/s) (b) of circular shaped pillars. (c) Flow velocity (m/s) of circular shaped pillars with a gap width of 0.1 mm and flow rate of $40mm^3/s$.

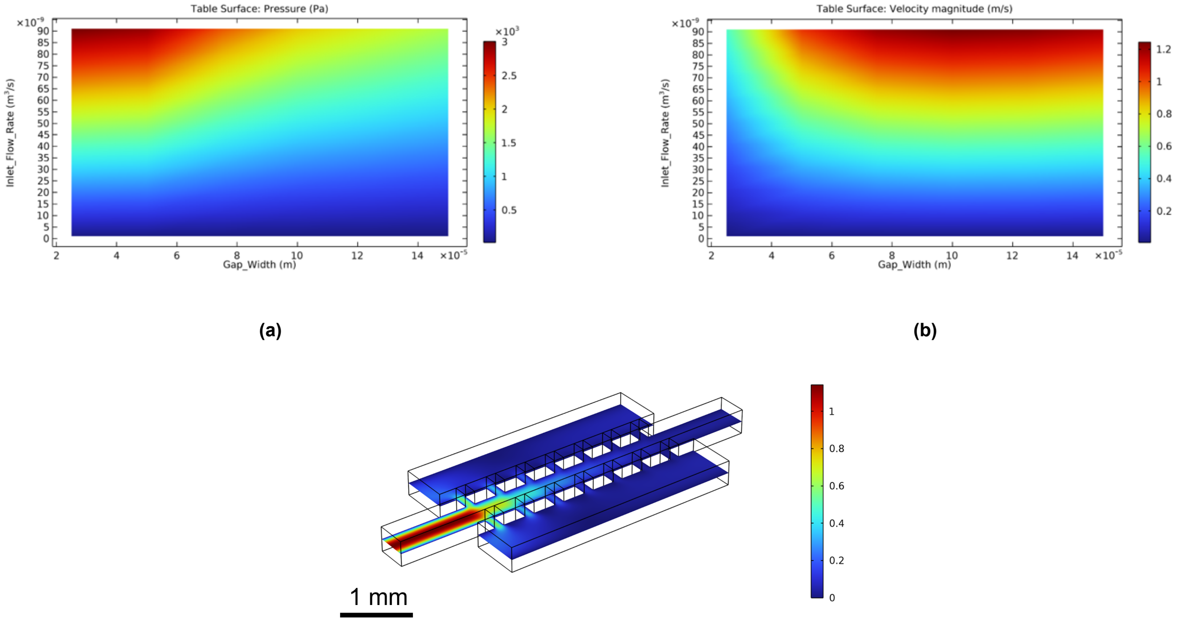

(a)

(b)

(c)

Figure E.3: Breakthrough pressure (Pa) (a) and velocity (m/s) (b) of square shaped pillars. (c) Flow velocity (m/s) of square shaped pillars with a gap width of 0.1 mm and flow rate of $40mm^3/s$.

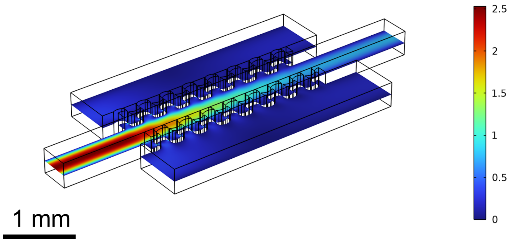

(a)

Figure E.4: Flow velocity (m/s) of curved pillars with a gap width of 0.025 mm and flow rate of $40mm^3/s$.

F

Literature review

Review of Pluronic F127 based hydrogels as a biodegradable wall option for vascularized cortical organoids in Organ-on-a-Chip applications

Maarten Lemmens (5609828)
Masters thesis review Biomedical Engineering, ECTM, TU Delft

***Abstract*—The goal of this literature review is to identify Pluronic F127 based hydrogels as a barrier option for Organ-on-a-chip (OoC) models. Organoid growth requires perfusion of vasculature to prevent cell necrosis. Therefore, co-culturing of vasculature and organoids on a single OoC platform is a promising solution. However, due to differences in required microenvironment of both cell cultures, the cell cultures need to be grown separately and come in contact only when fully developed. Therefore, a transient barrier needs to be placed in between and removed when needed. A systematic literature review is performed to identify Pluronic F127 based hydrogels as options for this barrier. The hydrogels should exhibit several properties, including thermoreversibility, transparency and stability in aqueous media. This review shows that di-acrylated- and thiol-terminated Pluronic F127 hydrogels are the most promising option. Di-acrylated Pluronic F127 hydrogels can be photo-polymerized to form stable hydrogels, while still being able to exhibit thermoreversible properties for lower concentrations. Simultaneously, thiol-terminated Pluronic F127 hydrogels form 3D stable structure through cross-linking with dopamine conjugated hyaluronic acid by Michael-type addition. A minor drawback of this hydrogel is a slight change in color. Finally, this review concludes with a set of proposed experiments to test these two hydrogels as a barrier option for vascularized organoid-on-a-chip.**

***Index Terms*—Organoid, Organ-on-a-chip, vascularization, Pluronic F127, hydrogel**

I. INTRODUCTION

Organ-on-a-chip (OoC) technology has revolutionized the biomedical research field by offering dynamic platforms which accurately mimic physiological environments of human tissue. This technology has become a promising option to study human biology *in vitro*, including disease modeling, drug screening and personalized medicine [1]. Organoids, 3D cell cultures derived from human stem cells, represent a promising tool to investigate 3D tissue growth *in vitro*. However, integration of vasculature in these organoids remains a significant challenge. Establishment of vasculature is essential to enable significant organoid growth, allowing nutrient and oxygen delivery and waste removal [2]. Therefore, co-culturing of vasculature and organoids on a single OoC platform evolved as a promising option to address these challenges. However, due to differences in chemical and mechanical requirements of the microenvironments of these tissues, a transient barrier is required in between these cell-cultures until sufficient growth of the organoid.
Pluronic F127 is a promising candidate to act as such a barrier. Pluronic F127 is known for its biocompatabiltiy, transparency and ability to exhibit thermoreversible properties [3].

This literature review aims to evaluate the utilization of Pluronic F127 based hydrogels as a barrier option between vasculature and cortical organoids on a single OoC platform. Literature is investigated to identify Pluronic F127 based hydrogels which comply to numerous requirements based on the growth process of both the vasculature cell cultures as well as the cortical organoids. The identified hydrogels were compared based on degradation rates in aqueous media at 37°C. Afterwards, the possibilities and limitations of these hydrogels are discussed.

A. Organ-on-a-Chip Technology

Traditionally, the most used methods for biological cell culturing and testing are 2D cell cultures and animal models. Traditional *in vitro* cell culturing utilizes 2D culture dishes as cell environment. This methods lacks complex living environment of cells and cannot stimulate cells through physical and chemical factors, such as biochemical gradients, fluid shear stresses and mechanical stress [2]. Therefore, cells cultured in 2D environments cannot self-assembly and represent physiological function of the tissue organ type.
The gold standard of biological testing *in vivo* is done with animal models. However, this has several limitations including differences in biological metabolism and immune response between animals and humans [2]. Because of the limitations of both models, developments of effective human models is vital and organ-on-a-chip models are a promising alternative solution. The structure of the chips can be adjusted towards the desired physiological and anatomical requirements, which enables the design of 3D mechanical and biochemical environments corresponding to the target organ.

Organ-on-a-chip models utilize microfluidics, which enable the precise fluidic manipulation of microenvironments [4]. Organ-on-a-chip research is focused on the elimination of animal models, while providing research on living 3D cell cultures. Due to the 3D structure, organ-on-a-chip models are very suitable to resemble human physiology. This can be employed in a wide range of biomedical applications including, drug screening, disease diagnosis and tissue engineering. Tissue engineering principles can also be applied to the development of human organoids. Organoids are *in vitro* miniaturized and simplified models of a specific human organ. Organoid models can be used for modeling of disease development, personalized medicine and drug screening [1]. The surrounding environments of organoids is highly dependent on the target organ [5]. The combination of organoids and OoC models can be used to address this challenge. Organoids offer more realistic organ models. However, the lack of proper vascularization limits the current possibilities. Human cell growth *in vitro* is possible, but most cells cannot survive when they are located more than 200 μm away from any blood vessel [2, 6, 7]. This is caused by the limited diffusion of nutrients and oxygen through cells. Therefore, co-culturing of organoids and vasculature tissue on a single OoC platform proves to have great potential.

1) Vascularization of organoids: Functional vascular networks can prevent cell death of growing tissue *in vitro* and therefore enable the engineering of large organoids [6]. The approach to obtain vasculature networks can be broadly categorized into two groups: templating and self-organizing methods. Templating methods include molding by needles, sacrificial materials and bioprinting [2, 6]. These models provide easy-to-use fabrication methods and can be used immediately after fabrication. However, the shape of the vasculature is pre-determined and cannot be dynamically adjusted to fit the environment. This inhibits vascular remodeling, which is an essential part for tissue development. In self-organizing methods, vascularization is induced by micropatterning, a supply of growth factors and culturing of supporting cells [6]. In microfluidics, vasculature is grown in central channel containing endothelial cells, smooth muscle cells, fibrinogen, thrombin and growth factors. Two parallel channel supply growth media containing growth factors, which is refreshed daily [8]. The morphology and permeability of these networks is similar to those found *in vivo*. Moreover, these vascular models allow for remodeling induced by environmental factors, in this case shear stress.

Vascularization of organoids on a chip aims at the co-culturing of self-organizing vasculature and organoids simultaneously. After the organoid has grown several weeks, the grown vasculature should perfuse the organoid to allow vasculature to grow within it. This should provide the organoid with needed oxygen and nutrients and prevent cell death within the organoid. Fig. 1 presents the theoretical model of vascularized organoids on a chip. To achieve this, a 3D printed microchip is used with an open-well design for the cortical organoid. In this chip, the cortical organoids can grow in the central chamber, whereas the vasculature can grow in the surrounding micro-channels. However, established protocol of organoid and vasculature growth are significantly different. The cortical organoid should grow for approximately 35 days, before vascular perfusion is required. Moreover, the organoid should grow in a stable and calm environment, not experiencing any mechanical stresses [10]. Simultaneously, the vasculature requires approximately seven days of growth and induced shear stress [8]. Therefore, to allow these two cell cultures to grow in the chip simultaneously, they should be separated until perfusion is required. The manufactured chip is designed in such a way, that a barrier can be placed between the two cell cultures. When perfusion is required, this barrier should be removed out of the chip, allowing the vasculature to grow into the organoid environment, inducing vasculature perfusion in the organoid.

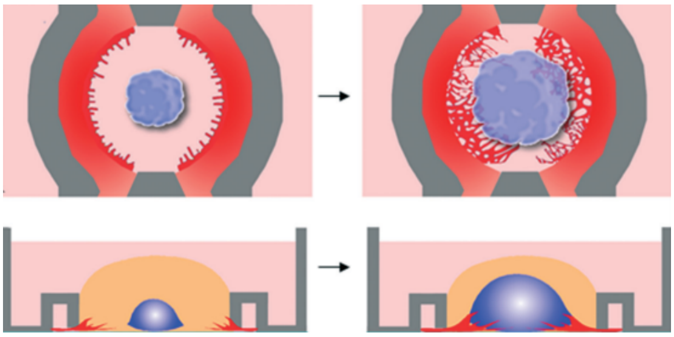

Fig. 1: Theoretical model of the vasculature perfusion of organoids on a chip. The organoid is grown in a central chamber of the chip. The vasculature is grown in the channels surrounding the central chamber. Media channels are placed on the outside of the vasculature channels to allow nutrient supply and provide shear stress. After the organoid has grown sufficiently, the vasculature is allowed to enter the central chamber and perfuse the organoid [9].

2) Barrier requirements: The transient barrier located in between the vascularized OoC platform and the growing cortical organoid should comply with several important requirements. The environment of the growing organoid should remain calm from the start of growth until vascular perfusion. To maintain this environment, the barrier placed in between should be non-permeable as well as be able to withstand the shear stress to which it is exposed from vascular hydrogel injection. The membrane should also be biocompatible and biodegradable to ensure that both cell cultures remain unharmed by the presence and removal of the barriers and its potential side-products. Moreover, since cell cultures are grown at 37°C to simulate human body environment, the barrier should remain stable at this temperature.

The growth time of both cell cultures and the fabrication of the OoC platform brings additional requirements. Due to geometric constraints of the designated channel, which is prefabricated on the chip, the barrier should be injectable in the OoC platform. Additionally, the barrier should be transparent to aid in visualization on the already transparent OoC platform. Because the cortical organoid have a growth period of more than 30 days and the vascular perfusion is not allowed to happen before the 35th day, the barrier should remain stable in aqueous environments at 37°C for more than the specified 35 days. After this period, the barrier should be able to be easily removed though, for example, thermoreversibility or chemical activation. Therefore, the barrier should provide a mean to control opening of the channel by external activation.

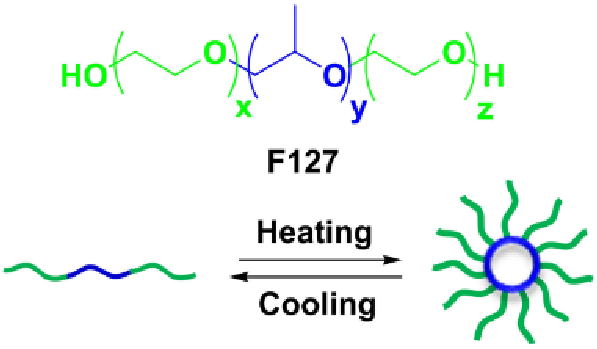

Fig. 2: Gelation principle of Pluronic F127 hydrogels. X = 65, Y = 99, Z = 65. Above the critical micelle temperature and critical micelle concentration, pluronic molecules will form micelle structures with the hydrophobic PPO blocks (blue) in the centre and the hydrophilic PEO blocks (green) at the edge [14].

Pluronics can be considered as a promising option for this application, as it could potentially comply to all above mentioned requirements. Pluronics form hydrogel when dissolved in aqueous media at body temperatures, while the can be easily flushed away at lower temperatures due to its thermoreversible properties [11]. However, Pluronic hydrogels can also exhibit poor mechanical stability in aqueous media over longer time. Therefore, this literature research aims to find Pluronic based hydrogel structures which are adjusted to comply to all above requirements for the successful perfusion of cortical organoids on a chip.

B. Pluronics

Pluronics are widely used and studied for a number of biomedical applications, including the generation of vasculature on a chip, encapsulation vehicles for drug delivery systems and post-surgery anti adhesion barriers. Especially Pluronic F127 is extensively investigated for its application and (together with Pluronic F68) is the only FDA approved type of Pluronic [3].

1) Properties: Pluronic F127 is a water-soluble, biocompatible poloxamer that consists of polyoxyethylene (PEO) and polyoxypropylene (PPO) with two 99-unit hydrophilic PEO blocks surrounding one 65-unit hydrophobic PPO block (Fig. 2 shows the PEO blocks (green) and PPO blocks (blue)) [12]. The nomenclature of these polymers consist of a letter to indicate the physical form at room temperature (liquid (L), paste (P) and flake (F). The first one or two figures provide 1/300 of the approximate molar mass of the PPO block per unimer. The last figure shows one-tenth of the molar mass percentage of PEO blocks per unimer [13]. Pluronic F127 solutions undergo a phase transition which is both concentration and temperature dependent [11]. The sol-gel transition happens above the critical micelle concentration (CMC) and critical micelle temperature (CMT), where Pluronics form micelles, which lead to gelation.

The gelation of Pluronic is based on their amphiphilic structure. The PEO blocks are hydrophilic, while the PPO blocks are hydrophobic, which makes them self-assemble into micelles in aqueous solutions above the CMC and CMT [15]. The viscosity of Pluronic F127 hydrogels is dependent on the concentration, where higher concentrations of Pluronic result in a higher viscosity of the hydrogel, both in solvent and gel state[16]. At temperatures below the gelation temperature, Pluronic solutions show Newtonian fluid behaviour. At temperatures above the gelation temperature, Pluronic hydrogels appear to show shear thinning behaviour for high shear rates [17, 18]. Pluronic F127 solutions have a gelation time of less than ten minutes for all concentrations. Additionally, gelation time increases with decreasing concentrations [18].

A major drawback of the usage of Pluronic F127 hydrogels is the fast degradation rate in aqueous media at body temperature [3].

2) Applications: As mentioned previously, Pluronic F127 hydrogels are widely studied for several different applications.

Pluronics as sacrificial materials: Pluronic F127 has been studied as sacrificial materials for tissue engineering, 3D bioprinting and the creation of branched vasculature within hydrogel-based systems [19]. The branched vascular channels can be seeded with endothelial cells to produce vessel-like structures [19].

The gelation temperature of Pluronic F127 can be adjusted by manipulating the concentration in deionized water or Phosphate Buffered Saline (PBS), where a higher concentration results in a lower gelation temperature [18]. The gelation temperature is defined as the temperature when G' (storage modulus) exceeds the G" (loss modulus) (Fig. 3). For visoelastic materials, the loss modulus represents the viscous behavior and the storage modulus represents the elastic behavior. Therefore, when the storage modulus exceeds the loss modulus, the material is considered to be in a viscoelastic solid state (or gel state). Additionally, a higher concentration also results in a significantly higher elastic modulus at body temperatures (15.7 kPa and 1 kPa for 25 wt% and 16 wt% respectively) [12]. Which means that higher concentration hydrogel are significantly stiffer at body temperature compared to lower concentration hydrogels.

Pluronic F127 can be 3D printed at ambient temperatures due to their shear thinning behavior. Through this way Pluronic channels can be printed surrounded by 3D printed GelMA [20]. After the full print is made, the Pluronics can be completely removed by lowering the temperature below 4°C [11, 19]. At this temperature, all Pluronic solutions will form liquids, which allows them to be easily removed.

Especially, F127 with a concentration of 25 wt% appeared to be suitable for bioprinting, due to fast gelation (< 5 min) at physical conditions, proper viscoelastic properties and fast viscosity recovery (< 5 sec) after shearing [18]. However, F127 mixtures of up to 40 wt% are used as fugitive inks, as these mixtures have a critical micelle temperature below 10°C and exhibit strong shear-thinning response [20, 21]. After decreasing the temperature below the lower critical gelation

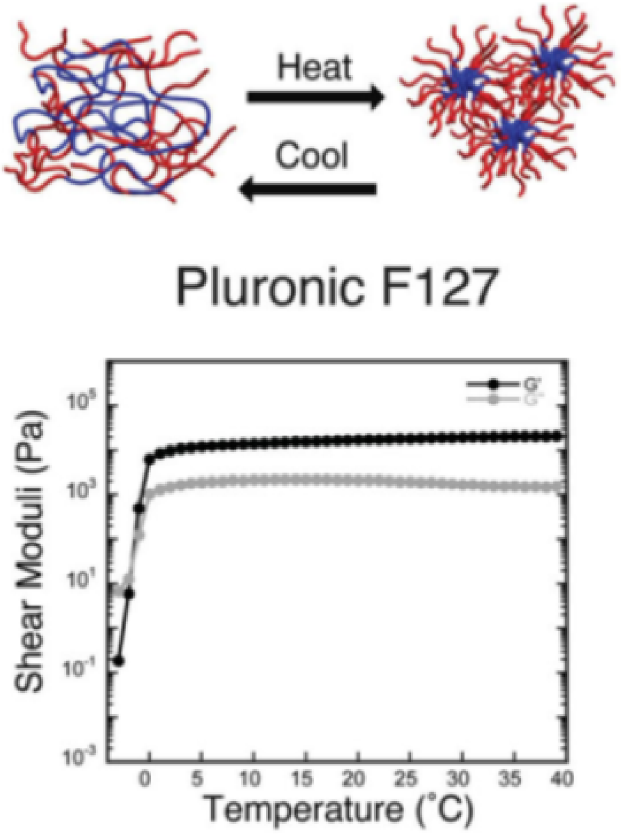

Fig. 3: Gelation of Pluronic F127 hydrogels. When the storage modulus (G') exceeds the loss modulus (G"), Pluronic F127 solutions form hydrogels [20].

temperature, the mixture can be washed away.

Pluronics are also used for passive flow control in microfluidic devices. Due to a heating induced gelation, they can be used for flow control. Here, the flow rate is modulated in response to temperature changes. Additionally, they can be used in microfluidic devices for localized gel formation to temporarily block channels. As mentioned, the gelation of Pluronics is concentration and temperature dependent. Above the critical micelle temperature, the viscosity of Pluronic mixtures increases by two order of magnitude within a few tenths of a degree Celsius [22].

Pluronics as Encapsulating Hydrogels: Because of the sol-gel transition near physiological temperature and pH, Pluronic F127 is also widely used in tissue engineering. Although Pluronics inhibit tissue adhesion, they have been successfully used as scaffolds in tissue engineering [3, 15].

The most suitable concentration of cell encapsulation is 20 wt%. This concentration has a gelation temperature of approximately 25 °C and a storage modulus of 7.2 kPa at body temperature. However, hydrogels made solely of Pluronic F127 might dissolve in aqueous medium in less than one hour [12]. Addition of carboxymethyl hexanoyl chitosan (CA) and glutaraldehyde (GA) can keep these hydrogels insoluble for more than one month [12]. This makes hydrogels made of Pluronic F127 with CA and GA more applicable as a scaffold for cell culturing. Moreover, the gelation temperature of this hydrogel is approximately 30 °C, making it easy to use.

Furthermore, the addition of heparin in Pluronic F127 hydrogels was successfully used to systematically deliver fibroblast growth factors to induce angiogenesis for over a month *in vivo* [23].

Pluronics as Anti-Adhesion barriers: Pluronics have also been used as tissue anti-adhesion barriers, which could have a potential application for organ on a chip application where prevention of cell adhesion is desired [24]. The Pluronics should be fluidic solutions before administration and form gels under physiological conditions [25].

Pluronic F127 has a low critical solution temperature (LCST) of 4 –20°C, which is optimal for applications *in vivo*, but has a rapid absorption rate due to dilution in fluids. Pluronics F68 has an LCST above 40°C, which exceeds body temperatures. Both these Pluronics are known to be biocompatible and least toxic among the Pluronic series. The LCST can be altered by adjusting the ratio and concentration of Pluronics F127/F68 mixtures [24]. A polymer concentration of 30 wt% with a Pluronic ratio of F127/F68 of 7/3 appeared to have a gelation temperature around 30°C, which makes it fluid at room temperature and a gel at body temperature [24]. The addition of sodium alginate (0.6 w%) and/or ibuprofen resulted in lower tissue adhesion of the Pluronic mixtures. Sodium alginates are widely used as drug delivery carriers, since they are biocompatible, degradable and nontoxic [24].

However, these Pluronic mixtures appeared to be completely dissolved in bodily fluids after five days. The addition of Pluronic P123 extends this period up to nine days, while it doesn't affect the gelation temperature of the above-mentioned mixtures [24]. Moreover, tissue adhesion appeared to be lower with the addition of P123 as well, without having an effect on inflammation in the body.

Pluronics are non-degradable materials and can be removed by dissolution in water. This also results in the relatively poor mechanical properties and dissolution in aqueous media which makes Pluronics suffer from a short persistence time *in vivo* [25, 26]. However, Pluronic F127 has many advantages including low toxicity, biologically inert, thermo-reversible properties and ease of use [27]. Therefore, chemically modified Pluronic polymers are studied to increase stability and integrity of the hydrogels.

II. METHODS

A systematic literature review was performed by the acquisition of papers through Web of Science, Scopus and manual addition of relevant papers. Added relevant papers were found as citations in papers (but not included by search terms) or recommended by colleagues. Since the relevant literature of Pluronic hydrogel modification dates back to the early 2000s and the objective of this study is not dependent on the newest research, no time restrictions are used in this search. The search term used in Web of Science and Scopus was: ”(pluronic OR f127) AND (*gel* OR inject*) AND (degrad* OR revers*) AND stab* ”, and was limited to search in the title, abstract and keywords of papers. In this search term, the star sign (”*”) means that all words including the words before or after the star sign are included in the search (i.e. inject* includes injected, injection, injectable, etc.). This search term includes papers based on Pluronic (f127), which either form gels or are injectable, include information about degradation or thermoreversibility and are stable. This resulted in 177 papers on Web of Science and 172 papers on Scopus. Based on the information about Pluronic F127 described above, relevant literature was added to the systematic search based on internal referencing within the papers used above. This resulted in 40 additional added papers. All papers were exported to Mendeley Reference Manager, where all duplicate papers were removed. This resulted in 248 unique papers. These papers were screened based on title and abstract and excluded if the information was not relevant (criteria explained below) for this literature search. This resulted in 84 remaining papers, which were screened based on the full text. The flowchart of this literature search is shown in Fig. 4.

The screening of papers on full text was based on the barrier requirements described in Sec. I-A2. Exclusion based on biocompatibility, biodegradability and injectability are not included as this is assumed to apply for all papers included by the search term. Papers were first screened on the availability of information of the stability over time of the Pluronic hydrogels. If this was not specified, the papers were excluded. Afterwards, for papers which specified the stability over time, the papers were screened based on the requirements listed in in Sec. I-A2. If the degradation or stability over time was not long enough for the application of vascularized cortical organoids on a chip, the papers were excluded. Papers which did provide substantial stability over time, but achieved this in a way which made the hydrogel not removable were also excluded. This included papers which used different additional polymerizable molecules, which resulted in cross linked structures, as these structures did not exhibit thermoreversibility or other easily removable features. Papers which used chemically modified Pluronic with additional cross-linked molecules in a later stadium were not excluded. Papers which used other Pluronic types or included supplements which made the hydrogel not transparent were excluded as well. Finally, reviews or irretrievable papers were excluded. After this systematic research, six papers were included in this review.

III. Results

Based on the systematic literature research, six papers were included in this review. A summary of the six Pluronic F127 based hydrogels is shown in Tab. I, the degradation rates of these chemically modified Pluronic F127 hydrogels are shown in Fig. 5. The resulting hydrogels from all six papers were biocompatible. These papers will be discussed in chronological order.

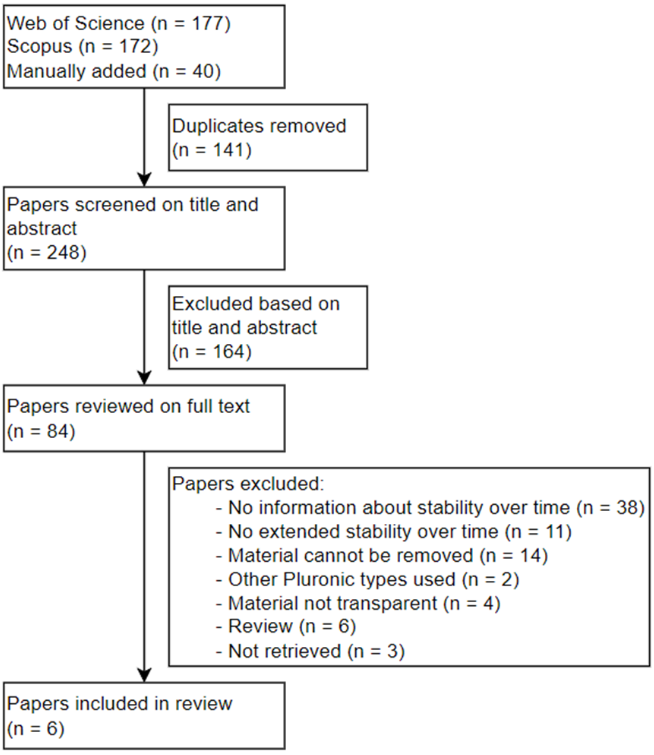

Fig. 4: Flowchart of literature review process

Lee et al. (2004) created photo-crosslinkable hydrogels through di-acrylation of Pluronic F127 without the addition of other monomers or macromers [28]. It was expected that polymerization would occur based on the cross-linking of the acrylate groups in self-assembled Pluronic micelles. This should result in a non-dissolving semi-solid hydrogel [28]. Solutions of di-acrylated Pluronics F127 (F127DA) were made at 4°C and dissolved. The obtained hydrogels formed a gel at room temperature. For these solutions, the strength of the hydrogels depended on the concentration, where a higher concentration resulted in a higher strength. Fig. 5a shows that the degradation of di-acrylated Pluronic solutions in PBS at 37°C is concentration dependent, where a higher concentration results in a lower degradation rate. For all three different concentrations used (15, 20 and 25%), the hydrogels had a remaining mass fraction of 80% after more than ten days. Moreover, after 30 days, all di-acrylated Pluronic hydrogels had a reaming mass fraction of more than 50% [28]. It should be noted that the obtained degree of acrylated end groups in the Pluronic molecules was determined to be 72%. Therefore, unmodified Pluronic molecules could still be present in these solutions.

Lee et al. (2007) chemically modified Pluronic F127 molecules with di-acrylated end groups as well. Similar to Lee et al. (2004), the F127DA hydrogels showed thermoreversible properties before photo-polymerization [29].

TABLE I: Summary of chemically modified Pluronic F127 hydrogels

		Degradation in PBS at 37°C			
Principle	**Thermoreversible**	**Ratio gel/PBS**	**20%**	**100%**	**Ref.**
Photo-polymerization of di-acryalted pluronic F127	Before polymerization	NA	$\sim$ 12 days	$>$ 40 days[1]	[28]
Photo-polymerization of di-acryalted pluronic F127	Before polymerization	1/20	10 - 30 days	$>$ 40 days[1]	[29]
Photo-polymerization of di-acryalted pluronic F127	Before polymerization	NA	$\sim$ 15 days	$>$ 40 days[1]	[23]
Michael-type catechol-thiol reaction	Yes	1/1[2]	$>$ 40 days[1]	$>$ 40 days[1]	[30]
Enzymatic catechol reaction	Yes	2/1[2]	$\sim$ 3 days	$>$ 40 days[1]	[31]
Hexamethylene diisocyanate and hyaluronic acid	Before addition of hyaluronic acid	1/2[2]	$\sim$ 3 days	$\sim$ 30 days	[32]

[1] No exact data

[2] With PBS refreshments at every time point

This allows the hydrogels to be injected in a liquid state, form a gel in the micro-channels and be polymerized afterwards to increase stability and lower degradation rates. Lee et al. (2007) modified Pluronics in a similar manner as Lee et al. (2004), but achieved a degree of acrylation of 98% [29]. Fig. 5b shows the degradation rates of F127 and F127DA hydrogels in PBS at 37°C. In this test, 0.5 ml of the produced F127 and F127DA hydrogels were injected in 10 ml of PBS. This figure is especially useful, as it elaborates on the differences in degradation rates between normal Pluronic F127 hydrogels and di-acrylated Pluronic F127 hydrogels. It can be seen that normal Pluronic F127 hydrogels degrade completely within ten days. Simultaneously, F127DA hydrogels remain stable significantly longer. Compared to Lee et al. (2004), these results are even more promising, as the concentrations of the hydrogels are lower, but the degradation rates are slower. This could be explained through the difference in the degree of acrylation (72% vs. 98%). These results show that even for lower concentrations (9 wt%), F127DA hydrogels have a remaining mass fraction of more than 60% for more than 30 days [29].

This paper also tested the mechanical strength (measured through elastic modulus using rheometry) of hydrogels for different UV cross-linking parameters. The polymerization of the F127DA hydrogels can be modified by alternating these parameters. The strength of these hydrogels increased for higher UV intensities, longer irradiation times and higher concentrations of photo-initiators [29]. While testing for each of these parameters, the other parameters were kept constant. Moreover, lower concentrations of F127DA, required longer irradiation times to form stable polymerized hydrogels. These results suggest that strength, and potentially the degradation rates, of the hydrogels can be modified be adjusting UV irradiation parameters.

Additionally, Yoon et al. (2007) studied the effect of cross-linking F127DA molecules with APMMA conjugated heparin [23]. They achieved an acrylation degree of 87%. The hydrogels were photo-polymerized after both F127DA molecules and APMMA conjugated heparin were dissolved in PBS. Fig. 5c shows the degradation rates of these hydrogels in PBS at 37°C. In this figure, the results for ”A” include no cross-linked heparin, while ”B”, ”C” and ”D” have increased quantities of cross-linked heparin, respectively. Therefore, the results from ”A” shows the polymerization of solely F127DA molecules. In this figure, a concentration of 30 wt% F127DA in PBS was used. The results are similar as the previous two results, were F127DA hydrogels have a slow degradation rate, with 80% mass fraction reaming after approximately 15 days. While, complete degradation took longer than 40 days. From these results can also be concluded that the influence on degradation rates of the addition of APMMA conjugated heparin is minimal [23].

Lee et al. (2010) produced lightly cross-linked hydrogels made of hyaluronic acid (HA) conjugated with dopamine and thiol end-capped Pluronic F127 molecules [30]. Thiol-terminated Pluronic F127 (Plu-SH) molecules were made by conjugating cysteamine on the terminal groups of F127 molecules. Plu-SH and dopamine conjugated HA were dissolved in PBS. Chemical crosslinking happened between the catchol-groups created on the HA molecules and the thiol groups on the Pluronic F127 molecules [30]. This resulted in a significantly lower critical micelle concentration at room temperature, compared to normal Pluronic F127 hydrogels. This inter-micellar crosslinking is caused by Michael-type catechol-thiol reaction. This also causes a slight change in color from completely transparent to slightly yellowish [30]. Interestingly, HA/Plu-SH hydrogels exhibited thermally reversible transitions, even after chemical crosslinking. This is probably caused due to the cross-linking already below the gelation temperature. The change in elastic- and viscous modulus caused by change in temperature is shown in Fig. 6. It can be seen that the change happens immediately after the temperature change, while the sol-gel transition remains repeatable over time. Compared to photo-polymerized materials, which don’t show thermoreversible properties after crosslinking.

The HA/Plu-SH hydrogels could be injected in PBS at 37°C without showing any detectable dissolution or disintegration for more than a month [30]. The hydrogel remained stable and precipitated in excess amounts of PBS. This is different compared to conventional Pluronic F127 hydrogels, which dissolute in excess amounts of aqueous solutions. Fig. 5d shows the degradation rates of HA/Plu-SH hydrogels in PBS at 37°C. Here, one gram of hydrogel was tested for degradation in 1 ml of PBS. The PBS was refreshed at all given time points. Depending on the concentrations, the degradation rates differed enormously. HA/Plu-SH hydrogels with a concentration of 12 wt% completely degraded within ten days. Hydrogels with a concentration of 16 wt% showed extreme resistance against erosion in aqueous solutions. Simultaneously, these

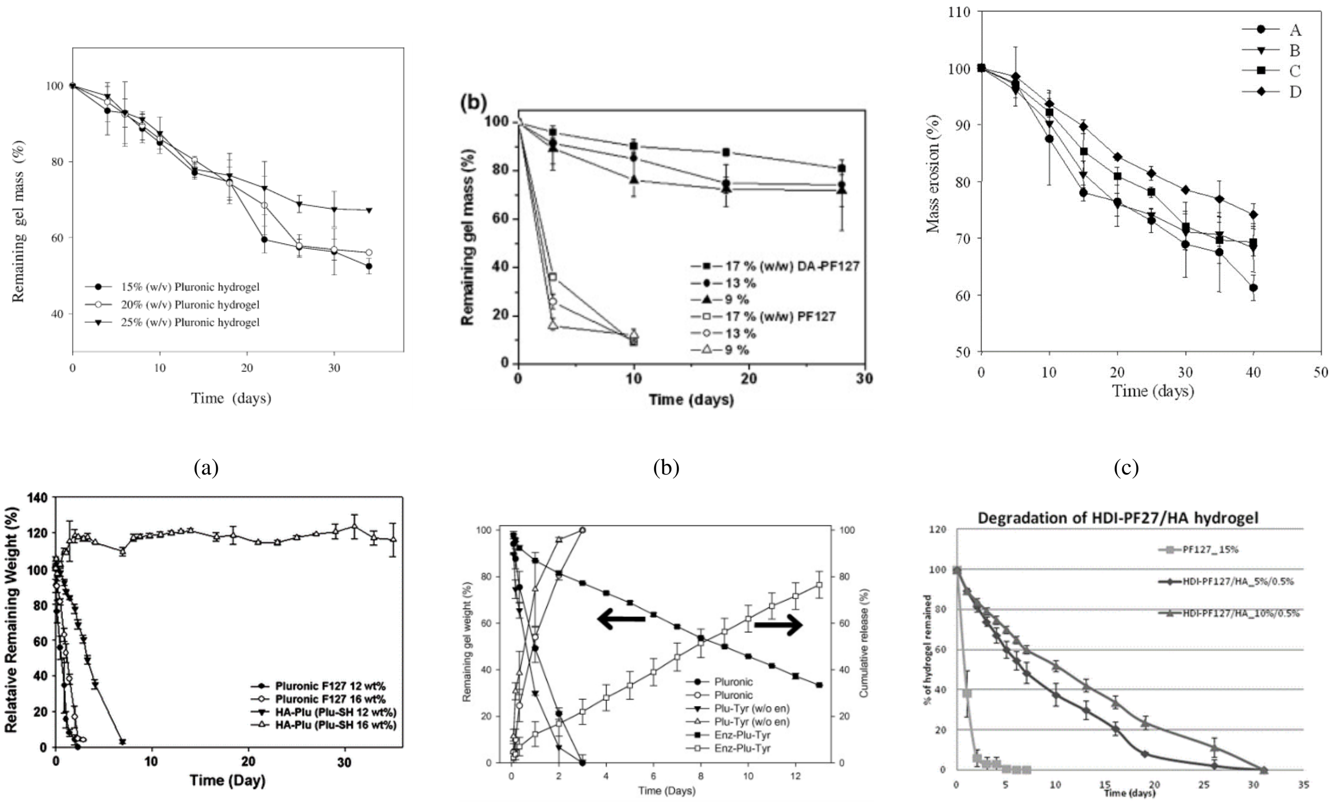

(a) (b) (c)

(d) (e) (f)

Fig. 5: Degradation rates of different chemically modified (and cross-linked) Pluronic F127 hydrogels in PBS at 37°C. (a) Degradation of di-acrylated Pluronic F127 hydrogels with concentrations of 15, 20 and 25 wt% [28]. (b) Degradation rates of normal and di-acrylated Pluronic F127 hydrogels with concentrations of 9, 13 and 17 wt% [29]. (c) Degradation rates of 30 wt% di-acrylated Pluronic F127 hydrogels with cross-linked APMMA conjugated heparin. Wt% of APPMA conjugated heparin: A = 0%, B = 0.3%, C = 3% and D = 9% [23]. (d) Degradation of thiol end-capped Pluronic F127 hydrogels cross-linked with dopamine conjugated hyaluronic acid with concentrations of 12 and 16 wt% [30]. (e) Degradation (black) and drug release (white) patterns Pluronic F127 hydrogels with conjugated tyramine (Plu-Tyr) and tyrosinase enzymes (Enz-Plu-Tyr) [31]. (f) Degradation of Pluronic F127 hydrogels with hexamethylene diisocyanate (HDI) cross-linked with 0.5 wt% hyaluronic acid (HA). Concentrations used were 5 and 10 wt%, with normal 15wt% Pluronic F127 hydrogel as control [32].

hydrogels with higher concentrations could still be injected as a solvent at room temperatures [30].

Lee et al. (2011) cross-linked individual Pluronic micelles through the additions of conjugated tyramine on the Pluronic F127 end groups, while using tyrosinase enzymes [31]. The tyramine could be oxidized to catechol groups by tyrosinase enzymes, after which the micelles cross-linked. The reaction caused by the tyrosinase enzymes changed the color of the hydrogel from transparent to brown (still transparent) [30]. Similar to the catechol-thiol reaction, this hydrogel also remained thermoreversible after cross-linking (same principle as shown in Fig. 6). This suggest that this hydrogel has cross-linked molecules before micelles formation as well. Moreover, this hydrogel can be injected at room temperature as well. Fig. 5e shows the degradation rates (in black) of Pluronic-tyramine molecules. The degradation was tested by using 1ml of hydrogel in 0.5ml of PBS with refreshing of PBS at given time points. It can be seen that the degradation rate is significantly lower than normal Pluronic F127 hydrogels when tyrosinase enzymes are added. However, 20% degradation already happened after several days, even for the hydrogel with the lowest degradation rates [31].

Last, Chen et al. (2013) extended Pluronic F127 molecules with hexamethylene diisocyanate (HDI) [32]. HDI was added as a cross-linking agent to provide inter micellar cross-linking. HDI-F127 molecules were still able to form micelles above the critical micelle temperature and/or concentration. The modified HDI-F127 molecules were dissolved in deionized water, after which HA was added. This resulted in significantly lower gelation temperatures, compared to normal Pluronic F127 hydrogels. After the addition of hyaluronic acid, the hydrogels did not exhibit thermoreversible behavior anymore. This suggest that the addition of HA caused the creation of a stable network. Fig. 5f shows the degradation rates of these hydrogels at 37°C in PBS. This was tested by injecting 1ml of

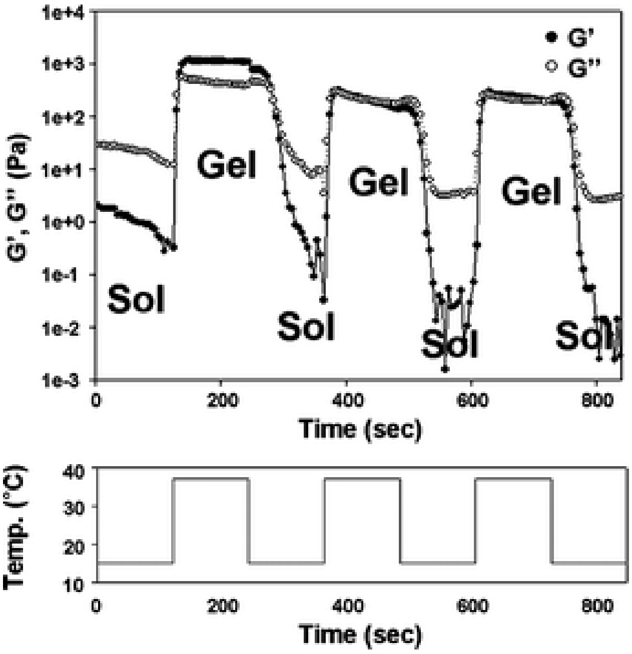

Fig. 6: Change of elastic (G') and viscous (G") modulus of HA/Plu-SH hydrogels with temperature cycles of heating (37°C) and cooling (5°C) [30]

hydrogel in 2ml of PBS with refreshments at given time points. HDI-F127 hydrogels have a significantly slower degradation rate, compared to conventional F127 hydrogels [32]. However, 20% is already degraded within three days, while the complete hydrogels were degraded within a month.

IV. DISCUSSION

Based on the requirements of the barrier described in Sec. I-A2, it can be concluded that two viable options remain. The first three results from the literature research indicated that the degradation rate and strength of Pluronic F127 hydrogels could be increased by cross-linking acrylated terminal ends of Pluronics [23, 28, 29]. Alternatively, Lee et al. (2010) and Lee et al. (2011) achieved similar results by chemically cross-linking Pluronics, causing catechol-thiol reactions [30, 31]. The last result from Chen et al. (2013) is discarded, as these results were the least promising of all, while the fabrication methods were extensive and needed additional polymerization of cross-linked materials [32]. Although the results of the first two methods are similar, both methods have several advantages and disadvantages.

A. Di-acrylated Pluronic F127

Pluronic F127 can be chemically modified to form terminally di-acrylated Pluronics. Compared to normal Pluronic F127, F127DA has a lower gelation temperature and concentration [33]. Pluronic F127 doesn't form hydrogels for concentrations below 20 wt%, whereas F127DA form hydrogels for concentrations as low as 10 wt%. The formed acrylated end groups on the pluronic are hydrophobic and replace the OH groups (hydrophilic) on the Pluronic molecules. This could cause the micelles to have a lower gel forming temperature and/or concentrations [33]. This feature can be suitable as a barrier for OoC applications. As a lower gelation concentration allows for an easier mixing protocol. Higher concentrated hydrogels require vigorous stirring, mostly in advanced machines, whereas lower concentration hydrogels can be easily manufactured by manual stirring. Moreover, a lower gelation temperature prevents unintended liquefaction for lower hydrogel concentrations.

In the results of Lee et al. (2004), Lee et al. (2007) and Yoon et al. (2007) on di-acrylated pluronics, it can be seen that the degradation rates of Pluronic F127DA hydrogels differs significantly. Unfortunately, only the results from Lee et al. (2007) included the volumes of hydrogel and PBS in the degradation testing [29]. This test was performed with 1g of hydrogel in 20ml of PBS, without refreshments. These results indicate a very slow degradation rate in aqueous media. The other two studies show less promising results, although still promising for OoC applications. However, since the degradation testing did not include PBS refreshments, it cannot represent the degradation for the application in this study, as the growth media (based on PBS) of the cortical organoids is refreshed every two to three days. Therefore, to determine degradation rates of hydrogels used in OoC applications, more research should be done.

The acrylated end groups of the Pluronic molecules provided cross-linking possibilities between the Pluronic micelles [34]. These hydrogels still showed thermereversible and biodegradable properties for lower concentrations [33, 35]. Di Biase et al. (2011) found that photo-polymerization of di-acrylated end caps, without additional monomers did not significantly improve the rheological behavior of Pluronic F127DA [33]. Without additional cross-linking monomers, the photo polymerization cross-linked the end cap micelle structures. This created covalent bonding between micelles, which improves mechanical behavior. To allow di-acrylated pluronic F127 to be removed from the barrier channel, it should be possible to wash the complete hydrogel out of the channels. Therefore, when these hydrogels are made through photo-polymerization into stable 3D structures, they can not be removed through thermoreversible properties anymore. This is one of the properties by which pluronics were chosen as a barrier option. Di Biase et al. (2011) found that di-acrylated pluronic F127 hydrogels could still exhibit thermoreversible properties after photo-polymerization (Fig. 7) [33]. This was only possible for hydrogels with a concentration below 15 wt% in combination with lower polymerization temperatures. However, since the study from Lee et al. (2007) showed that lower concentration F127DA hydrogels already showed a significant decrease in degradation rates, these hydrogels could be very promising [29]. To find the optimal F127DA hydrogel fabrication method, more research should be done. Additionally, this should include the identification of optimal photo-polymerization conditions, including the intensity, duration and temperature. Therefore, the combined results

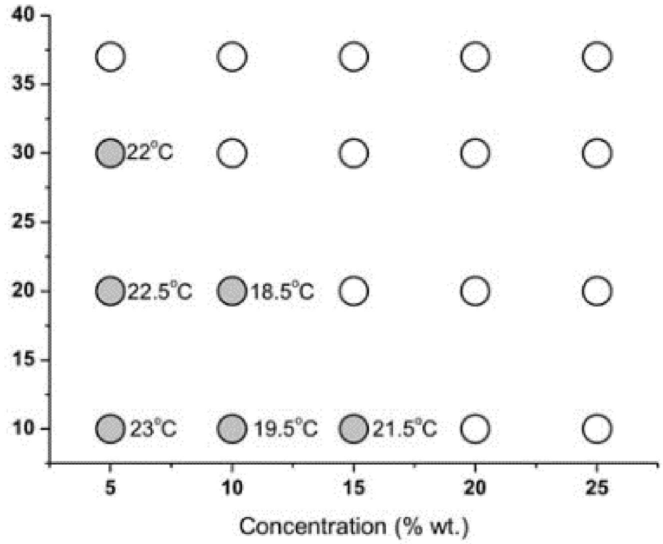

Fig. 7: Di-acrylated Pluronic F127 hydrogels which exhibit thermoreversible properties after photo-polymerization (shown in gray). The Y-axis shows the photo-polymerization temperature. The temperatures indicated at each sample is the gelation temperature at which the hydrogels. Lower F127DA concentrations and/or lower polymerization temperatures cause the hydrogels to exhibit thermoreversible behavior [33].

of the degradation rates of the di-acrylated Pluronic F127 hydrogels mentioned in Sec. III and the results of Di Biase et al. (2011) suggest that thermoreversible, slow degrading di-acrylated hydrogels can be made by polymerizing micelle end caps. However, since Lee et al. (2007) used different polymerization methods and Pluronic and photo-initiator concentrations compared to Di Biase et al. (2011), it remains highly uncertain if di-acrylated Pluronic hydrogels exhibiting thermoreversible properties and low degradation rates can be developed.

Lee et al. (2007) studied the effect of photo-polymerization methods on the elastic modulus of di-acrylated pluronic hydrogels. For constant concentrations (9wt%) of Pluronic F127DA, the mixture did not form a hydrogel for low UV intensities, UV irradiation times and initiator concentration [29]. Moreover, for each of these parameters, higher values resulted in a higher elastic modulus of the formed hydrogel. This suggest that the mechanical parameters can be regulated towards the desired properties by adjusting curing parameters.

Bhusari et al. (2023) found that the viscoelastic properties of Pluronic hydrogels can be regulated by adjusting di-acrylation fraction in Pluronic micelles [34]. Although additional cross-linking monomers are required for the creation of long term stable hydrogels, photo-polymerization of di-acrylated Pluronics without monomers already improves mechanical stability of the formed hydrogels. Differences in di-acrylation fraction were also studied by Muller et al. (2015). Different ratios of di-acrylated pluronic molecules in a hydrogel resulted in nanostructured hydrogels for cell encapsulation [36]. After photo polymerization of acrylated micelles terminal ends, the regular Pluronic F127 molecules were washed out by lowering the temperature, this resulted in ”porous” nanostructured hydrogel. For barrier applications in OoC’s, this can be suitable, by changing the hydrogels porosity when needed. In this manner, the barrier material won’t be washed out when the vascularization of the brain organoids is needed, but the material will be made porous. Since, Pluronics are considered to be biocompatible and are already used as encapsulating hydrogels, it could be tested if vascularization occurs after washing.

A study by Camana et al. (2023) compared Pluronic F127DA to modified Pluronic F127 with thioacetate (F127TA) and multi-acrylate (F127HA), to find optimal chemical modification for specific biomedical applications [26]. An interesting phenomenon for the application of barrier on OoC is that F127DA hydrogels have relatively low swelling ratios at room temperature and at body temperature compared to the other two modified Pluronics. This means that at physiological conditions, the hydrogel would not swell through any gaps on the chip, but would remain in its assigned channel. Moreover, the swelling degrees decrease with increasing concentration due to a rise in physical cross-linking [26] . The other modified Pluronics showed swelling ratios of approximately 100% at physiological temperatures. This makes those modified Pluronics less suitable for OoC applications. The swelling ratios can also be compared to conventional Pluronic F127 hydrogels, which appear to have swelling ratios above 200% at physiological temperature [37]. This suggest that modification of Pluronic F127 with di-acrylate end caps results in improved swelling ratios for OoC applications.

Lee et al. (2007) showed that di-acrylated Pluronic hydrogel have an hysteresis pattern in their gelation and ”melting” behaviour. Hydrogels with 17 wt% Pluronic F127 had a gelation temperature of 27°C, and a melting temperature of 17°C [38]. They also showed that the morphology of Pluronic F127DA hydrogels can be accurately controlled through concentration and cross-linking temperature. This hysteresis pattern can be especially useful in OoC barrier applications. As the gelation temperature can be relatively high, it is relatively easy to handle at room temperature. Meanwhile, a significantly lower ”melting” temperature prevents unintentional melting at room temperature.

Therefore, di-acrylated Pluronic F127 hydrogels are a promising option for the application as a barrier for vascularized organoids on a chip. The di-acrylated Pluronic F127 hydrogels shows slower degradation rates for similar concentrations, compared to conventional Pluronic F127 hydrogels. The mechanical properties of the hydrogels can be adjusted by alternating concentrations and photo-polymerization parameters. Simultaneously, the results above suggest that these hydrogels can still exhibit thermoreversible properties for lower concentrations. However, this needs ot be further investigated.

Moreover, adjusting the polymerization methods to allow for thermoreversibility might significantly increase degradation rates of these hydrogels. Based on the requirements mentioned in Sec. I-A2, di-acrylated Pluronic F127 hydrogels are a promising option. Theoretically, it can comply to all mentioned requirements.

B. Thiol end-capped Pluronic F127

The thiol end-capped Pluronic F127 hydrogels also showed promising results to be suitable as a barrier in OoC applications. Pluronic hydrogels modified with hyaluronic acid (HA) are studied because of the biocompatibility, biodegradability, anti-adhesive properties and extended stability [30]. Hyaluronic acid is a naturally occurring glucosaminoglycan in the human body. Lee et al. (2010) made Pluronic F127HA hydrogels by modification of Pluronic terminal end with cysteamine, mixed with dopamine-conjugated HA. Hydrogels consisting of more than 16 wt% Pluronics showed initial swelling and long-term stability. The degradation testing was performed in equal amounts of hydrogel and surrounding aqueous media, with repeating PBS refreshments. This resembles the eventual degradation process in applications for a barrier in vascularized organoids as surrounding growth media in this applications also occurs repeatedly. This makes these hydrogels very suitable for OoC applications.

Moreover, the fact that these hydrogels still exhibit thermoreversible properties allows them to be washed out of the barrier channels at any given time. This property, in combination with the extremely slow degradation rate, make this hydrogel the most promising chemically modified pluronic-based hydrogel. Additionally, the gelation temperature of these hydrogels, with a concentration above 15 wt%, is slightly below room temperature [30]. This allows for easy handling and prevent unintended liquefaction as the temperature doesn't have to be lowered significantly for the hydrogels to be washed out of the channels.

However, a possible implication of this hydrogel is that the Michael-type reaction causes the hydrogel to become slightly yellowish [30]. Transparency is considered to be a highly preferable property of hydrogels in OoC application. The exact color change for hydrogels with suitable properties needs to be determined. If the color change cause the hydrogel to by non-transparent, this can form a serious implication. Moreover, the addition of chemically modified hyaluronic acid chains causes the fabrication methods to be significantly more extensive compared to di-arcylation of Pluronic F127. The modification of thiol end-caps in Pluronic F127 is similar to modification methods of di-acrylation.

Based on the requirements of the barrier mentioned in Sec. I-A2, thiol end-capped Pluronic F127 hydrogels cross-linked with hyaluronic acid show promising results. These chemically modified Pluronics comply to most requirements. These hydrogels are stable for long time in aqueous media, exhibit thermoreversible properties and can be injected at room temperature. However, the color change caused by Michael-type reactions might inhibit the viability of this hydrogel for the application as a barrier in vascularized organoids on a chip.

C. Alternatives

The results from the literature are based on extended degradation rates of Pluronic F127 hydrogels in aqueous media. However, as degradation rate might severely differ from permeability of hydrogels in OoC channels, other Pluronic F127 based hydrogels are discussed below.

Yap & Yang (2016) mixed Pluronic F127 with carboxymethyl hexanoyl chitosan (CA) and glutaraldehyde (GA) [12]. These hydrogels can be synthesized relatively easily by mixing all mentioned substances in PBS. The dissolution time of these hydrogels in aqueous media is increased to more than a month, due to the addition of CA and GA (crosslinker) [12]. However, the addition of CA increase the gelation temperature of hydrogels with 20 wt% Pluronic from 20°C to 30°C. Moreover, these hydrogels exhibit swelling ratios in aqueous media of more than 500%. Due to the high swelling ratios, these hydrogels were not considered as a viable option for the barrier application in OoC.

Lippens et al. chemically modified Pluronic F127 with alanine (amino acid) and lactic acid to tailor degradation rates of cell encapsulating Pluronic hydrogels [3]. This chemically modified Pluronic-ALA-L hydrogel showed slower degradation rates in PBS at body temperature than conventional Pluronic F127 hydrogels. With 30 wt%, hydrogels made of this polymers showed remaining gel weights of more than 80% after 20 days. This would suit the application as barrier function for OoC models. Moreover, the hydrogel remained biodegradable and nontoxic. Pluronic-ALA-L is made through modification of Pluronic F127 with methacylated alanine as end caps and cross-linked of vinyl side groups through UV irradiation [3]. Therefore, due to extensive cross-linking of additional molecules, this hydrogel was excluded from the results above. However, if the hydrogel can be tailored to degrade in 35 days, it might still be promising as a barrier option.

Sun et al. (2014) chemically co-polymerized Pluronic F127DA with acrylamide [39]. This cross-linked hydrogel showed ultra stretchable behavior and stronger mechanical properties compared to Pluronic F127DA hydrogels without additional cross-linking monomers. This makes these hydrogels very suitable for applications where flexibility is required. However, the gelation temperature exceeded 30°C, which makes these hydrogels difficult to use as barriers for OoC applications [39].

Sohn et al. (2016) fabricated Pluronic F127DA hydrogels cross-linked with acrylated hyaluronic acid through photo-polymerization. Addition of photo polymerized acrylated hyaluronic acid chains in the hydrogel increases the stiffness of the hydrogel [40]. However, this option of polymerization resulted in swelling ratios of more than 500%. Alternatively, the hyaluronic acid chains could be methacrylated. Hyaluronic acid was modified to acquire vinyl end groups and form methacrylated HA. This hydrogel also showed increased stability over time compared to conventional Pluronic hydrogels, with similar results to the heparin cross-linked hydrogels [23, 41]. Exposure to UV light polymerizes the acrylated end groups of both molecules. Swelling ratios for those hydrogels appeared to be lower than 15% and 5% for hydrogels with a Pluronic F127DA concentration of more than 10 wt% and 20 wt%, respectively [4, 42, 43]. Moreover, these hydrogels are able to be injected and show high compressive toughness and fatigue resistance. This makes them a promising hydrogel for the OoC barrier application. The degradation of these hydrogels does not happen due to dissolution in surrounding aqueous media, as is the case for conventional Pluronic F127 hydrogels, but through hydrolysis of an acid labile ester linkage in the acrylated junction between the Pluronic and the polymerized polyacrylate backbone [35]. Therefore, these cross-linked hydrogels don't exhibit thermoreversibile properties as well. To achieve an open channel after 35 days (as mentioned in the requirements), these hydrogels should be exactly customized to degrade in this time span to allow for washing out of the channel.

Since, normal Pluronic hydrogels show low viscosity and high permeability levels at 37C, other chemically modified Pluronics have been studied as well. Sosnik et al. (2003) studied the effect or di-methacrylated Pluronic F127 hydrogels obtained through a reaction of Pluronics with methacryloyl chloride [44]. This modified Pluronics had significantly improved physical properties compared to normal Pluronic hydrogels. However, swelling rate were substantial for this hydrogel, with swelling ratios of approximately 700% [44, 45]. Moreover, the hydrogels appeared to degrade within five and fifteen days in dry conditions at body temperature and room temperature respectively [46]. Therefore, degradation rates of this hydrogel are considered to be too high. However, the permeability of this hydrogel might still be suitable for applications as barrier for OoC.

Pluronic F127 can also be modified to contain aldehyde terminal ends [14]. These modification induces self-healing and tissue adhesive properties in the hydrogels. These modified Pluronic F127 hydrogels are used in wound repair and generation and are able to perform gradual drug release. Tissue anti-adhesive effect can also be achieved through chemical modification. Pluronic F127 with alkoxyamine terminal ends showed anti adhesive properties to fibroblast, which makes them suitable for post surgery tissue-adhesion barriers [14]. This might be a suitable modification for OoC applications as it prevents tissue ingrowth in the hydrogels. Therefore, acting as a chemical barrier between two cell cultures.

Thermoreversible and biodegradable hydrogels made of polyester and poly-ether can be an interesting alternative to Pluronic F127 hydrogels because of their biodegradable properties and relatively longer persistence times [25]. Poly(3-caprolactone-co-lactide)-b-poly(ethylene glycol) -b-poly(3-caprolactone-co-lactide) (PCLAePEGePCLA) triblock copolymer hydrogel could serve as a barrier material to prevent postoperative intestinal adhesion [25]. This material has a sol-gel transition between room and body temperature at 20 wt%, which makes it more difficult to use, since the hydrogel will liquefy at room temperature. However, degradation studies showed that this polymers showed longterm integrity in PBS at body temperature. After twelve weeks, a gel fraction of 80% was still retained. This hydrogel is made from the central Pluronic F127 (PEG) chain and chemically modified with polycaprolactone through ring opening of caprolactone (CL) and lactide (LA) in presence of Pluronic [25].

Finally, additional Pluronic molecules can be mixed together. Oh et al. (2005), mixed Pluronic F127 and F68 molecules to fabricate anti-adhesive hydrogels [24]. The additions of Pluronic F68 lowers the adhesion of tissue to the hydrogels. However, Pluronic F68 significantly increase the gelation temperature of these hydrogels with lower concentrations. Alternatively, Pluronic F123 can be used. Mixtures of Pluronics containing P123 molecules slightly decrease the degradation rates of these hydrogels. Simultaneously, additions of Pluronic P123 lowers the degree of tissue even further [24].

V. CONCLUSION

Pluronic F127 molecules can be chemically modified to decrease the degradation rate of formed hydrogels in aqueous media. For the application as a barrier in vascularized organoids in Organ-on-a-chip, these hydrogels should remain stable in aqueous media for more than 35 days. To achieve this, two different chemically modified Pluronic F127 hydrogels show promising results. The Pluronic F127 molecules can be modified to acquire arcylated terminal ends, after which these are cross-linked through photo-polymerization. These hydrogels exhibit a significantly lower degradation rate than normal Pluronic F127 hydrogels. Simultaneously, it is also shown that di-acrylated Pluronic F127 hydrogels exhibit thermoreversible behaviour for lower concentrations. However, it remains to be investigated if both a low degradation rate and thermoreversible properties can be achieved simultaneously.

Pluronic F127 molecules can also be modified with thiol-end caps and chemically cross-linked with dopamine conjugated hyaluronic acid. These hydrogels exhibit thermoreversible properties after cross-linking and show extremely slow degradation rate in aqueous media. Therefore, these hydrogels are a promising option for the barrier application in vascularized organoids on a chip. However, the chemically cross-linking reaction causes the hydrogel to change color, which might severely inhibit the transparency of the hydrogel. This might cause this hydrogel to be unsuitable for biological applications.

VI. FUTURE WORK, OBJECTIVES AND RESEARCH PLAN

Based on the collected information in this review, a research plan for this master thesis to identify the optimal Pluronic F127 based hydrogel can be formulated. The objective of this research plan is to find a Pluronic F127 based hydrogel which can act as a transient barrier for vascularized organoids on a chip. First, the findings of this review concluded that both di-acrylated and thiol-end capped Pluronic F127 hydrogel show the most promising result to act as a barrier between vasculature and organoid growth. It was chosen to further investigate the potential of di-acrylated Pluronic F127 hydrogels through several experiments. The research plan for these hydrogels is divided in four different stages. First, the hydrogels will be synthesized based on present literature and tested for thermoreversible properties with different concentrations and photo-polymerization conditions. The results of several different papers will be combined. Lee et al. (2007) demonstrated that di-acrylated Pluronic F127 hydrogel exhibit slow degradation rates in aqueous media, while Di Biase et al. (2011) demonstrated that di-acrylated Pluronic F127 hydrogels with lower concentrations and low polymerization temperature exhibit thermoreversible properties [29, 33]. Therefore, findings of these two papers will be combined to test if di-acrylated Pluronic F127 based hydrogels can exhibit slow degradation rates in aqueous media while being thermoreversible simultaneously. Alternatively, Bhusari et al. (2023) found that the degradation rates of di-acrylated Pluronic F127 hydrogels can be adjusted by altering the ratios of F127/F127DA hydrogels. This can also be a promising option to allow hydrogels to remain thermoreversible. For all the obtained hydrogels, exhibiting thermoreversible properties, the degradation rate in PBS at 37°C and the permeability rate in PBS at 37°C will be tested for several different concentrations. The concentrations will be kept constant for all hydrogels to allow for proper comparison.

Second, the mechanical properties of each hydrogel will be tested with a rheometer and through differential scanning calorimeter (DSC). With the rheometer, the storage modulus, loss modulus and viscosity of the hydrogels can be obtained, while DSC allows to find the precise micellation temperature and possible hysteresis patterns.

Based on the found properties in the second step, the barrier channel on the chip can be accurately modeled. After modeling the channel, the chip will be 3D printed using digital light processing and it will be tested if the hydrogels do indeed remain within the channel.

Finally, an optimal injection protocol will be formulated. This will included the optimal injection volumes and temperature, as well as the photo-polymerization parameters.

Successfully execution of all steps should results in the establishment of the optimal di-acrylated Pluronic F127 based hydrogel to act as a barrier for vascularized organoids on a chip.

REFERENCES

[1] Hofer, M., & Lutolf, M. P. (2021). Engineering organoids. *Nature Reviews Materials*, *6*, 402–420.

[2] Zhao, X., Xu, Z., Xiao, L., Shi, T., Xiao, H., Wang, Y., Li, Y., Xue, F., & Zeng, W. (2021). Review on the vascularization of organoids and organoids-on-a-chip. *Frontiers in Bioengineering and Biotechnology*, *9*.

[3] Lippens, E., Swennen, I., Gironès, J., Declercq, H., Vertenten, G., Vlaminck, L., Gasthuys, F., Schacht, E., & Cornelissen, R. (2013). Cell survival and proliferation after encapsulation in a chemically modified pluronic® f127 hydrogel. *Journal of Biomaterials Applications*, *27*, 828–839.

[4] Shen, C., Li, Y., Wang, Y., & Meng, Q. (2019). Non-swelling hydrogel-based microfluidic chips. *Lab on a Chip*, *19*, 3962–3973.

[5] McCauley, H. A., & Wells, J. M. (2017). Pluripotent stem cell-derived organoids: Using principles of developmental biology to grow human tissues in a dish. *Development*, *144*, 958–962.

[6] Nashimoto, Y., Hayashi, T., Kunita, I., Nakamasu, A., Torisawa, Y.-s., Nakayama, M., Takigawa-Imamura, H., Kotera, H., Nishiyama, K., Miura, T., & Yokokawa, R. (2017). Integrating perfusable vascular networks with a three-dimensional tissue in a microfluidic device. *Integrative Biology*, *9*, 506–518.

[7] LaMontagne, E., Muotri, A. R., & Engler, A. J. (2022). Recent advancements and future requirements in vascularization of cortical organoids. *Frontiers in Bioengineering and Biotechnology*, *10*.

[8] Cuenca, M. V., Cochrane, A., van den Hil, F. E., de Vries, A. A., Oberstein, S. A. L., Mummery, C. L., & Orlova, V. V. (2021). Engineered 3d vessel-on-chip using hipsc-derived endothelial- and vascular smooth muscle cells. *Stem Cell Reports*, *16*, 2159–2168.

[9] Salmon, I., Grebenyuk, S., Fattah, A. R. A., Rustandi, G., Pilkington, T., Verfaillie, C., & Ranga, A. (2022). Engineering neurovascular organoids with 3d printed microfluidic chips. *Lab on a Chip*, *22*, 1615–1629.

[10] Eigenhuis, K. N., Somsen, H. B., van der Kroeg, M., Smeenk, H., Korporaal, A. L., Kushner, S. A., de Vrij, F. M. S., & van den Berg, D. L. C. (2023). A simplified protocol for the generation of cortical brain organoids. *Frontiers in Cellular Neuroscience*, *17*.

[11] Wu, W., DeConinck, A., & Lewis, J. A. (2011). Omnidirectional printing of 3d microvascular networks. *Advanced Materials*, *23*.

[12] Yap, L.-S., & Yang, M.-C. (2016). Evaluation of hydrogel composing of pluronic f127 and carboxymethyl hexanoyl chitosan as injectable scaffold for tissue engineering applications. *Colloids and Surfaces B: Biointerfaces*, *146*, 204–211.

[13] Pitto-Barry, A., & Barry, N. P. E. (2014). Pluronic® block-copolymers in medicine: From chemical and biological versatility to rationalisation and clinical advances. *Polym. Chem.*, *5*, 3291–3297.

[14] Li, S., Yang, C., Li, J., Zhang, C., Zhu, L., Song, Y., Guo, Y., Wang, R., Gan, D., Shi, J., Ma, P., Gao, F., & Su, H. (2023). Progress in pluronic f127 derivatives for application in wound healing and repair. *International Journal of Nanomedicine*, *Volume 18*, 4485–4505.

[15] Shirwaiker, R., Purser, M., & Wysk, R. (2014). Scaffolding hydrogels for rapid prototyping based tissue engineering. Elsevier.

[16] Lenaerts, V., Triqueneaux, C., Quartern, M., Rieg-Falson, F., & Couvreur, P. (1987). Temperature-dependent rheological behavior of pluronic f-127 aqueous solutions. *International Journal of Pharmaceutics*, *39*, 121–127.

[17] Jalaal, M., Cottrell, G., Balmforth, N., & Stoeber, B. (2017). On the rheology of pluronic f127 aqueous solutions. *Journal of Rheology*, *61*, 139–146.

[18] Gioffredi, E., Boffito, M., Calzone, S., Giannitelli, S. M., Rainer, A., Trombetta, M., Mozetic, P., & Chiono, V. (2016). Pluronic f127 hydrogel characterization and biofabrication in cellularized constructs for tissue engineering applications. *Procedia CIRP*, *49*, 125–132.

[19] Fitzsimmons, R. E., Aquilino, M. S., Quigley, J., Chebotarev, O., Tarlan, F., & Simmons, C. A. (2018). Generating vascular channels within hydrogel constructs using an economical open-source 3d bioprinter and thermoreversible gels. *Bioprinting*, *9*, 7–18.

[20] Kolesky, D. B., Truby, R. L., Gladman, A. S., Busbee, T. A., Homan, K. A., & Lewis, J. A. (2014). 3d bioprinting of vascularized, heterogeneous cell-laden tissue constructs. *Advanced Materials*, *26*, 3124–3130.

[21] Kolesky, D. B., Homan, K. A., Skylar-Scott, M. A., & Lewis, J. A. (2016). Three-dimensional bioprinting of thick vascularized tissues. *Proceedings of the National Academy of Sciences*, *113*, 3179–3184.

[22] Stoeber, B., Hu, C.-M. J., Liepmann, D., & Muller, S. J. (2006). Passive flow control in microdevices using thermally responsive polymer solutions. *Physics of Fluids*, *18*.

[23] Yoon, J. J., Chung, H. J., & Park, T. G. (2007). Photo-crosslinkable and biodegradable pluronic/heparin hydrogels for local and sustained delivery of angiogenic growth factor. *Journal of Biomedical Materials Research Part A*, *83A*, 597–605.

[24] Oh, S. H., Kang, J. G., & Lee, J. H. (2018). Co-micellized pluronic mixture with thermo-sensitivity and residence stability as an injectable tissue adhesion barrier hydrogel. *Journal of Biomedical Materials Research Part B: Applied Biomaterials*, *106*, 172–182.

[25] Zhang, Z., Ni, J., Chen, L., Yu, L., Xu, J., & Ding, J. (2011). Biodegradable and thermoreversible pcla–peg–pcla hydrogel as a barrier for prevention of post-operative adhesion. *Biomaterials*, *32*, 4725–4736.

[26] Camana, G., Tavano, M., Li, M., Castiglione, F., Rossi, F., & Cellesi, F. (2023). Design of functional pluronic-based precursors for tailoring hydrogel thermoresponsiveness and cell-adhesive properties. *Materials*, *16*, 2749.

[27] Shamma, R. N., Sayed, R. H., Madry, H., Sayed, N. S. E., & Cucchiarini, M. (2022). Triblock copolymer bioinks in hydrogel three-dimensional printing for regenerative medicine: A focus on pluronic f127. *Tissue Engineering Part B: Reviews*, *28*, 451–463.

[28] Lee, J. B., Yoon, J. J., Lee, D. S., & Park, T. G. (2004). Photo-crosslinkable, thermo-sensitive and biodegradable pluronic hydrogels for sustained release of protein. *JOURNAL OF BIOMATERIALS SCIENCE-POLYMER EDITION*, *15*, 1571–1583.

[29] Lee, S.-Y., & Tae, G. (2007). Formulation and in vitro characterization of an in situ gelable, photo-polymerizable pluronic hydrogel suitable for injection. *Journal of Controlled Release*, *119*, 313–319.

[30] Lee, Y., Chung, H. J., Yeo, S., Ahn, C.-H., Lee, H., Messersmith, P. B., & Park, T. G. (2010). Thermo-sensitive, injectable, and tissue adhesive sol–gel transition hyaluronic acid/pluronic composite hydrogels prepared from bio-inspired catechol-thiol reaction. *Soft Matter*, *6*, 977.

[31] Lee, S. H., Lee, Y., Lee, S.-W., Ji, H.-Y., Lee, J.-H., Lee, D. S., & Park, T. G. (2011). Enzyme-mediated cross-linking of pluronic copolymer micelles for injectable and in situ forming hydrogels. *Acta Biomaterialia*, *7*, 1468–1476.

[32] Chen, Y. Y., Wu, H. C., Sun, J. S., Dong, G. C., & Wang, T. W. (2013). Injectable and thermoresponsive self-assembled nanocomposite hydrogel for long-term anticancer drug delivery. *LANGMUIR*, *29*, 3721–3729.

[33] Biase, M. D., de Leonardis, P., Castelletto, V., Hamley, I. W., Derby, B., & Tirelli, N. (2011). Photopolymerization of pluronic f127 diacrylate: A colloid-templated polymerization. *Soft Matter*, *7*, 4928.

[34] Bhusari, S., Hoffman, M., Herbeck-Engel, P., Sankaran, S., Wilhelm, M., & Campo, A. D. (2023). Rheological behavior of pluronic/pluronic diacrylate hydrogels used for bacteria encapsulation in living materials. *bioRxiv*.

[35] Lee, J. B., Chun, K. W., Yoon, J. J., & Park, T. G. (2004). Controlling degradation of acid-hydrolyzable pluronic hydrogels by physical entrapment of poly(lactic acid- co -glycolic acid) microspheres. *Macromolecular Bioscience*, *4*, 957–962.

[36] Müller, M., Becher, J., Schnabelrauch, M., & Zenobi-Wong, M. (2015). Nanostructured pluronic hydrogels as bioinks for 3d bioprinting. *Biofabrication*, *7*, 035006.

[37] Cellesi, F., Tirelli, N., & Hubbell, J. A. (2002). Materials for cell encapsulation via a new tandem approach combining reverse thermal gelation and covalent crosslinking. *Macromolecular Chemistry and Physics*, *203*, 1466–1472.

[38] Lee, S.-Y., Tae, G., & Kim, Y. H. (2007). Thermal gellation and photo-polymerization of di-acrylated pluronic f 127. *Journal of Biomaterials Science, Polymer Edition*, *18*, 1335–1353.

[39] Sun, Y.-n., Gao, G.-r., Du, G.-l., Cheng, Y.-j., & Fu, J. (2014). Super tough, ultrastretchable, and thermoresponsive hydrogels with functionalized triblock copolymer micelles as macro-cross-linkers. *ACS Macro Letters*, *3*, 496–500.

[40] Sohn, S. S., Revuri, V., Nurunnabi, M., Kwak, K. S., & Lee, Y.-k. (2016). Biomimetic and photo crosslinked hyaluronic acid/pluronic f127 hydrogels with enhanced

mechanical and elastic properties to be applied in tissue engineering. *Macromolecular Research*, *24*, 282–291.

[41] Kim, M. R., & Park, T. G. (2002). Temperature-responsive and degradable hyaluronic acid/pluronic composite hydrogels for controlled release of human growth hormone. *Journal of Controlled Release*, *80*, 69–77.

[42] Zhang, H., Ren, P., Jin, Y., & Ren, F. (2019). Injectable, strongly compressible hyaluronic acid hydrogels via incorporation of pluronic f127 diacrylate nanomicelles. *Materials Letters*, *243*, 112–115.

[43] Ren, P., Zhang, H., Dai, Z., Ren, F., Wu, Y., Hou, R., Zhu, Y., & Fu, J. (2019). Stiff micelle-crosslinked hyaluronate hydrogels with low swelling for potential cartilage repair. *Journal of Materials Chemistry B*, *7*, 5490–5501.

[44] Sosnik, A., Cohn, D., Román, J. S., & Abraham, G. A. (2003). Crosslinkable peo-ppo-peo-based reverse thermo-responsive gels as potentially injectable materials. *Journal of Biomaterials Science, Polymer Edition*, *14*, 227–239.

[45] Vandenhaute, M., Schelfhout, J., Vlierberghe, S. V., Mendes, E., & Dubruel, P. (2014). Cross-linkable, thermo-responsive pluronic® building blocks for biomedical applications: Synthesis and physico-chemical evaluation. *European Polymer Journal*, *53*, 126–138.

[46] Vandenhaute, M., Snoeck, D., Vanderleyden, E., Belie, N. D., Vlierberghe, S. V., & Dubruel, P. (2017). Stability of pluronic® f127 bismethacrylate hydrogels: Reality or utopia? *Polymer Degradation and Stability*, *146*, 201–211.